PHOTONIC SWITCHING

TECHNICAL DIGEST

MARCH 1-3, 1989
SALT LAKE CITY, UT

1989 PHOTONIC SWITCHING
REGISTRATION LIST

LASTNAME	FIRSTNAM	ORGANIZA	ADDRESS1	ADDRESS2	MAILCODE	COUNTRY
ADAMS	MICHAEL J	BRITISH TELECOM RES LABS	RT233 MARTLESHAM HEATH	IPSWICH SUFFOLK	IP5 7RE	UK
AIDA	TAHITO A	ATR OPT & RADAR COM RES	TWIN21 MID 2-1-61	HIGASHI-KU OSAKA	540	JAPAN
ALFERNESS	ROD	AT&T BELL LABS	CRAWFORDS CORNER RD	HOLMDEL, NJ	07733	USA
ASOM	MOSES T	AT&T BELL LABS	600 MOUNTAIN AVE	MURRAY HILL, NJ	07974	USA
BAETS	ROEL G	UNIV OF GENT IMEC	LEA SINT PIETERSN	B-9000 GENT		BELGIUM
BERGH	ARPAD A	BELLCORE		MORRISTOWN, NJ	07960	USA
BERRY	MARK H	NAVAL OCEAN SYSTEMS CTR	271 CATALINA BLVD	SAN DIEGO, CA	92152	USA
BERTHOLD	JOSEPH E	BELLCORE	331 NEWMAN SPRINGS RD	RED BANK, NJ	07701	USA
BESSE	PIERRE A	ETH-ZURICH SWISS	HPT F10 8093	ZURICH		SWITZERLAND
BIZE	DANIEL	ONERA CERT	2 AVE ED BELIN BP 4025	TOULOUSE	31055	FRANCE
BLACK	RICHARD J	CECOLE POLYTECHNIQUE	ENG PHYS CP6079 STN A	MONTREAL	H3C3A7	CANADA
BLUMENTHAL	DANIEL J	UNIV OF PENNSYLVANIA	200 S 33RD ST MOORE	PHILADELPHIA, PA	19118	USA
BOTTELDOOREN	DICK B	UNIV OF GENT IMEC	LEA SINT PIETERSN	B-9000 GENT		BELGIUM
BOYD	GARY D	AT&T BELL LABS	ROOM 4B 537	HOLMDEL, NJ	07733	USA
BOYSEL	ROBERT M	TEXAS INSTRUMENTS	PO BOX 655936 MS 134	DALLAS, TX	75075	USA
BRACKETT	CHARLES A	BELLCORE	445 SOUTH STREET	MORRISTOWN, NJ	07960	USA
BRASHER	JAMES D	TELEDYNE BROWN ENG	300 SPARKMAN DRIVE NW	HUNTSVILLE, AL	35807	USA
BRENNER	KARL-HEINZ	UNIV OF ERLANGEN	ERWIN ROMMELSTR 1	ERLANGEN 8520		FED REP GER
BULLER	GERALD S	HERIOT-WATT UNIVERSITY	RICCARTON	EDINBURGH EH144AS		UK
BURDGE	GEOFF	LAB FOR PHYSICAL SCIENCE	4928 COLLEGE AVENUE	COLLEGE PARK, MD	20740	USA
CAPRON	BARBARA A	BOEING ELECTRONICS HTC	MS 7J-27 PO BOX 24969	SEATTLE, WA	98124	USA
CATHEY	W THOMAS	UNIVERSITY OF COLORADO	OPTOELECTRONIC COMP SYS	BOULDER, CO	80309	USA
CAVAILLES	JEAN	L E P	3 AVE DESCARTES	LIMEIL BREVANNES	F 94450	FRANCE
CHAN	Y ELLEN	EASTMAN KODAK	1669 LAKE AVE B65 FL1	ROCHESTER, NY	14650	USA
CHAO	TIEN-HSIN	JET PROPULSION LAB	4800 OAK GROVE DRIVE	PASADENA, CA	91109	USA
CHENEVAS PAULE	ANDRE A	CEA CENT DLETI DOPT	85 X	GRENOBLE	38041	FRANCE
CHENG	STEVEN	BELLCORE	445 SOUTH STREET	MORRISTOWN, NJ	07960	USA
CHIARULLI	DONALD M	UNIV OF PITTSBURGH	COMP SCI DEPT, 212M1B	PITTSBURGH, PA	15260	USA
CHIROVSKY	LEO M	AT&T BELL LABORATORIES	600 MOUNTAIN AVENUE	MURRAY HILL, NJ	07974	USA
CHU	KWONG W	SANDIA NATL LABS	DIV 1415	ALBUQUERQUE, NM	87185	USA
CHUROUX	PASCAL	CERT ONERA	2 AVE EDOUARD BELIN	BP 4025 TOULOUSE	31055	FRANCE
CINATO	PAOLA	CSELT	VIA REISS ROMOLI 274	TUPIN 10148		ITALY
CLOONAN	THOMAS J	AT&T BELL LABORATORIES	200 PARK PLAZA	NAPERVILLE, IL	60566	USA
COOPER	LARRY	OFFICE OF NAVAL RESEARCH	CODE 1114SS	ARLINGTON, VA	22217	USA
CRAFT	NICHOLAS C	AT&T BELL LABS	DEPT 11356	HOLMDEL, NJ	07733	USA
DASARO	L A	AT&T BELL LABS	600 MOUNTAIN AVENUE	MURRAY HILL, NJ	07974	USA
DAVISON	STEPHEN A	CAMBRIDGE UNIVERSITY	ENG DEPT TRUMPINGTON ST	CAMBRIDGE ENGLAND	CB2 1PZ	UK
DAWSON	PETER H	NATL RES COUNCIL	DIV OF PHYSICS	OTTAWA, ONT.	K1A OR6	CANADA
DAY	CLIVE R	BRITISH TELECOM RES LABS	RT233 MARTLESHAM HEATH	IPSWICH SUFFOLK	IP5 7RE	UK
DEEG	EMIL W	AMP INC	PO BOX 3608 MS 140 28	HARRISBURG, PA	17105	USA
DERSTINE\	MATTHEW W	BOEING ELECTRONICS HTC	PO BOX 24969	SEATTLE, WA	98124	USA
DICKEY	FRED M	SANDIA NATL LABS	DIV 1415	ALBUQUERQUE, NM	87185	USA
DICKINSON	ALEX	AT&T BELL LABS	CRAWFORDS CORNER ROAD	HOLMDEL, NJ	07701	USA
DOWNS	MARALENE M	AT&T BELL LABS	CRAWFORDS CORNER RD	HOLMDEL, NJ	07733	USA
DRAKE	MARVIN D	THE MITRE CORPORATION	BURLINGTON RD, MS 050	BEDFORD, MA	01730	USA
DUTHIE	PETER J	PLESSEY RESEARCH CASWELL	CASWELL TOWCESTER	NORTHANTS	NN128EQ	UK
ELMAN	BORIS S	GTE LABORATORIES INC	40 SYLVAN ROAD	WALTHAM, MA	02254	USA
ENG	KAI Y	AT&T BELL LABORATORIES	CRAWFORDS CORNER ROAD	HOLMDEL, NJ	07733	USA
ENG	SVERRE T	JET PROPULSION LAB	4800 OAK GROVE DRIVE	PASADENA, CA	91109	USA
ENGLERT	THAD	UNIV OF WYOMING	BOX 3295 UNIV STATION	LARAMIE, WY	82071	USA
FALK	R AARON	BOEING AEROSPACE	PO BOX 3999 MS 37 50	SEATTLE, WA	98124	
FELD	STEWART	COLORADO STATE UNIV	1705 HEATHERIDGE 6201	FT COLLINS, CO	80526	USA

1989 PHOTONIC SWITCHING
REGISTRATION LIST

LASTNAME	FIRSTNAM	ORGANIZA	ADDRESS1	ADDRESS2	MAILCODE	COUNTRY
FIDDY	MICHAEL A	UNIVERSITY OF LOWELL	DEPT OF ELECTRICAL ENG	LOWELL, MA	01854	USA
GABRIAGUES	JEAN-MICHEL	LABS DE MARCOUSSIS	ROUTE DE NOZAY	MARCOUSSIS	91460	FRANCE
GABRIEL	CHRIS	AT&T BELL LABS	46524 CRAWFORDS CRNR RD	HOLMDEL, NJ	07733	USA
GALBRAITH	IAN	PHILIPS RES LABS	CROSS OAK LANE	REDHILL RH1 5HA		UK
GAYLORD	THOMAS K	GEORGIA TECH	SCHOOL OF ELEC ENG	ATLANTA, GA	30332	USA
GIGLMAYR	JOSEF J	HEINRICH HERTZ INST	FUR NACHRICHTENTECHNIK	BERLIN D-1000	20742	FED REP GER
GILES	C LEE	AFOSR	BLDG 410 BOLLING AFB	WASHINGTON, DC	20332	USA
GIORDMAINE	JOE	NEC RESEARCH INSTITUTE	67 MOUNTAIN BLVD EXT	WARREN, NJ	07060	USA
GLEESON	JAMES N	AMOCO TECHNOLOGY CO	PO BOX 400 MS F8	NAPERVILLE, IL	60566	USA
GODSALVE	CHRISTOPHER	HERIOT WATT UNIVERSITY	RICCARTON CAMPUS	EDINBURGH		UK
GOODMAN	JOSEPH W	STANFORD UNIVERSITY	DURAND 127	STANFORD, CA	94305	USA
GOODWIN	MARTIN J	PLESSEY RESEARCH	CASWELL TOWCESTER	NORTHANTS	NN128EQ	UK
GOOSSEN	KEITH W	AT&T BELL LABS	ROOM 4B519	HOLMDEL, NJ	07733	USA
GRANESTRAND	PER	ERICSSON TELECOM	S-126 25	STOCKHOLM		SWEDEN
GROTE	JAMES G	USAF	WRDC/WLOT	W-P AFB, OH	95433	USA
HAMILTON	MICHAEL C	BOEING HIGH TECH CENTER	PO BOX 24969 MS 7J-04	SEATTLE, WA	98124	USA
HAMMER	JACOB	DAVID SARNOFF RES CTR	CN5300	PRINCETON, NJ	08543	USA
HANEY	MICHAEL W	BDM CORPORATION	1915 JONES BRANCH DR	MCLEAN, VA	22102	USA
HARVEY	AL	NATL SCIENCE FOUNDATION	1800 G ST, RM 134-36	WASHINGTON, DC	20550	USA
HASHIMOTO	MASASHI	NTT TRANSMISSION SYS LAB	1-2356 TAKE YOKOSUKA	KANAGAWA	238-03	JAPAN
HEALEY	PETER	BRITISH TELECOM RESEARCH	MARTLESHAM HEATH	IPSWICH IP57RE		UK
HENRY	JILL É	AT&T BELL LABS	CRAWFORDS CORNER RD	HOLMDEL, NJ	07733	USA
HESTER	CHARLES S	TELEDYNE BROWN ENGIN	CUMMINGS RESEARCH PARK	HUNTSVILLE, AL	35807	USA
HILL	ALAN M	BRITISH TELECOM RES LABS	IPSWICH	SUFFOLK	IP5 7RE	UK
HINTERLONG	STEVE J	AT&T BELL LABORATORIES	2E 234 200 PARK PLAZA	NAPERVILLE, IL	60566	USA
HINTON	HARVARD S	AT&T BELL LABS	200 PARK PLAZA 2F-235	NAPERVILLE, IL	60566	USA
	NOBUKI	MITSUI PETROCHEMICALS LT	250 PARK AVE, STE 950	NEW YORK, NY	10177	USA
	INOUE	HITACHI LTD	CENT RES, KOKUBUNJI	TOKYO 185		JAPAN
	JOHN H	ROCKWELL SCIENCE CTR	1049 CAMINO DOS RIOS	THOUSAND OAKS, CA	91360	USA
[illegible]	ALAN	AT&T BELL LABS	46514 CRAWFORDS CRNR RD	HOLMDEL, NJ	07733	USA
HU[illegible]	SHIUH	IBM T J WATSON RES CTR	PO BOX 704	YORKTOWN HGTS, NY	10598	USA
ILTAIF	[illegible] A	HERIOT-WATT UNIVERSITY	PHYSICS DEPT	EDINBURGH EH144AS		UK
ISHIHARA	SATOSHI	OITDA	2-7-4 NISHI-SHIMBASHI	MINATO-KU TOKYO	105	JAPAN
ISLAM	MOHAMMED N	AT&T BELL LABS	ROOM 4D 411	HOLMDEL, NJ	07733	USA
JATAR	SHASHANK	BNR	1500 CARLING AVE	OTTAWA ONT	K2K1X5	CANADA
JENKINS	KEITH	USC	PHE 306	LOS ANGELES, CA	90089	USA
JEONG	JAE WOO	ETRI OPTICAL COMM SEC	PO BOX 8, DAEDUG DANGI	CHUNG NAM	302-350	KOREA
JEWELL	JACK	AT&T BELL LABS	46520 CRAWFORDS CRNR RD	HOLMDEL, NJ	07733	USA
JOHNS	JURGEN	AT&T BELL LABS	46510 CRAWFORDS CRNR RD	HOLMDEL, NJ	07733	USA
JOHNSTON	ALAN R	JET PROPULSION LAB		PASADENA, CA	91109	USA
JONECKIS	LANCE	UNIVERSITY OF MARYLAND	4928 COLLEGE AVENUE	COLLEGE PARK, MD	20740	USA
JONES	KEVIN	AT&T BELL LABS	CRAWFORDS CRNR RD 4F323	HOLMDEL, NJ	07733	USA
KATAYAMA	YOSHIFUMI	OPTOELECTRONICS TECH RES	5-5 TOHKODAI	TSUKUBA	300-26	JAPAN
KAWABE	YUTAKA	UNIVERSITY OF ARIZONA	OPTICAL SCIENCES CENTER	TUCSON, AZ	85721	USA
KAWAI	SHIGERU	NEC CORPORATION	1-1 MIYAZAKI 4-CHOME	KAWASAKI-SHI	213	JAPAN
KAZHRINOV	RUDOLF	AT&T BELL LABS	600 MOUNTAIN AVE	MURRAY HILL, NJ	07974	USA
KOBAYASHI	IKUTARO	NTT	3-9-11 MIDORI-CHO	MUSASHINO, TOKYO	180	JAPAN
KOGELNIK	HERWIG	AT&T BELL LABS	RM L215	HOLMDEL, NJ	07733	USA
KOMATSU	KEIRO	NEC CORPORATION	4-1-1 MIYAZAKI, MIYAMAE	KAWASAKI	213	JAPAN
KORN	MANFRED O	UNIV OF STUTTGART	PFAFFENWALDRING 57	STUTTGART	D7000	FED REP GER
KOROTKY	STEVEN K	AT&T BELL LABORATORIES	HO 4F-313	HOLMDEL, NJ	07733	USA
KOSTRZEWSKI	ANDREW	CITY COLLEGE OF NEW YORK	138TH STR, CONVENT AVE	NEW YORK, NY	10031	USA

1989 PHOTONIC SWITCHING
REGISTRATION LIST

LASTNAME	FIRSTNAM	ORGANIZA	ADDRESS1	ADDRESS2	MAILCODE	COUNTRY
KOTELES	EMIL S	GTE LABORATORIES INC	40 SYLVAN ROAD	WALTHAM, MA	02254	USA
KOWALSKY	WOLF GANG K	UNIV OF BRAUNSCHWEIG	SCHLEINITZSTR 23 PB3329	BRAUNSCHWEIG	D-3300	FED REP GER
KRUG	WILLIAM P	BOEING ELECTRONICS	PO BOX 24969 MS 75-27	SEATTLE, WA	98124	USA
KUO	JENN MING	AT&T BELL LABS	600 MOUNTAIN AVENUE	MURRAY HILL, NJ	07974	USA
KUROKAWA	TAKASHI	NTT OPTO-ELECTRONICS LAB	3-1 MORINOSATO WAKAMIYA	ATSUGI, KANAGAWA	243-01	JAPAN
KURPIS	GEDI P	BELL CANADA	1170 TALISA COURT	MISSISSAUGA, ON	L5C 1B2	CANADA
KUZNETSOV	ALEXANDER A	ACAD OF SCIENCES OF USSR	VAVILOV STR 38	MOSCOW	117942	USSR
LARKINS	ERIC C	STANFORD UNIVERSITY	MCCULLOUGH BLDG RM 226	STANFORD, CA	94305	USA
LENTINE	ANTHONY L	AT&T BELL LABS	RM 2F-229 200 PK PLAZA	NAPERVILLE, IL	60566	USA
LI	TINGYE	AT&T BELL LABS	CRAWFORD HILL LAB	HOLMDEL, NJ	07733	USA
LIN	SAMUEL S	AEROSPACE CORPORATION		LOS ANGELES, CA	90009	USA
LINKE	RICHARD A	AT&T BELL LABS	CRAWFORD HILL LAB	HOLMDEL, NJ	07733	USA
LIU	HUA-KUANG	JPL	4800 OAK GROVE DRIVE	PASADENA, CA	91109	USA
LIVESCU	GABRIELA	AT&T BELL LABS	600 MOUNTAIN AVE	MURRAY HILL, NJ	07974	USA
LOHMANN	ADOLF W	PHYSIKALISCHES INST	EIWIN ROMMEL STR 1	ERLANGEN 8520		FED REP GER
MACDONALD	R I	A T R C	4245 97TH STREET	EDMONTON ALTA	T6E 5Y4	CANADA
MACKENZIE	HUGH A	HERIOT-WATT UNIVERSITY	RICCARTON	EDINBURGH EH144AS		UK
MAKOTO	NISHIO	NEC CORPORATION	4-1-1 MIYAZAKI, MIYAMAE	KAWASAKI 213		JAPAN
MARK	JANNIK	TFL TELECOMM RES LAB	LYNGSO ALLE 7	HORSHOLM DK 2970		DENMARK
MARRAKCHI	ABDELLATIF	BELLCORE	331 NEWMAN SPRINGS RD	RED BANK, NJ	07701	USA
MARTINSON	THOMAS	ASCOM TECH	BELPSTRASSE 23	BERN 14	CH3000	SWITZERLAND
MCCORMICK	FREDERICK B	AT&T BELL LABORATORIES	IHP2F231 200 PARK PLAZA	NAPERVILLE, IL	60566	USA
MEEKS	KENT	SANDIA NATIONAL LABS	DIV 5166, PO BOX 5800	ALBUQUERQUE, NM	87185	USA
MELMAN	PAUL	GTE LABORATORIES	40 SYLVAN ROD	WALTHAM, MA	02254	USA
MIDWINTER	JOHN E	UNIV COLLEGE LONDON	TORRINGTON PLACE	LONDON	WC1E 7J	UK
MILLER	DAVID A	AT&T BELL LABS	CRAWFORDS CORNER ROAD	HOLMDEL, NJ	07733	USA
MITSUHITO	SAKAGUCHI M	NEC CORPORATION	4-1-1 MIYAZAKI. MIYAMAE	KAWASAKI 213		JAPAN
MORGAN	ROBERT A	AT&T BELL LABS	600 MOUNTAIN AVENUE	MURRAY HILL, NJ	07974	USA
MORI	MASAHIKO M	ELECTROTECHNICAL LAB	1-1-4 UMEZONO	TSUKUBA		JAPAN
MORK	JESPER	TFL TELECOMM RES LAB	LYNGSO ALLE 7	HORSHOLM DK 2970		DENMARK
MOROZOV	VALENTIN	LEBEDEV INST ACAD OF SCI	LENINSKY PR 53	MOSCOW		USSR
MORRISON	RICK L	AT&T BELL LABORATORIES	2E 234 200 PARK PLAZA	NAPERVILLE, IL	60566	USA
MURDOCCA	MILES J	AT&T BELL LABS	46526 CRAWFORDS CRNR RD	HOLMDEL, NJ	07733	USA
MURPHY	TIMOTHY	AT&T BELL LABS	CRAWFORDS CORNER RD	HOLMDEL, NJ	07733	USA
NAKAGAMI	TAKAKIYO	FUJITSU LABS	1015 KAMIKODANAK	KAWASAKI 211		JAPAN
NOBUYOSHI	TERUMI	OKAYAMA RIKA UNIV	RIDAI CHO 1-1	OKAYAMA SHI 700		JAPAN
NOETHE	STEFFEN	PHYSIKALISCHES INST DER	UNIV HEIDELDERI	HEIDELBERG	06900	FED REP GER
NOLAN	DANIEL A	CORNING GLASS	SP/FR/1/7	CORNING, NY	14830	USA
NORDIN	RONALD A	AT&T BELL LABS	200 PARK PLAZA	NAPERVILLE, IL	60566	
NOVOTNY	ROBERT A	AT&T BELL LABORATORIES	200 PARK PLAZA	NAPERVILLE, IL	60566	USA
ODAGAWA	TETSUFUMI	FUJITSU LABS LTD	10-1 MORINOSATO-WAKAMIY	ATSUGI	243-01	JAPAN
OHLANDER	ULF R	INSTITUTE OF OPTICAL RES	LINDSTEDTSV 24	STOCKHOLM	210099	SWEDEN
OKAMOTO	HIROSHI	FURUKAWA ELEC CO	2-4-3 OKANO NISHI-KU	YOKOHAMA 220		JAPAN
OREN	MOSHE	E I DUPONT DENEMOURS CO	ENG PHYS LAB PDB 80357	WILMINGTON, DE	19880	USA
ORSIC	MILO	AT&T BELL LABORATORIES	200 PARK PLACE	NAPERVILLE, IL	87185	USA
PANKOVE	JACQUES I	UNIVERSITY OF COLORADO	OPTOELECTRONIC COMP SYS	BOULDER, CO	80309	USA
PARK	SEUNG HAN	UNIVERSITY OF PITTSBURGH	348 BENEDUM HALL	PITTSBURGH, PA	15261	USA
PAULIAT	GILLES	INST D'OPTIQUE CNRS	BAT 503	ORSAY CEDEX BP43	91 406	FRANCE
PAYNE	WILLIAM A	AT&T BELL LABORATORIES	200 PARK PLAZA, 2F-247	NAPERVILLE, IL	60566	USA
PEDOROV	WIATCHESLAB	ACAD OF SCIENCES OF USSR	COMP CTR OF COLL USE	MOSCOW		USSR
PEZESHKI	BARDIA	STANFORD UNIVERSITY	MCCULLOUGH BLDG RM 226	STANFORD, CA	94305	USA
PHILLIPS	ALFRED	IBM	EAST FISHKILL ZIP 47A	HOPEWELL JCT, NY	12533	USA

1989 PHOTONIC SWITCHING
REGISTRATION LIST

LASTNAME	FIRSTNAM	ORGANIZA	ADDRESS1	ADDRESS2	MAILCODE	COUNTRY
PILLOFF	HERSCH	ONR	CODE 11260 800 N QUINCY	ARLINGTON, VA	22217	USA
PRISE	MICHAEL E	AT&T BELL LABS	46526 CRAWFORDS CRNR RD	HOLMDEL, NJ	07733	USA
PRUCNAL	PAUL	PRINCETON UNIVERSITY	DEPT OF ELECTRICAL ENG	PRINCETON, NJ	08544	USA
REIHLEN	ECKART H	UNIVERISITY OF UTAH	MATERIALS SCI DEPT	SALT LAKE CTY, UT	84112	USA
REJMAN-GREENE	MAREK A	BRITISH TELECOM RES LABS	RT233 MARTLESHAM HEATH	IPSWICH SUFFOLK	IP5 7RE	USA
REN	RIUSHI	OHIO STATE UNIVERSITY	2015 NEIL AVE ECE DEPT	COLUMBUS, OH	43210	USA
RONALDSON	DAVID	HERIOT WATT UNIVERSITY	RICCARTON CAMPUS, RIC	EDINBURGH		UK
ROOSEN	GERALD	INST D OPTIQUE CNRS	BAT 503	BP43 ORSAY CEDEX	91406	FRANCE
SAHLEN	OLOF	INST OF OPTICAL RESEARCH	ROYAL INST OF TECH	STOCKHOLM S-100	44	SWEDEN
SANTORO	MARIO A	AT&T BELL LABORATORIES	CRAWFORDS CORNER 4F535	HOLMDEL, NJ	07733	USA
SARUWATARI	MASATOSHI	NTT TRANSMISSION SYS LAB	TAKE 1-2356	YOKOSUKA-SHI	238-03	JAPAN
SAWCHUK	ALEXANDER A	UNIV OF SOUTHERN CALIF	MC 0272	LOS ANGELES, CA	90089	USA
SCHLOSSBERG	HOWARD	AFOSR	BLDG 410 BOLLING AFB	WASHINGTON, DC	20332	USA
SCHWARZ	ROBERT	HERCULES AEROSPACE	HERCULES PLAZA	WILMINGTON, DE	19894	USA
SCHWEIZER	HEINZ	SEL RES CTR STUTTGART	LORENZSTR 10	STUTTGART	BW7000	FED REP GER
SELFRIDGE	RICHARD	BYU	459 CB	PROVO, UT	84602	USA
SETCHELLI	ROBERT E	SANDIA NATIONAL LABS	DIV 5166 PO BOX 5800	ALBUQUERQUE, NM	87185	USA
SHIGEFUMI	MASUDA	FUJITSU LABS LTD	1015 KAMIKODANAKA	KAWASAKI 211		JAPAN
SHIGERU	KAWAI	NEC CORPORATION	1-1 MIYAZAKI 4-CHOME	KAWASAKI-SHI 213		JAPAN
SHIMOE	TOSHIO T	FUJITSU	1015 KAMIKODANKA	KAWASAKI NAKAHAMA		JAPAN
SHIN	SANG-YUNG	KOREA ADV INST SCI TECH	PO BOX 150 CHEONGRYANG	SEOUL		KOREA
SHUMATE	PAUL W	BELLCORE	445 SOUTH STREET	MORRISTOWN, NJ	07960	USA
SIEWERT	RON O	MITRE CORP	120 BURLINGTON ROAD	BEDFORD, MA	01730	USA
SILBERBERG	YARON	BELLCORE	331 NEWMAN SPRINGS RD	RED BANK, NJ	07701	USA
SIZER	TOD	AT&T BELL LABS	46530 CRAWFORDS CRNR RD	HOLMDEL, NJ	07733	USA
SMITH	PETER W	BELLCORE		RED BANK, NJ	07701	USA
SNOWDON	JOHN F	HERIOT-WATT UNIVERSITY	RICCARTON	EDINBURGH EH144AS		UK
SOCCOLICH	CARL E	AT&T BELL LABS	CRAWFORDS CORNER ROAD	HOLMDEL, NJ	07733	USA
SOILA	RISTO O	NOKIA TELECOMMUNICATIONS	PO BOX 33	ESPOO SF	02601	FINLAND
SPITZ	ERICH	THOMSON	173 BOULEVARD HAUSSMANN	PARIS FR	75000	FRANCE
STEPHENS	WILLIAM E	BELLCORE	445 SOUTH ST MRF 2L-133	MORRISTOWN, NJ	07960	USA
STEVENS	PETER J	UNIV COLLEGE LONDON	DEPT OF EE, TORRING. PL	LONDON	WC1E7JE	UK
SU	SHING FONG	GTE LABORATORIES	40 SYLVAN ROAD	WALTHAM, MA	02254	USA
SUSSMANN	RICARDO S	AMOCO TECHNOLOGY CO	PO BOX 400 MS F4	NAPERVILLE, IL	60566	USA
SUYAMA	TAKAHIRO	SHARP CORP	CENTRAL RESEARCH LABS	TENRI NARA	632	JAPAN
SYUJI	SUZUKI	NEC CORPORATION	4-1-1 MIYAZAKI, MIYAMAE	KAWASAKI 213		JAPAN
TANIDA	JUN	OSAKA UNIVERSITY	2-1 YAMADAOKA	SUITA 565		JAPAN
TAYLOR	BRAD K	E I DUPONT DE NEMOURS	PO BOX 80357	WILMINGTON, DE	19880	USA
TAYLOR	MICHAEL G	UNIV COLLEGE LONDON	DEPT OF EE, TORRING. PL	LONDON, ENGLAND	WC1E7JE	UK
TAYLOR	GEOFF	AT&T BELL LABS	CRAWFORDS CORNER RD	HOLMDEL, NJ	07733	USA
THALMANN	RUEDI	UNIVERSITY OF NEUCHATEL	INST DE MICROTECHNIQUE	NEUCHATEL CH2000		SWITZERLAND
THIENPONT	HUGO	VRIJE UNIVERSIT. BRUSSEL	PLEINLAAN 2	BRUSSELS	1050	BELGIUM
THOMPSON	RICHARD A	AT&T BELL LABORATORIES	600 MOUNTAIN AVENUE	MURRAY HILL, NJ	07974	USA
THYLEN	LARS	ERICSSON TELECOM	S-126 25	STOCKHOLM		SWEDEN
TICKNOR	TONY	LOCKHEED	10215 EMPIRE AVENUE	CUPERTINO, CA	95014	USA
TOMBLING	CRAIG C	UNIV COLLEGE LONDON	DEPT OF EE, TORRING. PL	LONDON, ENGLAND	WC1E7JE	UK
TOOLEY	FRANK A	HERIOT-WATT UNIVERSITY	RICCARTON	EDINBURGH EH144AS		UK
TORCHIN	LUCIEN	LABS DE MARCOUSSIS	ROUTE DE NOZAY	MARCOUSSIS	91460	USA
TROMBORG	BJARNE	TFL TELECOMM RES LAB	LYNGSO ALLE 7	HORSHOLM DK 2970		DENMARK
TSANG	DEAN Z	MIT LINCOLN LAB	PO BOX 73	LEXINGTON, MA	02173	USA
TUCKER	RODNEY	AT&T BELL LABS	ROOM HOH-L137	HOLMDEL, NJ	07733	USA
UKACHI	TAKASHI	CORNELL UNIVERSITY	189 CLARK HALL	ITHACA, NY	14853	USA

1987 PHOTONIC SWITCHING
REGISTRATION LIST

LASTNAME	FIRSTNAM	ORGANIZA	ADDRESS1	ADDRESS2	MAILCODE	COUNTRY
VAN ECK	TIMOTHY	LOCKHEED	3251 HANOVER ST	PALO ALTO, CA	94306	USA
VEACH	ROBERT S	AT&T BELL LABS	200 PARK PLAZA	NAPERVILLE, IL	60566	USA
VERBER	CARL M	GEORGIA TECH	SCHOOL OF ELEC ENG	ATLANTA, GA	30332	USA
VESELKA	JOHN	AT&T BELL LABS	CRAWFORDS CORNER RD	HOLMDEL, NJ	07733	USA
VOUNCKX	ROGER	VRIJE UNIVERSIT. BRUSSEL	PLEINLAAN 2	BRUSSELS	1050	BELGIUM
WAGNER	KELVIN H	UNIV OF COLORADO BOULDER	DEPT OF ECE BOX 425	BOULDER, CO	80309	USA
WALKER	SUE	AT&T BELL LABS	46532 CRAWFORDS CRNR RD	HOLMDEL, NJ	07733	USA
WALTER	HERBERT	DEUTSCHE BUNDESPOST FTZ	PO BOX 5000	DARMSTADT D-6100		FED REP GER
WANG	JIANMING	UNIV OF SO CALIFORNIA	SIPI, DEPT OF EE	LOS ANGELES, CA	90089	USA
WATKINS	LAURENCE S	AT&T BELL LABORATORIES	PO BOX 900	PRINCETON, NJ	08560	USA
WATSON	TOM	AT&T BELL LABORATORIES	8392C ROSWELL RD NE	ATLANTA, GA	30350	USA
WEINER	ANDREW	BELLCORE	331 NEWMAN SPRINGS RD	RED BANK, NJ	07701	USA
WEISBUCH	CLAUDE C	THOMSON CSF	LCR BP10	91401 ORSAY		FRANCE
WEST	LAWRENCE C	AT&T BELL LABS	46518 CRAWFORDS CRNR RD	HOLMDEL, NJ	07733	USA
WHITE	IAN H	CAMBRIDGE UNIV	ENG DEPT TRUMPINGTON ST	CAMBRIDGE, ENG	CB2 1PZ	UK
WHITEHEAD	NIGEL	BRITISH TELECOM RESEARCH	MARTLESHAM HEATH	IPSWICH SUFFOLK	IP124QR	UK
WHITEHEAD	MARK	UNIV COLLEGE LONDON	DEPT OF EE, TORRING. PL	LONDON, ENGLAND	WC1E7JE	UK
WILLIAMSON	RICHARD C	MIT LINCOLN LAB	PO BOX 73	LEXINGTON, MA	02173	USA
WOLFF	ULRICH W	SIEMENS AG	OTTO-HAHN-RING 6	83 MUENCHEN	D8000	FED REP GER
YAMABAYASHI	YOSHIAKI	NTT TRANSMISSION SYS LAB	TAKE 1-2356	YOKOSUKA-SHI 238	87185	JAPAN
YAMAKOSHI	SHIGENOBU	FUJITSU LABS LTD	10-1 MORINOSATO	WAKAMIYA ATSUGI	243-01	JAPAN
YAMANISHI	MASAMICHI	HIROSHIMA UNIV	DEPT OF PHYS ELEC	HIGASHI-HIROSHIMA	724	JAPAN
YAN	RAN HONG	U C SANTA BARBARA	DEPT ECE	SANTA BARBARA, CA	93106	USA
YASUI	TADAHIKO T	NTT TELECOM	3-9-11 MIDORICHO	MUSAHINO, TOKYO	180	JAPAN
YASUO	KAN	HIROSHIMA UNIVERSITY	SHITAMI SAIJYO	HIGASHIHIROSHIMA	724	JAPAN
YOKOYAMA	HIROYUKI	NEC CORPORATION	4-1-1 MIYAZAKI, MIYAMAE	KAWASAKI 213		JAPAN
YU	JEFFREY JW	JET PROPULSION LAB	4800 OAK GROVE DRIVE	PASADENA, CA	91109	USA
ZIARI	MEHRDAD	UNIV OF SOUTHERN CALF	UNIVERSITY PARK	LOS ANGELES, CA	90254	USA
ZUCKER	JANE	AT&T BELL LABS	RM 4F 319 BELL LABS	HOLMDEL, NJ	07733	USA

TOTAL ATTENDANCE = 234

Unclassified

SECURITY CLASSIFICATION OF THIS PAGE

REPORT DOCUMENTATION PAGE

1a. REPORT SECURITY CLASSIFICATION unclassified	1b. RESTRICTIVE MARKINGS n/a
2a. SECURITY CLASSIFICATION AUTHORITY n/a	3. DISTRIBUTION / AVAILABILITY OF REPORT approved for public release distribution unlimited
2b. DECLASSIFICATION / DOWNGRADING SCHEDULE n/a	
4 PERFORMING ORGANIZATION REPORT NUMBER(S)	5. MONITORING ORGANIZATION REPORT NUMBER(S) AFOSR-TR- 90-0415
6a. NAME OF PERFORMING ORGANIZATION Optical Society of America 6b. OFFICE SYMBOL (If applicable)	7a. NAME OF MONITORING ORGANIZATION Air Force Office of Scientific Research
6c. ADDRESS (City, State, and ZIP Code) 1816 Jefferson Place, NW Washington, DC 20036	7b ADDRESS (City, State, and ZIP Code) Building 410 Bolling Air Force Base Washington, DC 20332
8a. NAME OF FUNDING / SPONSORING ORGANIZATION Same as 7a 8b. OFFICE SYMBOL (If applicable) NP	9 PROCUREMENT INSTRUMENT IDENTIFICATION NUMBER AFOSR-89-0266
8c. ADDRESS (City, State, and ZIP Code) Same as 7b	10. SOURCE OF FUNDING NUMBERS PROGRAM ELEMENT NO: 61102F; PROJECT NO.: 2301; TASK NO.: A1; WORK UNIT ACCESSION NO.
11 TITLE (Include Security Classification) (U) PHOTONIC SWITCHING. Technical Digest.	
12. PERSONAL AUTHOR(S)	
13a. TYPE OF REPORT Final 13b. TIME COVERED FROM 02/01/89 TO 31 Jan 90	14. DATE OF REPORT (Year, Month, Day) 90/01/31 15. PAGE COUNT
16 SUPPLEMENTARY NOTATION 1989 Optical Society of America Photonic Science Topical Meeting Series	

17 COSATI CODES			18 SUBJECT TERMS (Continue on reverse if necessary and identify by block number)
FIELD	GROUP	SUB-GROUP	

19. ABSTRACT (Continue on reverse if necessary and identify by block number)

The Optical Society of America sponsors topical meeting on subjects in which many rapid advances are taking place so that contributors to the field may interchange ideas to their mutual benefit. The Photonic Science Topical Meeting Series included the following subjects: a) Nonlinear Guided Wave Phenomena: Physics and Applications, b) Microphysics of Surfaces, Beams and Adsorbates, c) Optical Computing, d) Photonic Switching, e) Quantum Wells for Optics and Optoelectronics, f) Picosecond Electronics and Optoelectronics, g) High Intensity Laser Radiation on Atoms and Surfaces, h) Quantum Limited Imaging and Information Processing, and i) Signal Recovery and Synthesis.

20. DISTRIBUTION / AVAILABILITY OF ABSTRACT ☒ UNCLASSIFIED/UNLIMITED ☒ SAME AS RPT. ☒ DTIC USERS	21. ABSTRACT SECURITY CLASSIFICATION unclassified
22a. NAME OF RESPONSIBLE INDIVIDUAL Dr Howard R. Schlossberg	22b. TELEPHONE (Include Area Code) 202/767-4906 22c. OFFICE SYMBOL NP

DD FORM 1473, 84 MAR 83 APR edition may be used until exhausted. All other editions are obsolete.

SECURITY CLASSIFICATION OF THIS PAGE

UNCLASSIFIED

90 05 10 143

PHOTONIC SWITCHING

CONFERENCE EDITION

Summaries of papers presented at the Photonic Switching Topical Meeting

March 1-3, 1989

Salt Lake City, Utah

PRICE-$69.00 per Optical Society of America, 1816 Jefferson Place, NW Washington, DC 20036
TELECON 5/10/90 VG

Cosponsored by

Optical Society of America
Air Force Office of Scientific Research
National Science Foundation

Optical Society of America
1816 Jefferson Place, N.W.
Washington, D.C. 20036
(202) 223-8130

Articles in this publication may be cited in other publications. In order to facilitate access to the original publication source, the following form for the citation is suggested:

Name of Author(s), Title of Paper, Photonic Switching, Technical Digest, (Optical Society of America, Washington, D.C. 1989) pp. xx-xx.

ISBN Number
Conference Edition 1-55752-082-8 (softcover)

Library of Congress Catalog Card Number
Conference Edition 88-62710

This material is based upon work supported by the National Science Foundation under Grant No. EET-8901312. The Government has certain rights in this material Any opinions, findings, and conclusions or recommendations expressed in this material are those of the author(s) and do not necessarily reflect the views of the National Science Foundation.

TABLE OF CONTENTS

PROGRAM v

WA PLENARY SESSION 1

WAA JOINT PHOTONIC SWITCHING AND OPTICAL COMPUTING PLENARY SESSION 9

ThA DEVICES FOR TIME-DIVISION SWITCHING SYSTEMS 17

ThB POSTER SESSION: 1 31

ThC FREE-SPACE SYSTEMS 49

ThD FREE-SPACE DEVICES 65

ThE MULTI-DIMENSIONAL SWITCHING SYSTEMS 85

FA PACKET SWITCHING SYSTEMS 105

FB POSTER SESSION: 2 119

FC TIME-DIVISION SWITCHING SYSTEMS 133

FD SEMICONDUCTOR DEVICES 149

FE SPACE-DIVISION SWITCHING 167

KEY TO AUTHORS, PRESIDERS AND PAPERS 187

TUESDAY, FEBRUARY 28, 1989

SALON FOYER

6:00 PM-9:00 PM REGISTRATION/RECEPTION

WEDNESDAY, MARCH 1, 1989

SALON D

7:00 AM-8:30 AM BUFFET BREAKFAST

SALON FOYER

7:00 AM-5:30 PM REGISTRATION/SPEAKER CHECKIN

SALON G

8:30 AM-8:45 AM
OPENING REMARKS
Peter W. Smith, *Bellcore*

8:45 AM-12:15 PM
WA PLENARY SESSION
Peter W. Smith, *Bellcore, Presider*

8:45 AM (Plenary paper)
WA1 Broadband Electronic Switching, J. E. Berthold, *Bellcore.* Electronic switching research is rapidly advancing channel bandwidth, number of channels possible on a switch chip, and the rate of channel connection changes. (p. 2)

9:30 AM (Plenary paper)
WA2 Photonic Switching Systems Experiments in the European RACE Program. Nigel Whitehead, *British Telecom Research Laboratories, U. K.;* Nick Parsons, *Marconi Research Centre, U. K.;* Paul Vogel, *ASCOM Central Dept., Switzerland;* Goren Wicklund, *ELLEMTEL, Sweden.* Some photonic switching systems experiments are described which exploit space, wavelength and time-division techniques under development within the European RACE program. (p. 3)

SALON D

10:15 AM-10:45 AM COFFEE BREAK

WEDNESDAY, MARCH 1, 1989—*Continued*

SALON G

10:45 AM (Plenary paper)
WA3 Devices for Photonic Switching, Lars Thylen, *Ericsson Telecom., Sweden.* State-of-the-art devices for photonic switching are reviewed emphasizing the time and space switching areas. (p. 6)

11:30 AM (Plenary paper)
WA4 A New Direction in Photonic Switching, Paul R. Prucnal, *Princeton U.* Limitations in conventional photonic switching architectures, including time division, wavelength division, and space division, are reviewed. A novel "shared-medium switch" is proposed that permits all signals to share a single high-bandwidth transmission path. (p. 7)

12:15 PM-2:00 PM LUNCH BREAK

SALON F

2:00 PM-5:30 PM
WAA JOINT PHOTONIC SWITCHING AND OPTICAL COMPUTING PLENARY SESSION
Joseph W. Goodman, *Stanford University, Co-presider*
John E. Midwinter, *University College London, U.K., Co-presider*

2:00 PM (Plenary paper)
WAA1 OEIC Technology for Photonic Switching, S. Yamakoshi, *Fujitsu Laboratories, Ltd., Japan.* OEIC technology promises to construct new optical systems such as photonic switching, routing and other optical processing operations. The state-of-the-art and future prospects of OEICs for photonic switching are discussed. (p. 10)

2:45 PM (Plenary paper)
WAA2 Quantum Well Devices for Optical Computing and Switching, David A. B. Miller, *AT&T Bell Laboratories.* Quantum well electroabsorptive self-electrooptic-effect devices are attractive for 2-D arrays for switching and processing. Novel integrated configurations and progress toward arrays are summarized. (p. 11)

SALON D

3:30 PM-4:00 PM COFFEE BREAK

SALON F

4:00 PM (Plenary paper)
WAA3 Switching in an Optical Interconnect Environment, Joseph W. Goodman, *Stanford U.* The requirements placed on switching in an optical interconnect environment differ significantly from those present in long distance telecommunications, allowing new approaches to switch realization. (p. 14)

4:45 PM (Plenary paper)
WAA4 Relationship Between Photonic Switching and Optical Computing, H. Scott Hinton, *AT&T Bell Laboratories.* An outline of the relationship between the hardware requirements of photonic switching and optical computing systems, is presented. (p. 16)

SALON D

6:00 PM-7:30 PM CONFERENCE RECEPTION

SALON F

8:00 PM-10:00 PM
PANEL DISCUSSION "Impedimenta"

Photonic switching is advancing rapidly. When will it be possible to make use of these advances and what are the problems that must first be solved? A panel discussion to sense the current status will be held after the reception. The panel will consider the question:

What are the impediments to practical photonic switching systems?

Audience participation will be encouraged. Comments on matters such as signal processing, network control, packaging, multidimensional extension of switches, and opinions on devices, systems, services and potential uses are sought.

SALON D

7:00 AM-8:30 AM BUFFET BREAKFAST

SALON FOYER

7:30 AM-5:30 PM REGISTRATION/SPEAKER CHECKIN

SALON E

8:30 AM-9:45 AM
ThA DEVICES FOR TIME-DIVISION SWITCHING SYSTEMS
T. Nakagami, *Fujitsu Laboratories, Ltd., Japan, Presider*

8:30 AM (Invited Paper)
ThA1 Encoding and Decoding of Femtosecond Pulses for Code-Division Multiple Access, A. M. Weiner, J. A. Salehi, J. P. Heritage, M. Stern, *Bellcore.* We demonstrate encoding and decoding of femtosecond optical pulses, and propose and analyze a code-division multiple access communications system based on such encoding and decoding. (p. 18)

9:00 AM
ThA2 Velocity Matched Ti:LiNbO$_3$ Switch for 16-Gbit/s Optical Time-Division Multiplexing, J. J. Veselka, Steven K. Korotky, *AT&T Bell Laboratories.* We demonstrate a Ti:LiNbO$_3$ switch at 1.3-μm wavelength that is optimized for 8-GHz operation using velocity matching via periodic phase reversal. Crosstalk values of -16 dB at 8 GHz were achieved for both switch states with a low drive power of 234 mW. (p. 21)

9:15 AM
ThA3 Improved Operation of a Two-Core Fiber All-Optical Switch Using Femtosecond Square Optical Pulses, Y. Silberberg, A. M. Weiner, H. Fouckhardt, D. E. Leaird, M. A. Saifi, M. J. Andrejco, P. W. Smith, *Bellcore.* We measure all-optical switching in a dual-core fiber nonlinear coupler. By using femtosecond square pulses, we obtain enhanced power transfer and sharp switching transitions. (p. 24)

9:30 AM
ThA4 Novel All-Optical Kerr Amplification with Wavelength Switching in a Single-Mode Birefringent Fiber, A. S. Davison, I. H. White, *Cambridge U., U. K.* A new form of all-optical amplification is demonstrated where a singal is amplified and switched to the pump wavelength, using the high speed Kerr effect. (p. 27)

SALON D

9:45 AM–10:30 AM
ThB POSTER SESSION
Refreshments served

ThB1 Novel Optically Bistable Optoelectronic Device for Infrared Signal Processing, H. A. MacKenzie, A. Ilaif, J. Hughes, J. J. Hunter, D. Ronaldson, *Heriot-Watt U., U. K.* A new InSb cw bistable device has been developed which can be switched either optically or electrically and which can communicate interactively with conventional computing systems. (p. 32)

ThB2 Optical Bistable Switch Based on Self-Focusing in an Artificial Kerr medium, N. P. Walker, *Kings College London, U. K.;* D. R. Drury, M. A. Fiddy, *U. Lowell.* A new design is proposed for an optically bistable device based on the self-focusing properties of light using an artificial Kerr medium. (p. 35)

ThB3 Time Response of a Crossed Resonator, B. A. Capron, M. W. Derstine, D. A. Holm, *Boeing Electronics High Technology Center.* We present theoretical results showing the time response of an optical switch consisting of two crossed nonlinear Fabry-Perot etalons for both pulsed and sinusoidal inputs. (p. 37)

ThB4 A pnpn Light-Emitting Optical Switch, J. L. Pankove, R. Hayes, A. Majerfeld, M. Hanna, E. G. Oh, D. M. Szmyd, D. Suda, *U. Colorado at Boulder;* S. Asher, R. Matson, *Solar Energy Research Institute;* D. J. Arent, G. Borghs, *IMEC, Belgium;* M. G. Harvey, *David Sarnoff Research Center.* This pnpn photo-thyristor is a threshold device capable of logic functions and optical gain. On-Off response times of 10 ns have been obtained. (p. 40)

ThB5 Photonic Switching in InGaAsP Dynamic Memory Devices, W. Kowalsky, M. Port, K. J. Ebeling, *Braunschweig Technical U., F. R. Germany.* The dynamic memory characteristics of InGaAsP photonic switching devices are investigated. An on-off ratio of 5.5:1 and hold times greater than 10 ns enable clocked data processing. (p. 44)

SALON E

10:30 AM–12:00 M
ThC FREE-SPACE SYSTEMS
A. L. Lentine, *AT&T Bell Laboratories, Presider*

10:30 AM (Invited paper)
ThC1 Free-Space Optical Systems for Switching, Interconnections, and Computing, B. Keith Jenkins, *U. Southern California.* The use of free-space optical systems for photonic switching, optical and hybrid computing is discussed, including architectural tradeoffs and comparisons with electronics. (p. 50)

THURSDAY, MARCH 2, 1989—*Continued*

11:00 AM
ThC2 Optical Interconnection Networks Employing Multiplexed Crosspoints, P. Healey, *British Telecom Research Laboratories, U. K.* New image switching networks employing spatially multiplexed crosspoints and birefringent interconnects are described, which simultaneously minimize both the crosspoint count and the switch control complexity. (p. 51)

11:15 AM
ThC3 Spatial Extension of Multistage Interconnection Networks, Josef Gigimayr, *Heinrich Hertz Institute, F. R. Germany.* Three questions are discussed for 3-D multistage interconnection networks: 1) most appropriate regular interconnection pattern, 2) number of stages, and 3) optimal size of the switching modules. (p. 54)

11:30 AM
ThC4 Nonblocking Photonic Space Switch Architectures Utilizing Acoustooptic Deflectors, P. C. Huang, W. E. Stephens, S. S. Cheng, T. C. Banwell, L. A. Reith, *Bellcore.* The unique IO characteristics of AO deflectors makes possible the construction of large switches with minimal insertion loss and crosstalk. This was confirmed by an experimental 4 × 4 switch. (p. 58)

11:45 AM
ThC5 All-Optical Shift Register Using Symmetric Self-Electrooptic Effect Devices, F. B. McCormick, A. L. Lentine, L. M. F. Chirovsky, L. A. D'Asaro, *AT&T Bell Laboratories.* We demonstrate an all-optic shift register using a single reflective symmetric self-electrooptic effect (S-SEED) device array, using techniques that are extensible to large arrays of devices. (p. 61)

12:00 M–1:30 PM LUNCH BREAK

SALON E

1:30 PM–3:00 PM
ThD FREE-SPACE DEVICES
David A. B. Miller, *AT&T Bell Laboratories, Presider*

1:30 PM
ThD1 Exciton-Enhanced Photonic Switching in GaAs/AlGaAs Fabry-Perot Resonators, W. Kowalsky, T. Hackbarth, K. J. Ebeling, *Braunschweig Technical U., F. R. Germany.* Exciton-enhanced photonic switching in GaAs/AlGaAs Fabry-Perot resonators is demonstrated. Switching contrast of 10:1 is achieved at 1-mW control power. (p. 66)

1:45 PM
ThD2 Transverse Modes and Waveguide Dispersion in Submicron GaAs/AlAs Microresonators, J. L. Jewell, S. L. McCall, A. C. Gossard, J. H. English, *AT&T Bell Laboratories;* A. Scherer, *Bellcore.* GaAs/AlAs microresonators ~0.5–1.5 μm in diameter show well-defined transverse modes and waveguide dispersion. Smaller diameter devices seem to be nearly single-mode. (p. 69)

2:00 PM
ThD3 InGaAs/InP MQW 3 × 3 Planar Spatial Light Modulator Grown by Gas-Source Molecular Beam Epitaxy, M. A. Z. Rejman-Greene, E. G. Scott, E. McGoldrick, *British Telecom Research Laboratories, U. K.* Fabrication details and measurements are presented on the first, we believe, planar, 2-D semiconductor optical modulator arrays using InGaAs/InP MQW layers. (p. 72)

2:15 PM
ThD4 Batch Fabricated Symmetric Self-Electrooptic Effect Devices, L. M. F. Chirovsky, L. A. D'Asaro, C. W. Tu, A. L. Lentine, G. D. Boyd, David A. B. Miller, *AT&T Bell Laboratories.* A design of symmetric self-electrooptic effect devices with an internal dielectric mirror has enabled fabrication of arrays of devices suitable for digital optics system tests. (p. 75)

2:30 PM
ThD5 Diffusion-Assisted Optical Switch: A New Optical Logic Device, Theodore Sizer II, Gabriela Livescu, Jack Cunningham, David A. B. Miller, *AT&T Bell Laboratories.* Theoretical and experimental results from a new optical logic device are presented which indicate that it has speeds of many GHz, sub-100 femtojoule energies, and is easily fabricated. (p. 78)

2:45 PM
ThD6 Optical Back Plane Interconnect Technology for Computers, J. M. Hammer, Sr., *David Sarnoff Research Center;* H. D. Hendricks, *NASA Langley Research Center.* We describe and analyze a novel approach for optically interconnecting any row of one $M \times N$ back plane array to any row of a second array. (p. 81)

SALON D

3:00 PM–3:30 PM COFFEE BREAK

THURSDAY, MARCH 2, 1989—*Continued*

SALON E

3:30 PM–5:15 PM
ThE MULTI-DIMENSIONAL SWITCHING SYSTEMS
Lars Thylen, *Ericsson Telecom, Sweden, Presider*

3:30 PM (Invited paper)
ThE1 Dense WDM Networks and Applications, Charles A. Brackett, *Bellcore.* Recent progress in dense wavelength division multiplexing and its use in new network architectures is reviewed, including wavelength division switching and local distribution. (p. 86)

4:00 PM
ThE2 High-Speed Hitless Switching Using Ti:$LiNbO_3$, J. R. Erickson, R. F. Huisman, K. D. Major, R. A. Nordin, R. S. Veach, *AT&T Bell Laboratories.* Using a combination of high-speed bank switches and dual switching fabrics, we demonstrate the feasibility of high-speed time-multiplexed switching with guided-wave photonics. (p. 89)

4:15 PM
ThE3 Experimental Modular Switching System with a Time-Multiplexed Photonic Center-Stage, R. A. Thompson, R. V. Anderson, J. V. Camlet, P. P. Giordano, *AT&T Bell Laboratories.* An experimental time-space-time switching system has been constructed. Multiuser switching modules are interconnected by a lithium niobate switching network, under distributed control. Channels with high data rates are mixed with conventional channels. (p. 92)

4:30 PM
ThE4 Extendible Optical Interconnection Network, D. W. Smith, P. Healey, S. A. Cassidy, *British Telecom Research Laboratories, U. K.* A new bus oriented, hierarchical multiple access, optical interconnection network is presented. It offers extendibility and huge capacity by combining numerous degrees of switching freedom. (p. 95)

4:45 PM
ThE5 Experiment with Photonic Wavelength-Division and Time-Division Hybrid Switching, M. Nishio, S. Suzuki, N. Shimosaka, T. Numai, T. Miyakawa, M. Fujiwara, M. Itoh, *NEC Corp., Japan.* Fast wavelength tuning of a filter and laser diode over four of eight wavelengths is confirmed. It shows eight-wavelength-division and four-time-division hybrid switching capability. (p. 98)

5:00 PM
ThE6 Passive Spectral Commutator and the Architectures of Usual and Optical Networks, E. M. Dianov, A. A. Kuznetsov, S. M. Nefjodov, G. G. Voevodkin, *Academy of Sciences of the U.S.S.R.* A passive spectral commutator is proposed and realized. In optical net abonent changes the wavelength (mutual address), in usual net tunable lasers before commutator are necessary. (p. 101)

5:15 PM–8:00 PM DINNER BREAK

SALON E

8:00 PM–9:00 PM
POSTDEADLINE PAPER SESSION
H. S. Hinton, *AT&T Bell Laboratories, Presider*

SALON D

7:00 AM–8:30 AM BUFFET BREAKFAST

SALON FOYER

7:30 AM–5:30 PM REGISTRATION/SPEAKER CHECKIN

SALON E

8:30 AM–9:45 AM
FA PACKET SWITCHING SYSTEMS
Paul R. Prucnal, *Princeton University, Presider*

8:30 AM (Invited paper)
FA1 Optical Processing in Photonic Switching Systems, Ikutaro Kobayashi, *NTT Communication Switching Laboratories, Japan.* The advanced features of optical technologies will trigger further evolution in communication switching systems. This evolution will, in turn, stimulate the evolution of optical processing. (p. 106)

9:00 AM
FA2 Optical Technology in Fast Packet Switching, Paola Cinato, Alfredo de Bosio, *Turin CSELT, Italy.* An electro-optical fast packet switching mode model for the public telecommunication network is proposed, and the main optical switching matrix requirements are investigated. (p. 109)

9:15 AM
FA3 Photonic Packet Switch Using Optical Buffer Memories, S. Suzuki, H. Suzuki, K. Kasahara, M. Fujiwara, T. Takeuchi, *NEC Corp., Japan.* Extremely high-speed photonic packet switches, using wavelength-division multiplexed fiber loop buffer memories or a massively parallel interconnected optical memory 2-D array, are proposed. (p. 112)

9:30 AM
FA4 InP Based 4 × 4 Optical Switch Module and Its Application to ATM Switching, H. Inoue, T. Kato, Y. Sasaki, K. Ishida, K. Mizuishi, E. Amada, *Hitachi, Ltd., Japan;* S. Kashimura, *Hitachi Cable, Ltd., Japan.* The module hosting a 4 × 4 polarization independent optical switch with an original fiber attachment was fabricated and tested. Its use in ATM switching is proposed. (p. 115)

SALON D

9:45 AM-10:30 AM
FB POSTER SESSION
Refreshments served

FB1 Optical Parallel Processor for Control of Photonic Switching Networks, Daniel J. Blumenthal, *U. Pennsylvania.* A parallel optical processing architecture for the control of photonic switching networks is proposed. The high space-bandwidth product of bulk optics and holographic optical elements improves throughput and delay while concurrent processing allows simultaneous control of switch cross-points. (p. 120)

FB2 Characterization of High-Speed Electrodes for LINbO$_3$ Electrooptic Switch Arrays, R. A. Nordin, M. T. Ratajack, *AT&T Bell Laboratories.* High-speed lossy electrodes for electrooptic switch arrays display superior performance when unterminated, compared with properly terminated electrodes, thus relieving routing and power constraints. (p. 123)

FB3 All-Optical Signal Routing Using Bistable Interferometers, G. S. Buller, S. D. Smith, A. C. Walker, *Heriot-Watt U., U. K.* An examination of the potential use of bistable interferometers in signal routing is presented. Device contrast, switch networks, and wavelength routing are discussed. (p. 126)

FB4 Self-Routing Optical Switch Using Ring Topology, S. F. Su, K. T. Koai, *GTE Laboratories.* A self-routing optical switch using ring topology is proposed. This switch self-routes multiple optical packets simultaneously because transfers of data inside the switch are parallel. (p. 129)

SALON E

10:30 AM-12:00 M
FC TIME-DIVISION SWITCHING SYSTEMS
T. Yasui, *NTT Telecommunication Networks Laboratories, Japan, Presider*

10:30 AM (Invited paper)
FC1 Time Multiplexed Optical Systems, R. S. Tucker, G. Eisenstein, Steven K. Korotky, *AT&T Bell Laboratories.* We survey recent progress in optical time-division multiplexed systems, with special emphasis on transmission and switching at multigigabit per second data rates. (p. 134)

11:00 AM
FC2 Experimental 512-Mbit/s Time-Division Photonic Switching System, T. Shimoe, S. Kuroyanagi, K. Murakami, H. Rokugawa, N. Mekada, T. Odagawa, *Fujitsu Laboratories, Ltd., Japan.* We have developed a high-speed thermally stable photonic time-division switching system. Stable 512-Mbit/s switching was obtained with the optical and electrical modules mounted in a single rack. (p. 136)

FRIDAY, MARCH 3, 1989—*Continued*

11:15 AM
FC3 Self-Clocked Optical Time-Slot Interchanger, Philippe A. Perrier, Paul R. Prucnal, Michel W. Chbat, *Princeton U.* A novel time division photonic switch is reported. Fiber delays are used as optical memories, no reading gate is required, and the switch operated asynchronously. (p. 139)

11:30 AM
FC4 Efficient Clock Distribution in a High-Speed Time-Multiplexed-Switched Optical Network, Steven K. Korotky, A. Azizi, *AT&T Bell Laboratories.* We demonstrate an efficient method for clock distribution in time-multiplexed-switched optical local area networks. The local clock of a 4-Gbit/s terminal on an experimental network is synchronized to the switch master clock located 5 km from the terminal. (p. 142)

11:45 AM
FC5 Experiments on the Optical Drop/Insert Function Using Bistable Laser Diodes for Optical Access Nodes, S. Masuda, N. Fujimoto, H. Rokugawa, K. Yamaguchi, S. Yamakoshi, *Fujitsu Laboratories, Ltd., Japan.* A novel approach to optical signal access is proposed. We successfully made the optical direct drop/insert function from/to a 50-Mbit/s data highway using bistable laser diodes. (p. 145)

12:00 M-1:30 PM LUNCH BREAK

SALON E

1:30 PM-3:15 PM
FD SEMICONDUCTOR DEVICES
R. I. MacDonald, *Alberta Telecommunications Research, Canada, Presider*

1:30 PM (Invited paper)
FD1 Bistable Laser Amplifiers as Optical Memories/Regenerators in Photonic Switching Systems, M. J. Adams, *British Telecom Research Laboratories, U. K.* Recent progress in the nonlinear properties of semiconductor laser optical amplifiers is reviewed with especial attention to potential use in switching and signal regeneration. (p. 150)

2:00 PM
FD2 Optical Flip-Flop Operation of a Bistable Laser Diode Using One-Wavelength Light Signals, T. Odagawa, S. Yamakoshi, *Fujitsu Laboratories, Ltd., Japan.* Optical flip-flop operation of a bistable laser diode has been demonstrated using one-wavelength light signals that have different pulse width or pulse intensity. (p. 153)

2:15 PM
FD3 Effect of Absorber Position in Bistable InGaAsP Lasers, Ulf Ohlander, Olof Sahlen, *Royal Institute of Technology, Sweden.* Threshold current, hysteresis width, luminescence wavelength, and carrier redistribution depend strongly on whether the middle section or the end-facet section is used as an absorber in a bistable laser. (p. 156)

2:30 PM
FD4 Traveling Wave Semiconductor Laser Amplifiers for Simultaneous Amplification and Detection: Systems Experiments, Mats Gustavsson, Lars Thylen, Anders Djupsjobacka, *Ericsson Telecom, Sweden;* Anders Karlsson, *Royal Institute of Technology, Sweden.* We present results on systems experiments on a near traveling wave semiconductor laser amplifier used simultaneously for amplification and detection of optical signals. Bit error rate as well as bandwidth measurements are reported. (p. 159)

2:45 PM
FD5 Compact InGaAsP Quantum Well Electrooptic Waveguide Switch, J. E. Zucker, K. L. Jones, M. G. Young, B. I. Miller, U. Koren, *AT&T Bell Laboratories.* We have utilized the large excitonic electrorefraction and tunable band gap in high quality InGaAsP quantum wells to produce compact directional couplers operating at 1.55-μm wavelength. (p. 162)

3:00 PM
FD6 High-Gain Optical Transistors Resistant to Pump Instability, Alex A. Maier, *Academy of Sciences of the U. S. S. R.* Self-switching of radiation in nonlinear systems with two 1-D distributionally coupled waves is considered for the general case when both waves are fed into the system and their nonidentity is taken into account. The possibility is discussed of optical transistors with a high gain that are resistant to pump intensity instability. (p. 165)

SALON D

3:15 PM-3:45 PM COFFEE BREAK

SALON E

3:45 PM-5:30 PM
FE SPACE-DIVISION SWITCHING
S. S. Cheng, *Bellcore, Presider*

3:45 PM (Invited Paper)
FE1 HDTV Photonic Space-Division Switching System Using 8 × 8 Polarization Independent $LiNbO_3$ Matrix Switches, S. Suzuki, H. Nishimoto, M. Iwasaki, S. Kajitani, M. Kondo, M. Shikada, M. Ashibe, F. Akashi, *NEC Corp., Japan.* A photonic switching system using a 3-stage network with newly developed 8 × 8 polarization independent $LiNbO_3$ switches successfully operated in switching HDTV signals, transmitted through ordinary optical fibers. (p. 168)

FRIDAY, MARCH 3, 1989—*Continued*

4:15 PM
FE2 Systems Experiments with a Packaged 4 × 4 Polarization Independent Switch Matrix, Per Granestrand, Lars Thylen, *Ericsson Telecom, Sweden;* Bjorn Stoltz, Jan-Erik Falk, *Ericsson Components AB, Sweden.* We report systems experiments involving transmission of 2-Gbit/s signals through a 4 × 4 polarization independent switch matrix. Influence of crosstalk on bit error rate is investigated. (p. 171)

4:30 PM
FE3 Comparison of Linear and Reflective 4 × 4 Ti:$LiNbO_3$ Switch Arrays, P. J. Duthie, M. J. Wale, I. Bennion, *Plessey Research Caswell, Ltd., U. K.* A $LiNbO_3$ reflective 4 × 4 crossbar switch array has been compared with a conventional crossbar array. Significantly reduced length and interface complexity have been demonstrated. (p. 174)

4:45 PM
FE4 Small Size Low-Crosstalk GaAs/AlGaAs Electrooptic Directional Coupler Switches with Alternation $\Delta\beta$ for Long Wavelength Matrix Switches, K. Komatsu, M. Sugimoto, A. Ajisawa, A. Suzuki, *NEC Corp., Japan.* Small size (2-mm long) GaAs/AlGaAs directional couplers, with crosstalk as low as -16 dB at $\lambda = 1.3$ μm without a requirement for precise device dimensions control, have been achieved by using an alternating $\Delta\beta$ technique. (p. 177)

5:00 PM
FE5 Switch Matrix with Semiconductor Laser Amplifier Gate Switches: A Performance Analysis, Mats Gustavsson, Lars Thylen, *Ericsson Telecom, Sweden.* A performance analysis of a space division switch matrix based on semiconductor laser amplifier gate switches is presented in terms of technological and systems requirements. (p. 180)

5:15 PM
FE6 A Linear Torsion-Hinged Deformable Mirror Device for Optical Switching Applications, R. Mark Boysel, T. Gus McDonald, Jeffrey B. Sampsell, *Texas Instruments, Inc.* We will describe a deformable mirror device and discuss its system-dependent optical performance in two applications: optical crossbar switching and frequency excision. (p. 183)

5:30 PM-5:45 PM CLOSING REMARKS
John E. Midwinter, *University College London, U.K.*

WEDNESDAY, MARCH 1, 1989

SALON G

8:45 AM–12:15 PM

WA1–WA4

PLENARY SESSION

Peter W. Smith, Bellcore, *Presider*

BROADBAND ELECTRONIC SWITCHING

J.E. Berthold
Bellcore
Room 3Z331
331 Newman Springs Road
Red Bank, NJ 07701

Electronic switching research is rapidly advancing channel bandwidth, number of channels possible on a switch chip, and the rate of channel connection changes.

Photonic Switching Systems Experiments in the European RACE Programme.

Nigel Whitehead,
British Telecom Research Laboratories,
Martlesham Heath,
Ipswich, IP5 7RE, England.

Nick Parsons,
Marconi Research Centre,
Great Baddow,
Chelmsford, CM2 8HN, England.

Paul Vogel
ASCOM Tech. Research Laboratories,
Belpstrasse 23,
CH 3000 Bern 14, Switzerland.

Göran Wicklund
ELLEMTEL
PO Box 1505
S 12525 Älvsjö, Sweden.

Some photonic switching systems experiments are described which exploit space, wavelength and time division techniques under development within the European RACE programme.

Introduction

Over the last decade optical transmission has come to dominate telecommunications networks, in conjunction with digital time division in both transmission and switching. If photonic systems are also to enter the switching arena, devices will probably be needed which are able to operate synchronously with the payload bitstream. Thus in these experiments we have sought to exploit some photonic techniques which break into the bit stream and which might be relevant to future high capacity switching applications.

The first systems experiment to be described uses an optical time multiplexed space switch (TMSS) within a digital network similar in concept to that proposed by Habara and Kikuchi [1], but with a number of novel features which provide the capability for use within a wide area fibre optic network (see Figure 1). The photonic switch is integrated with remotely located electronic time switches to create a strictly non blocking switching fabric supporting initially about 35000 x 64kbit/s channels or equivalent payload capacity in broadband channels.

A second experiment exploits photonic switching in a very high speed optical loop system (VHSOL). Some reported systems [2 & 3] have used photonic switching elements for protection and healing. With the VHSOL system we want to go a step further in using photonic switching devices for handling high speed optically coded information. The resulting network is designed to carry multiple broadband and narrow band services using Asynchronous Transfer Mode (ATM) at a maximum rate per ring of 8 M cells/s.

A third systems experiment will be described in the presentation which explores the possibilities for network access control on fibre optic subscriber lines in which photonic switching elements are used to provide flexible access to broadband networks and services.

Time Multiplex Switched Network Design

The photonic space switch employs a splitter/combiner architecture [4] and is constructed from sixteen 1 x 16 Lithium Niobate passive splitter arrays and sixteen 16 x 1 active combiners. The two stages are cross-connected using an interconnection array comprising 256 waveguides. The splitter/combiner architecture has a number of significant advantages when it is used in a time multiplexed network as proposed. It can be constructed such that all possible paths through the switching structure exhibit a common optical path length and common insertion loss. The crosstalk performance of splitter/combiner arrays is good and hence favourable signal to noise ratios (SNR) through the switch can be achieved. In addition the high speed control of a binary tree structured switch is relatively simple.

Hybrid Mach-Zehnder unit cells [5] are used to

Figure 1 **Time Multiplex Switched Network**

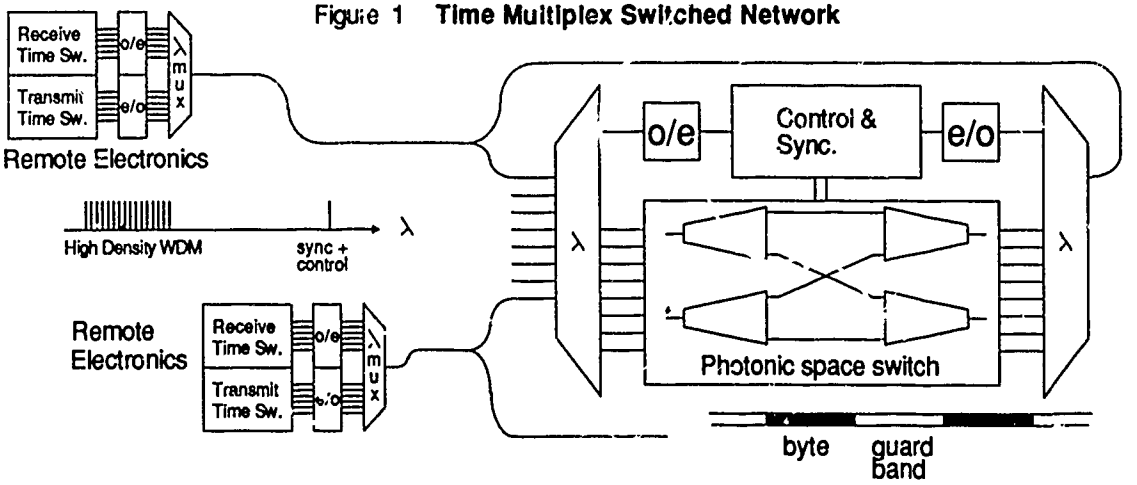

construct the active 16 x 1 combiner arrays, and simple Y-junction unit cells are used in the passive 1 x 16 splitters. The active unit cells are controlled using separate DC bias voltages and high speed switching voltages. Polarisation insensitivity is traded for a low switching voltage of less than 5 volts, thus permitting the switch to be operated with switch transition times of under 5ns. The switching elements exhibit an optical bandwidth of about 50nm thus permitting the switch throughput capacity to be extended using a wavelength division multiplex.

Sixteen electronic time switches are employed in the network, each comprising a receive and transmit channel store. The time switches are designed to operate at a data rate of 155 Mbit/s with the intention of moving to compatibility with the Synchronous Digital Hierarchy (SDH) standard. In order to maintain a strictly non blocking switching fabric, the time switches support n x 2n channels. Thus the interface to the space switch is a serial data stream of 2n channels. In addition before optoelectronic signal conversion, each byte is interleaved with a guard band of byte length, 12.5 ns.

Synchronisation and control of the network is centralised at the space switch. An optical path ranging scheme may be used to determine the delays between each of the time switches and the central space switch. The operation of the time switches can thus be synchronised with the reconfiguration cycle of the time multiplexed space switch by means of a feedback mechanism within the tolerance imposed by the guard band. A configuration store provides cyclic control of the photonic switching matrix, and local configuration stores are provided within each time switch. Requests for channel switching are processed by the central control which updates the space and time switch configuration stores.

A key feature of the splitters used in the network is that they each incorporate a polarisation scrambler on the optical inlet. Likewise the combiners incorporate polarisation filters on their optical inlets. Thus the passive interconnection array does not need to maintain polarisation. In addition, optical compatibility between the photonic switch matrix and existing standard singlemode fibre networks is achieved at the cost of an additional 3dB insertion loss. This feature, together with the use of centralized synchronisation control permits the time switches to be located remotely from the time multiplexed space switch, greatly enhancing the applications potential of the network.

The initial TMSS configuration permits byte switching on a single wavelength. The system capacity can be extended by the introduction of cell switching in which each byte of a 32 octet cell is carried in parallel on a different wavelength (see Figure 1) in a high density wavelength division multiplex. It is possible to design the read/write structure of the time switch payload stores in a way which would greatly facilitate a cell parallel output to the WDM lasers and receivers. The single wavelength TMSS has a

total payload capacity of 2.4 Gbit/s at 64kbit/s channel granularity. This is not very short of the maximum switching capacity of today's digital electronic central office systems. The proposed multi wavelength network offers many times that capability.

Very High Speed Optical Loop Design

The VHSOL is configured as a hierarchical structured multiple fibre ring system comprising a backbone double ring, and secondary rings (see Figure 2). Fixed length slots of 36 octets are used. Full slots contain a complete ATM cell and empty slots contain unmodulated light. Guard bands carrying slot status information for the Medium Access Protocol (MAC) are introduced between consecutive slots. A key system feature is the use of the *spread header* principle in which the header belonging to a certain slot is spread over the time interval of the preceding filled slot.

Fibre loop access (LAP) is implemented on the secondary rings based on 1x2 directional coupler switches in Lithium Niobate which are used to listen, switch and modulate. In the listen state relatively low power has to be coupled out from the fibre loop for header detection. If the header processor recognises its own node address, the information field in the next following full slot is extracted, switching maximum coupled optical power to the receiver. Data is coupled to the ring by the modulation of empty slots. A certain number of LAPs can be connected to the fibre loop before optical regeneration becomes necessary or connection is made to the backbone ring. In the initial design, access between the secondary rings and the backbone uses lasers and receivers, but more advanced designs are being considered using integrated optoelectronics.

Figure 2
VHSOL

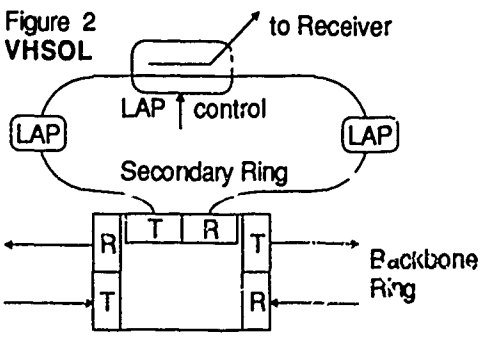

Potential

We have shown that high data throughputs can be achieved using photonic switching in ways which integrate with time multiplexed digital structures and with fibre local access networks. In the future, very much more capable photonic switch fabrics may be built. For example, zero insertion loss switches and modulators may soon be available for systems applications using compound semiconductor materials, with integrated photonic amplifiers and electronic elements. In addition photonic signal retiming may be introduced, opening up the possibilities of all-optical clock distribution and synchronisation control. These possibilities are being examined with a view to enhancing the systems we have described.

Acknowledgements

This work is partly supported by the European Commission under RACE Contract R1033.

References

[1] K Habara and K Kikuchi, "Optical Time-Division Space Switches using Tree-structured Directional Couplers", Electronics Letters, Vol 21 No 14, 4 July 1985.

[2] Flatman & Caves, "FDDI-II A new standard for Integrated services High Speed LANs", Wideband Communications (1986), Online Publications, UK.

[3] N Fugimoto, P Ishihara, A Paniguchi, H Yamashita and K Yamaguchi "Experimental Broadband Drop/Insert/Cross Connect System: 1.8Gb/s Optical Shuttle Bus", Proc. IEEE Globecom 1988.

[4] R A Spanke, "Architectures for Large Nonblocking Optical Space Switches", IEEE Journal of Quantum Electronics, Vol. QE22, No. 6, June 1986, pp. 964-967.

[5] T Pohlmann, A Neyer and E Voges, "Ti:LiNbO3 Interferometric Activated X-switch for high-speed applications", Electronic Letters, Vol 24 No 9, 28 April 1988.

DEVICES FOR PHOTONIC SWITCHING

Lar Thylen, Ericsson Telecom
Integrated Optics and Photonic Switching
S-126 25 Stockholm, Sweden

State-of-the-art devices for photonic switching are reviewed emphasizing the time and space switching areas.

A New Direction in Photonic Switching

Paul R. Prucnal
Department of Electrical Engineering
Princeton University
Princeton, NJ 08544

Limitations in conventional photonic switching architectures, including time division, wavelength division, and space division, are reviewed. A novel "shared-medium switch" is proposed that permits all signals to share a single high-bandwidth transmission path.

NOTES

WEDNESDAY, MARCH 1, 1989

SALON F

2:00 PM–5:30 PM

WAA1–WAA4

JOINT PHOTONIC SWITCHING AND OPTICAL COMPUTING PLENARY SESSION

Joseph W. Goodman, Stanford University,
Co-presider

John E. Midwinter, University College London, U.K.,
Co-presider

OEIC Technology for Photonic Switching

S. Yamakoshi
Fujitsu Laboratories, Ltd.
10-1, Morinosato-Wakamiya, Atsugi 243-01, Japan

OEIC technology is promising to construct the new optical systems such as photonic switching, routing and other opitcal processing operations. The state-of-the-arts and future prospects of OEICs for photonic switching are discussed.

Quantum Well Devices for Optical Computing and Switching

D. A. B. Miller,

AT&T Bell Laboratories,

Holmdel, NJ 07733

The future prospects for both optical computing and photonic switching are clearly very dependent on advances in devices. This is especially true in the case of large scale applications requiring arrays of devices. Not only must the individual devices have good physical performance, they must also (i) operate at very low energies so that the array can be powered optically if required and have sufficiently low overall dissipation, (ii) be fabricatable in uniform arrays, and (iii) have sufficiently sophisticated functionality to allow efficient design of complex systems. Any one of these requirements suggests integration; taken together, we can see that a technology that offers straightforward integration of large numbers of flexible devices is essential for such array applications. Given that there are very few physical mechanisms that can offer sufficiently low operating energies for optical devices regardless of integration, we can see that this is a hard problem.

The potential return for a suitable technology is, however, large. Not only are there many architectural advantages in parallel optics, there are also now clear and relatively fundamental physical arguments why optics is actually better than electronics for communicating inside processors; the impedance transformation performed by optical devices can actually reduce the energy required for communication inside the processor.[1] To exploit this impedance transformation also requires integration since the capacitance of any connections between the opto-electronic devices and the electronic devices should be smaller than the device capacitances themselves. Indeed, it is arguable that much of the desire to avoid optical-electronic-optical conversions is because of lack of integration.

Quantum well devices have emerged over the past few years as strong candidates for optical switching and logic devices, especially for high-performance two-dimensional arrays compatible with free-space optics. One physical reason for this is the quantum-confined Stark effect electroabsorption mechanism,[2] which offers a low energy means for getting optical information out of a system, and is sufficiently strong that it can be used for modulation of beams propagating perpendicular to the chip surface, as required for two-dimensional arrays. A technological reason for the attractiveness of these devices is that the layered semiconductor growth techniques used to fabricate the thin semiconductor layers required for quantum wells and the lithographic techniques used for quantum well devices are also well suited to integration, both of many quantum well devices on one chip and of quantum well devices with other electronic and optical components.

The concept of combining photodetectors and quantum well modulators to give an optically controlled device with optical outputs is the principle of the self-electrooptic-effect device (SEED).[3] Such devices only offer low energy performance when they are integrated so that there are no parasitic capacitances associated with the interconnections between the different parts of the device. Integration of simple bistable devices was demonstrated first.[4] Although these large ($200\times200\ (\mu m)^2$) devices did not have particularly low switching energies (~ 1 - 2 nJ), they had the property that they could be scaled to smaller size ($60\times60(\mu m)^2$) with an approximately proportional improvement in switching energy and in increase in the size of the arrays (6×6).[5]

Systems experiments with simple bistable devices have problems because of the critical biasing requirements of simple bistable devices. The next step was therefore the symmetric SEED (S-SEED), which is a device that employs two quantum well diodes in series and is bistabie in the ratio of two beam powers.[6] This S-SEED is in effect a three-terminal optical device, greatly simplifying system design. This device is now being scaled to larger arrays of smaller devices, with 16×8 arrays of devices with $13.5\times14\ (\mu m)^2$ mesas.[7] These devices are now being used for more complex optical circuit experiments.[8] There has also been recent work to extend the functionality of S-SEEDs further by including yet more diodes in series to make a multistate SEED (M-SEED).[9] Such a device can have N or 2^N stable states for N light beams on N series diodes depending on the biasing conditions.

Other opportunities with the SEED concept include the integration of more electronic components. Integration of bipolar transistors has been proposed,[3,10] and integration with field-effect transistors (F-SEED) has been demonstrated[11]. Importantly, the F-SEED integration is compatible with standard GaAs field effect transistor processing, and so we may contemplate integration of arbitrary amounts of electronics to expand the functionality of the optical module if we wish. It is also becoming increasingly likely that the quantum well modulators can be integrated with silicon circuits.[12]

In the future, we can expect continued miniaturization of SEEDs; indeed we cannot expect the necessary performance out of these devices for real applications unless and until they are fabricated with dimensions comparable to small electronic devices. We can also expect increasing flexibility in the functionality of the devices so that they are more suitable for particular systems applications. Finally, we can anticipate that a natural consequence of these developments will be to offer us the choice as to where we make the interface between optics and electronics so that we may have the best of both worlds.

[1] D. A. B. Miller, Optics Lett. (to be published, Jan. 1989)

[2] D. A. B. Miller, D. S. Chemla, T. C. Damen, A. C. Gossard, W. Wiegmann, T. H. Wood, and C. A. Burrus, Phys. Rev. **B32**, 1043 (1985); D. A. B. Miller, J. S. Weiner, and D. S. Chemla, IEEE J. Quantum Electron. **QE-22**, 1816 (1986).

[3] D. A. B. Miller, D. S. Chemla, T. C. Damen, T. H. Wood, C. A. Burrus, A. C. Gossard, and W. Wiegmann, IEEE J. Quantum Electron. **QE-21**, 1462 (1985);

D. A. B. Miller, U. S. Patents 4,546,244 and 4,716,449.

[4] D. A. B. Miller, J. E. Henry, A. C. Gossard, and J. H. English, Appl. Phys. Lett. **49**, 821 (1986).

[5] G. Livescu, D. A. B. Miller, J. E. Henry, A. C. Gossard, and J. H. English, Optics Lett. **13**, 297 (1988).

[6] A. L. Lentine, H. S. Hinton, D. A. B. Miller, J. E. Henry, J. E. Cunningham, and L. M. F. Chirovsky, Appl. Phys. Lett. **52**, 1419 (1988).

[7] L. M. F. Chirovsky, L. A. D'Asaro, C. W. Tu, A. L. Lentine, G. D. Boyd, and D. A. B. Miller, submitted to Photonic Switching Conference.

[8] F. B. McCormick, A. L. Lentine, L. M. F. Chirovsky, and L. A. D'Asaro, submitted to Photonic Switching Conference.

[9] A. L. Lentine, D. A. B. Miller, J. E. Henry, J. E. Cunningham, and L. M. F. Chirovsky, Paper FBB1, OSA Annual Meeting, Santa Clara, November 1988.

[10] P. Wheatley, P. J. Bradley, M. Whitehead, G. Parry, J. E. Midwinter, P. Mistry, M. A. Pate, and J. S. Roberts, Electron. Lett. **23**, 93 (1987).

[11] D. A. B. Miller, M. D. Feuer, T. Y. Chang, S. C. Shunk, J. E. Henry, D. J. Burrows, and D. S. Chemla, Paper TUE1, CLEO, Anaheim, April 1988.

[12] W. Dobbelaere, D. Huang, M. S. Unlu, and H. Morkoc, Appl. Phys. Lett. **53**, 94 (1988); K. W. Goossen, G. D. Boyd, J. E. Cunningham, W. Y. Jan, D. A. B. Miller, D. S. Chemla, and R. M. Lum, submitted to Quantum Wells for Optics and Optoelectronics Conference.

Switching in an Optical Interconnect Environment

Joseph W. Goodman
Department of Electrical Engineering
Stanford University

Optical interconnects are gaining importance in a wide range of applications, ranging from interconnection of supercomputers and workstations to interconnection of multiple chips on a single board. With the development of any interconnect technology, eventually the need for switching arises. Thus the switching of optical interconnects is a topic of much current interest.

Some applications of switching in the interconnect environment include, for example: 1) connection of a multitude of workstations to several shared resources, such as high-speed disk drives, laser printers, high-speed scanners, etc.; 2) connection of a multitude of backplanes in a tightly coupled multiprocessing machine; and 3) connection of a multitude of boards on an optical backpiane in a single computer. The data rates and switch reconfiguration times required in these applications can differ significantly.

The lengths of the interconnects in these applications are typically quite short, ranging from perhaps hundreds of meters at one extreme (machine to workstation interconnection) to a few centimeters at the other (chip to chip on a board). The losses associated with the interconnect medium are therefore typically quite small (only a few dB), and both modal and material dispersion effects are often negligible. The consequences of these facts are several: 1) switching architectures with significant loss may still be of interest; 2) the choice of an operating wavelength (0.8 μm, 1.3 μm, etc.) is dictated by reliability rather than material dispersion; and 3) the use of multimode solutions is quite acceptable.

While switch loss appears not to be a critical parameter, nonetheless the issue does warrant further thought. When one considers the most fundamental motivations for the use of optics (as opposed to electronics) in interconnect problems, it appears that low drive power per length-bandwidth product can be one important advantage. When the internal loss of a switch is too great, optical interconnects may lose some of their

attractiveness when compared with electronic solutions, due to the increased electrical power required to drive the optical links.

With these facts in mind we examine several alternative approaches to optical switch construction for these applications. Most direct is the use of an electronic switch interfaced to optical receivers and transmitters. An intermediate electro-optic approach is a switch based on an array of forward- and back-biased detectors, interfaced to an array of optical transmitters [1,2]. All optical approaches include the optical matrix-vector [3,4], switches based on beam deflection, either through the use of stripe domain gratings in magneto-optic materials [5] or through acousto-optic deflection [6], and switches based on wavelength selective switching (e.g. [7]). Finally, LiNb switchable couplers, under intense development for long-distance telecommunications, are a candidate in this application as well (e.g. [8]). Each approach has its own unique advantages and disadvantages.

References

1. R.I. MacDonald, "Optoelectronic switch matrices: recent developments", *Optical Engineering*, Vol. 24, pp. 220-224 (1985).
2. G.L. Tangonen, V. Jones, J. Pikulski, D. Jackson, J. Persechini, G. Thornebooth, "8*8 optoelectronic crossbar switch", *Electronics Letters*, Vol. 24, No. 5, pp. 275-277 (1988).
3. A. Himeno, M. Kobayashi, "4x4 optical gate matrix switch", *J. Lighwave Technology*, Vol. LT-3, pp. 230-235 (1985).
4. A.R. Dias, R.F. Kalman, J.W. Goodman, A.A. Sawchuk, "Fiber-optic crossbar switch with broadcast capability", *Optical Engineering*, Vol. 27, No. 11, pp. 955-960 (1988).
5. E.J. Torok, J.A. Krawczak, G.L. Nelson, B.S. Fritz, W.A. Harvey, F.G. Hewitt, "Photonic switching with stripe domains", in *Photonic Switching*, T.K. Gustafson and P.W. Smith, Eds., Springer-Verlag, pp. 46-49 (1988).
6. P.C. Huang, W.E. Stephens, T.C. Banwell, L.A. Reith, "4x4 Acoustooptic photonic space switch with multicasting capability", *Paper Summaries*, OSA Annual Meeting, Paper TuK6, October 1988.
7. S. Suzuki, K. Nagashima, "Optical broadband communication network architecture utilizing wavelength-division switching technology", in *Photonic Switching*, T.K. Gustafson and P.W. Smith, Eds., Springer-Verlag, pp. 134-137 (1988).
8. H.S. Hinton, "Applications of photonic switching devices", *Proceedings of the SPIE*, Vol. 835, pp. 11-16 (1988).

The Relationship Between Photonic Switching and Optical Computing

H. S. Hinton

AT&T Bell Laboratories

Naperville, Illinois 60566P

The purpose of this talk is to outline the relationship between the hardware requirements of photonic switching and optical computing systems. The majority of the talk will address the hardware requirements of digital optical switching and computing systems with the exception of a brief discussion on analog switching and computing. It will include a review and comparison of the devices, interconnects, and systems that have been proposed for both types of systems.

THURSDAY, MARCH 2, 1989

SALON E

8:30 AM–9:45 AM

ThA1–ThA4

DEVICES FOR TIME-DIVISION SWITCHING SYSTEMS

T. Nakagami, Fujitsu Laboratories, Ltd., Japan,
Presider

Encoding and Decoding of Femtosecond Pulses for Code-Division Multiple-Access

A.M. Weiner, J.A. Salehi, J.P. Heritage, and M. Stern

Bellcore
331 Newman Springs Road
Red Bank, NJ 07701-7020

The speed of current fiber-optic communications systems is limited in part by the speed of electronic processors used for signal processing. Optical signal processing potentially can be much faster than electronic processing and could be utilized to achieve higher data rate transmission and to provide added flexibility for network design. One application of optical processing, which is receiving increasing consideration, is code-division multiple-access (CDMA), a communications environment in which multiplexing is achieved by assigning different, minimally interfering code sequences to different subscriber pairs [1,2]. This approach to multiplexing can provide many users with an asynchronous, random access, communication link.

In this paper we discuss the possibility of an ultrahigh speed optical CDMA system based upon encoding and decoding of coherent ultrashort light pulses. We first describe experiments demonstrating the ability to encode femtosecond pulses into picosecond-duration pseudonoise bursts and to decode such pseudonoise bursts back into fsec pulses [3]. We then propose a novel multiplexing scheme utilizing these manipulations and comment on the advantages of and the issues facing this approach. Finally, we present results of recent bit error rate calculations for the proposed ultrashort pulse CDMA system [4].

We accomplish encoding and decoding by utilizing a powerful new technique for synthesizing arbitrarily shaped ultrashort pulses [3]. As described previously [3], pulses are encoded by spatial masking within an apparatus consisting of a pair of diffraction gratings placed at the focal planes of a unit magnification, confocal lens pair [5]. A spatially patterned phase mask, placed midway between the lenses, adjusts the phases of the optical frequency components which are spatially dispersed at that point. By utilizing a pseudorandom phase mask to scramble (encode) the spectral phases, incident fsec pulses are spread into low intensity, picosecond-duration, pseudonoise bursts. Decoding is achieved by using a second, phase conjugate mask to unscramble (decode) the spectral phases, thus restoring the original fsec pulse. Autocorrelation measurements of uncoded, coded, and decoded pulses are shown in Fig. 1 [3]. The dramatic contrast in the peak intensities could be used in a CDMA system to discriminate between correctly and incorrectly addressed information.

The proposed ultrashort pulse CDMA system is shown in Fig. 2 [3]. N subscriber stations are connected via a passive N X N coupler. Each transmitter spreads coherent ultrashort pulses

into low intensity pseudonoise bursts; each receiver attempts to decode the incoming pseudonoise bursts back into intense ultrashort pulses. Incoming signals which are successfully decoded are detected by the optical thresholder; signals which are not successfully decoded are rejected.

A key motivation for this approach is that individual subscribers would operate at data rates compatible with electronic modulation and processing. Encoding and decoding would serve to provide asynchronous multiplexing and immunity to collisions. Furthermore, by using a fast multielement phase modulator within the encoder, the system could achieve rapid reconfigurability. Of course, several issues must be faced before an ultrashort pulse CDMA system can be practically realized. We will comment on the need for a compact subpicosecond source and a low power optical thresholder, discuss the effect of fiber dispersion, and describe a set of codes which will provide a large number of addresses while minimizing interference.

We have analyzed the bit error rate (BER) of the proposed CDMA system as a function of number of users, code lengths, individual bit rates, and threshold [4]. Power budget considerations were not included, and the phase codes were taken as sequences of binary (0 or π) random variables. Figure 3 shows the BER plotted vs. threshold, assuming a code of length 128, an individual bit rate of 100 Mbit/sec, and a 0.8 psec input pulse (or 1 Gbit/sec for 80 fsec input pulses). For an "ideal" thresholder, active only at the instant when the properly decoded pulse is expected, the system can handle 20 users at a BER of 10^{-9} or 100 users at a BER of 3×10^{-7}. For a "practical" thresholder, active during the entire data frame but easier to implement, the BER increases by a factor of 10. The BER decreases drastically with increasing code length.

In summary, we have demonstrated encoding and decoding of fsec pulses and have proposed it as a basis for ultrashort pulse CDMA. We expect that fsec pulse shaping techniques, which utilize parallel modulation in the frequency domain to provide effective serial modulation rates as high as 10 THz, will stimulate a new class of ultrashort pulse optical communications systems.

References

1. P.R. Prucnal, M.A. Santoro, and T.R. Fan, IEEE J. Lightwave Technol. LT-4, 547 (1986).
2. J.A. Salehi and C.A. Brackett, Proceedings of the IEEE International Conference on Communications, 1601 (1987).
3. A.M Weiner J.P. Heritage, and J.A. Salehi, Opt. Lett. 13, 300 (1988).
4. J.A. Salehi, A.M. Weiner, and J.P. Heritage, submitted to Opt. Lett.
5. C. Froehly, B. Colombeau, and M. Vampouille, in Progress in Optics, E. Wolf, ed. (North Holland, Amsterdam, 1983), pp. 115-121.

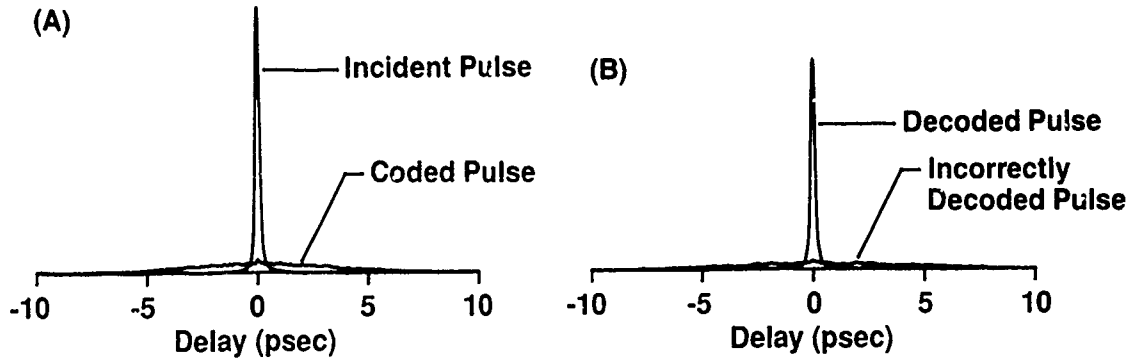

Fig. 1 Intensity autocorrelation measurements of uncoded, coded and decoded pulses. (A) Uncoded and coded pulses. (B) Successfully and unsuccessfully decoded pulses.

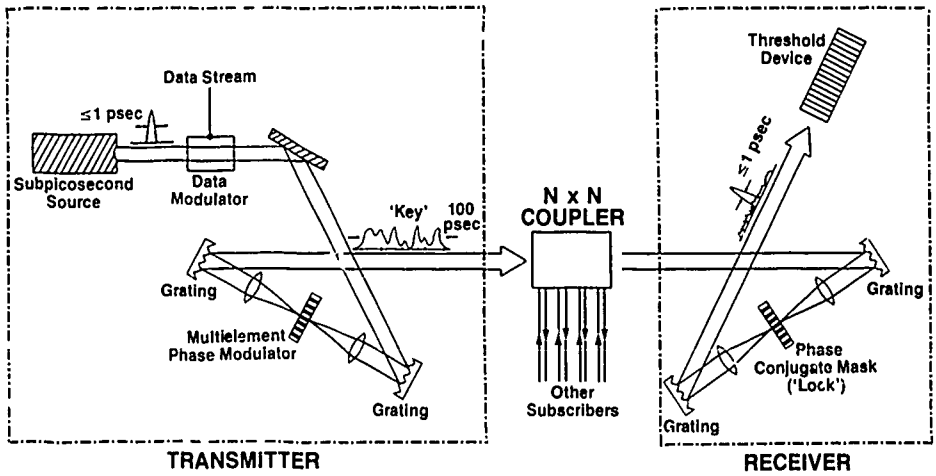

Fig. 2 Proposed ultrashort pulse, CDMA communications network. Data is received only when the incoming encoded signal (the "key") is matched to the decoder (the "lock").

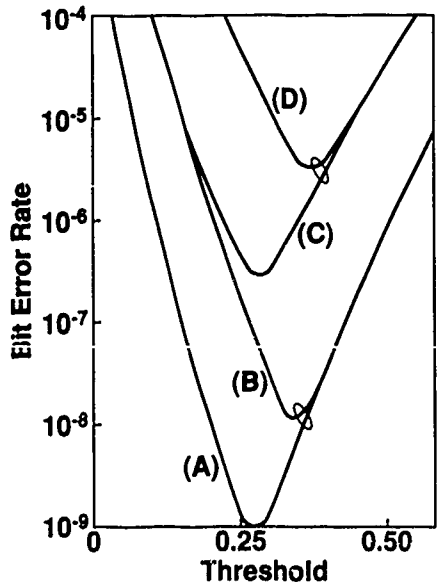

Fig. 3 Bit error rate as a function of threshold, for a code of length N=128. A threshold of 1.0 corresponds to the intensity of a properly decoded pulse. For this example we set the individual bit rates to $0.01(N\tau)^{-1}$, where τ is the starting pulse width, and assume that the receiver detects a '1' if the decoded intensity exceeds the threshold at any time within an interval of duration $\beta\tau$. β=1 corresponds to an "ideal" thresholder, active only at the instant when the desired data is expected. For β=128 the thresholder is active over a longer interval (128τ) equal to the duration of a coded pulse. (A) β=1, M=20 = # of users; (B) β=128, M=20; (C) β=1, M=100; (D) β=128, M=100.

Velocity-Matched Ti:$LiNbO_3$ Switch for 16 Gb/s Optical Time-Division Multiplexing

J.J. Veselka and S.K. Korotky

AT&T Bell Laboratories
Crawfords Corner Road
Holmdel, NJ 07733
(201) 949-5213

Optical time-division multiplexing (OTDM) offers the ability to increase the transmission capacity of fiber communication systems by circumventing the speed/power limitations of broadband electronic multiplexer, driver, and decision circuits and of optoelectronic transducers [1]. It accomplishes this while still requiring only a single laser per transmitter, and thus permitting operation at the fiber zero-dispersion wavelength. A key element of OTDM systems is the optical switch used in the demultiplexer. At present, data transmission speeds of 16 Gb/s have been achieved using fast Ti:$LiNbO_3$ waveguide electrooptic switches [2]. However, at that rate a system power penalty of -2.9 dB was caused by crosstalk in the demultiplexer. This penalty was largely attributable to insufficient drive voltage to the switch performing the first stage of demultiplexing, which was operated at 8 GHz and driven with 1 W (50 Ω). Here we report a Ti:$LiNbO_3$ 2×2 switch operating at the 1.3 μm optical wavelength that incorporates electrical/optical velocity matching to achieve a low required drive power of 234 mW at 8 GHz. We demonstrate a measurement-limited crosstalk performance of -16 dB for both switch states for those same conditions.

The 2×2 switch utilizes a waveguide Mach-Zehnder (MZ) interferometer structure [3], as shown in Fig. 1, and was fabricated on z-cut $LiNbO_3$ by titanium diffusion. It consists of a pair of directional couplers that form the input splitter and output combiner of the interferometer. Electrodes on the 4 mm long couplers are used to adjust the coupler crossover efficiencies to 50%. The arms of the interferometer between the couplers are 29.4 mm in length and are separated by 20 μm at the inner edges of the waveguides. Three electrodes are placed over the interferometer to introduce a relative phase shift between light in the two branches. Of these, two provide a total length of 6 mm to DC-bias the interferometer to the desired operating point. The third is a coplanar-waveguide (CPW) traveling-wave electrode and is used to implement the high-speed switching. Since the switch is intended to serve as a 1-to-2 demultiplexer for a 16 Gb/s OTDM pulse stream, we have designed the CPW electrode structure to achieve a low required drive voltage at 8 GHz. This was accomplished by choosing the width and gap dimensions of the CPW electrode to achieve high electrooptic overlap efficiency [4] and low RF attenuation. In addition, we implemented the effective velocity matching of the electrical and optical waves via the periodic lateral shifting of the CPW electrode relative to the interferometer waveguides [5].

The CPW electrode consists of a 18 μm wide center conductor separated by 12 μm on each side from two 100 μm wide ground planes. It was gold-plated to a thickness of ~4 μm and had a center conductor end-to-end resistance of 7.1 Ω. An ~2200 Å thick SiO_2 buffer layer separates the electrodes from the surface of the $LiNbO_3$ substrate. We have calculated [7] and measured the microwave characteristics of this CPW structure with consistent results. The values for the impedance, Z, and microwave index, N_m, are $Z = 34\ \Omega$ and $N_m = 3.8$. The RF attenuation coefficient was measured and is described by $\alpha = 0.8$ dB $+ 0.8$ dB/cm $\times \sqrt{f\,(\mathrm{GHz})}$. To implement velocity matching, and thereby utilize an electrooptic interaction length many times the walkoff length of $LiNbO_3$ waveguide devices, the CPW was divided into six reversal-sections. The length of each section of the CPW electrode is given by $L = c/2(N_m \pm N_o)f_d$ where f_d is the design frequency, c is the speed of

light in a vacuum, N_m is the effective microwave refractive index along the electrode, N_o is the effective refractive index of the optical mode ($N_o \simeq 2.1$) , and the + or - sign is used if the optical field and applied electric field are counter-propagating or co-propagating [4]. To make use of the shortest section length, we have chosen to counter-propagate the RF and optical waves, which for 8 GHz results in a section length of 3.1 mm.

Single-mode fibers were attached to the four input/output waveguides of the Ti:$LiNbO_3$ switch with standard techniques. TM-pass waveguide polarizers ~2 mm long were fabricated at one end of the device using proton-exchange to assist in minimizing optical crosstalk [6]. By fabricating the polarizers to have an optical mode size between those of the fiber and the titanium-diffused waveguide we achieved polarizers with a measured insertion loss of 0.0 ± 0.2 dB.

To measure the small-signal electrooptic frequency response, we biased the device at its linear operating point. We drove the CPW electrode with the signal from a network analyzer and observed the modulated light with a high-speed detector whose output was amplified and fed back to the network analyzer. As shown in Fig. 2, there is very good agreement between the measured and calculated frequency response, which includes the effects of the electrical attenuation.

Under DC operation we could achieve crosstalk levels of -23 dB in both switch states of the device using the MZ bias electrodes. To determine the crosstalk levels at 8 GHz we used an optical sampling technique [7]. A stream of optical pulses (~10 ps FWHM) from a mode-locked grating-extended-cavity laser operating at a 2.020 GHz repetition rate was input to the device. The amplitude and DC-bias of the drive signal was adjusted to toggle the switch between its crossover and straight-through states. This was observed by offsetting the switch drive frequency by 100 Hz relative to the fourth harmonic of the laser pulse rate, detecting the output with a slow detector, and displaying the signal on an oscilloscope. The trace for 8.080 GHz operation is shown in Fig. 3 and illustrates the expected nonlinear behavior of the switch. To make quantitative measurements, the frequency offset was eliminated and a phase shifter was used to adjust the arrival time of the input optical pulses to coincide, in turn,to either the crossover or straight-through states. For each of the states, the average optical powers from the two output waveguides were measured and the crosstalk of the switch was calculated. Crosstalk values of -16 dB were obtained for both switch states with a low cw RF drive power of only 234 mW (50 Ω). We note that these crosstalk values were limited by the laser optical pulse width used for the sampling.

In summary, we have demonstrated an optical switch requiring low drive power at 8 GHz. The first crosstalk measurements at this high a frequency were reported with results of -16 dB for both states of the switch. We thank R. Bosworth and J. Lutz for the mask programming, G. Eisenstein for the optical amplifier, and F. Heismann for his assistance.

REFERENCES

[1] R.S. Tucker, G. Eisenstein, and S.K. Korotky, J. Lightwave Technol. **LT-6**, 1737 (1988).

[2] R.S. Tucker, G. Eisenstein, S.K. Korotky, L.L. Buhl, J.J. Veselka, G. Raybon, B.L. Kasper, and R.C. Alferness, Elec. Lett. **23**, 1270 (1987).

[3] V. Ramaswamy and R.D. Standley, Bell Sys. Tech. J. **55**, 767 (1976).

[4] D. Marcuse, in *Tech. Dig. Top. Meet. on Num. Sim. and Anal. in Guided-Wave Optics and Optoelectronics*, Houston, 1989.

[5] R.C. Alferness, S.K. Korotky, and E.A.J. Marcatili, IEEE J. Quantum Electron. **QE-20**, 301 (1984).

[6] J.J. Veselka and G.A. Bogert, Electron. Lett. 23, 265 (1987).

[7] J.J. Veselka, D.A. Herr, T.O. Murphy, L.L. Buhl, and S.K. Korotky, in *Tech. Dig. Conf. on Integ. and Guided-Wave Optics*, Sante Fe, 1988, paper WD2.

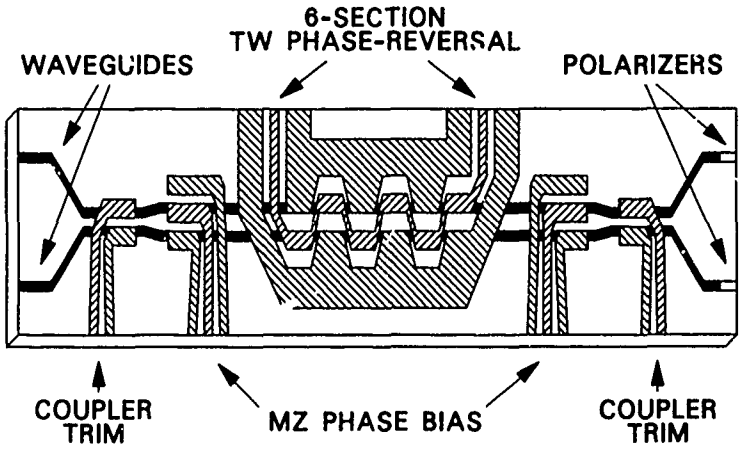

Fig. 1: Schematic of velocity-matched Ti:$LiNbO_3$ Mach-Zehnder switch showing waveguides, electrodes, and polarizers.

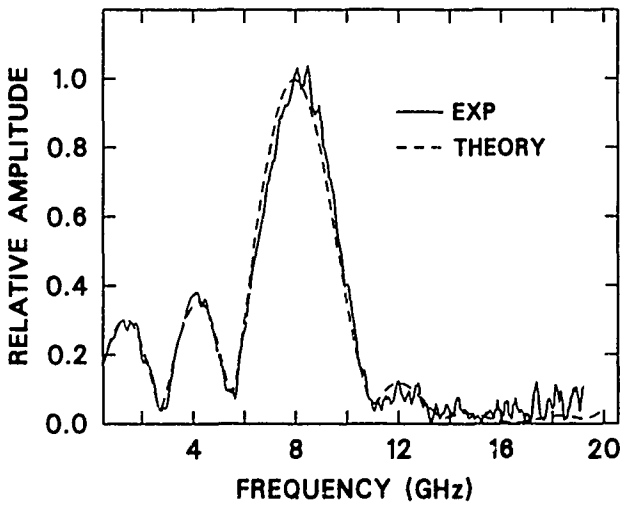

Fig. 2: Measured and calculated frequency response of 6-section phase-reversal switch designed for 8 GHz.

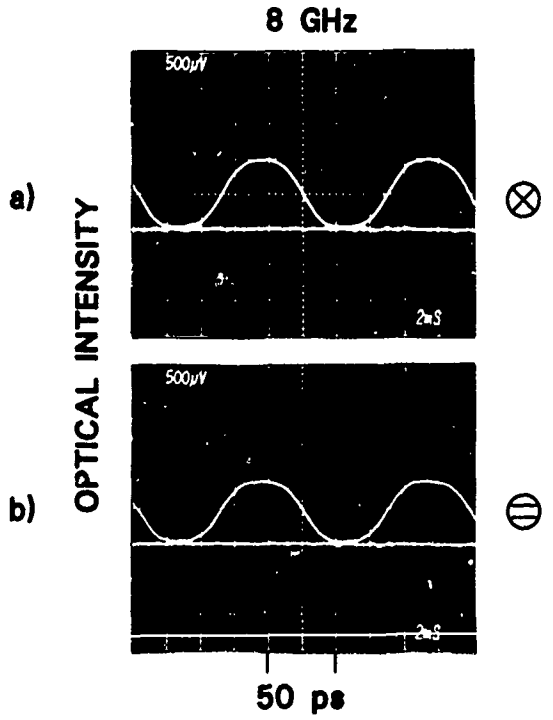

Fig. 3: Measured switching waveform for 8 GHz drive frequency.
a) output of crossover waveguide
b) output of straight-through waveguide

Improved Operation of a Two-Core Fiber All-Optical Switch Using Femtosecond Square Optical Pulses

Y. Silberberg, A. M. Weiner, H. Fouckhardt, D. E. Leaird,
M. A. Saifi, M. J. Andrejco and P. W. Smith

Bellcore
331 Newman Springs Road, Red Bank, NJ 07701-7020

Light controlled switches that operate through nonlinear optical interactions have the potential of providing ultrafast switching speeds, much higher than those possible with electronic or electrooptic devices. Such high switching rates are likely to be necessary in future high-speed communications and computing systems.

One switching element that is considered for all-optical switching is the nonlinear directional coupler (1). In the usual configuration a coupler of one coupling-length is used. Low-power signals which are introduced into one guide emerge from the second guide. High-power signals induce a refractive index change which frustrates the coupling, causing them to stay in the input guide. The directional coupler switch is a traveling-wave device, which can route incoming signals according to their intensity. The solid line in Fig. 1 shows the expected power output from each of the two waveguides as a function of input power for a cw input signal. Complete switching is possible.

The temporal response of the directional coupler switch depends on the nature of the nonlinear process. The electronic nonlinearity of some transparent materials can be extremely fast. We have recently demonstrated a two-core fiber directional coupler switch that operated with 100 fsec pulses (2). One of the problems that are associated with short pulse operation is that such pulses usually come with a bell-shaped temporal profile; the device may switch the peak of the pulse to the input guide, while leaving the weak wings in the other guide. This break-up of the pulse tends to increase the crosstalk and to make the switch response more gradual; the broken line in Fig. 1 shows the energy fraction that emerges from each core for a sech^2 shaped pulse. The reduced contrast is obvious.

Proposals have been made to solve the pulse break-up problem by using solitons (3). A simpler cure to this problem is to use square optical pulses, in which the intensity across the pulse is constant, except for finite rise and fall times. The response to square pulses should approach the ideal cw response of the device. In this talk we will present the first experimental results using square optical pulses to improve nonlinear optical switching.

We have previously described a technique for nearly arbitrary reshaping of ultrashort pulses (4,5), and we use this technique to generate femtosecond square pulses. Briefly, 75 fsec, 620 nm pulses from a CPM dye laser and copper vapor laser pumped amplifier are shaped by a lens and grating apparatus. In this setup, spatially patterned amplitude and phase masks are imposed on the spatially dispersed frequency components of the pulse. The shape of the output pulse is the Fourier transform of the patterned spectrum. Using this technique

we have generated a 540 fsec long square pulse with a rise and fall time of approximately 100 fsec. A cross-correlation of this pulse with a 90 fsec standard pulse is shown in Fig. 2.

These pulses were used to switch a 5 mm long dual-core fiber coupler device. This device has two pure silica cores, about 4.5 μm in diameter with center to center separation of 7.7 μm, a fluorine doped silica cladding and core-clad index difference of 0.003. This coupler showed no long term degradation which had been observed in the germanium doped fibers used previously (2). Fig. 3 shows the measured switching characteristics as a function of the peak input power for the square pulses as well as for standard (bell-shaped) 90 fsec pulses. Comparing these curves with the theoretical prediction of Fig. 1, we can clearly recognize the sharper transition, the lower switching power and the more complete switching associated with the square pulses. Note, however, that due to the finite rise and fall times the square pulses are not switched completely, and that the observed response tends to average over the oscillations predicted for cw signal. Switching occurred at peak level of about 90 KW.

Of practical importance is the question of crosstalk between channels in a self-switching environment. Consider a pulse stream which contains pulses of two kinds, having different peak intensities. The pulses are to be routed in the switch according to their intensity. Ideal square pulses can in principle be routed with only minimal crosstalk, if their amplitude are carefully chosen. It is clear, however, that in general there will be significant crosstalk. The most severe interference will be caused by the unswitched component of the high-intensity pulses. For example, to ensure better than 2:1 discrimination in the output pulse train, the intensity ratio at the input for two sech^2 pulses should exceed 2.3:1, whereas for square pulses with a rise time which is .2 of the pulse duration (similar to the pulses in our experiments) this ratio is only 1.37:1. To obtain a much better discrimination a fast rising square pulse is required. These considerations will be discussed in detail.

In conclusion, we have demonstrated ultrafast all-optical switching with femtosecond square pulses to overcome the pulse break-up problem. We have obtained steep switching curves and enhanced power transfer compared with those obtainable with standard pulses. Shaping of ultrafast optical pulses could prove to be an important tool to overcome some of the problems of all-optical photonic switching.

References:

1. S. M. Jensen, IEEE J. Quantum Electron. **QE-18**, 1580 (1982).
2. S. R. Friberg, A. M. Weiner, Y. Silberberg, B. G. Sfez, and P. W. Smith, Opt. Lett. 13, 904 (1988).
3. S. Trillo, S. Wabnitz, E. M. Wright, and G. I. Stegeman, Opt. Lett. **13**, 672 (1988).
4. A. M. Weiner, J. P. Heritage, and J. A. Salehi, Opt. Lett. **13**, 300 (1988).
5. A. M. Weiner, J. P. Heritage, and E. M. Kirschner, J. Opt. Soc. Am. B5, 1563 (1988).

Figures

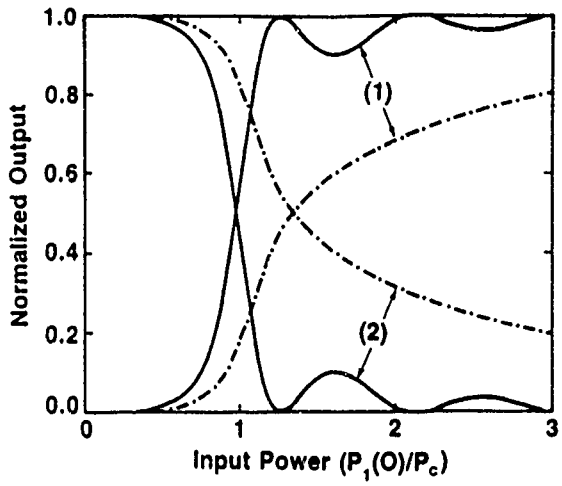

1. Calculated fractional output power emerging from the two cores. The power is in units of the critical switching power Pc. The solid line is the cw signal, the broken line is the response integrated over a $sech^2$ pulse intensity profile.

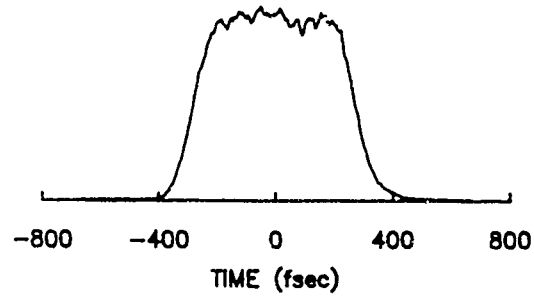

2. The cross correlation of a square pulse with a standard 90 fsec pulse.

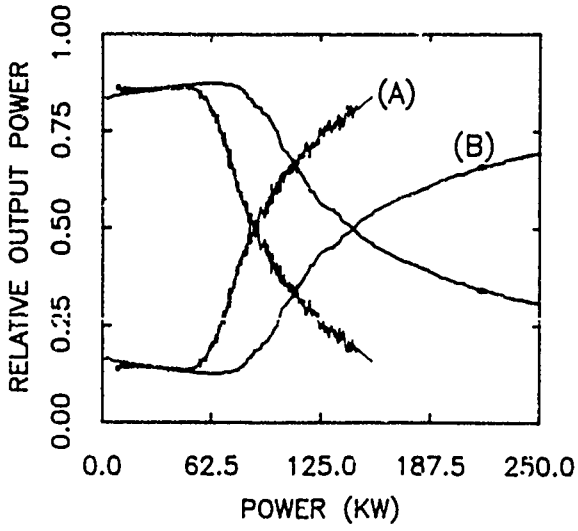

3. The measured fractional output power through the two cores as a function of peak intensity for (A): a 540 fsec long square pulse with 100 fsec rise and fall times, and (B): a 90 fsec long $sech^2$ pulse.

Novel, All-Optical, Kerr Amplification with Wavelength Switching, in a Single Mode Birefringent Fibre

A.S. Davison, I.H. White, Cambridge University Engineering Dept., Trumpington St., Cambridge, CB2 1PZ, United Kingdom

This paper reports for the first time, a novel, all-optical amplifier using a single mode optical fibre. The amplifier uses the Kerr effect to amplify an input optical signal, forming the output at the wavelength of the optical pump. The amplifier gain is proportional to the optical pump power, and can be varied at high speeds due to the ultra-fast response time of the optical Kerr effect. These characteristics are suitable for a broadband, low noise and very fast optical amplifier, appropriate to time division multiplexed signals and wavelength division switching. Although the threshold of other non-linear effects apart from the Kerr effect limits the amplification of a single stage device, a novel form of cascading these amplifiers is shown to greatly increase the potential maximum gain.

The apparatus used is shown schematically in Figure 1. The principle of the structure is similar to the ultrafast switching demonstrated by Morioka [1]. A strong optical pump is injected into the birefringent fibre with its polarisation at an angle of 45° to the fibre axes. A small optical signal, coupled onto one of the fibre axes, is able using the Kerr effect, to induce phase shifting and consequently polarisation rotation of the pump. A polariser converts this polarisation rotation to an amplitude modulation. At sufficiently high pump powers, the modulation depth becomes greater than the original signal power. Thus signal information is amplified and switched to a new carrier wavelength.

When the polarisation of the pump light from the output of the fibre is conditioned by direct phase control or a quarter-waveplate, it can be shown that the pump power transmitted through the polariser is given by

$$P_t = P_p/2 + \{ 2\pi n_2 P_p L / 3 \lambda A \} P_s = P_p/2 + P_m \qquad (1)$$

where n_2 is the Kerr coefficient, P_p, P_s and P_m are the pump, signal and modulated output powers, λ is the pump wavelength, A is the effective area of the fibre core and L is the length of the fibre. By using a sufficiently high pump power, $\{....\}$ is made greater than unity. Thus with the amplitude of the modulation P_m exceeding the input signal power, amplification is achieved, proportional to the power of the pump.

In the experiment to demonstrate the principle, the signal was generated by a diode laser of wavelength 1.3 μm. This signal modulated pump light from a NdYAG mode-locked laser of wavelength 1.064 μm, which coupled pulses with a peak-power of 8W into the birefringent fibre. The fibre used was only 38m long, highly birefringent, and had a small 4.5μm^2 elliptical core area with a high Germania content.

Figure 2 shows a typical trace of the modulation obtained using a slow rise time detector to smooth out the individual mode-locked pump pulses. A 6mW signal induced 0.15% modulation of the total pump power of 8W. Hence the modulation was 12mW, and the gain was 2. Walk-off between the components of the pump pulses on the birefringent axes, reduced the extinction ratio of the pump at the output to 2:1 and hence reduced the gain. Simple cut and

splice adaptions to the fibre, to improve the extinction ratio, would have raised the gain to 6.

In a single stage amplifier the pump power, and hence the gain, will ultimately be limited by other non-linear optical effects apart from the Kerr Effect, which introduce noise above a threshold pump power, due to random photon removal from the pump. In this case, the pump was limited to 8W by the cut-in of four photon mixing.

In general the gain limit may be improved, by dividing the length limit into a number of sections and cascading. Each axis of a birefringent fibre acts like a polarising filter, so splicing a second amplifier section to the first with the axes rotated by 45°, the polarisation rotation induced modulation appears on the birefringent components of the second fibre. After the first section, further modulation is self induced at the pump wavelength, rather than cross induced by the original signal.

If for a given pump power the maximum length due to non-linearities is L_{max}, then for an internally cascaded amplifier divided into n equal sections, the overall gain will be

$$G = (K L_{max} / n)^{n} \qquad (2)$$

where $K = 2\pi n_2 P_p / 3 \lambda A$. Figure 3 shows the rapid increase in gain that is possible as $K L_{max}$ increases. Such high gains will be stable because amplification only occurs in the forward direction.

Conclusion:

In conclusion therefore, a new form of optical amplification with wavelength switching has been demonstrated. The optical fibre device uses the Kerr effect to generate an amplified form of an optical input, the output being super-imposed on the optical pump signal. The gain of a single stage amplifier is limited by the cut in of other non-linear effects, but dividing into lengths and cascading the amplifier within that limit allows the possibility of much higher gain. The transmission characteristics of the amplifier are determined by the optical pump and can potentially be varied at ultra-fast rates.

Acknowledgements:

The authors would like to thank Dr. R. Dyott of Andrew Corporation for the supply of the fibre, and Mr. R.E. Epworth of STC Technology Ltd for the supply of diode lasers and fibre couplers, used in this experiment. We are grateful to the UK Science and Engineering Research Council and the Department of Education for N.Ireland for support.

Reference:

1 Morioka T., Saruwatari M., Takada A., Electron. Lett., 1987, 23, pp.453-454.

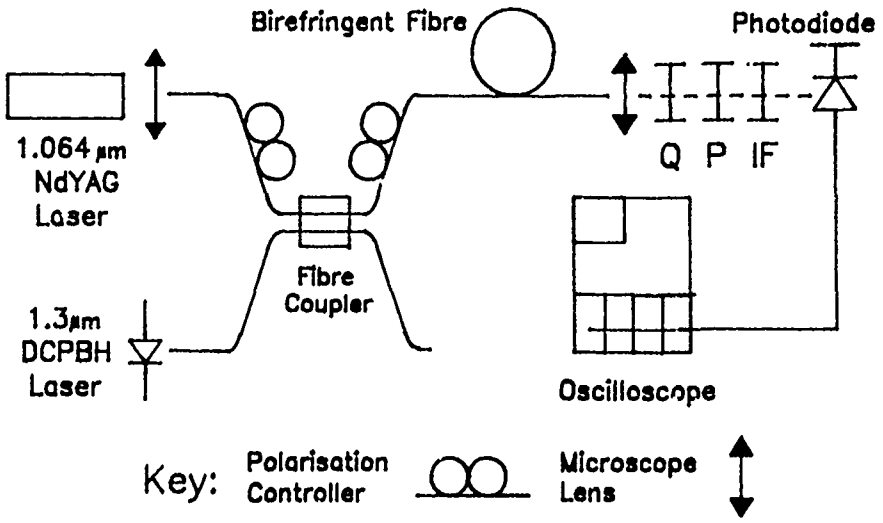

Figure 1. Schematic Diagram of Experimental Apparatus
Q = Quarter-wave Plate P = Polarising Filter
IF = Interference Filter

Figure 2.
Oscilloscope trace
of Kerr induced
modulation of high
power optical pump

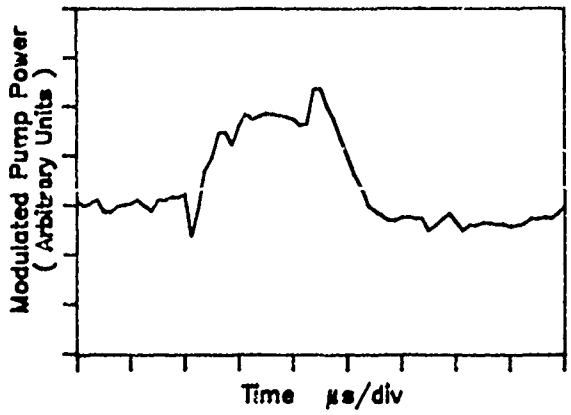

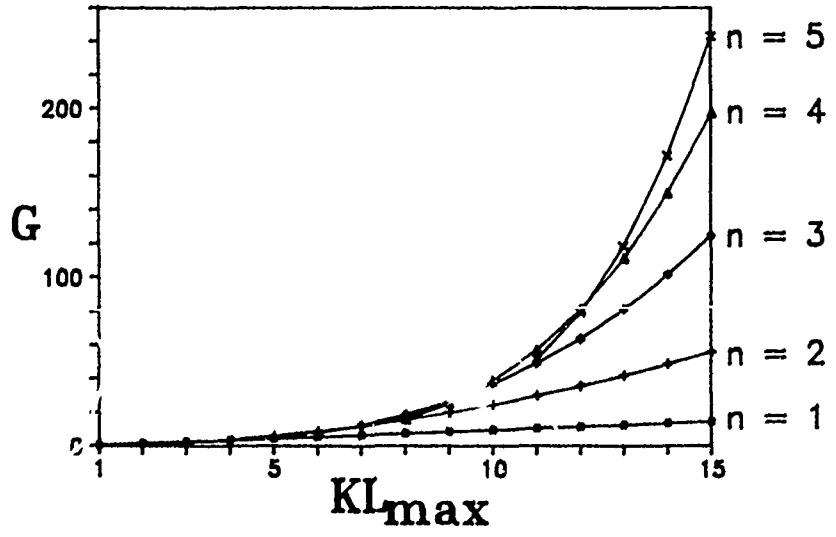

Figure 3. Gain limit G for n-stage amplifier vs gain limit for single stage amplifier KL_{max}

NOTES

THURSDAY, MARCH 2, 1989

SALON D

9:45 AM–10:30 AM

ThB1–ThB5

POSTER SESSION: 1

A Novel Optically Bistable Optoelectronic Device for Infrared Signal Processing

H.A. MacKenzie, A. Iltaif, J. Hughes, J.J. Hunter and D. Ronaldson

Department of Physics, Heriot-Watt University, Riccarton, Edinburgh EH14 4AS, Scotland, U.K.

Since the first observation of optical bistability in an InSb etalon (1) the device has been under continuous investigation and development. The long-term stability and reproducibility of the InSb system makes it ideal for the systematic study and optimization of bistable operating parameter both in single channel and array configurations (2). The refractive nonlinearity is electronic in origin so that the optical state of the bistable device may be controlled either by the photogeneration of carriers or, as we will describe, by the the direct injection of carriers from an electrode system. In the present work, we report, for the first time, the practical development of this concept to achieve an optically bistable optoelectronic (OBOE) device which can make complete and interactive communication between an all-optical element and conventional electronic circuitry and computing systems.

The well established all-optical switching characteristics of the InSb system have been retained throughout this work and, by fully optimizing the operating parameters (3), a new generation of low energy bistable switches have evolved. The etalon consists of a 50 μm thick wafer of n-type InSb with multilayer coatings to give a reflectivity of 85% at each face. The system was driven by a CO laser operating at an output frequency of 1927 cm^{-1} and, when the laser beam was focussed to a spot size of 40 μm diameter, bistable switching was achieved at an input power of 500 μW. The switch ON time was 100 nS and the switch OFF time was 200 nS. These switch times are a major improvement on previous results and are attributed to the dominance of

surface recombination processes in the photo-generated carrier dynamics due to the comparatively thin etalon. The consequent switching energy (50 pJ) per channel makes the array operation of such devices a feasible proposition. In addition, the inherent stability of the InSb system permits stable operation within 1% (5 μW) of the switch point and, since the electronic refractive nonlinearity is achieved in a region of very low optical absorption ($\alpha \sim 0.1$ cm^{-1}) minimal thermal dissipation results.

The bistable state of the device may be monitored electrically (4) and, typically, there is a 25 μV increment in the Hall-voltage when the system transfers between the ON and OFF states. In the present work, in addition to such a monitoring system, we have incorporated carrier injection contacts at the ends of the bistable etalon. When the system is optically biased close to the switch point with a CO laser beam, an electrical pulse to the injection electrodes creates sufficient carrier population in the optical beam region to achieve c.w. bistable switching, with indefinite hold in the ON state. The optoelectronic characterisation and optimization of the electrode assembly is presently under development.

A prolonged electrical pulse may also be used to switch the device OFF via the onset of the thermal nonlinearity (5) after which the device returns to the holding point.

Thus by electrical monitoring, injection switching and electro-thermal switch-OFF, the OBOE device is in complete interactive communication with external systems whilst retaining an all-optical signal processing capability. Thus, the optical state of the device may be both interrogated or commanded by conventional electronics and computing making it a useful new component in optical computing architecture. This OBOE device will be developed in an array format to create an intelligent detector interface for

pattern recognition, optical signal processing and encoding. Other applications including spatial light modulation and adaptive optics are being investigated.

References:

(1) D.A.B. Miller, S.D. Smith and A.M. Johnston
App. Phys. Lett., 35, 658 (1979).

(2) J. Young, H. Richardson, H.A. MacKenzie and E. Abraham
J. Opt. Soc. Am. B., 5 3 (1988).

(3) B.S. Wherrett, D. Hutchings and D. Russell
J. Opt. Soc. Am. B., 3 (1986).

(4) H.A. MacKenzie, G.R. Allan, J.J. Hunter, D.C. Hutchings and B.S. Wherrett
Opt. Comm. 63, 73 (1987).

(5) H.A. MacKenzie, J.J.E. Reid, H.A. Al-Attar and E. Abraham
Opt. Comm. 60, 181 (1986).

An optical bistable switch based on self-focusing in an artificial Kerr medium

N. P. Walker
Department of Physics, Kings College,
Strand, London, WC2R 2LS, UK

D. R. Drury & M. A. Fiddy
Department of Electrical Engineering, University of Lowell,
Lowell, MA 01854, USA

Seven years ago an optically bistable device based on the self-focusing properties of light in a nonlinear medium was proposed and demonstrated[1]. It was shown that by reflecting a self-focused beam back on itself, the device would exhibit hysteresis; a simple theoretical model was later developed in order to explain the performance characteristics of the device[2]. Unfortunately, reflecting a fraction of what would otherwise be an output signal back on itself significantly reduces the efficiency of this particular arrangement. In this letter a new design is proposed in which the feedback and output signals are combined, thus increasing the efficiency of a device based on the same basic principle.

In the demonstration of the original device[1], sodium vapour was used as the nonlinear optical medium. Later, using a slightly modified design, it was show that a liquid suspension of dielectric particles could be used as the nonlinear medium[3]. The input lens focuses the incident light on to the face of the cell containing the nonlinear medium. At input powers below some critical threshold power, P_{cr}, required for self-focusing to occur, the beam diverges. Only a small fraction of the incident beam is imaged by the output lens to pass through the detector aperture. At input powers above P_{cr}, self-focusing will occur and the beam will then follow the path indicated by the solid line. The output lens now focuses a large fraction of the incident beam onto the detector. The exit face of the cell containing the nonlinear medium was a 95% reflecting mirror, from which it follows that for the self-focused case, 95% of the incident illumination is reflected back on itself thus reinforcing the self-focusing effect due to the nonlinearity. This feedback mechanism indicates that it is possible to maintain the self-focused and high output state for incident power levels that drop below P_{cr}. It is this mechanism that leads to bistability.

One of the advantages of a device based on self-focusing, is that its operation is not dependant on on the presence of a resonant optical cavity. This removes restrictions on the frequency and bandwidth of the light used, offering the possibility for broad band operation. As was pointed out previously, one of the disadvantages of this design is that the percentage of the input power that can be transmitted in the high output state is limited by the highly reflecting mirror at the exit of the cell. With a 95% reflecting mirror, the transmitted percentage can be at best 5% of the incident power. However, a simple modification to the design can lead to an increase in this percentage.

Consider an input beam is focused by a lens on to a concave mirror to a point inside the cell. For input powers above some P_{cr}, self-focusing will occur and the beam can be confined to a narrow filament that is subsequently reflected back on itself from a small diameter mirror at the entrance surface of the cell. The self-focused beam can then pass through an aperture in the concave exit mirror to an output detector. For input powers below P_{cr}, the incident beam will pass through the focal point within the cell and diverge significantly, before impinging on the small diameter mirror. Consequently, little light will be reflected by this mirror and subsequently pass through the aperture in the exit mirror. The reverse path taken by the self-focused beam, between the focal point and the small mirror, provides the feedback and thus reinforcement of the nonlinear process that results in the hysteresis.

With the design proposed here, 100% of the incident light reflected by the small mirror is used in the feedback process and contributes to the output signal. This is to be compared with the 95% to 5% split in energy arising with the original design.

Self-focusing or self-trapping has been reported using liquid suspensions of dielectric particles, the beam diameter being of the order of $2\mu m$[4]. We describe results based upon a cell of the kind described above, and in which artificial Kerr media are used as the nonlinear medium. We present an evaluation of the performance characterisitics of the device as a function of the properties of the particle suspensions used as the Kerr media.

References

1. J. E. Bjorkholm, P. W. Smith, W. J. Tomlinson and A. E. Kaplan," Optical bistability based on self-focusing", Opt. Lett., **6**, 345, (1981).

2. J. E. Bjorkholm, P. W. Smith and W. J. Tomlinson, " Optical bistability based on self-focusing: an approximate analysis" , IEEE J. Quantum Electron., **QE-18**, 2016, (1982).

3. P. W. Smith, A. Ashkin, J. E. Bjorkholm and D. J. Eilenberger, " Studies of self-focusing bistable devices using liquid suspensions of dielectric particles", Opt. Lett., **10**, 131, (1984).

4. A. Ashkin, J. M. Dziedzic and P. W. Smith, " Continuous-wave self-focusing and self-trapping of light in artificial Kerr media", Opt. Lett., **7**, 276, (1982).

Time Response of a Crossed Resonator

B. A. Capron, M. W. Derstine and D. A. Holm
Boeing Electronics High Technology Center
P. O. Box 24969 MS 7J-27
Seattle, Wa. 98124-6269

INTRODUCTION

A device consisting of two intersecting Fabry-Perot etalons filled with a nonlinear medium has the potential of a useful optical switch. In this device the light in one cavity (referred to as the control) tunes the other cavity and controls the emerging beam (referred to as the bias). Such a device has several advantages over the more conventional single nonlinear Fabry-Perot. It can be used in a three-dimensional geometry separating the output from the input and thereby acts as a true three port device. A theoretical model of the steady state performance[1] shows that the power output *vs.* power input characteristic curve has both a sharper turn on and flatter wings allowing for less sensitivity to the input power. These are desirable characteristics for an optical switch. However, any realistic architecture using such a device would require pulsed inputs to impress information on the signal as well as for energy considerations. We have developed a time-dependent model of the crossed resonator and present sample curves showing the gain achievable for both pulsed and sinsusoidal inputs.

THEORY

The starting point for the theoretical model is the steady-state model developed earlier.[1] The medium is assumed to have a Kerr-like nonlinearity such that its index of refraction varies like $n = n_0 + n_2 I$ where n_0 is the background index, n_2 the nonlinearity and I is the intensity. An intensity independent absorption is also assumed. In the new model presented here, the full time dependence of the input fields and phases are allowed. The dependence of the phase on the medium response time is described by the Debye equation:

$$\tau_d \frac{\partial \Delta\phi_{1,2}}{\partial t} + \Delta\phi_{1,2} = c_{11,21} I_1 + c_{12,22} I_2$$

where the subscripts 1,2 refer to the bias and control beams, τ_d is the medium response time, $\Delta\phi$ is the nonlinear phase change, I is the transmitted intensity and the c's are functions of the material parameters such as α, n_2, the mirror reflectivities, and the operating wavelength. Instead of using the method of integrating the Debye equation and summing up all the reflected waves within the cavity,[2] we derive and solve difference equations describing the intracavity fields and use the Fabry-Perot boundary conditions to obtain the transmitted and reflected intensities. This method is less computationally intensive and in the limits assumed, both methods are equivalent.

EXAMPLES

We solve the equations for a number of interesting cases and show here two representative examples for integrated optic geometries. The first example is for both bias and control beams that are gaussian functions of time. This configuration allows net gain in that the difference in the output energy between cases with and without a control beam is much larger than the energy of the control beam. Fig. 1 illustrates such a case using parameters appropriate for the nonlinear organic polymer polydiacetylene. The transmitted intensity is shown for the case of no control beam as well as with a control beam. The gain for this example is around 7. It is useful to note that the transmitted beam does not break up as has been shown to occur in coupled mode geometries[3] and thus can be used as the input to another device. We examine the influence of the device parameters such as pulse duration, medium response time and pulse timing on the output intensity. Fig. 2 illustrates examples of a constant bias pulse with a sinusoidally modulated control pulse. For this configuration the gain is defined as the ratio of the output modulation to the input modulation. As expected, for the two input modulation frequencies in the example (8 and 16 GHz) the gain is reduced at the higher frequency. Through analysis of this configuration we determine useful gain-bandwidth figures of merit for the device as a function of model parameters.

CONCLUSIONS

We have developed a time dependent model for the crossed resonator device. As an optical switch, this device has several advantages over a single Fabry-Perot. We model the performance of the device for different forms of input pulses and examine the device figures of merit such as gain and gain-bandwidth products as a function of device parameters.

REFERENCES

1. Capron, B. A. and Holm, D. A., *Crossed resonator configurations for photonic switching*, Optical Society of America Annual Meeting, paper TuG6, November, 1988.

2. Bischofberger, T. and Shen, Y. R., *Theoretical and experimental study of the dynamic behaviour of a nonlinear Fabry-Perot interferometer*, Phys. Rev. A **19**, 1169, (1979).

3. Trillo, S. *et al.*, *Experimental observation of polarization instability in a birefringent optical fiber*, Appl. Phys. Lett. **49**, 1224, (1986).

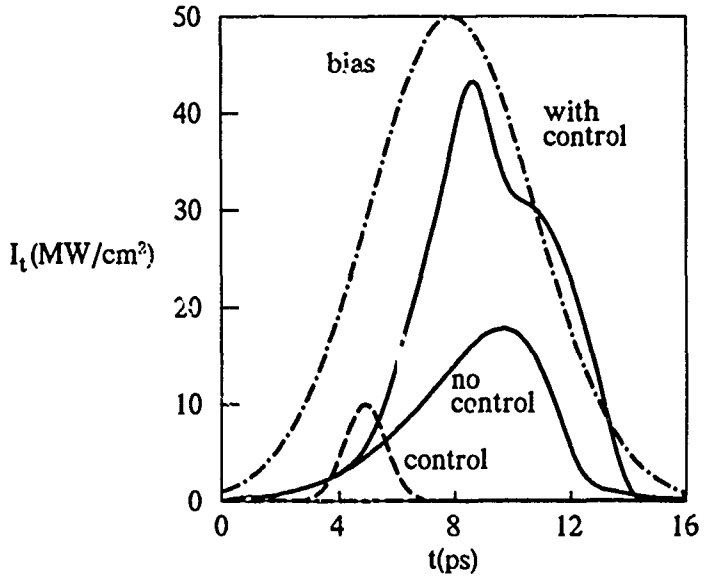

Fig. 1. Output intensity (solid curves) with and without control pulses for bias pulse of 50 MW/cm² and 8 ps (dot-dashed curve) and a control pulse (dashed curve) of 10 MW/cm² and 2 ps. The nonlinear index is 5.9 x 10^{-6} cm²/MW, the medium response time is 0.25 ps. and the cavities are 10 μm long. The gain is 7.3.

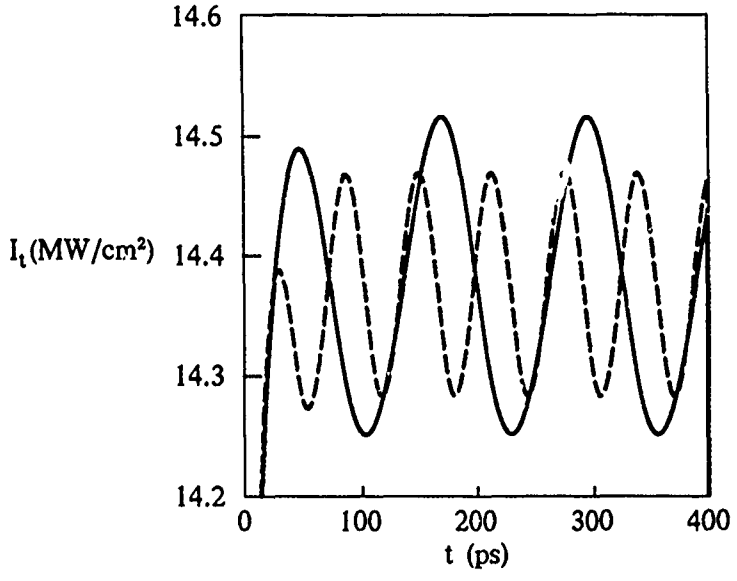

Fig. 2. Transmitted outputs for two sinusoidal control inputs at different frequencies. The cavity parameters are the same as in Fig. 1. The bias pulse is constant at 50 MW/cm². The control pulses have a DC value of 1.64 MW/cm² and peak-to-peak modulation of 0.02 MW/cm². The solid line represents the output for an input frequency of 8 GHz and the dashed line for a frequency of 16 GHz.

A pnpn Light-Emitting Optical Switch

J. I. Pankove, R. Hayes, A. Majerfeld,
M. Hanna, E. G. Oh, D. M. Szmyd, D. Suda
Center for Optoelectronic Computing Systems,
University of Colorado at Boulder
Boulder, Colorado 80309-0425

S. Asher, R. Matson
Solar Energy Research Institute
Golden, Colorado 80401

D. J. Arent, G. Borghs
IMEC
Leuven, Belgium

M. G. Harvey
David Sarnoff Research Center
Princeton, New Jersey 08540

1. INTRODUCTION

The pnpn optical switch was devised in response to the needs of optical computing. The device should emit light in response to incident light, emitting more light than incoming light, and it should be capable of synchronization. The present device is a photothyristor, wherein the detector and emitter functions are integrated into a single body. The device can be made into a laser to insure the desired optical gain. It turns out that, although the device can respond to the same wavelength as it emits, it can also respond to other wavelengths, which may be useful in architectures involving parallel processing at different wavelengths with intersecting networks.

2. DEVICE STRUCTURE AND OPERATION

In our pnpn light-emitting optical switch, the inner two layers are made of a direct-gap semiconductor, while the outer two layers are made of a wider-energy-gap material.

In operation (Fig. 1), the central pn homojunction is reverse-biased, while the outer two heterojunctions are forward-biased. Most of the applied voltage appears across the central pn junction. As the applied voltage is increased, breakdown eventually results from either avalanching (when a critical field is exceeded at the reverse-biased junction), or from punch-through (when a depletion layer extends to the nearest forward-biased heterojunction).

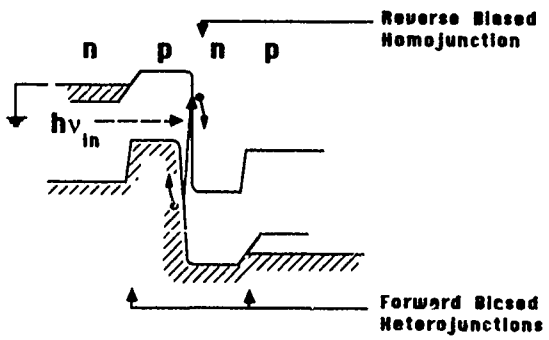

Fig. 1. Energy-band diagram of biased optical switch showing carrier generation in the reverse-biased pn junction.

After breakdown, double injection occurs, flooding the central, narrower gap region with electrons and holes that are stopped by the potential barriers at the heterojunction, as shown in Fig. 2. This is the same carrier-confinement condition obtained in double-heterojunction injection lasers. And, in fact, with a proper Fabry-Perot cavity, the device should lase. If the applied bias

does not exceed the breakdown voltage, breakdown can be induced by irradiating the device with photons that can be absorbed in the narrower gap region. The presence of a high electric field in the junction lowers the photon energy to which the device is sensitive (Franz-Keldysh effect) (1). Essentially, the absorbed photons produce electron-hole pairs that are separated by the electric field. These charges accumulate on either side of the pn junction, lowering the potential barrier to the injection of carriers from the outer layers. Then double-injection occurs. The sensitivity of the device to the exciting light can be adjusted by the voltage applied across the device.

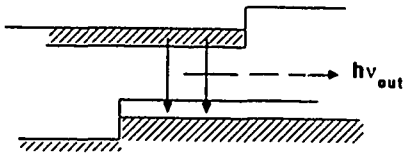

Fig. 2. Energy-band diagram of device of Fig. 1 after breakdown. Cross-hatched regions represent electrons.

A search of prior art revealed that, in 1972, a pnpn laser structure was first demonstrated by Alferov et al. (2). Improved structures were made in 1974 by Lockwood et al. (3) as well as by Alferov et al. (4) It consisted of two GaAs inner layers and GaAlAs outer layers deposited by liquid-phase epitaxy on GaAs. The device operated as a laser, emitting pulses with rise- and fall-times of less than 30 nsec. When the device was switched optically by another light source, an optical gain of 10^4 was obtained. Copeland et al. (5) built another variation of this structure, with an etched well to receive the triggering light pulse from an optical fiber; a second optical fiber could carry out the emitted light. This device worked as an optical repeater, but it was not structured as a laser. Lee et al. (6) built still another variation of the pnpn optical switch, where two narrow-gap layers were spaced by a wider-gap central section, thus forming two thinner carrier-confinement regions to reduce the threshold current and increase the breakdown voltage; however, this device was not operated with optical input.

Although the fundamental principle of the pnpn optical switch has been demonstrated, this device has not been developed into a commercial product. Perhaps this development is waiting for the optoelectronic computer as its customer.

3. DEVICE FABRICATION

We have grown pnpn structures both by metalorganic chemical vapor deposition (MOCVD) and by molecular beam epitaxy (MBE) in the GaAs/GaAlAs lattice-matched system. A thin capping layer of heavily doped GaAs is used as a final layer of the structure. Finally, both surfaces are metallized. Then the wafer is cleaved into parallelepipeds that are mounted on a copper heat sink. Other materials for other spectral ranges are possible. With a well etched into the GaAs substrate, the device works as a surface-emitter. If the opposite edges of the structure are cleaved to form a Fabry-Perot cavity, the device can operate as a laser.

The device can be addressed by one or more input optical fibers, as shown in Fig. 3. The output is channeled into one or two output optical fibers which can be organized according to the signal-processing requirements.

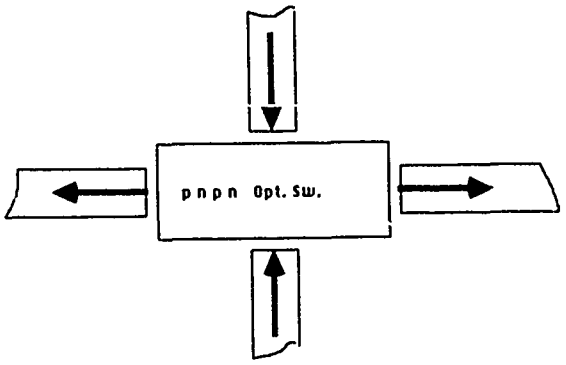

Fig. 3. Optical fiber coupling to pnpn device.

4. DEVICE PERFORMANCE

The I(V) characteristics of a typical device are shown in Fig. 4. A current-controlled negative resistance is obtained when the breakdown voltage is exceeded. In the presence of external illumination, the breakdown voltage is reduced. In the broken-down mode, injection luminescence is obtained that can be monitored with an image converter or measured with a spectrometer, as shown in Fig. 5.

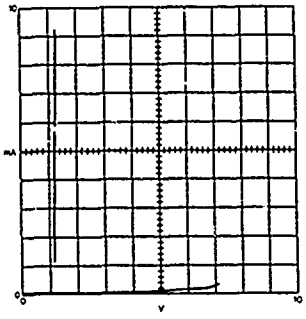

Fig. 4. I(V) dark characteristic of typical device.

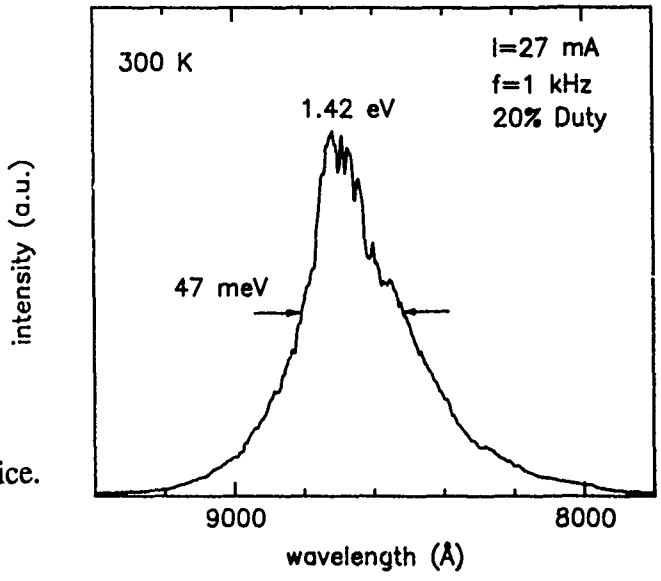

Fig. 5. Light-emission spectrum from pnpn optical switch.

The optical switching effect that we obtained is demonstrated in Fig. 6. The pnpn device is mounted in tandem with a laser diode operated in the LED mode. A biasing pulse 400 nsec long is applied to the pnpn device. Another pulse 80 nsec long is applied to the LED. At low voltage across the LED, the pnpn device sustains the sub-breakdown voltage (Fig. 6a). When the LED intensity is increased, the pnpn device switches into the conducting mode and the voltage drops to the 1.4-volt sustaining value (Fig. 6b). The LED pulse can be translated in time with respect to the pnpn device biasing pulse. This causes the breakdown and consequent light-emission to follow the position of the LED pulse. The rise and fall times of light emission are less than 10 nsec, instrument-limited.

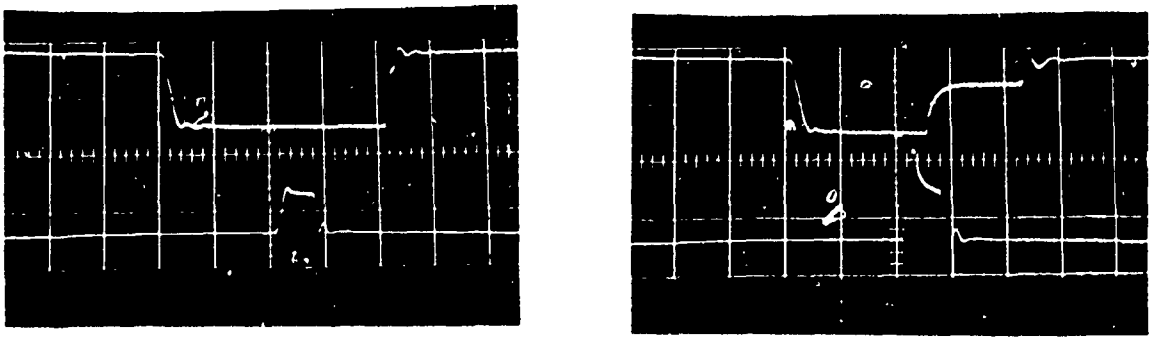

Fig. 6. Time-dependence of voltage applied across pnpn device (upper curve) and of voltage applied across triggering pn diode: a) low drive across diode does not disturb pnpn device; b) high drive across diode causes switching of pnpn device. Scale 100 ns/div. and 2V/div.

5. FUTURE PROSPECTS

The pnpn optical switch is essentially a threshold device. For a given electrical bias, the breakdown depends on the light input's exceeding a threshold value. This threshold can be achieved by the summation of several simultaneous optical inputs that may occur at different wavelengths. In this sense, the device already has the logical functions: AND, OR. To make the device more useable, one will need to address the problem of "pig-tailing" in order to attach optical fibers for input/output interconnections. Since the dimensions of the device are comparable to the cross-section of the optical fiber, mounting the device will be a non-trivial problem. Heat dissipation and thermal stability will be another area of concern. Eventually, switching speed will become a limitation. There, one has the option of compromising between carrier lifetime and incorporating luminescence efficiency. For faster operation, the lifetime can always be degraded by incorporating deep impurities or lattice damage. Finally, it is possible to make linear arrays of such devices for optical crossbar applications, and in the surface-emitting configuration, an x-y–addressed, 2-D array should be feasible.

6. CONCLUSION

A semiconductor optical switch is under exploration to satisfy the needs of optical computing. The device is electrically biased and emits light when stimulated by light. The input can be at the same or at a different wavelength than the output light. Optical gain of 10^4 and response times of 30 nsec have been reported in the past for such devices. We expect to exceed this performance – the response time is already shorter (≤10 nsec) – and we intend to provide computer architects with easy-to-use components.

7. ACKNOWLEDGMENTS

This work was supported at the University of Colorado by NSF grants #ECE-8616908 and #CDR-8622236. We are grateful to the managements of SERI, DSRC and IMEC for their valuable contributions.

8. REFERENCES

1. L. V. Keldysh, *Soviet Physics–JETP* 7, 788 (1958); W. Franz, *Z. Naturforsch.*, 13a, 484 (1958).
2. Zh. I. Alferov, V. M. Andreev, V. I. Korol'kov, V. G. Nikitin, E. L. Portnoi, and A. A. Yakovenko, "Recombination Radiation Emitted by Four-Layer Structures Based on GaAs-AlAs Heterojunctions," *Soviet Physics-Semiconductors* 6 (1972).
3. H. Lockwood, K.-F. Etzold, T. E. Stockton, and D. P. Marinelli, "The GaAs P-N-P-N Laser Diode," *IEEE J. of Quantum Electron.* QE-10, 567 (1974).
4. Zh. I. Alferov, F. A. Akhmedov, V. I. Korol'kov, and A. A. Yakovenko, "Electroluminescent photothyristors based on GaAs-AlAs heterojunctions," *Sov. Phys. Semiconductors* 8, 1741 (1974).
5. J. A. Copeland, A. G. Dentai, and T. P. Lee, "p-n-p-n Optical Detectors and Light-Emitting Diodes," *IEEE J. of Quantum Electron.* QE-14 , 810 (1978).
6. C. P. Lee, A. Gover, S. Maragalit, I. Samid, and A. Yariv, "Barrier-controlled low-threshold PNPN GaAs heterostructure laser," *Appli. Phys. Lett.* 30, 535 (1977)
7. S. M. Sze, Physics of Semiconductor Devices, Second Edition, Wiley, 1981, Chapter 4.

Photonic Switching in InGaAsP Dynamic Memory Devices

W. Kowalsky, M. Port, K. J. Ebeling

Institut für Hochfrequenztechnik
Technical University of Braunschweig
D-3300 Braunschweig
Federal Republic of Germany

The dynamic memory characteristics of InGaAsP photonic switching devices are investigated. An on-off-ratio of 5.5 : 1 and hold time greater than 10 ns enable clocked data processing.

Optically controllable gates are of decisive importance for the implemation of logical operations in all-optical data processing. Promising approaches to matrices of switching devices operated at incidence normal to the surface for processing in parallel have been demonstrated [1 - 4]. Buffered information input and output as well as clocked data processing cycles can be attained by additional use of optical memory devices. Static memory elements have been realized by optically bistable switches [5 - 7]. In the present paper we explore dynamic memory characteristics of InGaAsP switching devices. We achieve a hold time greater than 10 ns which enables clocked data processing. A switching contrast of 5.5 : 1 is demonstrated with negligible insertion loss in the on-state. A basic analysis in terms of ambipolar diffusion provides a good description of the dynamic memory characteristics.

Fig. 1 illustrates clocked data processing in the InGaAsP photonic switching device. A Control (write) and a signal (read) beam are focused on to the surface to overlap. The focal diameter is about 4 μm. The signal light pulses with wavelength $\lambda_t = 1.3\mu m$, close to the fundamental absorption edge of the InGaAsP compound are nearly completely absorbed in the epilayer but pass the larger band gap InP substrate without additional attenuation. The switching state of this photonic switch is controlled by an advanced control pulse of same or different wavelength λ_c. Underlaying mechanism is dynamic band filling [8]. Excess carriers generated by the control pulse reduce the absorption coefficient at the test wavelength and thus switch to the on-state. The hold time is determined by excess carrier lifetimes and ambipolar diffusion.

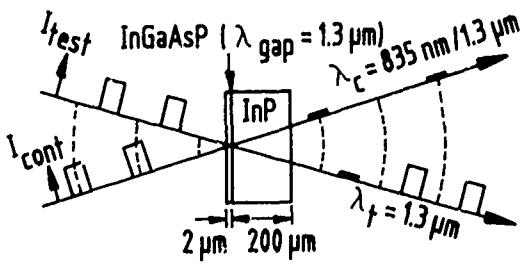

Fig. 1 Schematic of clocked data processing in the InGaAsP photonic switching device.

In the experiments a control pulse of power P_c with τ_c =10 ns width at $\lambda_c = 835nm$ wavelength is used. By continuous delay of the 200 ps test pulse P_c the dynamic memory characteristics are derived. Fig. 2 shows the modulation depth given by

$$m = \frac{P_t(P_c) - P_t(P_c = 0)}{P_t(P_c)} \tag{1}$$

and the on-off-ratio in dependence on delay time. During the control pulse modulation increases with growing excess carrier concentration. Beyond the control pulse efficient modulation is detected for more than 10 ns. A 3 dB decrease is observed after 15 ns. This memory effect is due to excess carrier lifetimes but is reduced by carrier diffusion. Equivalent experimental results are achieved using the same wavelength for test- and control beam. As depicted in Fig. 3 modulation depth exceeds 50 % and a 3 dB hold time of more than 10 ns is observed which should be sufficient for clocked optical data processing.

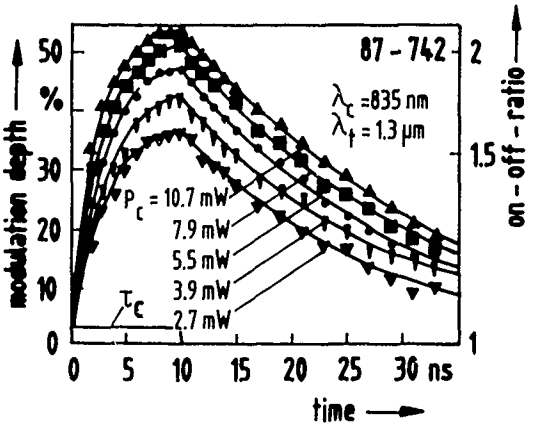

Fig.2 Modulation characteristics in dependence on delay time for a control pulse of τ_c = 10ns width.

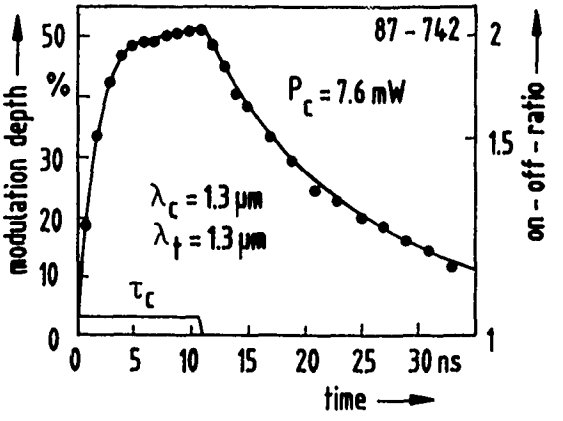

Fig.3 Modulation depth as a function of delay time using the same wavelength for test- and control beam.

In the on-state the insertion loss of the switching devices is negligible. Total bleaching of InGaAsP epitaxial layers is achieved experimentally by a reduced spot size of 2 μm. The modulation depth in dependence on control power is depicted in Fig. 4 for two InGaAsP epitaxial layers of different thicknesses d and slightly varying absorption coefficients α_0 at the test wavelength λ_t ($87 - 742 : d = 2.2\mu m, \alpha_0 = 5500cm^{-1}$, 88-858 : d = 3.5 μm, $\alpha_0 = 6000cm^{-1}$). The modulation depth increases considerably with control power but then saturation is observed at about $m = 72\%(82\%)$ corresponding to an on-off-ratio of 3.5:1 (5.5:1) with epitaxial layer no. 87-742 (88-858). From the material properties an insertion loss in the off-state of 5.3 dB (9 dB) is derived limiting the modulation to $m \approx 70\%(87\%)$ for total bleaching. These theoretical estimates are in good agreement with the experimental results confirming the negligible insertion loss in the on-state. Thus a suitable switching contrast can be obtained by optimization of layer thickness and composition and even at large on-off-ratios total bleaching is achieved at low control power levels.

For estimating the dynamic memory characteristics and the switching contrast theoretically we assume carrier induced absorption change [9] which can be approximated by

[10]

$$\frac{\Delta\alpha}{\alpha_0} \approx \frac{-\Delta n}{n_0 + \Delta n + N_c \exp(\frac{\hbar\omega_l - W_g}{kT})}, \tag{2}$$

where $\Delta\alpha$ denotes the absorption change, $n_0 \approx 10^{16} cm^{-3}$ the electron concentration of the epilayer, $N_c \approx 3 \cdot 10^{17} cm^{-3}$ the effective density of states in the conduction band, and Δn the excess carrier density. The band gap energy $W_g \approx 0.95eV$ is derived from absorption measurements in dependence on wavelength. Assuming carrier profile flattening in depth by diffusion and a Gaussian-distribution of the intensity in the control beam results in a spatial profile of the excess carrier generation rate

$$G(r) = G_0 \exp(-(r/a)^2) \tag{3}$$

with

$$G_0 = \frac{\hbar P_c}{\hbar\omega_c \pi a^2 d} \tag{4}$$

where $a = 2\mu m$ is the radius of the optical spot. Starting from the continuity equations of ambipolar diffusion [11] a rough estimate for Δn is obtained as

$$\Delta n = \Delta p = \begin{cases} \frac{G_0}{f}(1 - \exp(-ft)) \exp(-(r/a^2) & \text{for } t \leq \tau_c \\ \frac{G_0}{f}(\exp(f\tau_c) - 1) \exp(-ft) \exp(-r/a^2) & \text{for } t > \tau_c \end{cases} \tag{5}$$

with

$$f = \frac{1}{\tau} + 0.3\frac{4D_a}{a^2}. \tag{6}$$

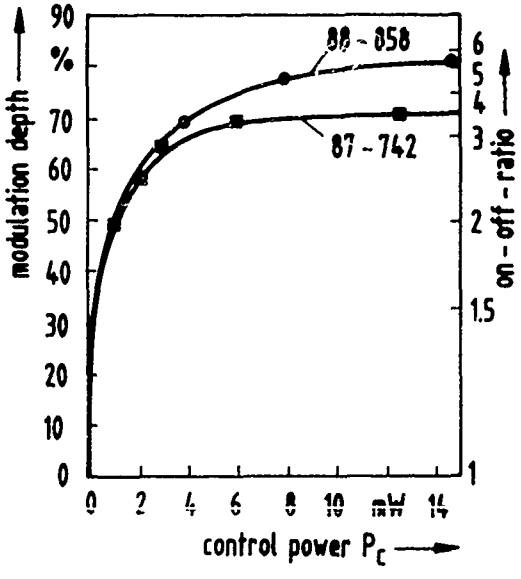

Fig.4 Control power dependence of modulation depth. Total bleaching of the epitaxial layers is achieved at about $P_c = 10$mW.

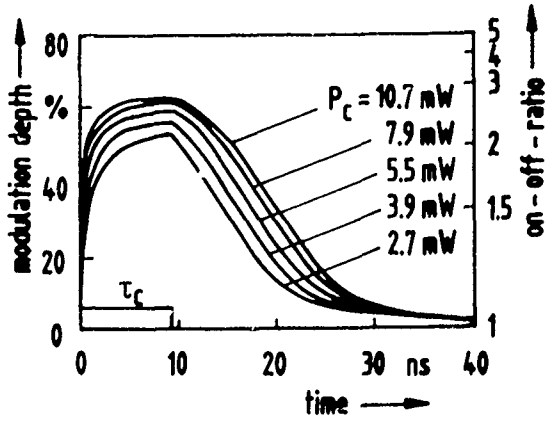

Fig.5 Theoretical description of the dynamic memory characteristics.

The ambipolar diffusion coefficient D_a is given by

$$D_a = \frac{\Delta p + (n_0 + \Delta n)}{\Delta p/D_n + (n_0 + \Delta n)/D_p}. \tag{7}$$

We use $D_n \approx 110 cm^2/s$ and $D_p \approx 3.75 cm^2/s$. Theoretical results assuming an excess carrier lifetime of $\tau = 30$ ns are depicted in Fig. 5. Modulation depth and dynamic memory characteristics are in good agreement with the experimental observations given in Fig. 2.

To conclude, we have investigated dynamic memory characteristics in InGaAsP photonic switching devices. The hold time of more than 10 ns due to excess carrier lifetimes enable clocked data processing. An on-off-ratio of 5.5 : 1 is achieved using an InGaAsP epitaxial layer of 3.5 μm thickness. Total bleaching of the epilayer is attained at a few mW control power. Thus the insertion loss of the switching device in the on-state is negligible. Because of the low control power level and the large switching contrast this device is well suited for parallel optical data processing.

We gratefully acknowledge the financial support by the Stiftung Volkswagenwerk and the Deutsche Forschungsgemeinschaft.

References

[1] G. D. Boyd, D. A. B. Miller, D. S. Chemla, S. L. McCall, A. C. Gossard, J. H. English, Appl. Phys. Lett. 50 (1987) 1119.

[2] J. L. Jewell, A. Scherer, S. L. McCall, A. C. Gossard, J. H. English, Appl. Phys. Lett. 51 (1987) 94.

[3] D. Hulin, A. Mysyrowicz, A. Antonetti, A. Migus, W. T. Masselink, H. Morkoc, H. M. Gibbs, N. Peyghambarian, Appl. Phys. Lett. 49 (1986) 749.

[4] W. Kowalsky, T. Hackbarth, K. J. Ebeling, 14th European Conference on Optical Communication, Brighton (1988) 308.

[5] D. A. B. Miller, D. S. Chemla, T. C. Damen, T. H. Wood, C. A. Burrus, A. C. Gossard, W. Wiegmann, IEEE J. Quant. Electron. $QE-21$ (1985) 1462.

[6] D. A. B. Miller, J. E. Henry, A. C. Gossard, J. H. English, Appl. Phys. Lett. 49 (1986) 821.

[7] G. Livescu, D. A. B. Miller, J. E. Henry, A. C. Gossrad, J. H. English, Opt. Lett. 13 (1988) 297.

[8] W. Kowalsky, K. J. Ebeling, Opt. Lett. 12 (1987) 1053.

[9] R. N. Hall, Solid State Electron. 6 (1963) 405. A. Yariv, Quantum Electronics, 2nd ed. (Wiley, New York, 1975) Chap. 10.

[10] W. Kowalsky, Appl. Phys. B 46 (1988) 27.

[11] K. Seeger, *SemiconductorPhysics* (Springer, Berlin, New York).

NOTES

THURSDAY, MARCH 2, 1989

SALON E

10:30 AM–12:00 M

ThC1–ThC5

FREE-SPACE SYSTEMS

A. L. Lentine, AT&T Bell Laboratories, *Presider*

FREE-SPACE OPTICAL SYSTEMS FOR SWITCHING, INTERCONNECTIONS, AND COMPUTING

B. Keith Jenkins
Signal and Image Processing Institute
University of Southern California
Los Angeles, CA 90089-0272

The use of free-space optical systems for photonic switching, optical and hybrid computing is discussed, including architectural tradeoffs and comparisons with electronics.

OPTICAL INTERCONNECTION NETWORKS EMPLOYING MULTIPLEXED CROSSPOINTS.

P. Healey.

Department RT2141, British Telecom Research Laboratories,
Martlesham Heath, Ipswich, UK., IP5 7RE.

Abstract:

New multi-stage image switching networks employing spatially multiplexed crosspoints and birefringent interconnects are described which simultaneously reduce both the crosspoint count and the switch control complexity to the theoretical minimum. The networks may be one-sided or two-sided, and both types are non-blocking in the strict-sense.

Introduction:

In a recent article [1] the author has demonstrated that the additional degrees of freedom available to the optical systems designer can be exploited in the realisation of highly-efficient optical switching networks. The spatial/angle multiplexing power of optics, combined with polarisation switching and routing, can lead to dramatic simplifications in hitherto unrealistic electro-mechanical/electronic switching network designs. For example, the simultaneous minimisation of crosspoint count and control complexity, for a strict-sense non-blocking generalised interconnection network, is now realisable for the first time [1].

The basic principle of crosspoint minimisation is based on spatial multiplexing, as shown in Fig 1. The lenses perform a 'wiring' function between the switch 'contacts' and its terminals, while polarisation is employed as the switching and routing mechanisms. This simple optical circuit is equivalent to a relay with many thousands of broad band changeover contacts. Clearly, the spatial multiplexing power of optics has allowed a vast saving in the number of physical crosspoints required, and furthermore, the interconnection power of optics has eliminated the wiring problem. The small physical size of the Fourier plane polarisation modulator/crosspoint is also compatible with high speed operation.

Architectures:

Similar multi-pole changeover 'relays' can be incorporated in the following switching network architectures:-

(i) Shannon's minimum separate memory Exchange [1,2],
(ii) passive splitter/active combiner [1,3],
(iii) active splitter/passive combiner [1], and
(iv) active splitter/active combiner [1,3].

Networks (i) (ii) and (iii) achieve the theoretical minimum control complexity and, by using multiplexed crosspoint, the theoretical minimum number of physical crosspoints. Networks (iii) and (iv) are binary self routing, and all four are strictly non-blocking. With optics, the switched circuits can comprise single beams or two-dimensional images (for example; 64 Bit computer data bus's) with no increase in crosspoint count or control complexity. A Generalised NxN connection network, such as (ii), is capable of implementing any mapping of inputs onto outputs (N^N settings) and may be used for one-to-one and one-to-many type communications [4]. (See Fig 2) The total number of controls and crosspoints in a generalised optical interconnection network employing multiplexed crosspoints is the theoretical minimum of only $N\log_2 N$. The minimum loss, however, is $10\log_{10} N$

(dB), due to the passive input signal distributors. Network (iv) eliminates this loss, and 1-st order crosstalk but, can only perform one-to-one permutations (ie, N! settings).

Optical Implementations:

A generalised interconnection network based on the components described in this paper is shown in Fig 2. Each signal distributor is arranged to create N equal intensity copies of each input image, and feed one copy to each select network. (An efficient image distributor is shown in Fig 3a.) The array of select networks is based on an assembly of N digital light deflectors [5], each operating in the select 1 from N mode [1]. Digital light deflection/selection is a method of addressing $N = 2^n$ locations using n optical modulators and n uniaxial birefringent crystals [1]. (Fig 3b) In this way, each output port of the switch can access its associated array of N inputs, independent of other output port settings. Thus, many output ports can make simultaneous access to any input port when broadcast, or one to many, type connections are required.

The operating principles of optical switching networks employing multiplexed crosspoints have been proven experimentally with a 1 to 16-way fibre switch [1]. Uniaxial calcite crystals were used as the polarisation routing mechanism, and twisted-nematic liquid crystals were used as switchable half-wave plates. A four stage digital light deflector was arranged to produce 16, binary addressed, 125 um deflection increments, to coincide with the fibre core spacing in the linear output array. A simple 4-f imaging setup completed the switch 'wiring'. Details of these results will be presented at the meeting.

Discussion and Conclusions:

Strict-sense non-blocking one-sided and two-sided optical switching networks have been described which exploit the spatial multiplexing properties of optical devices to achieve the theoretical minimum number of crosspoints and control lines. The switched paths possess both high temporal and spatial bandwidths and may be used, therefore, as dynamic broad band image (eg data-bus) interconnection networks. Experimental results confirm that large generalised switching networks should be possible with current optical technology.

Acknowledgments:
The author wishes to thank the Director of Research of British Telecom for permission to publish this paper.

References:

1] P. Healey.: "Optical Switching Networks Using Multiplexed Crosspoints", 14-th European Conference on Optical Communication, Brighton, UK. Conference Pub. 292-part 2 (Post-Deadline Papers) pp.53-56.

2] C. E. Shannon.: "Memory Requirements in a Telephone Exchange", Bell System Technical Journal (BSTJ) Vol.29, July 1950. pp. 343-349.

3] C.L. Wu., and T.Y. Feng.: "On a Class of Multistage Interconnection Networks", IEEE Trans. on Computers, Vol. C-29, No. 8, Aug 1980, pp. 694-702.

4] C.D. Thompson.: "Generalised Connection Networks for Parallel Processor Intercommunication", IEEE Transactions on Computers, Vol. C-27, No. 12, December 1978, pp. 1119-1125.

5] W. Kulcke., et-al.: "A Fast, Digital-Indexed Light Deflector", IBM Journal Research Develop, Vol. 8, January 1964, pp. 64-67.

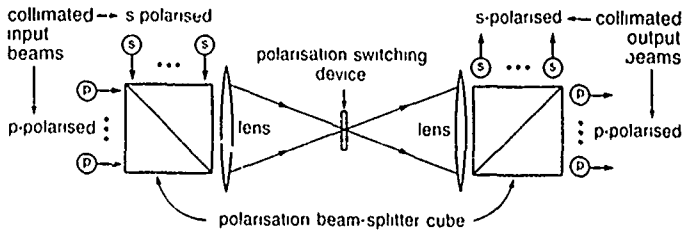

Figure 1. Multiplexed optical change-over 'relay' based on polarisation routing and switching. In the crossed state, the polarisation switching device interchanges the s and the p polarised beams.

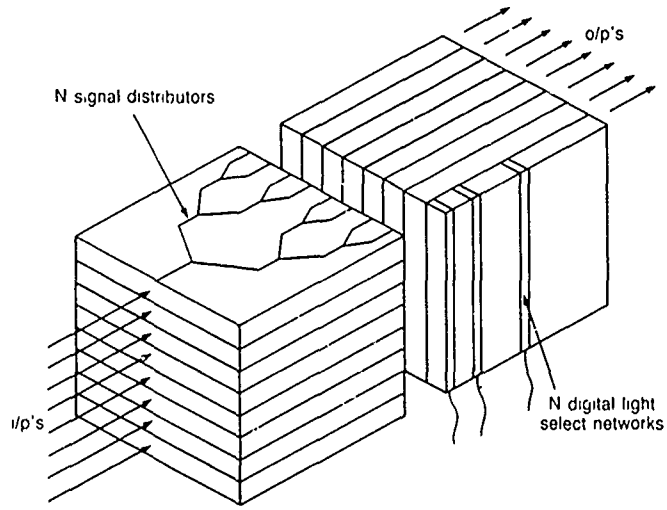

Figure 2. NxN Generalised interconnection network, comprising N distribution planes (Fig 3a) and N digital light selection planes (Fig 3b).

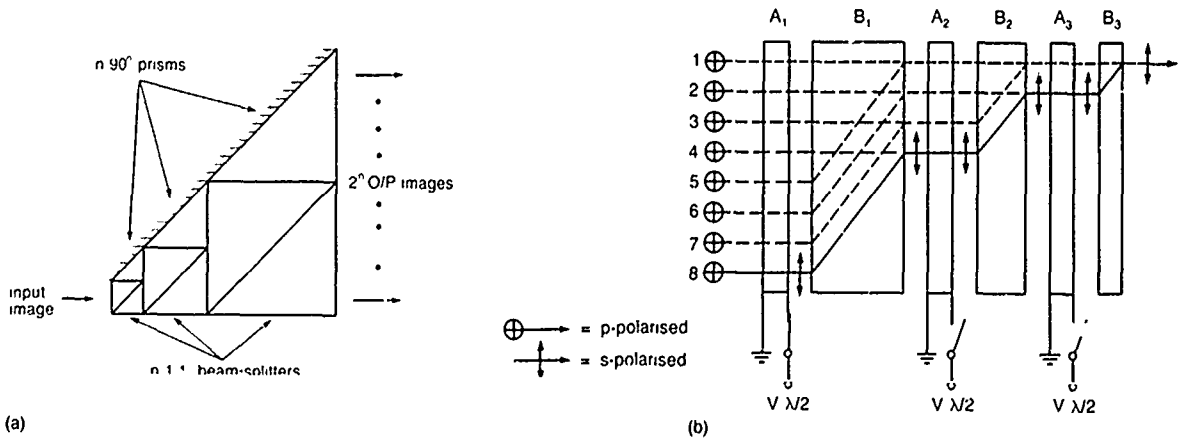

Figure 3. (a) Image distributor, (b) Digital light selection network, ⊕⟶ = p-polarised, ⊣⟶ = s-polarised light beams. A_i = switchable half-wave plate, B_i = Uniaxial birefringent crystal. (Although, for clarity, spatially multiplexed crosspoints are shown in Fig 3b, angularly multiplexed crosspoints can also be used.)

On the spatial extension of multistage interconnection networks

Josef Giglmayr
Heinrich-Hertz-Institut
für Nachrichtentechnik Berlin GmbH
Einsteinufer 37, D-1000 Berlin 10
Federal Republic of Germany

A large number of multistage interconnection networks (MIN's) have been proposed and analysed for the application in multiprocessor systems. There, the mapping of one-dimensional (1D)-inputs (vectors) onto 1D-outputs is obtained by means of 2D-MIN's which can be realized by the current VLSI-technology. In contrast, the need for a 3D-MIN arises naturally in the optical case where subsequently arranged arrays of optical bistabilities are interconnected by free space light beams. 3D-MIN's are expected to represent an important development step for connecting networks in telecommunications (Figure 1) as well as being the basis of the architecture of a pipeline-type digital optical processor [1].

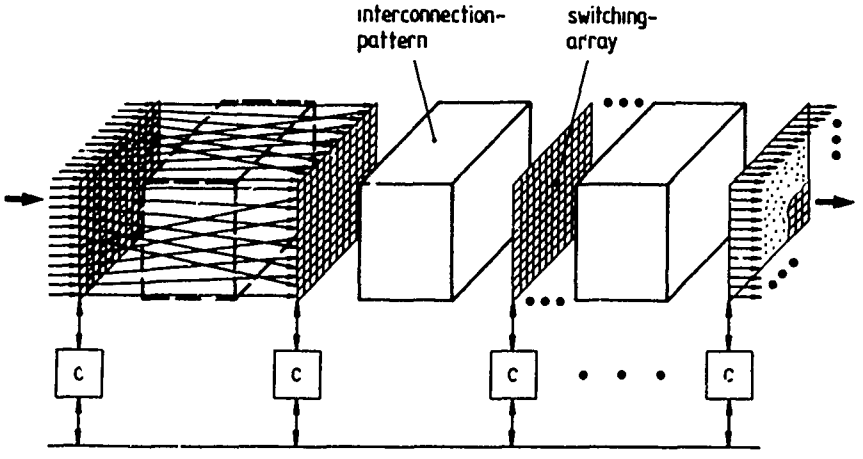

Figure 1. 3D-MIN with distributed control (C) and regular interconnections

Throughout this paper the 3D-extension of several MIN's will be analysed and discussed. We are starting with a 3D-MIN with shuffle interconnection patterns and switching modules with four inputs and four outputs. Then, the 3D-extension of some other important networks ("between" the 3D-omega net and the crossbar, cf. Figure 2) is analysed and discussed. From

the analysis of a 3D-MIN an answer to at least three questions is expected: 1) What is the most appropriate regular interconnection pattern, 2) how many stages are needed for establishing arbitrary connections (or for generating arbitrary permutations), and 3) what is the optimal size of the switching modules. Throughout this paper these problems are made transparent and some answers are presented.

A) 2D-generalized perfect shuffle

This pattern is easily constructed by means of the mixed radix number system (MRNS) of an array

$$(X,Y) = (\sum_i v_i x_i, \sum_j w_j y_j) \tag{1}$$

which provides the numbering of the graphs of the generalized perfect shuffle (GPS). Eq(1) together with the definition of the GPS allows the construction of a general class of 3D-MIN's which include the 3D-omega net. The second step will be the transformation of this 3D-pattern into its 2D-counterpart.

B) Transformation

The transformation is based on the separation property of the 2D-GPS (i.e. shuffling with respect to the columns is subsequently followed by shuffling with respect to the rows and vice versa). Appropriate equations for the transformation are derived from

$$S_{2D}(n_1,n_2) = [1_{n_1n_2} \otimes S(n_1,n_2)]S(n_1n_2,n_1n_2)[1_{n_1n_2} \otimes S(n_1,n_2)] \tag{2}$$

by means of Kronecker and shuffle algebra (a NxN data array is assumed where $N=n_1n_2$, 1_i is the unity matrix of i-th order, S are shuffle matrices and $\otimes$ is the notation for the Kronecker product). A 2D-MIN composed of several stages with the interconnection patterns described by the r.h.s. of eq(2) is isomorphic to the 3D-MIN and will be called generalized shuffle net (GSN).

C) Interconnection pattern

Comparing the performance of the 3D-omega net and its 2D-realization with the performance of the corresponding crossbar (Figure 2) it is easy to conclude that the 3D-omega net is superior to its 2D-realization: The bandwidth (mean number of requests accepted during one cycle, Figure 2a)

is higher and the delay (mean number of cycles a request needs to pass the MIN, figure 2b) is smaller. But the 3D-omega net is inferior to other MIN's (gamma net etc.). In particular, regular optical interconnects are requested which "fill" the space between the 3D-curves and the crossbar in Figure 2 (1st question).

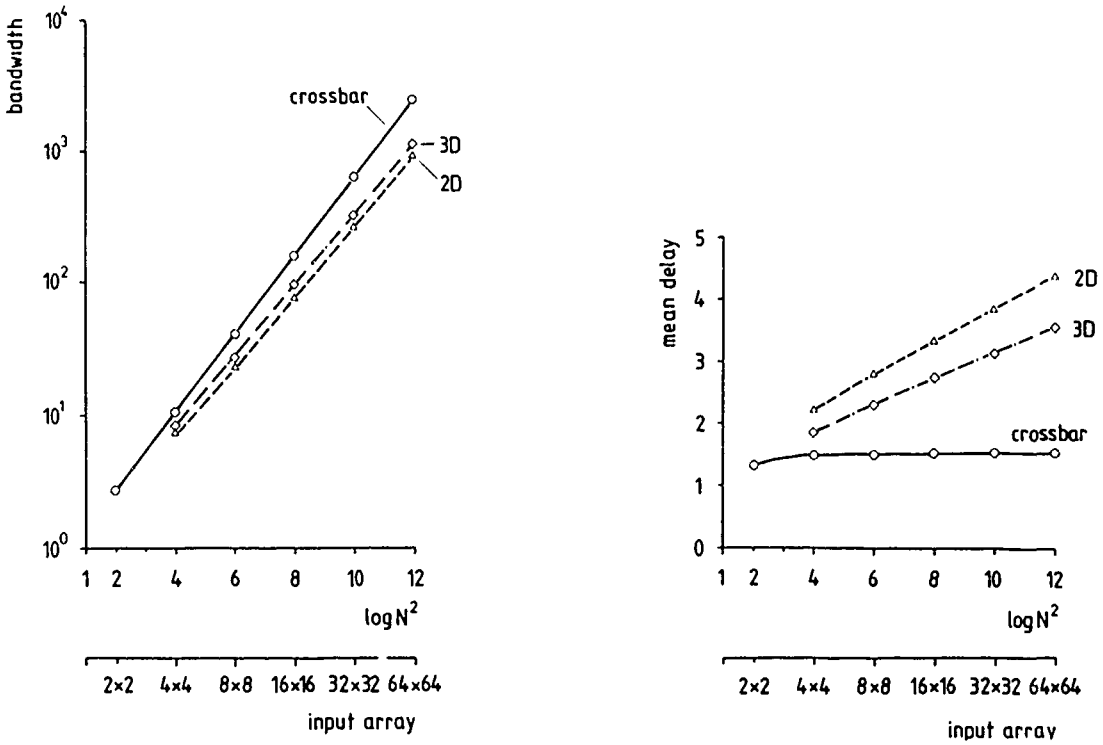

Figure 2. Performance of MIN's and crossbar

For improving the performance of MIN's the interconnection pattern has to be "expanded". Another design parameter is the controllability of the net. The following cases are considered presently: 1) Dilation of the 3D-omega net (duplicating etc. of links), 2) 3D-extension of nets superior to the omega net (gamma net etc.), and 3) 3D-extension of nets with simple control algorithms (sigma net etc.).

D) Design of the net

Given the size of the switches (4x4-crossbars) and the interconnection pattern transformed by eq(2) the number of stages needed to generate arbitrary permutations (multiprocessor system) or to connect any input with any output (connecting network) has to be determined (2nd question). Most of

the results on the number of passes and in turn on the number of stages are for centrally controlled MIN's (2logN-1 and 3logN-3 for the omega net) whereby precomputation of all states of the switching modules is assumed. But precomputation in real time (within one clock cycle) is impossible for MIN's of practical size. Thus, distributed control is required (i.e. a routing decision has to be made at each stage) and results are rather provided by the analysis of the random access through the MIN [2] than by permutation analysis.

For the distributed control of MIN's composed of logN stages the (expected) number of passes needed for the 3D- and 2D-case has been compared with the results for the corresponding centrally controlled 2D- and 3D-MIN's (the latter results are obtained by the transformation into their 2D-counterparts). In all cases considered, the number of passes obtained for distributed control was found to be less than the number of passes for centrally controlled nets.

E) Optimization

Finally, the 3D-MIN's have to be optimized (3rd question). In particular, increasing the complexity of the MIN (multiple paths) which implies an increase of the complexity of the switches (logic for the control of the ports) the number of passes through the net needed to generate arbitrary permutations etc. decreases. Thus, there exists a balance between the costs for the interconnection patterns and the costs for the ports of the switches. This balance has been analysed: Measuring the costs for the interconnection patterns by the delay we have to differ between dilation (where the costs decrease rapidly if the number of ports increases) and no dilation, i.e. an increase of the number of ports changes the type of the interconnection pattern (there, the costs decrease much slower). Both cases provide different solutions for the optimal number of ports of the switches.

References:

[1] J. Giglmayr, "On a three-dimensional interconnection system and its applications to optical computing" (submitted for publication)

[2] H. Patel, "Performance of processor-memory interconnections for multiprocessors", IEEE Trans. Computers, Vol. C-30, pp.771-780 (1981)

Nonblocking Photonic Space Switch Architectures Utilizing Acousto-Optic Deflectors

P.C. Huang, W.E. Stephens, S.S. Cheng, T.C. Banwell, L.A. Reith

Bellcore, 445 South Street, P. O. Box 1910, Morristown, NJ 07960-1910

1. Introduction

Optical switch architectures utilizing such 2x2 switching elements such as directional-coupler switches and crossing X-switches tend to be limited in size by substrate sizes, system attenuation, and system signal-to-noise ratio. Attempts to reduce the effects of these limitations typically result in trading off desirable architectural features. Spanke[1] achieved low system attenuation and good signal-to-noise ratio by using a switch-intensive and interconnection-intensive architecture. Padmanabhan[2] increased system signal-to-noise ratio by increasing the switch count of a more restrictive rearrangeable nonblocking architecture. A summary of these tradeoffs is given in Table 1.

TABLE 1. Comparison of Optical Switching Architectures

Architecture	# of Switching Devices	Insertion Loss (dB)	Crosstalk (dB)
Crossbar Switch	N^2	(2N-1)L+2W	X-10 $\log_{10}$(N-1)
Benes	(N/2)(2$\log_2$N-1)	(2$\log_2$N-1)L+2W	X-10 $\log_{10}$(2k-1)
Dilated Benes	(2N$\log_2$N)-(N/2)	(2$\log_2$N-1)L+2W	0
Multiple Substrate (EO Directional Coupler) ASAC	2N(N-1)	(2$\log_2$N)L+4W	2X-10 $\log_{10}$k
ASPC/PSAC	N(N-1)	$\log_2$N(3+L)+2W	X-10 $\log_{10}$k
(AO Bragg Cell) ASAC	2N	2L+4W	<-28 dB
ASPC/PSAC	N	L+3$\log_2$N+2W	<-28 dB

N=Size of Switch
L=Insertion Loss of Device
X=Extinction Ratio of Device
W=Waveguide/Fiber Coupling Loss
k=$\log_2$N

In this paper, we propose using an acousto-optic deflector (AOD) as a basic switching element for large optical space switches. We also propose partitioning the switch into multiple substrates in a manner that exploits the unique 1xN fanout structure of the AOD. We believe that crosspoint facility switches as large as 128x128, with low system attenuation and crosstalk, can be built from minimal hardware with control complexity of order N.

2. Acousto-Optic Switching Element and Architecture

The acousto-optic deflector diffracts incident light by means of an ultrasonic acoustic wave traveling through the crystal. The ultrasonic wave sets up an optical phase grating either on the crystal's surface or in it's interior by means of slight changes in the index of refraction through the photoelastic effect. The impinging optical beam is diffracted by an angle

$$\theta_i = \frac{f_i \lambda}{v} \qquad (i = 1,2,3,\ldots,n) \tag{1}$$

where f_i is the acoustic wave of frequency, λ is the optical wavelength and v is the velocity of the

sound wave traversing the media.[3] The AOD device can be implemented both in bulk optics and integrated-optics form. In the bulk device, the optical phase grating is generated by $LiNbO_3$ platelet transducers bonded to the side of the TeO_2 or GaP bulk crystals. In the integrated devices, the optical phase grating is generated by interdigital Surface Acoustic Wave (SAW) transducers attached to the crystal surface.[4]

The schematic for the multiple substrate architecture using acousto-optic deflector switches is illustrated in Figure 1.

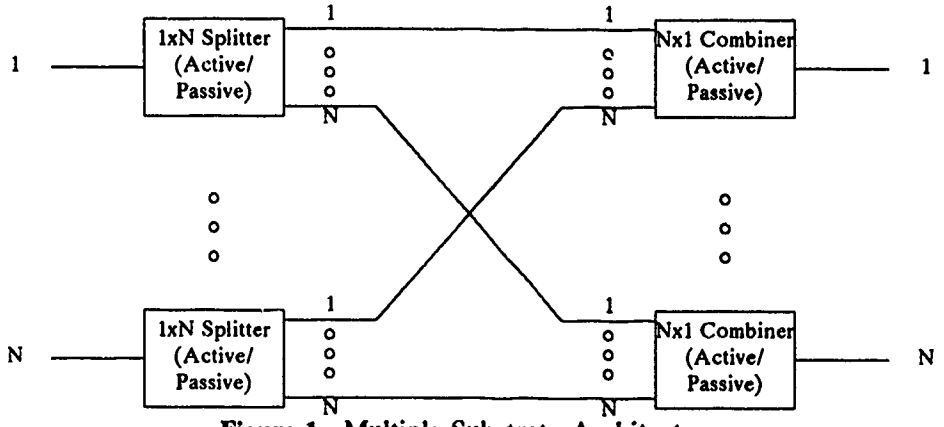

Figure 1. Multiple-Substrate Architecture

This architecture can be shown to be equivalent to the crossbar space switch. The principle of switching is as follows: The input optical signals are deflected to one of N spatial positions where they are summed or switched to form the crosspoints of the switch. Additional optical devices are needed to couple the optical beams in and out of the substrates and to interconnect the multiple substrates. This architecture is known to be interconnection intensive as opposed to switch intensive. Depending whether the input and output substrates are active or passive; three switch classes are possible, Active Splitting-Active Combining (ASAP), Active Splitting-Passive Combining (ASPC) and Passive Splitting-Active Combining (PSAC). (The Passive Splitting-Passive Combining architecture is not useful as an active switch as it is equivalent to a passive star coupler.) From Table 1, the ASAC architecture shows superior characteristics for point-to-point switching, while the PSAC and ASPC are desirable for point-to-multipoint switching. All three multiple switch architectures are strictly nonblocking.

A crosspoint switch built with acousto-optic deflectors offers several advantages. The required technology (both bulk and integrated) is mature. The system attenuation and crosstalk are determined solely by a single-stage switching device; thus, as device technology improves, these characteristics improve. The number of switch elements is of the order N; thus, the crosspoint requires minimal hardware and control complexity. With these features, crosspoints as large as 128x128 may be feasible. With the wired-OR functionality and the gray-scale capability, these architectures also look promising in optical neural networks.[3]

3. Experimental Results

To determine the feasibility of the proposed architecture, a 4x4 switch using an Active-Splitter Passive-Combiner architecture was constructed, as shown in Fig. 2. The input to each cell is a 1.3 μm single-mode fiber attached to a 0.25 pitch GRIN-ROD lens with a diameter of 1.8 mm. At $\lambda = 0.83$ μm, this fiber supports several modes. The pitch of the GRIN-ROD lens, chosen to collimate the light exiting the fiber, produces an output beam whose diameter is estimated to be 350 μm. A low-cost, commercially available acousto-optic Bragg cell with a 50 MHz bandwidth, centered at 200 MHz is used. A set of negative and positive cylindrical lenses in a Galilean-telescope configuration serves to reduce the overall switch size by a factor of two, since the deflection angle of the Bragg cell varies only from 1.65° to 2.75° over the frequency range of 150 to 250 MHz. The negative lens is designed

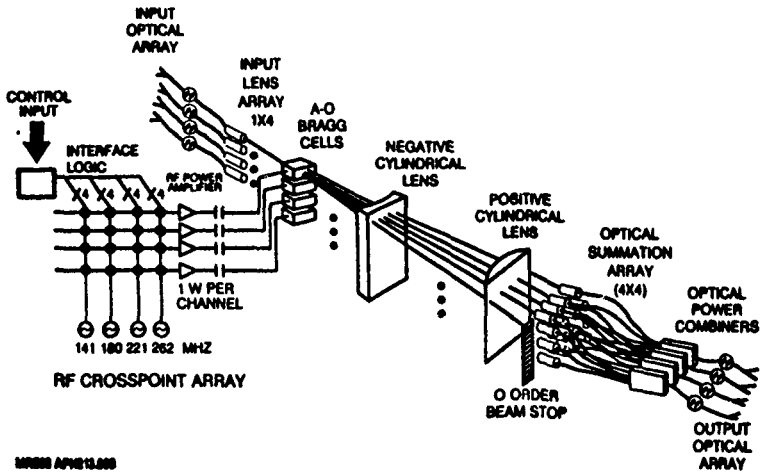

Figure 2. 4x4 Photonic Space Switch

with a focal length of 7.62 cm and is situated 7.95 cm from the GRIN-ROD lenses to double the deflection angle of the Bragg cell. The positive lens is designed with a focal length of 15.42 cm to bend the deflected beams parallel to each other such that they can be focused into the 4x1 multimode power combiners via an array of GRIN-ROD lenses. Coupling efficiency is increased by using multimode fiber with core diameter of 50 μm.

Measurements at $\lambda = 0.83\ \mu m$ indicate a 9.6 dB loss due to the input and output fiber coupling, a 3 - 8 dB diffraction loss from the Bragg cells, and a 1 dB loss from the multimode power combiners, adding up to a 13.6 -18.6 dB total insertion loss for the entire switch fabric. The large variations in the total insertion loss result from operating the Bragg cell beyond its 50 MHz bandwidth.

Polarization sensitivity measurements reveal a 0.8 dB variation between the deflection efficiency of the TM and TE waves in TeO_2 at 1 W of RF power. The reconfiguration time is 50 ns. The worst case crosstalk is less than -24 dB and the worst case extinction ratio is 33 dB. All switching modes of operation, point-to-point, point-to-multipoint and wired-OR, have been demonstrated.

Recent experiments indicate that the insertion loss variation can be kept within 3 dB and that crosstalk can be reduced to less than -30 dB by using an AOD Bragg cell with a phased-array piezo-electric transducer design. With properly phased delayed RF control signals, 10% diffraction efficiency at $\lambda = 1.3\ \mu m$ is achieved over a bandwidth of 200 MHz of 1 W RF.

4. Conclusion

A polarization-insensitive 4x4 photonic space switch with multicasting capability has been demonstrated using acousto- optic techniques at $\lambda = 0.83\ \mu m$. The switch's is active-splitting passive-combining architecture has the advantage of low switch count and requires control complexity of order N. This experiment is the basis for a more generic switch design that includes multiple substrate AOD switch elements and an interconnection matrix.

1. R. A. Spanke, "Architectures for Guided-Wave Optical Space Switching Systems," IEEE Communications Magazine; Vol. 25, (5) pp. 42-48; 1987.

2. K. Padmanabhan and A. N. Netravali; "Dilated Networks for Photonic Switching;" IEEE Trans. Comm.; Vol. COM-35 (12); pp. 1357-1365; (1987).

3. P. C. Huang, W. E. Stephens, T. C. Banwell, and L. A. Reith; "Fast Multicasting 4x4 Photonic Space Switch Utilizing Acousto-Optic Bragg Cells;" European Conference on Optical Communications (ECOC'88); Brighton, UK, Sept, 11-15; Conf. Pub. 292-Part 1, pp. 284-287; 1988.

4. M. K. Barnoski, B. U. Chen, T. R. Joseph, J. Y. Lee, and O. G. Ramer; "Integrated-Optic Specrum Analyzer;" IEEE Trans. Circuits and Sys.; Vol. CAS-26 (12) pp. 1113-1124 (1979).

An All-Optical Shift Register Using Symmetric Self Electro-optic Effect Devices

F. B. McCormick and A. L. Lentine
AT&T Bell Laboratories, Naperville, IL 60566

L. M. F. Chirovsky and L. A. D'Asaro
AT&T Bell Laboratories, Murray Hill, NJ 07974

Shift registers are a basic component of electronic switching and computing systems. In the development of optical switching and computing systems, applications for all optical shift registers are also forseen. These applications include serial-to-parallel and parallel-to-serial converters to match the inherent parallelism of free-space optics to the presently serial nature of optical transmission systems and most electronic systems, time division switching components such as time slot interchangers and elastic stores, and general purpose computing (binary multiplication, etc.). We present the first demonstration of an *all optical* shift register using reflection-mode symmetric self electro-optic effect devices (S-SEEDs)[1] [2]. An optical shift register with electronic shifting using charge coupled devices (CCDs) has been demonstrated[3], but the lack of optical logic/memory devices with reasonable switching energies has made the implementation of an extensible all optical shift register difficult. Symmetric SEEDs, which function as optical set-reset latches, provide this memory with reasonable power requirements. In addition their ability to operate without critical biasing over a wide range of power levels makes them an excellent choice for these initial system experiments. Previously, transmission-mode S-SEEDs have been cascaded in an optical ring counter arrangement[4], but the optical techniques used in that experiment were not extensible to many bits. The optical techniques used in the experiment that we describe here, are extensible, not only to larger shift registers, but to many shift registers operating concurrently using only a single array of devices.

In this experiment, four S-SEED latches on the same array were cascaded in a master-slave configuration to form a 2-bit shift register as shown schematically in Fig. 1.

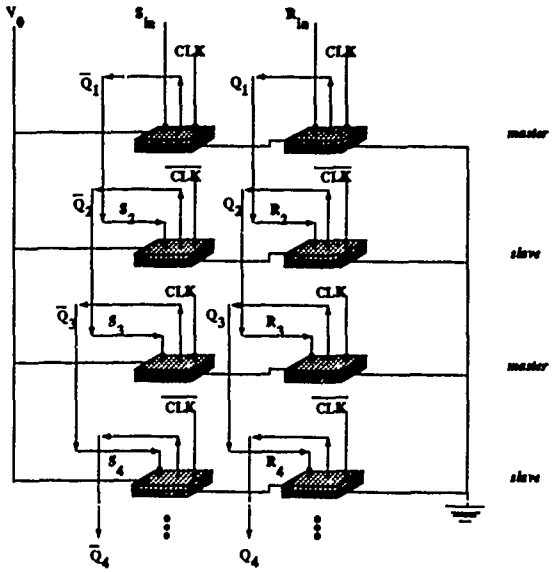

Figure 1. Shift register connections: each device's reflected outputs become the next devices inputs

Simultaneously clocking alternate devices (i.e.- all of the "master" latches or all of the "slave" latches) insures that the signal beams set the state of the devices before the clock beams are applied to read them out. Note that, since the S-SEEDs actually perform an inverting S-R latch function, the data is inverted once as it passes through the master latch and then again as it goes through the slave latch.

The optical information is this system is propagated as an array of collimated beams which are transformed into arrays of spots at the image planes. The two sets of clock beams, *CLK* and $\overline{CLK}$ are generated by current modulating two AlGaAs laser diodes at 850 nm, which are combined onto the same polarization via an optical isolator configuration. Both laser beams pass through a 1 x 2 binary phase grating (BPG) [5] [6] that produces two equal beams for each laser that ultimately are routed to th ective devices. (ie. the first and third devices are driven from one laser and the second and fourth devices d he other.) Each of these (four) beams pass through a second 1 x 2 PBG that generates a set of beams put beam [7] that are routed to the two optical windows (ie. set and reset) of each device. Zoom lenses w eeded to match the grating periods to the device window spacings. Two additional lasers provided the input signals to the first device.

Combining the two input signal beams, clock beams, and loopback or interconnection beams so that they can be imaged onto the device array is accomplished using a space-multiplexing technique[8], as illustrated in Fig. 2. Mirrors M_1 and M_2 consist a 2-D array of small mirrors deposited onto a thin glass substrate. Lenses image the clock, signal, loopback and output spot arrays onto and off of these mirror arrays. The input and loopback signals reflect off of M_2 and M_1, respectively. The clocks pass through M_1 and the reflected device outputs pass through M_2. The reflected outputs are also sampled by a pellicle beamsplitter and are imaged onto Si avalanche photodiodes. The lenses used to image spots onto the patterned reflectors have focal lengths of 40mm, whereas the final objective next to the device has a focal length of 7.7 mm. This results in a 5.19 magnification step between the devices and the mirror arrays and a lowered numerical aperture (N.A.) for the spots formed on the mirror array. This lowered N.A. results in easier alignment of the mirror arrays with the spots and devices, and a decrease in the spherical aberration introduced by the glass substrates on which the mirror arrays are fabricated.

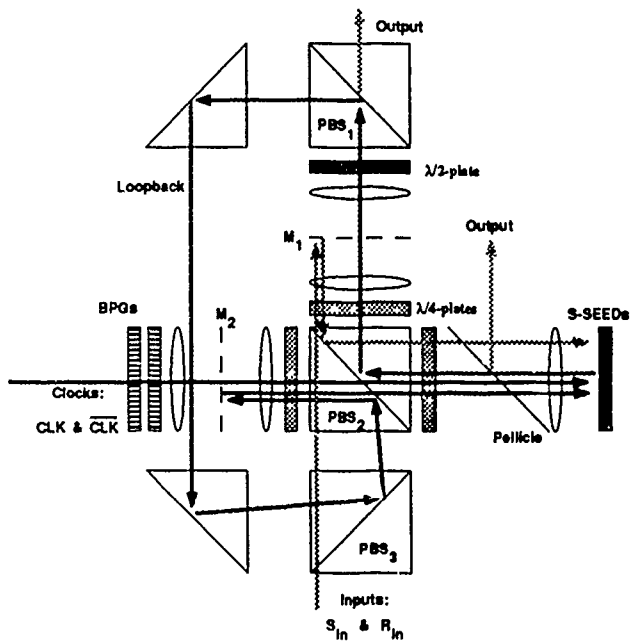

Figure 2. Simplified diagram of the optical shift register implementation (rays indicate connections performed, not actual propagation paths)

The signal and clock lasers were driven from the output of a digital word generator. Figure 3 shows the two optical input signals and the four Q outputs from each device. As we stated earlier, note that alternating outputs are inverted and that they are delayed by 1/2 clock cycle. The peak laser diode output powers were ~4.9mW. This resulted in clock powers of ~215μW on each mesa of the devices. The signal beams after the loopback path were estimated to be ~5.8μW and ~2.9μW for a logic one and zero respectively. The fastest measured switching speed of ~20μs is somewhat longer (~5×) than the expected speed based on a measured switching energy of 12 pJ for these devices [2]. Part of this may be due to the high leakage currents in these devices (~600nA at 16 volts), which can reduce the "differential current" that switches the device.

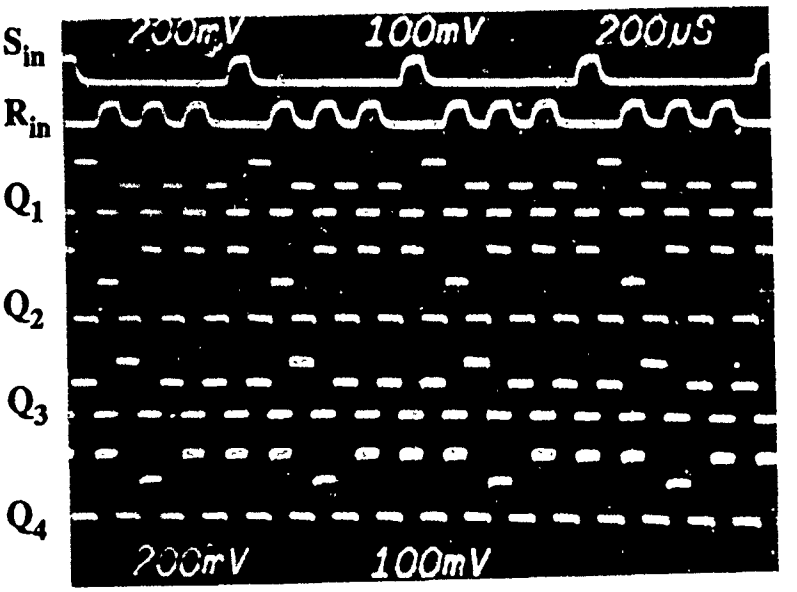

Figure 3. Optical inputs and outputs of the shift register

In conclusion, we have demonstrated an all optical shift register using reflection-mode S-SEEDs with relatively low switching energies. The implementation used easily fabricated patterned mirror reflectors and binary phase gratings along with conventional optics, and was driven by low-powered laser diodes. The techniques used are thermally and physically stable, relatively easily aligned, and extensible both to larger shift registers and to many shift registers operating on the same array.

We would like to thank Rick Morrison, Sonya Walker, and D. Bruce Buchholtz for fabricating and characterizing the BPGs used in this experiment.

REFERENCES

1. A. L. Lentine, H. S. Hinton, D. A. B. Miller, J. E. Henry, and J. E. Cunningham, and L. M. F. Chirovsky, "Symmetric Self Electro-Optic Effect Device: Optical Set-Reset Latch," *Applied Physics Letters* 52(17), 1419-1421 (1988).

2. L. M. F. Chirovsky, L. A. D'Asaro, C. W. Tu, A. L. Lentine, G. D. Boyd, and D. A. B. Miller, "Batch Fabricated Symmetric Self Electro-Optic Effect Devices," *submitted to Topical meeting on photonic switching, OSA (1989)*

3. K. B. Nichols, B. E. Burke, B. F. Aull, W. D. Goodhue, B. F. Gramstorff, C. D. Hoyt, and A. Vera, "Spatial light modulators using charge-coupled-device addressing and electro-absorption effects in multiple quantum wells," *Device Research Conference, Santa Barbara, CA, June, 1987.*

4. A. L. Lentine, D. A. B. Miller, J. E. Henry, and J. E. Cunningham, "Photonic Ring Counter and Differential Logic Gate using Symmetric Self Electro-optic Effect Devices," *Conference on Lasers and Electro-optics, paper Tue4, OSA (1988)*

5. H. Dammann and K. Gortler, "High-efficiency in-line multiple imaging by means of phase holograms," *Optics Communications 3*, 312-315, 1971

6. J. Jahns, M. E. Prise, M. M. Downs, S. J. Walker, and N. Streibl, "Dammann Gratings as Array Generators," *J. Opt. Soc. Am. A 4, (13), p 82 (1987)*

7. F. B. McCormick, Jr., "Generation of Large Spot Arrays from a Single Laser Beam via Multiple Imaging with Binary Phase Gratings," *OPTCON '88, (Annual Meeting of the OSA), paper WBB3 (1988).*

8. M. E. Prise, M. M. Downs, F. B. McCormick, S. J. Walker, and N. Streibl, "Design of an Optical Digital Computer," *OSA Topical Meeting on Optical Bistability (OB-4)*, March 1988.

NOTES

THURSDAY, MARCH 2, 1989

SALON E

1:30 PM–3:00 PM

ThD1–ThD6

FREE-SPACE DEVICES

David A. B. Miller, AT&T Bell Laboratories, *Presider*

Exciton Enhanced Photonic Switching in GaAs-AlGaAs Fabry-Perot Resonators

W. Kowalsky, T. Hackbarth and K. J. Ebeling

Institut für Hochfrequenztechnik, Technical University of Braunschweig, D-3300 Braunschweig, Federal Republic of Germany

Exciton enhanced photonic switching in GaAs-AlGaAs Fabry-Perot Resonators is demonstrated. Switching contrast of 10 : 1 is achieved at 1 mW control power.

Optically controlled photonic switching devices are key elements in prospective optical data processing [1]. Several approaches to matrices of surface normal switching elements towards parallel optical computing have been demonstrated [2 - 6]. In the present paper we investigate optically controlled switching in a GaAs-AlAs MQW etalon integrated with a multilayer dielectric reflector grown by molecular beam epitaxy. With a 20-period MQW etalon we achieve a switching contrast of 10 : 1 at less than 1 mW control power. Excess carrier lifetimes of a few ns allow for bit rates of ca. 100 Mb/s.

Optically controlled photonic switching in reflection is illustrated schematically in Fig. 1. The essential element is a GaAs-AlAs MQW etalon in front of a multi-layered dielectric reflector.

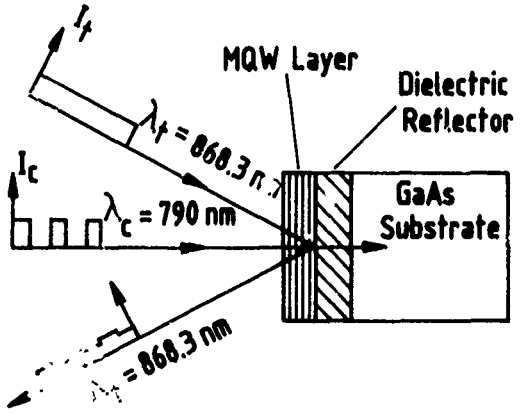

Fig. 1 Schematic of the GaAs-AlAs MQW etalon integrated with a multilayer dielectric reflector.

The total optical length of the etalon is optimized to attain a coincidence in wavelength of the excitonic absorption resonance of the quantum wells with a Fabry-Perot reflection minimum. The power of the reflected test beam at the resonance wavelength $\lambda_t = 868.3nm$ is influenced by a second superimposed control beam of same or different wavelength. Angle or polarisation diversity schemes may be used for beam discrimination. The control beam of power P_c bleaches the excitonic absorption resonance by generation of excess carriers resulting in increasing power of the reflected test beam. The effective spot size of about $44\mu m^2$ is mainly determined by carrier diffusion. Because of the low control power required several hundred channels per mm^2 can be operated in parallel without thermal problems.

The multilayer structure was grown in a Varian Gen II MBE system. The MQW etalon consists of 20 GaAs quantum wells (20 nm) embedded in AlAs spacer layers of 85 nm thicknesses. The reflectivity of the dielectric reflector (20 pairs of AlAs/$Al_{0.1}Ga_{0.9}As$ (69 nm/59 nm) quarter wave layers) is larger than 95 %. Due to excitonic absorption in coincidence with a Fabry-Perot reflection minimum the reflectivity of the device is diminished to about 5 % without excitation.

Since a slight increase of the carrier concentration is sufficient to suppress the excitonic absorption resonance, a strong switching contrast is achieved at only a few mW control power. The experimentally determined switching contrast in dependence on test wavelength for control power $P_c = 2.5mW$ is shown in Fig. 2.

At the resonance wavelength an on-off-ratio of 8 : 1 is observed. The control power dependence of the switching ratio is depicted in Fig. 3.

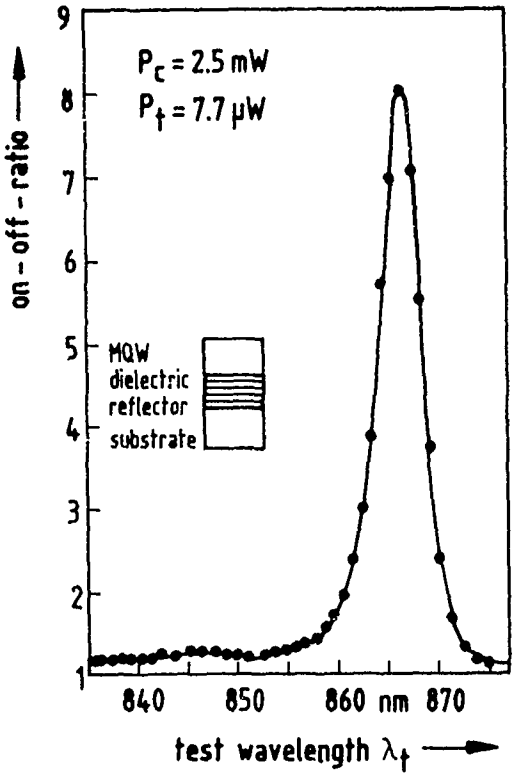

Fig. 2 Switching contrast in dependence of test wavelength.

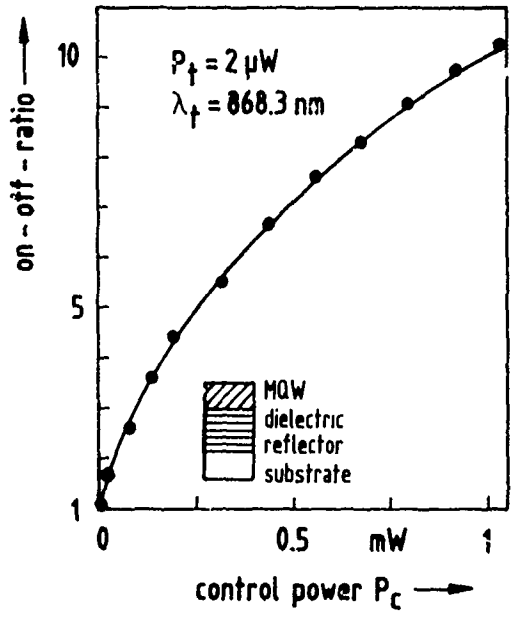

Fig. 3 On-off-ratio as a function of control power.

For optimized experimental conditions it increases nearly linearly with control power and is far from saturation. At only 1 mW control power a switching contrast better than 10 : 1 is achieved. This strong modulation at a low control power level is promising for densely spacing of parallel channels.

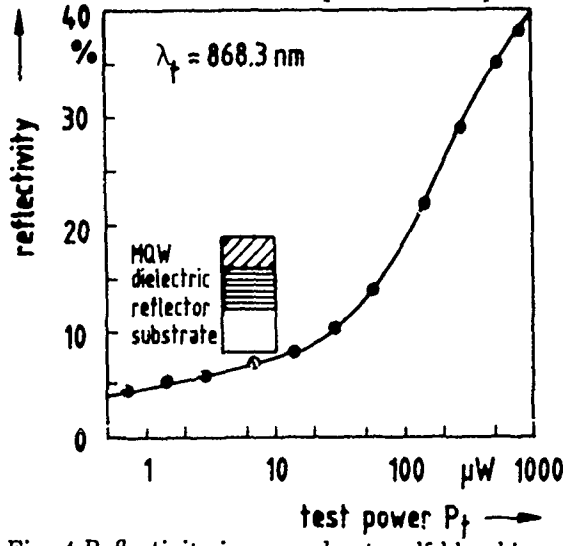

Fig. 4 Reflectivity increase due to self-bleaching by the test beam.

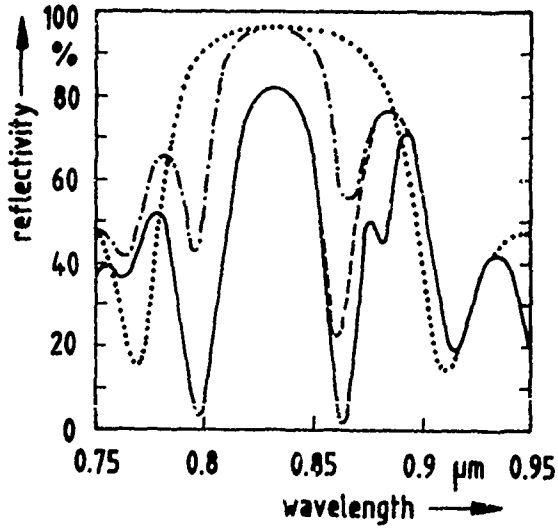

Fig. 5 Theoretical analysis of switching characteristics.

The dependence of the excitonic absorption coefficient on the excitation intensity is derived from the

reflectivity of the switching device as a function of test power. The experimental results are depicted in Fig. 4. The kink at about $P_t = 20\mu W(\sim 50W/cm^2)$ is probably caused by saturation of nonradiative recombination centers. From the distinct reflectivity increase at higher power levels the intensity dependence of excitonic absorption is estimated. Assuming a linear approximation $\alpha(I) = \alpha_0 + \alpha_2 I$ results in $\alpha_2 = 10...45cm/W$ which is in good agreement with earlier work [7].

Fig. 5 summarizes theoretical results on switching characteristics in dependence on test wavelength. Whereas the reflectivity of the dielectric reflector gives a broad platean indicated by the dotted line, adding the MQW etalon results in resonance minima at about 800 nm and 860 nm (dash-dotted line). Fundamental and additional excitonic absorption indicated by the broken and solid curve, respectively, reduce the reflectivity at 860 nm wavelength to only a few percent. Thus bleaching of the MQW etalon by optical excitation enables a high on-off-ratio as observed experimentally.

To conclude, we have investigated optically controlled photonic switching in GaAs-AlGaAs MQW Fabry-Perot Resonators. Excitonic absorption in coincidence with a Fabry-Perot resonance enables a strong switching contrast. An on-off-ratio of 10 : 1 is achieved at 1 mW control power. Dynamics are limited by excess carrier lifetimes to about 100 Mb/s. Because of the low power consumption this device is suitable for high speed parallel optical data processing.

We gratefully acknowledge the financial support by the Stiftung Volkswagenwerk and the Bundesministerium für Forschung and Technologie.

References

[1] A. Huang, IEEE Proc. 72 (1984) 780.

[2] D. A. B. Miller, D. S. Chemla, T. C. Damen, T. H. Wood, C. A. Burrus, A. C. Gossard, W. Wiegmann, IEEE J. Quant. Electron. $QE-21$ (1985) 1462.

[3] G. D. Boyd, D. A. B. Miller, D. S. Chemla, S. L. McCall, A. C. Gossard, J. H. English, Appl. Phys. Lett. 50 (1987) 1119.

[4] J. L. Jewell, A. Scherer, S. L. McCall, A. C. Gossard, J. H. English, Appl. Phys. Lett. 51 (1987) 94.

[5] D. Hulin, A. Mysyrowicz, A. Antonetti, A. Migus, W. T. Masselink, H. Morkoc, H. M. Gibbs, N. Peyghambarian, Appl. Phys. Lett. 49 (1986) 749.

[6] W. Kowalsky, K. J. Ebeling, Opt. Lett. 12 (1987) 1053.

[7] D. S. Chemla, D. A. B. Miller, P. W. Smith, Opt. Engineering 24 (1985) 556.

TRANSVERSE MODES AND WAVEGUIDE DISPERSION IN SUBMICRON GaAs/AlAs MICRORESONATORS

J.L. Jewell, S.L. McCall[a], A. Scherer[b],
A.C. Gossard[c] and J.H. English[c]

AT&T Bell Laboratories, Rm. 4G-520, Holmdel, NJ 07733 U.S.A.

INTRODUCTION

Miniaturization of optical devices is a key approach to minimizing their energy and time requirements. The formation of GaAs microresonators[1] was a step in this direction which reduced device diameters, controlling energies, and recovery times to about 1.5 μm, 600 fJ, and 200 ps respectively. Diameters of the studied devices was limited to $\sim$1.5 μm by our ability to focus the $\sim$875 nm light in air. More recently we have been able to study devices down to $<$0.5 μm diameter. Devices in the $\sim$0.5-1.5 μm "intermediate" range are difficult to operate due to the effects of multiple transverse modes. When diameters are $<$0.5 μm (the size range sought anyway), they appear to be single-mode, or nearly so.

EXPERIMENTS

Gating of the devices was observed with the same picosecond pump-probe apparatus[1] as before. A Kodak bi-aspheric molded glass lens with numerical aperture NA=0.55 provided tight focusing. Combining this with a 2-mm-radius hemisphere of $SrTiO_3$ (refractive index n=2.4; obtained from Hibshman Corp.), yielded an NA of $\sim$1.3 and theoretical focusing to $\sim$0.4 μm FWHM. Furthermore, we added a spatially incoherent illumination/imaging system allowing us to view many devices on a TV screen.

Figure 1 shows images of 4 "large" and 2 "small" microresonators at 5 different wavelengths. The "large"/"small" devices are 4-μm/3-μm center-to-center and 1.2-μm/0.8-μm in diameter. Since the light is reflected from the microresonators, a transmission resonance is indicated by *darker* images. At the longest wavelength the larger devices show a generally dark central region, which we interpret to be the lowest order mode. At 8911 Å they are very bright (no resonance), but at 8872 Å they show a dark ring with a bright spot in the center, the next-higher-order mode resonance. The next resonance occurs at 8794 Å and has a small dark region in the center.

Due to waveguide dispersion the smaller devices have resonances at different wavelengths than the larger ones. (Thickness variations of the multilayer structures are negligible over the several device separations.) A resonance occurs at 8911 Å, where there is no resonance for the large devices. Resonances also occur at the two shortest wavelengths where the reflected light patterns form a bright horizontal bar at 8849 A and a dark bar at 8794 Å. Since defocusing can change the appearance of these patterns, we focused at each wavelength to maximize sharpness of the devices' outer edges.

The validity of these mode patterns is strengthened by our pump-probe experiments on the larger devices. Since the probe beam can be focused to a size much smaller than the

devices, it can preferentially couple into different modes. For example, at 8872 Å with the probe focused at the center (bright region), the reflectivity switches from its initially high value to a lower one. Moving the probe to the dark ring results in switching from lower to higher reflectivity, and having the probe on the outside (bright) region again results in higher-to-lower reflectivity switching. We see similar behavior in the smaller devices.

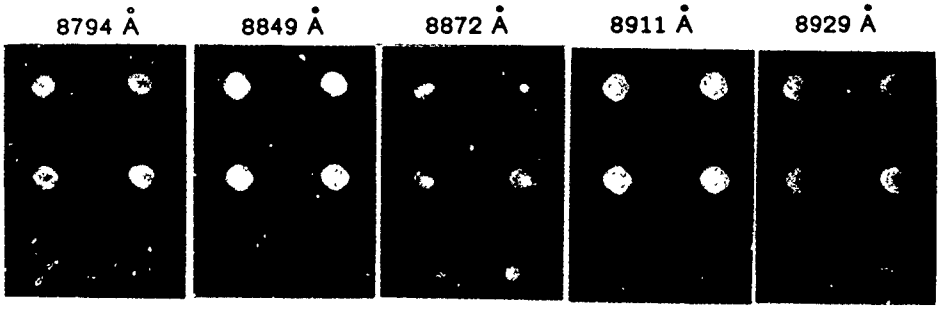

Figure 1

Due to the multiplicity of transmission peaks discretely separated in wavelength, devices in the $\sim$0.5-1.5 μm range show decreased modulation of the probe beam by the pump beam. In resonators larger than $\sim$2 μm diameter the resonances overlap and these effects are not observed. To achieve efficient modulation in the intermediate size range it would be necessary to match the intensity profile of our beam to a particular mode of the resonator. On the other hand, a sufficiently small device would have only a single transverse mode which should be better matched to our laser. This appears to be the case since the smallest devices observed, $<$0.5 μm diameter, show much larger modulation than do the $\sim$1 μm devices.

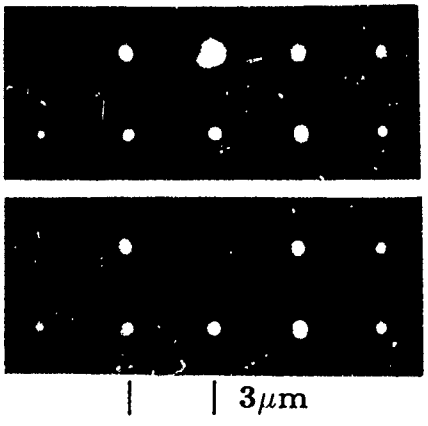

Figure 2

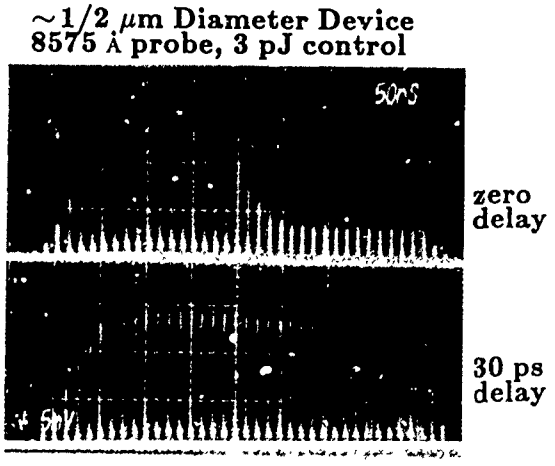

Figure 3

Figure 2 shows a region containing some $\sim$0.5 μm devices. Although the features on the mask used to make them were 1.5 μm in diameter, limitations and imperfections in the contact optical lithography resulted in their reduced sizes to the point that some are even missing as in the upper left corner. Quality of these device structures is not known. The spot sizes in Fig. 2 are at the diffraction limit of the imaging system. If an actual device was smaller

it would appear fainter but not much smaller on the TV screen. Thus we expect the device in the top center of the two photographs is the smallest in the field. The top photograph in Fig. 2 has the probe beam focused onto the device (making it appear much brighter), while the bottom photo has only the illumination beam incident. Its smaller size is further evidenced by its shorter wavelength resonance, consistant with our expectation from waveguide dispersion. Figure 3 shows the response of this device. It has about 80% modulation which is more than that of the larger devices. Full modulation would require a well-balanced resonator design and coupling of the entire beam into a single mode. Lack of either could easily cause the incomplete modulation. The pump energy was quite high, about 3 pJ, but this is not surprising because: 1) the pump beam was not focused as well as the probe, and 2) the resonance occurred at 8575 Å which is well inside the absorption band of the bulk GaAs. The modulation is due to large absorption saturation by a fraction of the 3 pJ pump. The device is also observed to recover in 30 ps. Its actual recovery time is smaller since the pulse duration overlap and relative jitter caused an *apparent* 13 ps rise time in the response. Thus the speed is in accordance with that expected from size scaling[2], while the energy requirements for such small devices have not yet been reasonably tested.

CONCLUSION

High-numerical-aperture focusing has allowed us to investigate the smallest optical resonators yet studied, about 4-μm long and as little as <0.5 μm in diameter. The "intermediate" size range, ~ 0.5-1.5 μm diameter, is difficult for device operation due to the effects of multiple transverse modes. They could be made single-mode by cladding with an appropriately high refractive index material. Smaller devices can be single mode even with low-index (i.e. air) cladding. We expect that the best performances (lowest energy and time requirements) will be obtained from the smallest devices into which one can couple the light.

REFERENCES

[1] J.L. Jewell, A. Scherer, S.L. McCall, A.C. Gossard, and J.H. English, Appl. Phys. Lett. **51**, 94-96 (1987).

[2] J.L. Jewell, S.L. McCall, Y.H. Lee, A.Scherer, A.C. Gossard, and J.H. English, Journal de Physique, **C2**, 39-42, (1988); Proceedings of the Topical Meeting on Optical Bistability IV, Aussois, France, March 1988.

a) AT&T Bell Laboratories, Murray Hill, NJ 07974
b) Bellcore, Redbank, NJ 07701
c) present address: Eng. Matls. Dept., University of California, Santa Barbara, CA 93106

InGaAs/InP MQW 3x3 Planar Spatial Light Modulator Grown by Gas-source Molecular Beam Epitaxy

M.A.Z. Rejman-Greene, E.G. Scott, and E. McGoldrick
British Telecom Research Laboratories,
Martlesham Heath, Ipswich IP5 7RE, United Kingdom

1. Introduction.

The practical realisation of two-dimensional spatial light modulators is a key requirement in the development of optical processing and all-optical switching. Among the more promising designs of SLM are those utilising the Quantum-Confined Stark Effect[1-8] in Multiple Quantum Well (MQW) layers. The use of III-V semiconductor materials offers the prospect of monolithic integration with other electronic and optical components. In particular, modulators grown on InP substrates simplify array operation in transmission, whereas in GaAs-based systems the substrate is removed for operation in the transmissive mode[1]. To date, devices in both systems have been formed for the most part by etching mesas[1][3][8]; however, a planar technology is preferred if robust arrays are to be produced, or more complex functionality is envisaged.

2. Fabrication of Arrays of Planar Modulators

The MQWs were grown on 2" diameter S-doped InP wafers by gas-source MBE, using conventional solid sources for the group III elements, and As_2 and P_2 beams obtained by passing arsine and phosphine through a low pressure cracker operated at 1000^0C. High quality interfaces were obtained by ramping the solid source temperatures, and by interrupting the growth during the changeover of group V sources. After epitaxial layer growth, individual modulators are made by etching windows in a PECVD silicon nitride layer, followed by zinc diffusion through these windows to a depth of 1.2μm. Finally, contacts are made to individual devices by patterning sputtered Ti-Au layers using conventional photolithographic techniques.(Fig.1)

Modulators, spaced at 500μm intervals, are designed to produce a sensitive area of diameter 45μm, together with an offset bond pad approximately 50μm in diameter for ease of bonding. By selecting a small device area, and reducing the doping of the MQW layers, the capacitance of unbonded modulators is 0.4pF at an operating voltage of -30V - promising very fast operation in system use.

Suitable arrays on the processed wafer are identified by measurement of the dark currents of individual devices using an automatic wafer prober. Chips from the wafer are cleaved and then bonded on to DIL headers over predrilled apertures. Thermocompression bonding to individual devices enables the low dark currents to be maintained through to the completion of processing of 3x3 arrays. (fig.2)

3.Array assessment

Transmission spectra have been obtained using a Bruker IFS88 FT-IR spectrometer coupled to an externally-mounted microscope and optimised for operation in the near-IR - a novel approach which enables fast assessment of a large number of devices. Fig. 3 shows typical absorbance spectra on a device from a 3x3 array located near the centre of the 2" InP wafer - 3dB modulation is realised at 1.525μm. The 5dB insertion loss should be substantially reduced by incorporating anti-reflection coatings. Measurement of the transmission through modulators in a line 12mm long shows that the variation in unbiased absorption edge is no more than 4nm, indicating a variation of 0.2dB in the 3dB modulation for these devices.

In conclusion, we have described a process for the fabrication of a uniform 3x3 array of electrically-addressed planar optical modulators - the first reported planar SLM array in the InGaAs/InP MQW system. The individual modulators are characterised by a low capacitance and dark current, and exhibit a 3dB modulation of the transmitted light at 1.525μm, close to the optimum wavelength of operation of optical fibre communication systems.

The authors thank Ms L. Davies for the diffusion and Ms L. Johnson for the device bonding; and Dr. P Turner from Bruker Spectrospin Ltd. Acknowledgement is made to the Director of Research British Telecom for permission to publish this paper.

References

1 Chemla, D. S. et al., Appl. Phys. Lett., **42**, pp. 864-866 (1983)
2 Chang,C.C. et al., SPIEVol.634 "Optical and Hybrid Computing",p.372 (1986)
3 Wakita, K. et al., Surface Science, **174**, pp. 233-237 (1986)
4 Goodhue, W.D. et al., J.Vac.Sci.Technol., **B4**, pp. 769-772 (1986)
5 Bradley, P.J. et al., Electron. Lett., **23**, pp. 213-215 (1987)
6 Hsu, T.-Y. et al., Opt. Engineering, **27**, pp. 372-384 (1988)
7 Singh, J. et al., J. Lightwave Technol., **6**, pp. 818-831 (1988)
8 Dobbelaere, W. et al., Electron. Lett., **24**, pp. 295-297 (1988)

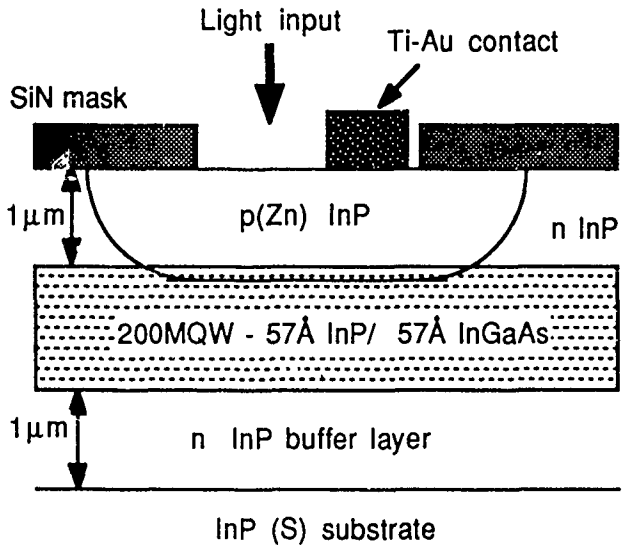

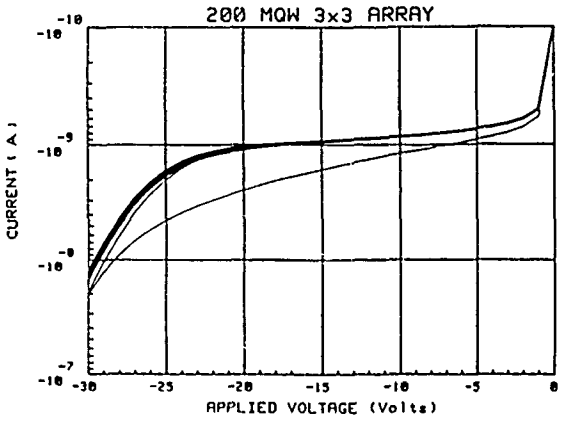

Fig1 InGaAs/InP MQW Modulator Fig2 Dark Currents of Individual Modulators

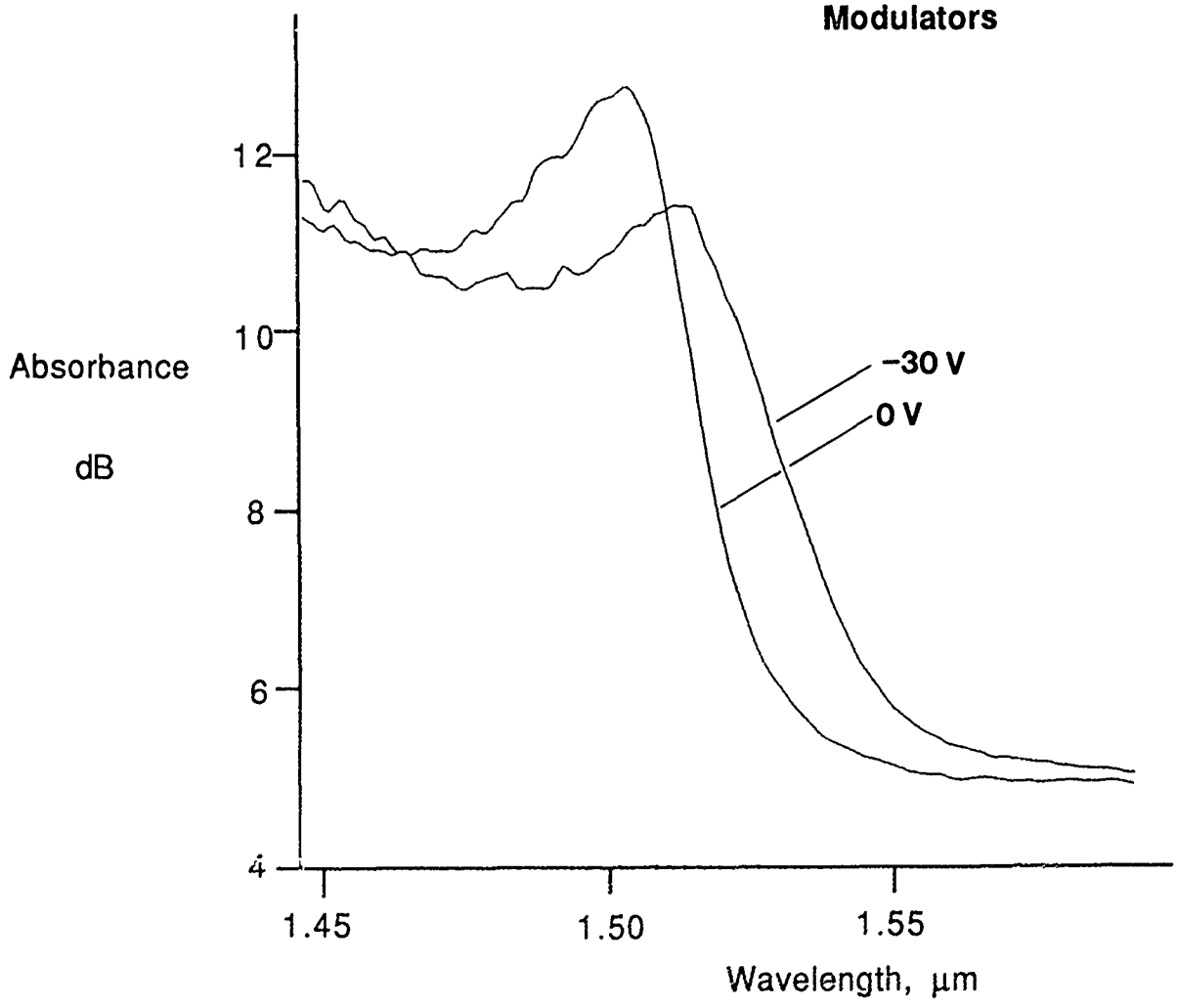

Fig3 Absorbance spectra of a single modulator

Batch Fabricated Symmetric Self Electro-optic Effect Devices

*L. M. F. Chirovsky, L. A. D'Asaro, C. W. Tu**
AT&T Bell Laboratories
Murray Hill, N.J. 07974

A. L. Lentine
AT&T Bell Laboratories
Indian Hill Park
Naperville, IL. 60566

G. D. Boyd, D. A. B. Miller
AT&T Bell Laboratories
Holmdel, N.J. 07733

Digital optics systems are expected to provide powerful new methods of processing and routing digital information. The power of these systems arises from the massive parallelism made possible by the high interconnectivity of free space optics. Up until the present it has not been possible to build such systems due to the unavailability of suitable devices. Although numerous device concepts are being investigated, presently the Symmetric Self Electro-optic Effect Device (S-SEED), has the most suitable blend of device characteristics for system tests.

The fundamental principles of operation of SEED's in general and the S-SEED in particular have been previously described in detail [1,2]; a summary follows. Exciton peak absorption at a wavelength λ_o persists in a Multiple Quantum Well Structure (MQWS) even at room temperature. By way of the Quantum Confined Stark Effect, an externally applied electric field, perpendicular to the MQWS, can significantly modulate the absorption at λ_o by red-shifting the exciton peak. In a p-i-n diode, with an undoped MQWS sandwiched between a p and an n layer, a reverse-bias voltage produces an electric field perpendicular to the MQWS, which controls the intensity of a light beam at λ_o that passes through the MQWS as well as the magnitude of the photocurrent that is generated. Such a diode, when reverse-biased through a load, can be made into an optically bistable device that is switchable by optical signals. This diode and load become a Self Electro-optic Effect Device (SEED) [1].

An especially robust device occurs when two such diodes are reverse-biased in series, as shown schematically in Fig. 1, so that each acts as the others' load. This Symmetric-SEED (S-SEED) is an all optical, three-terminal device which acts as an optical set/reset latch. It exhibits time-sequential gain and so is optically cascadable. The S-SEED utilizes two incident beams; thus it is dual rail device. This mode is a distinct advantage since the operation depends on the ratio of the intensities of the incident beams and not on their absolute intensities. In a system design this ratio dependence allows for a relaxation of the tolerance requirements on uniformity for arrays of devices and incident beams [2].

The assembly of digital optics systems requires large arrays of devices. This paper describes the design and fabrication of arrays of S-SEED's with an internal dielectric mirror [3]. The advantages of the reflective device design over transmissive S-SEED designs includes:

1) Amenability to batch fabrication using standard processing procedures;

2) Shorter switching times due to smaller device size made possible by batch fabrication;

3) Increased output beam contrast due to double passes by light beams through the active MQWS;

---

* Presently at University of California at San Diego, Ca.

4) Better heat sinking, because the back of the chip can be heat sunk.

A schematic cross-sectional profile of a reflective S-SEED is shown in Figure 2. A complex GaAs/AlGaAs heterostructure was grown by Molecular Beam Epitaxy (MBE), consisting of an undoped quarter-wave layer reflector stack, followed by an n^+ conducting AlGaAs layer, then by the MQWS topped off by a p^+ conducting layer. The subsequent fabrication included: mesa-etching down to the n^+ layer, isolation of individual p-i-n diodes with ion-implantation, ohmic metal contacts, an insulator deposition through which appropriate windows were provided, an interconnect metallization and an anti-reflection coating deposition. The procedures were performed with a set of lithographic masks to produce a variety of device dimensions, shown in Table 1., in various array sizes.

Figure 3 is a photograph of one such array. The interconnection is such that all devices are electrically biased in parallel. The optical windows are large enough for two separate beams of focussed light per diode. This is necessary for optical logic systems.

The arrays were evaluated by comparing the results of the following experiment performed on each individual device. While a constant intensity beam P_{in2} is incident on diode 2, Fig. 1., the intensity of the beam incident on diode 1, P_{in1}, is linearly ramped between 0 and $2P_{in2}$. The output intensity P_{out2} is then plotted against P_{in1}. The expected performance is the following. When $P_{in1} \simeq 0$, the device is in the state where V (voltage at a point between the two diodes) is equal to V_o and P_{out2} is dim. The device remains in this state until P_{in1} far exceeds P_{in2} whereupon V drops to 0, and P_{out2} becomes bright. The device then remains in this state until P_{in1} drops far below P_{in2} whereupon V rises back to V_o and P_{out2} again becomes dim. A plot of P_{out2} versus P_{in1} should then be a hysteresis loop, the vertical height of which gives the output contrast and the horizontal width the robustness of the latching states. Figure 4 shows a superposition of the hysteresis loops of 128 devices in one 8×16 array. All the devices operate, 126 devices exhibit uniform operating characteristics and two show reduced sensitivity. The results of the fabrication and testing show that large arrays of reflective S-SEEDs can be batch-fabricated and that these arrays are suitable for system tests.

[1] D. A. B. Miller, D. S. Chemla, T. C. Damen, T. H. Wood, C. A. Burrus, A. C. Gossard, and W. Wiegmann, IEEE J. Quantum Electron. QE-21, 1462 (1985).

[2] A. L. Lentine, H. S. Hinton, D. A. B. Miller, J. E. Henry, J. E. Cunningham, and L. M. F. Chirovsky, Appl. Phys. Lett. 52, 1419 (1988).

[3] G. D. Boyd, D. A. B. Miller, D. S. Chemla, S. L. McCall, A. C. Gossard, and J. H. English, Appl. Phys. Lett. 50, 1119 (1987).

TABLE 1. DEVICE SCALING

MESA (μm×μm)	CAPACITANCE (fF/MESA)	MAX. BEAM DIA. (μm)	SPACING (μm)
200×200	4,600	50	400
100×100	1,150	40	200
60×60	415	25	140
30×30	105	10	80
14×13.5	22	5	40

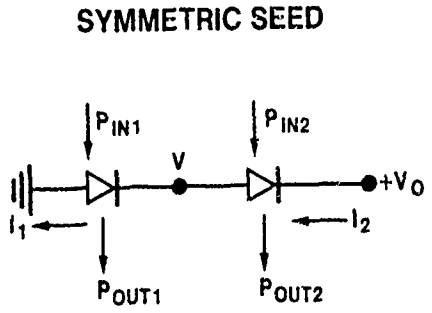

Figure 1. A schematic diagram of an S-SEED. Two MQW diodes are reverse-biased in series to V_o; their interconnection region assumes a voltage V. The input light beams P_{in1} and P_{in2} are transmitted or attentuated to P_{out1} and P_{out2} and corresponding photocurrents I_1 and I_2 are generated.

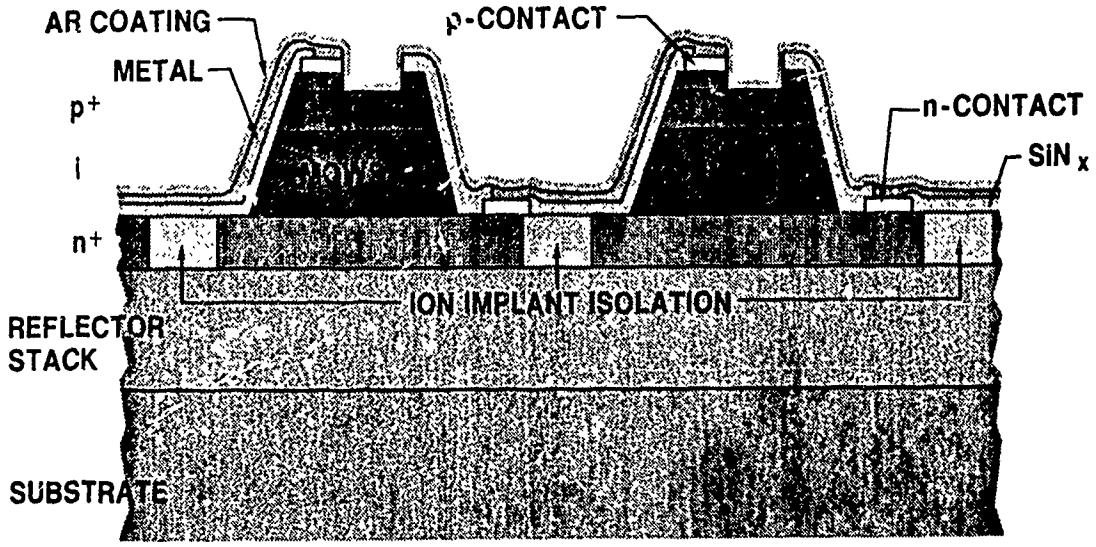

Figure 2. A schematic cross-sectional profile of a reflective S-SEED. This illustrates the MBE grown structure and the subsequent device processing.

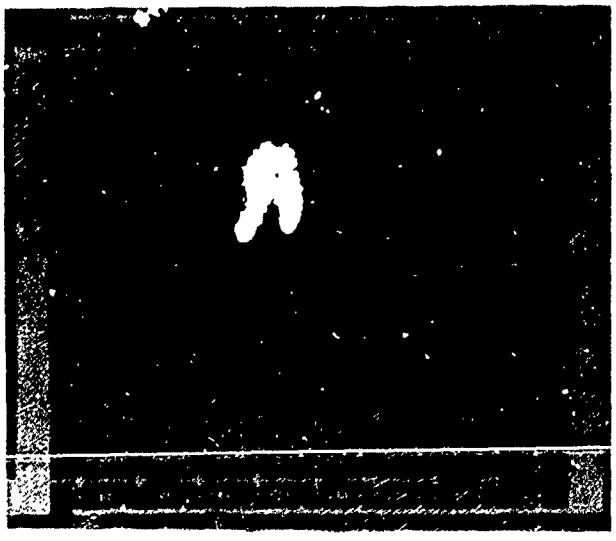

Figure 3. A photograph of an 8x16 array of S-SEED's.

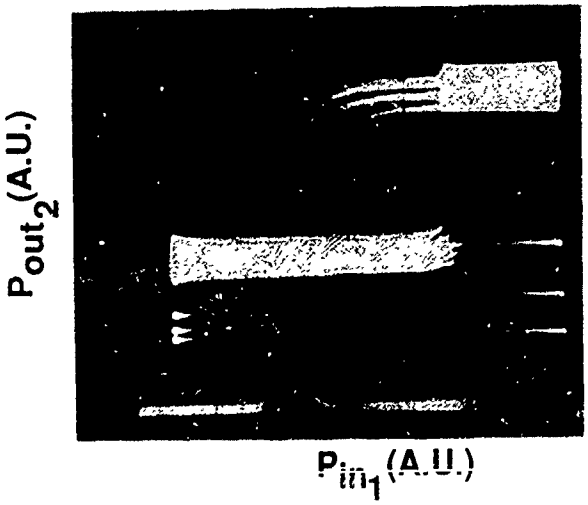

Figures 4. A storage oscilloscope superposition of the hysteresis loops which characterize device performance, for 128 S-SEED's in one 8x16 array. This data is obtained by plotting P_{out2} versus P_{in1}, when P_{in2} is constant and P_{in1} is ramped between 0 and $2P_{in2}$.

Diffusion Assisted Optical Switch: A new optical logic device

Theodore Sizer II, Gabriela Livescu, Jack Cunningham and David A.B. Miller
AT&T Bell Laboratories
Crawfords Corner Road
Holmdel, NJ 07733-1988

Both photonic switching and optical computing applications require that one have a device which uses one beam of light to switch either the amplitude or direction of another beam of light. Free-space imaging architectures are the most powerful in using large numbers of these devices in parallel. This places several requirements on the device parameters. First, the speed of the device must be compatible with either telecommunications or computing applications and as such must have a speed which is in excess of 1 GHz.[1] The optical energy to switch an individual device must be low since even a device with a 1 picojoule energy requirement when used at 1 GHz and in a 100X100 array requires a total switching power input of 10 Watts. This is a large amount of power which is presently unrealizable from lasers at the wavelengths required by current devices. The devices must also be cascadable and have a gain of at least two to allow the output of one device to drive two identical devices. The device should have a vertical structure (as opposed to waveguide) to allow for free-space imaging to large numbers of devices. Finally, the device should be fabricatable in large, closely packed, regular arrays.

What we describe here is a new device which satisfies many of the above requirements. The demonstration device uses GaAs - AlGaAs quantum wells in the intrinsic region of a reverse-biased PIN photodiode. The structure is very similar to the SEED modulator first demonstrated in 1984[2] which used a large mesa structure to define the PIN region. In this device, however, we employ a light spot which is many times smaller than the mesa itself. Used in this way with fast optical pulse inputs and precision timing between the logical inputs and outputs, the switching mechanism is considerably different than that of the SEED modulator. A series of diagrams which detail the operation of the device are shown in figures 1a-d. Figure 1e is an I-V curve taken with the input optical pulses tuned to be at the peak of the exciton near 0V bias voltage. This curve is related to the inverse of the transmission of the device providing for (at this input wavelength) a transmissive device at high voltages and an absorptive device at low voltages. At times before the input logic pulse (figure 1a) there is low light and as such the voltage provided is entirely across the high impedance PIN structure. When the pulse of light is incident on the mesa (figure 1b) the light is absorbed in the intrinsic region of the PIN; however, the electrons and holes are uniformly distributed throughout the intrinsic region and as such there is no change in the voltage in the focal region. At some later time, called T_1 (figure 1c), the electrons and holes transport out of the quantum wells and make their way to the P and N conductive regions. Since the applied field is solely in the vertical direction the electrons and holes are still bunched together in the plane of the wells. At this point the electrons and holes provide a screening field which is opposite in sign to the bias field which reduces the voltage in the focal region. Because the electrons and holes are localized, however, the voltage at any other position on the mesa remains at the bias voltage. As can be seen in figure 1e, this reduction in the voltage causes an increase in the absorption of the PIN structure in the focal region which can be used to provide a logical NOR operation. At a still later time, called T_2 (figure 1d), the electrons and holes laterally diffuse which causes the voltage in the focal region to recover. Thus, the risetime of this device is the transport time through the quantum wells while the falltime is the lateral diffusion in the P and N regions.

A device has been fabricated to test the device characteristics. Sixty-three periods of 105 angstrom GaAs wells and 80 angstrom $Al_xGa_{1-x}As$ barriers (x=0.4) were used as the intrinsic region of a PIN structure. A 200X200 μm mesa was defined and electrodes

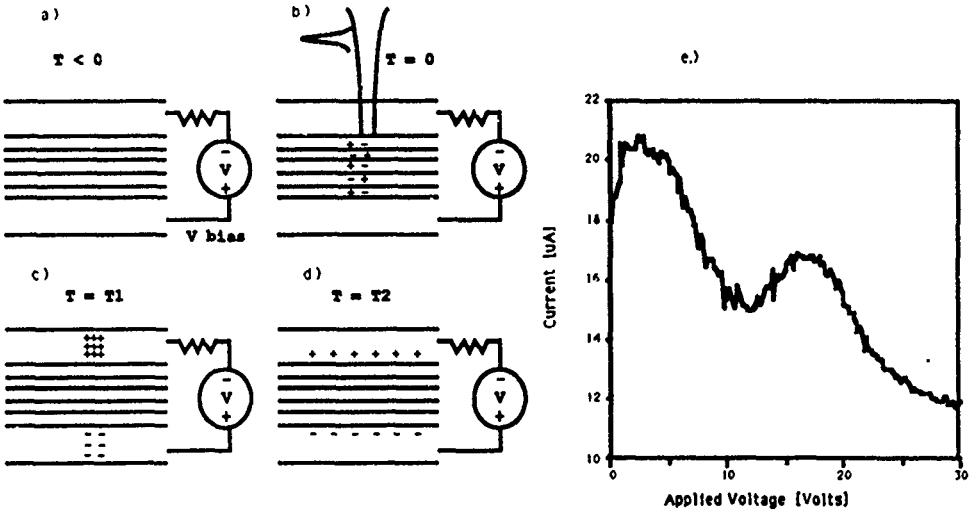

Figure 1: Diagram of device operation and IV curve for Quantum well based PIN structure.

were patterned to provide the reverse bias. Fifteen volts was used for the reverse bias. A modelocked dye laser was used for the pump-probe testing which had a repetition rate of 82 MHz at a tunable wavelength near 850 nm and a pulse duration of 2 picoseconds. The experimental results for three different values of the probe energy are shown in figure 2. In these curves the pump and probe are overlapped at T=15 psec which indicates that the transport time (time to maximum voltage change) is 35 picosecond while the diffusion time is near 60 picoseconds. The energy in the pump pulse is 80 femtojoules focussed to a 1.5 μm 1/e focal spot diameter. The change in transmission of the device was 20% which was less than expected. The reason for this is that diffusive conduction in the P and N regions is considerably faster than the transport time out of the wells for the tight focal spots used here. In the case of the 1.5 μm focal spot used here, the time to double the electron packet diameter is only 50 femotoseconds which indicates that as soon as the electrons escape from the quantum wells they diffuse laterally very quickly.[3] The number of electrons and holes created can be calculated accurately using the I-V curve data and the number created is sufficient to provide the contrast required for switching applications. Efforts to increase the diffusive conduction in the N and P regions are continuing and should approach the transport times ensuring that the electron and hole packets are maintained for a sufficient time.

The advantages of this device are many. First the area of the device is small and is determined by the focal spot diameter of the input optical logic signal rather than on fabrication of the device itself. It is generally easier to focus to small spots than fabricate small (about 1 μm) mesas. Since the energy of all optical logic devices is linearly related to the area of the device, the energy required for the device is also small. Theoretical values show that if the diffusion constants can be reduced, the energy to switch the device should be less than 10 femtojoules. Secondly, the device is cascadeable since there is gain (as illustrated in figure 2) and uses the same wavelength for both the input and output. Since the pump and probe are not overlapped in time, the gain is time sequential gain. The device is, therefore, a three terminal device. Thirdly the speed of the device is less than 200 picoseconds for a complete operation allowing for operation up to 5 GHz. The speed is given by diffusion times rather than RC time constants. Lastly the fabrication of the device is relatively simple involving only one large mesa to be created. Many different spots (and therefore logical operation sites) can be situated on the same

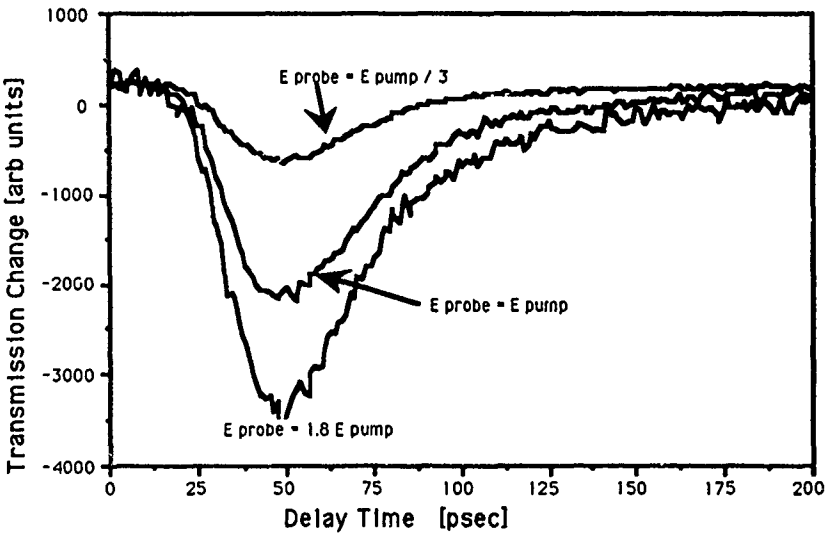

Figure 2: Transmission versus time plots for three different values of the probe energy - The pump energy is kept at 86 femtojoules.

mesa since it is the locallized electron and hole packets which provide the change in the voltage which subsequently changes the transmission. As the electrons and holes diffuse, however, there will be "cross-talk" between the adjacent spots. If 2 μm spots are used 20 μm apart, however, than the crosstalk between two adjacent spots will be a 1% modulation since the packets diffuse uniformly in the plane of the N and P regions. If a 1% crosstalk is acceptable than a 100x100 array of spots could be operated on a single 2x2mm mesa.

References

[1] T. Sizer "Light Sources for Optical Computing Applications", paper TuI-5, International Quantum Electronics Conference, Tokyo, Japan, July 19, 1988.

[2] D.A.B. Miller, D.S. Chemla, T.C. Damen, A.C. Gossard, W. Wiegmann, T.H. Wood, and C.A. Burrrus, "Novel hybrid optically bistable switch: The quantum well self electro-optic effect device," *Applied Physics Letters*, vol. 45 p.13-15, 1984.

[3] G. Livescu, D.A.B. Miller, T. Sizer, D. Burrows, J.E. Cunningham, A.C. Gossard, and J.H. English, "High speed absorption recovery in quantum well diodes by diffusive electrical conduction," Submitted to Applied Physics Letters

Optical Back Plane Interconnect (OBIT) Technology for Computers,
J. M. Hammer, David Sarnoff Research Center, CN 5300, Princeton, NJ 08543-5300 and H. D. Hendricks, NASA Langley ResearchCenter, MS 473, Hampton VA 23665,

We describe and analyse a novel approach to implementing an Optical Back Plane Interconnect Technology (OBIT) which is capable of optically connecting any row of a MxN back plane array to any row of a second MxN array. Each back plane array illustrated in Fig. 1 is formed monolithically on a wafer. The technology is based on the use of Grating-Surface-Emitting (GSE) waveguides [1] which are formed on a wafer containing quantum well and separate confinement waveguide layers. These layers serve a number of functions being used for transverse guiding, gain, modulation, detection [2] and for the the formation of wavelength tunable distributed Bragg reflector lasers.[3] The required ridges, electrodes and other surface structures are formed photolithographically. The GSE waveguides act as efficient antennae which radiate light at angles selected by tuning the wavelength of the lasers. In the receiving mode the same waveguides may be used as receiving antennae. See Fig. 2. Thus, wavelength tuning is used to direct light from each row of the transmitting array to the desired row of the receiving array.

Using our approach it should be possible, within the present state of the art, to have an optical backplane array with the following characteristics: Any row of an MxN GSE array may be optically connected to any row of a second MxN array. As an example, scanning the laser driver of a row of the transmitting array through a wavelength range of 100 Å, [3] any of 16 rows of the receiving array can be addressed. The number of addressable rows for a 200 Å scan is plotted against the output coupling angle at the center wavelength in Fig.3.

Each monolithic array can be used as both transmitter and receiver by switching the bias on the quantum well Switch-Detectors. Separate transmitting and recieving structures could be provided for duplex operation. For a 32 row device with a bit error rate of 10^{-9} at 100 M Hz data rate , a required laser power of 12 mW is calculated.

This approach has the following advantages:

- Uses an optical method to overcome complexity inherent in electronic switching for computer applications.
- Will be compact and power efficient because a complete backplane array is formed monolithically on a chip.
- Requires only one switch decision to switch M parallel connections to anyone of M positions.
- Can achieves a high level of performance (32 parallel connections to any of 32 positions with 10^{-9} BER at a 100 MHz data rate) with modest laser power.

Details of the theoretical calculations and some results of supporting experiments will be given.

[1] G.A. Evans, N.W. Carlson, J.M. Hammer, Optoelectronics-Devices and Technologies, 2, 363 (Dec.'87)
[2] Y. Kan, H. Nagai, M. Yamanishi, IEEE J. Quantum Electron.,QE-23, 2167 (12 Dec. 87)
[3] B. Broberg and S. Nilsson, Appl. Phys. Lett. 52, 1285 (18 April '88)

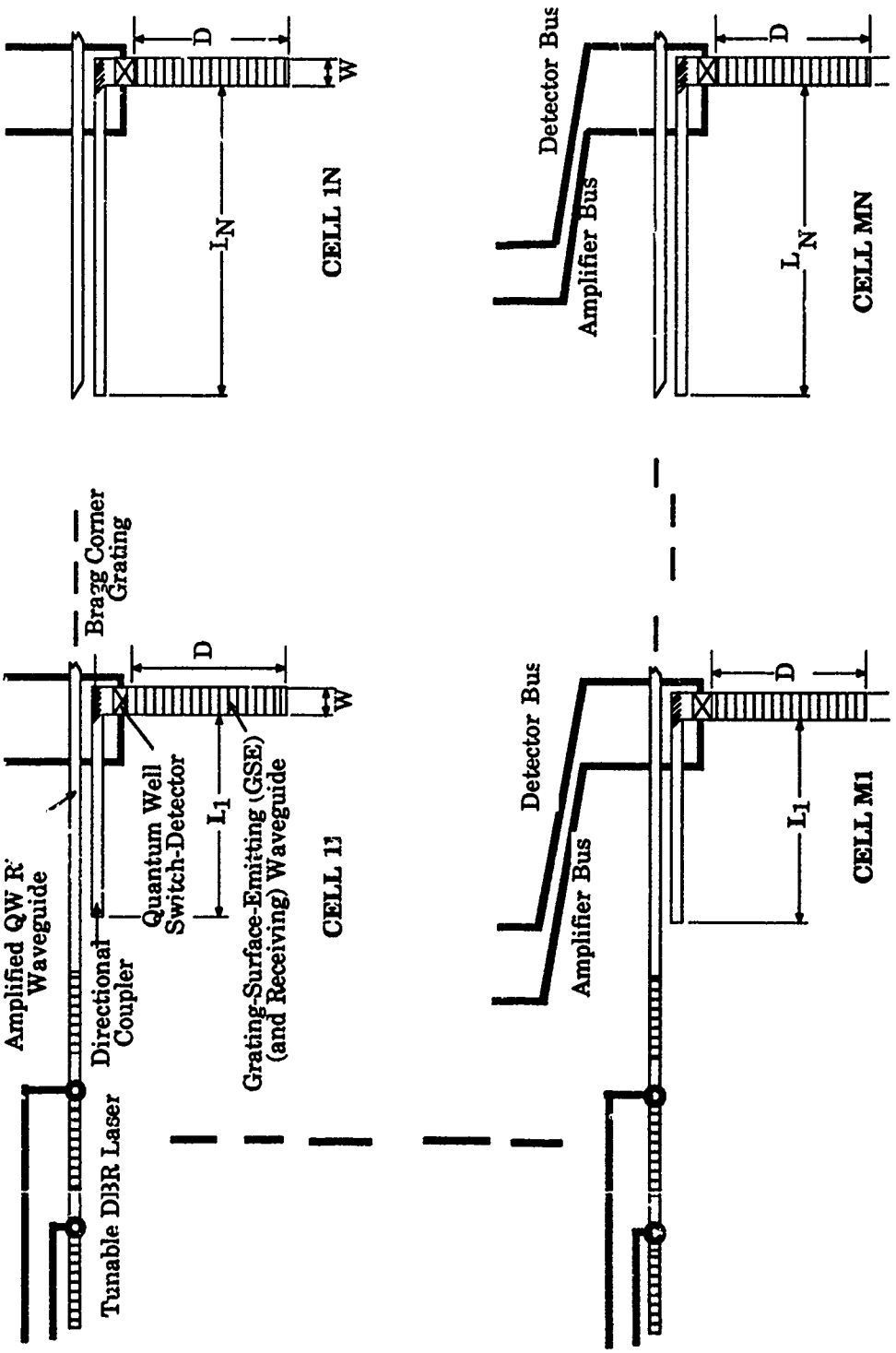

Figure 1. Schematic diagram of GSE waveguide array approach to OBIT. Light from the tunable laser is distributed to the unit cells of a row through the amplified waveguide and directional couplers. The GSE waveguides emit or receive light at angles which vary with wavelength.

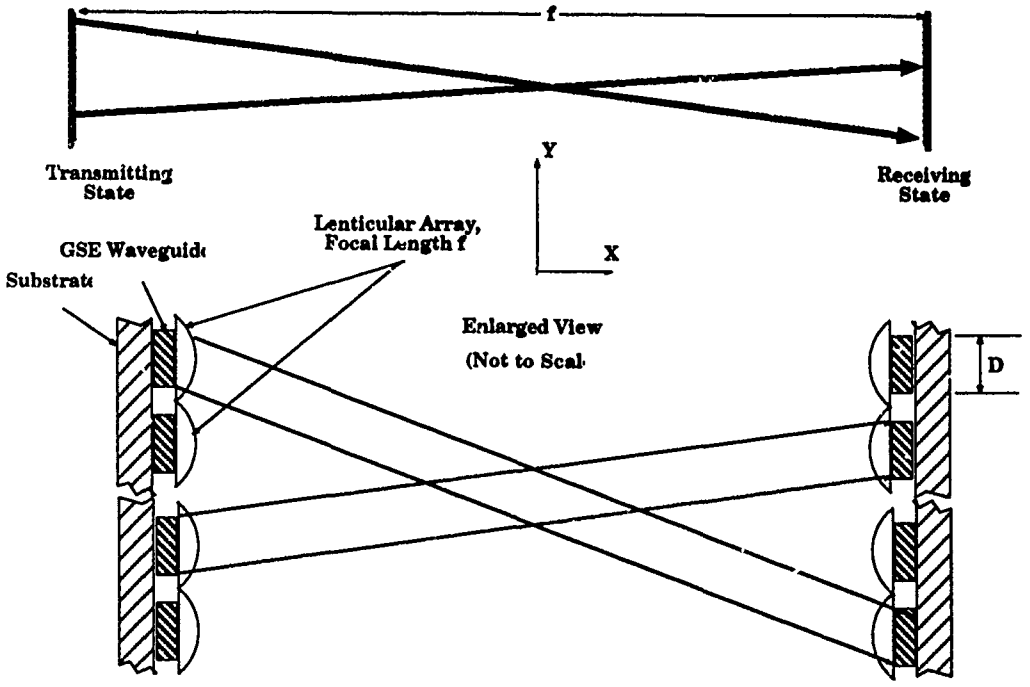

Fig. 2. Schematic of two GSE waveguide arrays arranged with lenticular arrays to act as transmitter and receiver for an optical back plane interconnect system.

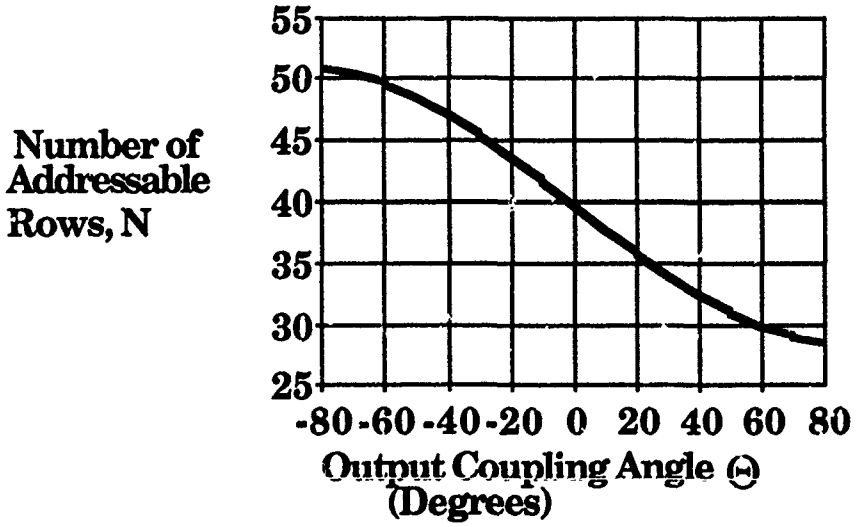

Fig.3 Number of addressable rows plotted against the output coupling angle measured from the normal to the waveguide plane when the the wavelength is tuned ± 100 Å around a center value of 0.83 μm. The GSE Waveguide grating length D = 500 μm, n_e = 3.4 and n_0 = 1.

NOTES

THURSDAY, MARCH 2, 1989

SALON E

3:30 PM–5:15 PM

ThE1–ThE6

MULTI-DIMENSIONAL SWITCHING SYSTEMS

Lars Thylen, Ericsson Telecom, Sweden, *Presider*

Dense WDM Networks and Applications

Charles A. Brackett
Bell Communications Research
Morristown, NJ 07960-1910
U.S.A.

INTRODUCTION

Wavelength-Division Multiplexing (WDM) began with the use of two-to-four wavelengths on single fibers for the purpose of increasing the information capacity between two fixed points in a communications network. It has evolved to experimental demonstrations of systems of up to twenty wavelengths[1] (with projections extending to hundreds and even thousands of wavelengths) in network architectures where wavelength is used as part of the very interconnection fabric of the network. In this paper, we will outline the types of network architectures that are evolving using dense WDM, review some of their potential applications, summarize experimental progress, and discuss some of the relevant technologies.

ARCHITECTURES AND APPLICATIONS

The broad goals for the application of optics to communications networks include: 1) increasing the information bandwidth available to the user, 2) creating a service-transparent network, 3) increasing the degree of interconnection flexibility, 4) providing relief to emerging switching bottlenecks, and 5) reducing the cost of broadband services.

The unique properties of optical systems that contribute to these goals are:

1. The very large bandwidth of the fiber medium. The low-loss regions of the fiber transmission spectrum provide a bandwidth of roughly 20 THz, implying a potential capacity of several Tb/s. Utilization of such a large bandwidth would almost certainly depend on using multiwavelength techniques. Such techniques were used to set the current capacity record, held by the 18-wavelength, 36 Gb/s, LAMBDANET demonstration, which uses DFB lasers with 2 nm channel spacings. Several experiments have demonstrated 8 - 10 wavelengths with 5 - 10 GHz spacings.

2. Signal Orthogonality. The ease of producing large numbers of wavelengths and their subsequent independent detection, using either filtering and direct-detection or coherent detection, means that new network structures can be considered in which all of these signals can be made available at each point of the network.

3. Passive Optical Components. In relative terms, both WDM filters and broadcast-star couplers are easy to make. Fiber stars with large dimensions have been used in experiments to demonstrate the feasibility of, for example, video distribution to 2048 subscribers.[2] These components, being passive, offer the promise of less expensive, highly reliable, local subscriber networks, in which the transport portions are insensitive to the service or bit-rate.

Two types of network architectures are evolving to the forefront of consideration: 1) Wavelength-Division Routing networks, and 2) Broadcast-and-Select networks.

In wavelength-routing networks, the path through the network is determined by the wavelength, with the possibility of several sequential branch-points. Such networks can be large both in number of terminations and in geographic size. Switching can be achieved by using wavelength- (or frequency-) agile sources; switching sources between wavelengths redirects signals from one output port to another. These networks feature non-blocking, single-stage switching, distributed routing, and wavelength-addressed outputs, but do not directly permit point-to-multipoint (either multicast or broadcast) switching. Such networks have been proposed for local-loop telephony since they allow the establishment of private channels over a shared fiber, with passive components.

In broadcast-and-select networks, the core of the network is currently a passive broadcast fiber star; the signals from each input port are thus broadcast to every output port simultaneously. The simplest form of such a network uses unique, fixed, wavelengths at each input. Each output port is then

terminated in either a wavelength-selective receiver, or a WDM unit and an array of unselective receivers. The availability of all network traffic at each output port gives these networks the most complete interconnectivity possible. The passivity of the switch again implies that the network intrinsically is transparent to the data and signal format. Such networks have been proposed for both circuit and packet switching, with a wide variety of switch-control algorithms, supporting multicast as well as point-to-point services. One commonly envisioned, though economically uncertain, application, is that of broadcast video local distribution, in which the subscriber would select channels by tuning a filter or local oscillator.

For some applications, not only the number of wavelengths and their interconnection network are important, but also the speed with which any of the wavelengths can be accessed or changed. Video program selection at the subscriber's terminal would require only a millisecond or so response time, but high-speed packet-switching, for instance, would likely require switching between any two wavelengths in a few nanoseconds[3].

In all of these cases, the discrete wavelengths serve to create an orthogonal set of carriers which can be separated, routed and switched without interfering with each other. It is this use of wavelength, and its processing in passive network elements, which distinguishes optical networks in general from other network technologies. The use of many wavelengths for these network functions of routing, selection and transmission-capacity enhancement is the natural exploitation of the fiber bandwidth. The full utilization of the fiber bandwidth by time-division multiplexing would require pulse durations on the order of femtoseconds duration in ordinary digital time division multiplexing. It would also require sophisticated high-speed electronics and substantial power dissipation. By comparison, dense WDM passive networks offer simple distributed-processing architectures.

THE CONTROL PROBLEM

It is common to consider only the information transport when talking about photonic switches. There has, however, been an increasing awareness in the photonic-switching community of what has been known for a long time in the electronic switching world: the throughput limitations of a switch are more often determined by the information processing requirements than by the signal transport technologies. This is especially true in packet switches and packet networks; it is also an important consideration in multiwavelength packet networks.[4]

The signal processing requirements that are an intimate part of switching are difficult to meet without electronic conversions and electronic processing. An often-stated goal for optical switching is to have an all-optical network, with electronic conversion only at the edges of the network. This must, however, be regarded as a very distant goal for any large-scale switching system. In a packet switch for example, a destination address is contained in the header. This address must be decoded and translated to an output-port address, with the packet being stored in a buffer memory during this header processing. There are forms of optical memory which can conceivably do this job, but not for large switches and long memory times. For circuit switches, one can consider separate signalling circuits, but those are normally packet channels themselves, and even so it is a non-trivial job to organize and synchronize the signalling and data channels, and then actually perform the switching operation, without a buffer memory.

In view of such considerations, it is natural to pursue hybrid switches, where the digital processing is done in electronics and the data transport is optical. When large-scale integrated optical memory becomes available, it may be possible to consider optical control.

RECENT RESULTS

A brief summary of network experiments and multiwavelength technology, including tunable lasers and filters, can be found in the ECOC '88 Conference Proceedings.[5] More recent results are summarized below:

1. ECOC '88:
   Several NEC papers on advances in tunable lasers reported tuning to 10 independent wavelength channels, and the tuning of DFB-amplifier based receivers to 8 independent channels. Both

devices were switched at high speed and were demonstrated in a space-division WDM switching experiment. A 10-channel coherent video distribution experiment with modularly packaged laser transmitters and automatic optical frequency locking and registration was also reported.

Bellcore presented several papers on hybrid optical packet switches with internal control and contention resolution, by using a broadcast star and tunable laser for the information routing, and a tunable DFB optical amplifier for the control function. The simulated packet switch was used to demonstrate 1ns switching times between Gb/s packets. This approach uses electronics to do the packet processing and uses optics to do the information and control signal transport.

Also presented was a demonstration of 20 wavelength simultaneous amplification in a laser amplifier, achieving 6 - 9 dB gain with no measurable crosstalk penalty, and an experiment using tunable etalons to perform the tunable receiver function in a multiwavelength video distribution system, showing 16 wavelengths at 600 Mb/s to 64 customer terminals, and at 2 Gb/s to 16 terminals.

2. GLOBECOM '88:
   An NEC paper [paper 29.2] presented several switch proposals with a multiplicity of wavelength and time division multiplexed switching. Switches both with and without wavelength conversion were examined, and application to Broadband ISDN switching systems was proposed.

3. OFC '89:
   Bellcore [papers ThG3, ThB3] introduced the use of both bulk and integrated acousto-optic tunable filters in WDM networks. These devices can select any wavelength on a fiber, tuning over virtually the entire 1.3 and 1.5 μm transmission bands, with switching times of a few μs and resolutions as good as 1 nm. A single filter can simultaneously select multiple wavelengths. The integrated ($LiNbO_3$) device required as little as 100 mW of rf drive power. They had previously demonstrated the use of the same filter to make an electronically tunable external cavity laser with an 83 nm tuning range with 3 μs tuning speed.[6]

CONCLUSIONS

A wide variety of applications all point to an increasing importance for dense WDM networks, where the wavelength becomes a part of the interconnection and switching fabric. Such systems may employ either direct or coherent detection. Their real significance lies in the fuller use of the fiber bandwidth potential to expand the network function.

REFERENCES

1. G. Coquin, et al, "Simultaneous amplification of 20-channels centered at 1.54μm in a multiwavelength distribution system," Proc. ECOC '88, postdeadline paper, pp. 41-44, 1988.

2. W.I. Way, et al, "90-channel FM video transmission to 2048 terminals using two inline travelling-wave amplifiers in a 1300nm subcarrier multiplexed optical system," Proc. ECOC '88, postdeadline paper, pp 37-40, Brighton, England, 1988.

3. M.S. Goodman, et al, "Demonstration of Fast Wavelength Tuning for a High Performance Packet Switch," in Conf. Proc., ECOC '88, Brighton, UK, 1988

4. E. Arthurs, et al, "HYPASS: an Optoelectronic Packet Switching System," IEEE J. on Selected Areas of Communications, vol. 6, pp 1500-1510, Dec. 1988."

5. C.A. Brackett, "Dense-WDM Networks," in Conf. Proc., ECOC '88, Brighton, England, 1988.

6. G. Coquin, K. W. Cheung, and M.M. Choy, "Single- and Multiple-Wavelength Operation of Acousto-Optically Tuned Semiconductor Lasers at 1.3 Microns," 11th IEEE Int. Semiconductor Laser Conf., Boston, 1988.

High-Speed Hitless Switching Using Ti:$LiNbO_3$

J.R. Erickson R.F. Huisman K.D. Major* R.A. Nordin R.S. Veach

AT&T Bell Laboratories, 200 Park Plaza, Naperville, Il., 60566

1. INTRODUCTION

In designing switching systems with Ti:$LiNbO_3$, one faces a dichotomy: couplers may be long with low voltage requirements and fast switching speed; or they may be short with higher integration but slower switching speed.

Modulators in Ti:$LiNbO_3$ have reached 40 GHz and time-division multiplexing at 16 Gb/s has been shown [1] [2]. These high-speed experiments used discrete modulators and switches with lengths > 1 cm and terminated traveling-wave electrodes. This combination of low voltage and careful electrical design allows switching speeds that can accommodate the needs of future multigigabit systems.

Using current device design constraints and moderate power budgets, architectures have been proposed for building Ti:$LiNbO_3$ switches with 32 inputs and 32 outputs[3] [4], with possible extensions to 512x512. Characteristics of proposed architectures include a range of blocking probabilities and signal-to-crosstalk ratio (SXR) alternatives broad enough to accommodate the connection and performance needs of most applications. In growing to architectures of these dimensions, however, individual coupler length shortens and switching speed slows. Power dissipation makes it unlikely we will have a substrate with 20 high-speed couplers at 15 volts, each with terminated transmission-line electrodes.

This paper proposes a marriage of long high-speed switches with slower more complex arrays to achieve a high-speed hitless switching system.

2. BANK SWITCHING

In bank switching, the input data stream is demultiplexed by high-speed traveling-wave-electrode switches. Each of the two demultiplexed streams is fed to one of two switching fabrics (see Figure 1). After switching and exiting the fabrics, the data streams are recombined into a contiguous stream. This approach allows us to relax the switching speed requirements on the large arrays at the expense of duplicating the fabric. Let: R = the data rate in bits per second, W = bits per word, $T_R = 1/R$ = bit period in seconds, $T_W = W/R$ = word period in seconds, and X = fraction of a bit time allowed for bank switching. Then the settling time for the high-speed bank switches is $X \cdot T_R$ and the settling time for the switch arrays is $T_W - X \cdot T_R$. If $W = 1$ the switch array must reconfigure in a single bit time, but if $W = 8$ as in the SONET standard that is gaining wide acceptance, the switching fabrics have approximately 8 bit times to reconfigure. Larger W relaxes the speed requirement on the

---

* Now at University of Pennsylvania, Philadelphia, 19104

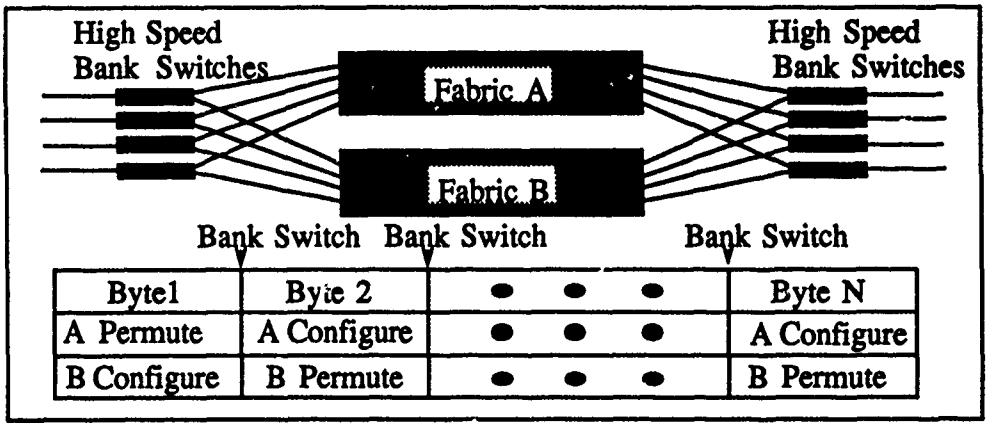

Figure 1. Bank Switching of a Byte-Multiplexed Format

switch fabric.

The switching speed required of the bank switches depends on the data coding. For Non-Return-to-Zero coding X must be small; for Return-to-Zero (RZ) coding, $X = 0.5$. A RZ, byte-multiplexed data stream at 2 Gb/s requires the high-speed bank switches to settle in 250 ps and the fabric switches to settle in 3.75 ns; with careful electrical design, both requirements can be met.

Since we are using the switching network as a time-multiplexed switch, the fabric need only be rearrangeably non-blocking and we can take advantage of the high SXR provided by the dilated networks proposed by Padmanabhan and Netravali[4].

Synchronization is a critical issue. Any two paths through the fabrics must be of equal length so that the final outgoing bitstream is contiguous. The high-speed switches must be phase synchronous with the data and must be driven by a square wave of $R/(2W)$ Hz. The fabrics can be driven with sequences derived from the R/W clock. Permutation decisions and routing must be pipelined.

3. BANK SWITCHING EXPERIMENT

An experiment to show feasibility of this bank switching approach is show in Figure 2.

3.1 Experimental Setup

The switching fabric used is a 4x4 Passive Splitter/Active Combiner (PSAC) switch that has lossy tranmission line electrodes. Fabric A is represented by switch 5 and fabric B by switch 8. These couplers are characteristic of the designs used in larger fabrics. To simplify the experiment, we use an electronic, input bank switch made from commercial gallium arsenide and a passive fused-fiber coupler in place of the output switch. The clock/8 output from the BER generator feeds the logic which drives the switches. Clock/16 drives the input demultiplexer such that every other byte goes to the same fabric.

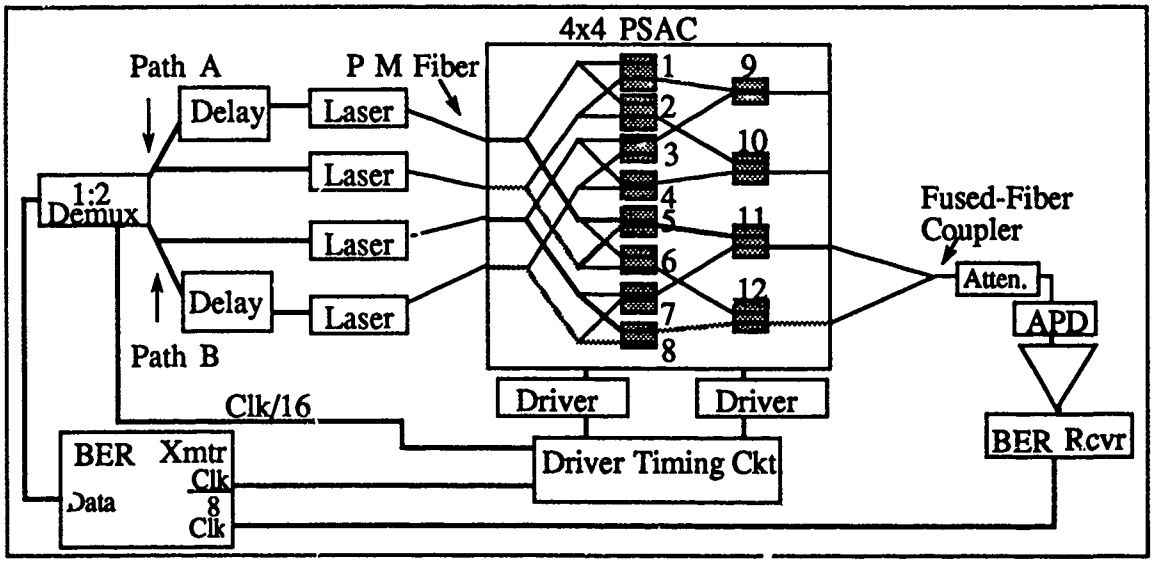

Figure 2. Bank Switching Experiment for Byte-Multiplexed Data

3.2 Experiment Scenario

A repetitive 8-bit pattern from the BER transmitter is sent to the 1:2 demux. One of each of the demultiplexed streams is delayed to uncorrelate it from the other bitstream. Each of the two bitstreams drives two lasers and each laser output is sent to the fabric. The high-speed bank switch alternates between Path A and Path B in Figure 2. Each path is switched as necessary to construct a consistent 24-bit pattern after the bitstreams from the two fabrics are coalesced. This consistent 24-bit pattern is then converted to electrical, amplified and fed to the BER receiver. Bit-error-rate testing at a data rate of 622 Mb/s on a byte-multiplexed stream yields an error rate of $\sim 3^{-11}$ at -34 dBm received power.

REFERENCES

1. Korotky et al., "Optical Intensity Modulation to 40 GHz Using a Waveguide Electro-Optic Switch", *Appl. Phys. Lett.*, 50(23), p. 1631, 8 June 1987
2. Tucker et al., "16-Gbit/s Optical Time-Division-Multiplexed Transmission System Experiment *OFC '88 Technical Digest*, Vol. 1,Paper THB2, OSA 1988, p. 149
3. S. Suzuki et al., "Thirty-Two-Line Optical Space-Division Switching System," *OFC '87 Technical Digest Series 1987* Vol. 3, WB4, OSA 1987, p. 146
4. K. Padmanabhan and A.N. Netravali, "Dilated Networks for Photonic Switching," *IEEE Trans. on Comun.*, Vol. COM-35, No. 12, Dec. 1987, pp. 1357-1365.

An Experimental Modular Switching System with a Time-Multiplexed Photonic Center-Stage

R. A. Thompson, R. V. Anderson, J. V. Camlet, and P. P. Giordano

A. T. & T. Bell Laboratories

600 Mountain Av

Murray Hill, NJ 07974 USA

(201)-582-6170

SUMMARY

This Experimental System supports N switching modules, interconnected by an N-by-N central network. Each module connects to the center-stage by a one-way single-mode optical fiber up-link and down-link. The implementation is electronic from each module outward toward its users and is photonic from the links inward toward, and including, the lithium niobate center-stage. Figure 1 reflects the current state of this prototype; with only 2 modules, although the center-stage is 8-by-8.

Switching is classical *time-space-time*, where the modules perform the time-division multiplexing. The center-stage is a time-multiplexed space switch, that connects N up-links to N down-links in parallel, reconfiguring for every time-slot in a pattern that cycles every frame. For example, in a telephone switching environment, a module with 256 time-slots could serve about one thousand users with an acceptably small probability of blocking. Then, with a 64-by-64 time-multiplexed center-stage, the total system with 64 modules could serve over 60,000 users, comparable to a large telephone switching office.

Since users are spatially concentrated by time-multiplexing in modules, the spatial central network is small. However, the data rate on the links must support the active user's data rate times the multiplexing factor. While a small switching network supports a large system, it must be capable of extremely high throughput. But its switching speed need not be high because the network is reconfigured at the time-slot rate, not the bit rate. Requirements of small size, high throughput, and modest switching speed match well with lithium niobate technology. Furthermore, the overall system allows that the data rate may be non-uniform from one time-slot to the next. Changes in this rate, by simply replacing the transmitters and receivers in a link interface, do not affect the center-stage.

A Time-Division Multiplexing Module is implemented with a commercial private branch exchange (PBX). This PBX's back-plane is time-multiplexed into 256 time-slots in 8000 frames per second. In the prototype, frame and time-slot in all modules are synchronized together and with the center-stage. An added Link Interface, in Figure 1, translates this parallel electronic back-plane with the serial optical up- and down-links. At 180 Mbps, an 8-bit word occupies a small part of a 488-ns time-slot. A telephone conversation, between T1 and T2, has been successful.

Similar boards, represented by "other e/o" in Figure 1, provide communications for 88 Mbps uncompressed digital video, in only 18 time-slots, by using 1.5 Gbps within these time-slots. These high-rate time-slots are interspersed with the conventional time-slots. In each module, the fibers from these boards are passively combined to the single up-link and down-link. Such calls are set-up by slightly modified existing software in the modules.

The Photonic Time-Multiplexed Center-Stage is an 8-by-8 Dilated Benes Network,[1] containing 48 directional couplers on two butt-coupled chips of Lithium Niobate.[2] The 48 electronic driver circuits[3] reconfigure the network in 5 ns at the beginning of every time-slot, well before the bits in the middle of the time-slot arrive at the switch. These bits may be an 8-bit audio sample or data packet at 180 Mbps or they may be several hundred bits at 1.5 Gbps; it doesn't matter to the network.

With only 2 modules now, the current center-stage has two configurations and the control processor is simple. This controller will become more complex as the experimental system expands toward N=8 modules in the future. While control of this network is centralized, overall call processing control is distributed.

REFERENCES

1. K. Padmanabhan and A. N. Netravali, *Dilated Networks for Photonic Switching*, OSA Top Mtg on Phot Sw in March 1987 and IEEE-TComm in Dec 1987.
2. J. J. Veselka, et al. *A Low-Voltage, Low-Crosstalk 8-by-8 Ti:LiNbO3 Switch for a Time-Multiplexed Switching System*, OFC in Feb 1989.
3. R. A. Thompson and P. P. Giordano, *An Experimental Photonic Time-Slot Interchanger Using Optical Fibers as Re-entrant Delay Line Memories*, OFC in Feb 1986 and IEEE-JLT in Jan 1987.

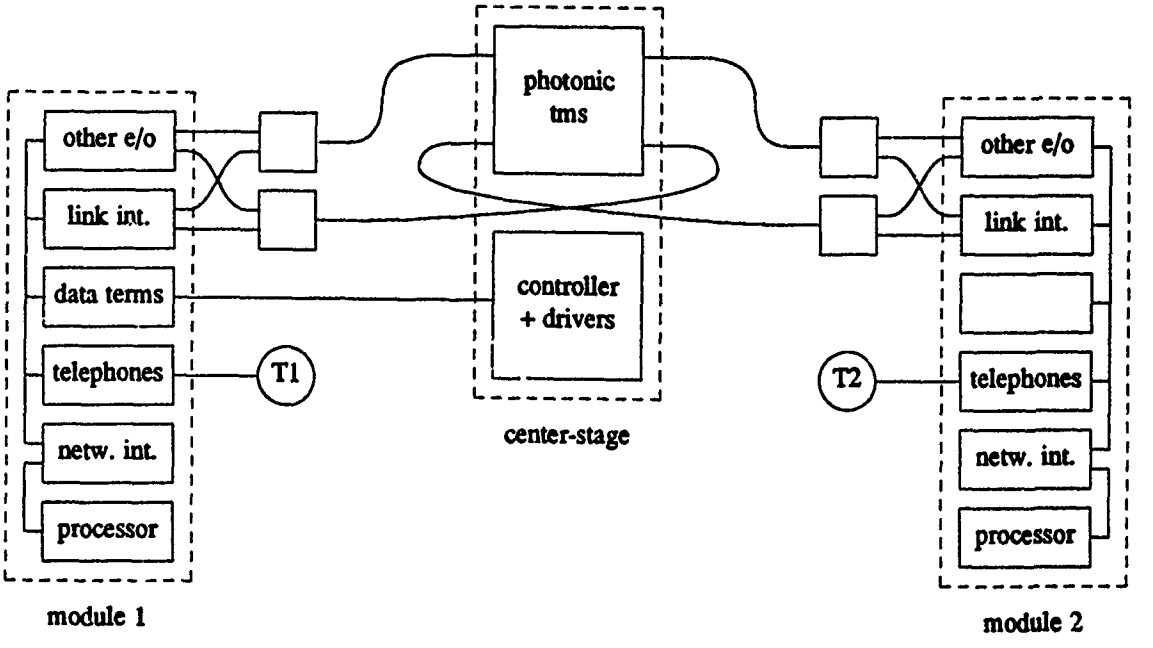

Figure 1. Modular Photonic Switching System

EXTENDIBLE OPTICAL INTERCONNECTION NETWORK.

D.W. Smith, P. Healey, S.A. Cassidy.

Department RT214, British Telecom Research Laboratories,
Martlesham Heath, Ipswich, UK., IP5 7RE.

Abstract:

This paper describes a new form of non-blocking extendible multi-stage optical interconnection network that combines one, two, or more degrees of switching freedom via access to a common multiple access bus. The common bus is capable of exploiting the spatial, spectral, and temporal multiplexing powers of optics, significantly reducing the number of physical interconnections required.

Introduction:

Photonics technology could play a significant role in future telecommunications and computer switching systems. Currently, the route ahead for large optical switching machines appears tortuous because of the unrealistic demands that must be made on the optical technology. In this paper a new approach is presented that could allow very large switches (eg 10000 x 10000) to be realised without any major technology breakthroughs.

The basic idea is to employ a hierarchical set of multiple access (MA) techniques (such as space 'S', frequency/wavelength 'F', time 'T', code 'C', ... etc) in such a way that each interconnect circuit is identified by a unique combination of channels from this set. The channels may be selected on a pre-assigned or demand assignment basis. The total number of interconnects is given by the product of the number of channels in each member of the MA set. For example, a MA set comprising (S,F,T) multiplexing, each with a dimension of 100 channels, corresponds to an interconnect power of 10^6.

The main advantages of this new approach to interconnection network design are:-

* It allows many of the developing photonics switching technologies, which by themselves offer limited switch size, to be combined in the realisation of very large interconnection networks.
* A bus architecture can be used to greatly simplify the practicable network implementation, whilst also offering extendible growth.

Architecture:

The architecture (Figure 1) is based on a multiple, multiplexed, bus approach. One parallel bus carries the multiplexed messages whilst a second bus carries the multiple access channel references. An interconnection path is established by selecting one channel from each of the multiple access reference buses, performing the channel product (eg, multiplying a selected frequency carrier by a selected time slot), modulating the resulting carrier by the message information, and then connecting the result to the selected space channel on the message bus. Thus, each space channel conveys a multiplex hierarchy of messages. In order to select a particular channel from the bus, the receiver effectively 'peels' off the multiplexing layers by first selecting the appropriate space channel, followed by the remaining de-multiplexing steps. To simplify this operation, the receiver also has access to the MA referencing channels via the common bus. Numerous channel allocation techniques can be

used, however, for brevity we will only describe a pre-assigned transmission channel approach using space and frequency (S,F) MA.

Figure 2 shows an example of a pre-assigned transmission channel (S,F) network architecture. Each input node is arranged to modulate a pre-assigned optical frequency from a multiplex of M frequency references. Each modulated optical carrier is then connected to one of N spatial paths on the common message bus. The message bus is connected, by power sharing, to all of the output selector switches. Connections are established by combinations of space switching and frequency tuning at each of the receivers Thus, each receiver has access to all NxM input nodes. Tunable optical receivers could be built using adjustable filters in front of the detector. However, a much more elegant technique in this instance is to use optical heterodyne detection. Optical heterodyne detection is relatively straightforward when all frequency sources are available on the reference bus. In this example, the interconnect path is chosen by the receiver selecting both the appropriate spatial path from the signal bus, and the appropriate local-oscillator (LO) path from the reference bus. Practicably, M and N may be limited to about 100 channels, but, combined in this way we can achieve a 10000x10000 switching network.

The number of crosspoints used in this network is considerably less than a simple single-stage network and yet, unlike the more complex multistage networks such as Clos, this network is very simple to extend. Power loss due to signal distribution via the bus could be compensated by suitable optical amplifiers.

The space switches could be based on a number of technologies, such as Lithium Niobate [1], Fibre switches [2], and Beam steering switches [3]. And numerous techniques for the stable generation of optical frequencies are known [4].

Discussion and Conclusions:

A new bus oriented, hierarchical multiple access, optical interconnection network has been described that allows many optical switching techniques to be combined into a single, extendible architecture. The number of switchable data paths grows as the power of the number of MA techniques, thus, rapidly yielding very large connectivity. Latest progress in demonstrating this concept in the laboratory will be presented at the meeting.

Acknowledgments:
The authors wish to thank the Director of Research of British Telecom for permission to publish this paper.

References:

1] R.A. Spanke.: "Architectures for Large Nonblocking Optical Space Switches", IEEE J. Quantum Electronics, Vol. QE-22, No. 6, pp. 964-967 (1986).
2] S.A. Cassidy, and P. Yennadhiou.: "Optimum Switching Architectures Using D-Fibre Optical Space Switches", IEEE J on Selected Areas in Communications, Vol. 6, No. 7, pp.1044-1051. (1988).
3] P. Healey.: "Optical Switching Networks Using Multiplexed Crosspoints", 14-th European Conference on Optical Communication, Brighton, UK. Conference Pub. 292-part 2 (Post-Deadline Papers) pp.53-56. (1988).
4] G.R. Hill, et-al.: "Evolutionary Wavelength Division Multiplexed Schemes for Broad-band Networks", OFC/IOOC87, Reno. (1987).

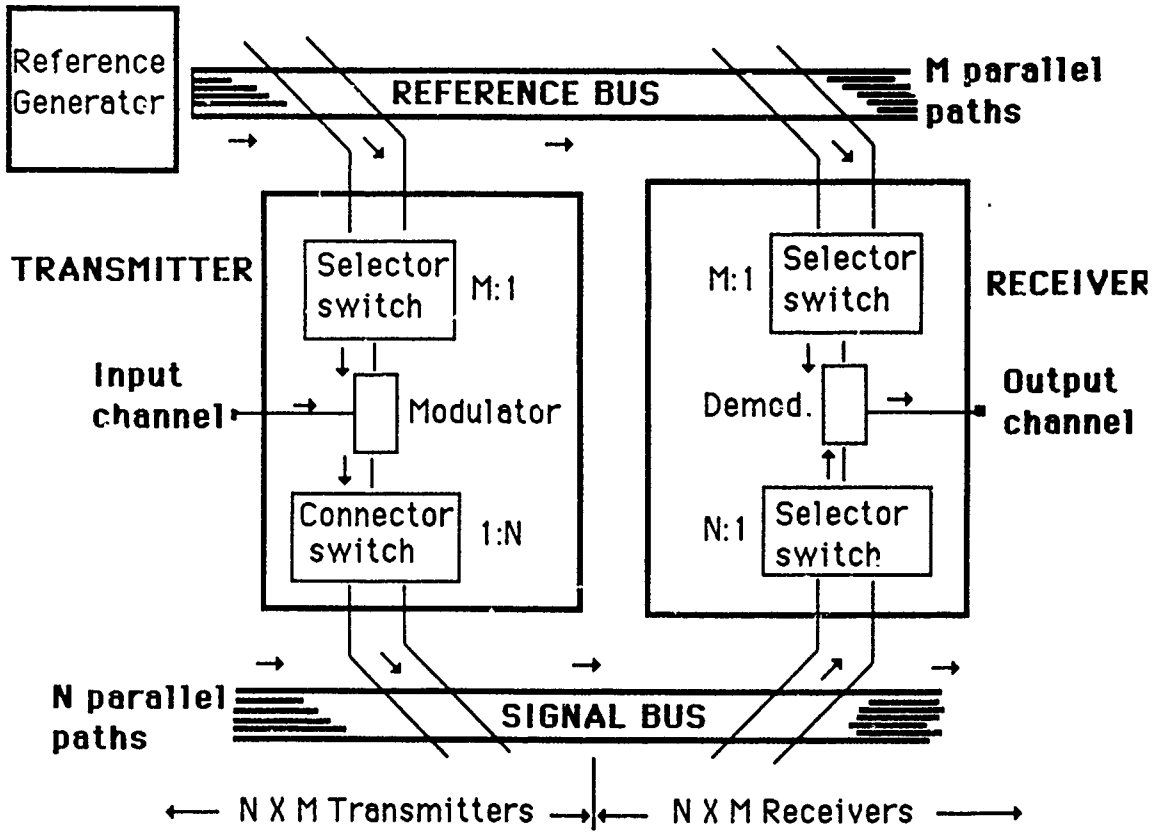

FIG1. **GENERALISED ARCHITECTURE OF MA BUS SWITCH**
Showing both transmitter channel assignment and receiver channel selection.

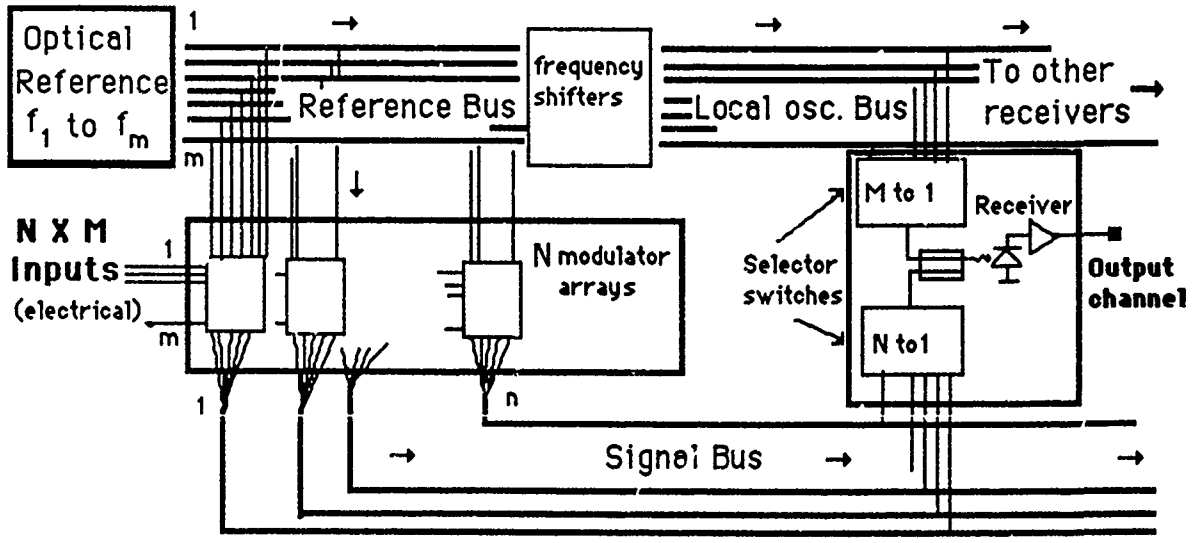

FIG2 **MA BUS SWITCH USING OPTICAL HETERODYNE SELECTION OF PRE-ASSIGNED CHANNELS**
(1 out of N X M receivers shown)

AN EXPERIMENT ON PHOTONIC WAVELENGTH-DIVISION AND TIME-DIVISION HYBRID SWITCHING

M. Nishio S. Suzuki N. Shimosaka* T. Numai*
T. Miyakawa* M. Fujiwara* M. Itoh**
C&C Systems *Opto-Electronics **R&D Planning and
Res. Labs. Res. Labs. Technical Service Div.
NEC Corporation 4-1-1 Miyazaki, Miyamae-ku, Kawasaki 213 Japan

1. Introduction Photonic wavelength-division and time-division (WD&TD) hybrid switching networks[1] can achieve large multiplexity, which is given by the product of individual wavelength-division and time-division multiplexities, and is expected to be suitable for large line capacity broadband switching systems. In these networks, fast wavelength tuning of both tunable filters and tunable laser diodes is necessary. Recently, measurements on the fast-tuning properties between two wavelength optical signals of tunable filters and tunable laser diodes have been reported[2],[3]. This paper describes an experiment on the fast tuning of filters and laser diodes among 4 of the 8 wavelength optical signals for the application of WD&TD switching with 32 total multiplexity of 100-Mbps signals.

2. WD&TD hybrid switching system Figure 1 shows the WD&TD hybrid switching system block diagram. In WD&TD multiplexer, nxm-channel input signals are WD (wavelength $\lambda 1 - \lambda n$) & TD (time-slot T1-Tm) multiplexed and multiplexed optical signals are led to the wavelength and time (W&T) hybrid switch. In W&T hybrid switch, WD&TD multiplexed optical signals are split and parts are led to individual wavelength tunable filters, each of which extracts a specific wavelength signal from the input signal. This selected wavelength may change every time-slot. The output signal from the tunable filter is then converted to an electronic signal and the electronic signal is applied to an electronic time switch (T switch), which interchanges time-slots on the input line. An electronic T switch output signal is sent to a tunable electronic-optical converter, which contains a tunable laser diode and changes its wavelength every time-slot. Finally, tunable electronic-optical converter output signals are combined to form a W&T hybrid switch output signal. Employment of electronic T switch is the most practical way. With future progress in photonic TD switching technology, photonic T switch will be used in the W&T hybrid switch. The WD&TD demultiplexer separates the W&T hybrid switch output signal into nxm-channel output signals. The W&T hybrid switch can exchange among arbitrary wavelengths and arbitrary time-slots. As a result, this system has nxm-multiplexity. In addition, large line capacity can be obtained by fabricating multi-stage switching network. For an example, 1024-line capacity can be achieved using a three-stage network with 32-multiplexity W&T hybrid switch.

3. Experiment Recently, 8 WD channel selectivity with 6-Å tuning range has been demonstrated[4] using a phase-shift-controllable DFB LD filter[5]. Phase-shift-controllable DFB LD can also be used as a light source with 6-Å tuning range. Therefore, 8 WD multiplexity can be obtained using the phase-shift-controllable DFB LD as a tunable filter and light source in the WD&TD switching network. The wavelength tuning time for this device is several nanoseconds. To achieve some TD multiplexity for broadband signals, such as 100-Mbps signals, using this device, a byte-interleaved form, which can insert guard-time between time-slots, is effective. In order to confirm the feasibility of 8 WD and 4 TD hybrid switching network, whose total multiplexity reaches 32 for 100-Mbps signals, fast wavelength tuning

experiment was performed. Experimental setup for wavelength fast tuning of tunable filter is shown in Fig. 2. The phase-shift-controllable DFB LD filter used for this experiment has constant 12-dB gain and constant 0.25-Å 3dB down bandwidth over 6-Å wavelength tuning range with 0.8-Å wavelength separation, by controlling active section current Ia and phase control current Ip. Four 100-Mbps electronic input signals were TD-multiplexed in a byte-interleaved form with 6.7-nsec guard time between adjacent channels, during which tunable filter executes wavelength switching. Consequently, total bit rate reaches 600-Mbps. Output lights from laser diodes, whose wavelengths are :$\lambda 1$, $\lambda 2$, $\lambda 3$ and $\lambda 8$, were combined and led to a modulator. The WD multiplexed light was intensity-modulated according to the 600-Mbps signal from TD multiplexer by using a $LiNbO_3$ modulator. The WD&TD multiplexed optical signal, as shown in Fig. 3(a), was then applied to the tunable filter. The signal selected by the tunable filter was converted to electronic signal and led to TD demultiplexer. The wavelength selected by the tunable filter, biased at Ia=0.98Ith, was switched sequentially from $\lambda 1$ to $\lambda 8$ according to Ia and Ip as shown in Fig. 3(b). As a result, the wavelength $\lambda 1$, $\lambda 2$, $\lambda 3$ and $\lambda 8$ signals were sequentially selected at individual time-slots within 6.7-nsec guard-time as shown in Fig. 3(c). The channel bit error rate was measured at every wavelength signals and BER<10^{-8} for the TD demultiplexer output signal was obtained for -28dBm filter input power.

Experimental setup for wavelength fast tuning of tunable laser diode is shown in Fig. 4. The light from tunable laser diode is intensity-modulated according to the electronic signal from TD multiplexer, whose output is supposed to that of a electronic T switch in Fig. 1. 6.7-nsec guard-time was also set for wavelength switching of tunable laser diode. Wavelength of tunable laser diode was changed sequentially from $\lambda 1$ to $\lambda 8$, as shown in Fig. 5(a). The WD&TD multiplexed optical signal was applied to fixed filter. Therefore, the output signal waveforms of fixed filter at $\lambda 1$, $\lambda 2$, $\lambda 3$ and $\lambda 8$ are shown in Fig. 5(b),(c),(d) and (e), respectively. BER<10^{-8} for the TD demultiplexer output signal was also obtained for -28dBm fixed filter input power.

4. Conclusion The fast wavelength tuning operation of a filter and a laser diode, among 4 of the 8 wavelength optical signals, within 6.7-nsec guard-time has been confirmed. These results show the feasibility of 8-WD and 4-TD hybrid switching for 100-Mbps signals.

Reference

[1]S. Suzuki et al., to be presented at GCOM'88, 29-2 [2]M. P. Vecchi et al., ECOC'88 part1 247 [3]M. S. Goodman et al., ECOC'88 part1 255 [4]M. Nishio et al., ECOC'88 part2 49 [5]T. Numai et al., ECOC'88 part1 243

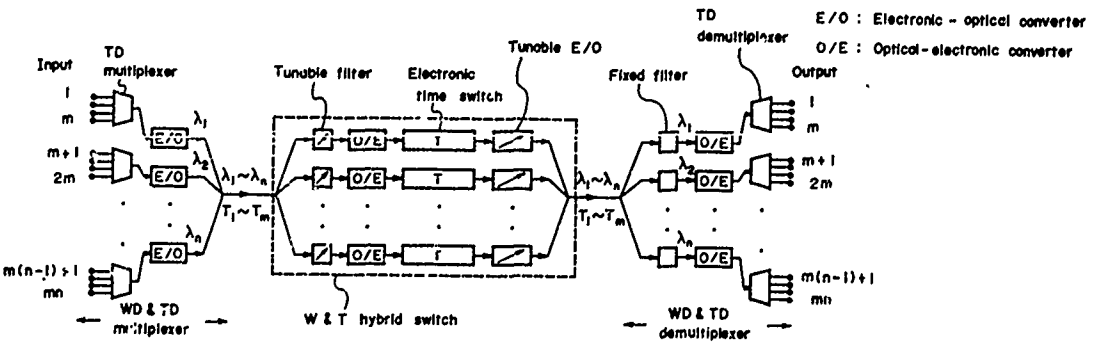

Fig. 1 WD & TD hybrid switching system block diagram

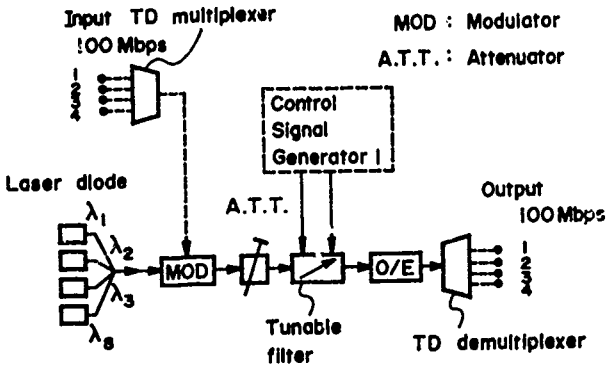

Fig. 2 Experimental setup for 4-channel wavelength sequential fast tuning of tunable filter

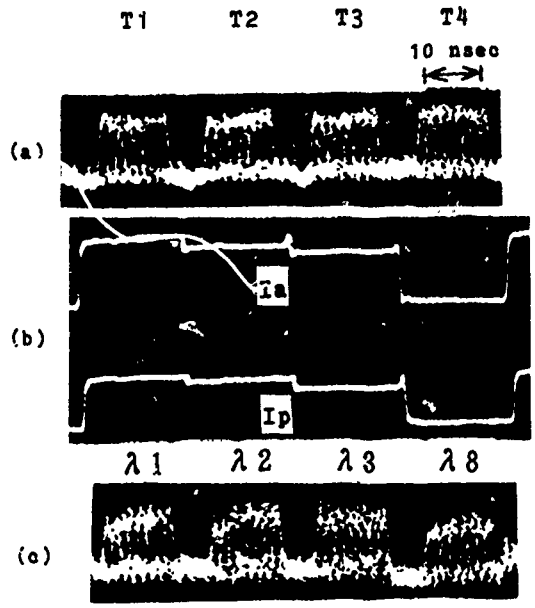

Fig. 3 Signal waveforms
(a)Tunable filter input signal
(b)Ia and Ip currents
(c)Tunable filter output signal

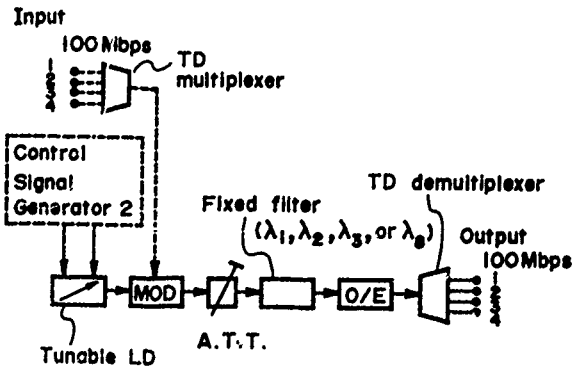

Fig. 4 Experimental setup for 4-channel wavelength sequential fast tuning of tunable laser diode

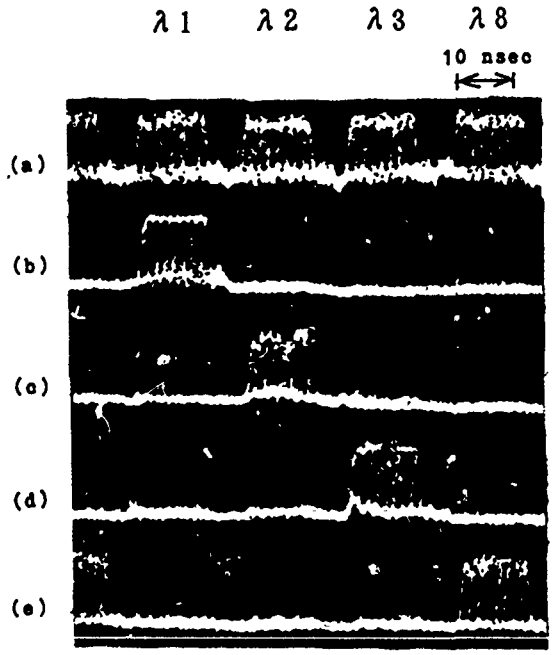

Fig. 5 Signal waveforms

(a)Fixed filter input signal
(b)Fixed filter at λ1 output signal
(c)Fixed filter at λ2 output signal
(d)Fixed filter at λ3 output signal
(e)Fixed filter at λ8 output signal

Passive spectral commutator and the architectures of usual and optical nets

E.M. Dianov, A.A. Kuznetsov, S.M. Nefjodov, G.G. Voevodkin

Academy of Sciencies of the USSR

General Physics Institute

Vavilov street, 38 117942 Moscow, USSR

We have proposed and realized passive spectral commutator (PSC)[1]. PSC is like to spectral demultiplexer for optical WDM links. Practically, usual WDM demultiplexer works as PSC, when the abonents, united by this demultiplexer, changes their communication wavelengthes.

The architectures of optical nets with PSC may be divided in two classes: the first architecture with tunable wavelength of each abonent and the second architecture with some standard wavelength. Let us begin from the first architecture.

In the optical net with tunable communication wavelength the output ends of the each abonent fiber are united in fiber arrow in PSC (Fig. 1). So, in this architecture all individual fibers from abonents must reach PSC. As a matter of fact, star architecture is necessary.

PSC working in such star architecture is absolutely passive and photonic namely. Initial knowledge in optics is enough to understand, that abonent i (Fig. 1) by tuning his wavelength can call abonent k. Due to ray reversal principle, this communication at the same wavelength is mutual for abonents i and k. The other wavelengthes will provide the talking with the other abonents.

Many simultaneous wavelengthes from one abonent will provide group talking. "White light" makes possible "general conference" talking.

It is very interesting, that single wavelength simultaneously provides the talkings between the different abonent pairs (up to N/2 pairs, where N - the number of the abonents). Such situation is impossible in similar radiotechnical commutator, as in optics only it is possible to localize exactly the energy from fiber i on the receiving face of fiber k.

We have described the details of PSC working earlier[1]. For all possible pair contacts between N abonents 2N wavelengthes are necessary. Full spectral range is then $\Delta\lambda = 2dN/FG$, where d - fiber diameter, F - objective focal length, G - grating lines number per millimeter. The first experimental abonent net may be projected for 100 abonents. If d = 100 μm, F = 50 mm and G = 600 mm^{-1}, the net will use the spectral range about of 600 nm (for example, in the region 0.8 - 1.4 μm). PSC parameters are like to demulteplexer parameters in WDM systems: cross-talking (optical power) about of -20...-30 dB, the losses in PSC at the connection of one abonent pair must be equal tc 2 - 3 dB. Nowadays many different spectral demultiplexers are known, and practically the each of them can be used as PSC. PSC are realizable on the base of integrated optics or as glass-block constructions.

The advantages of our passive spectral commutator are the next:

- simple passive channel commutation;

- the possibility of fabrication of PSC as monolithic (or integrated) glass block;
- the absence of moving elements and control voltages;
- the absence of power supply;
- small switching time (the time of beam run between two fibers in PSC - less than 1 ns).

These advantages of PSC are impressive enough to try to use PSC in any net architectures (not only in previously described one). Such use is possible in usual wire nets and in optical nets with standard single communication wavelength. But PSC must be complicated: at its periphery at the each fiber input (Fig. 1), corresponding to concrete abonent, the tunable lasers must be placed (Fig. 2). Information signal from the each abonent must change the laser wavelength, id est the address. Of course, star architecture is preferable again (for both electrical and optical nets). For other architectures it is possible to install special electronic block, which must distribute the signal from concrete abonent (information and control signal for laser) to corresponding laser at the periphery of PSC.

Thus, in principle the different architectures of usual and optical nets with passive spectral commutators are possible. The most real architecture is star optical one with tunable abonent transmitter. Less practical, but yet real architectures are star wire net and star optical net with standard wavelength. In this case "mini-star" is necessary around PSC with controlled tunable lasers at its ends. The other architectures, unfortunately, are more speculative, than real.

Optical star-type net with PSC seems us as the interesting, simple and useful abonent net with pure photonic switching inside PSC. We suppose, that such net will be realized for some special applications.

1. G.G. Voevodkin, A.A. Kuznetsov, S.M. Nefjodov. Passive optical commutator for optical fiber abonent net with spectral multiplexing. - Radiotechnika, 1988, No. 7, p. 65-67.

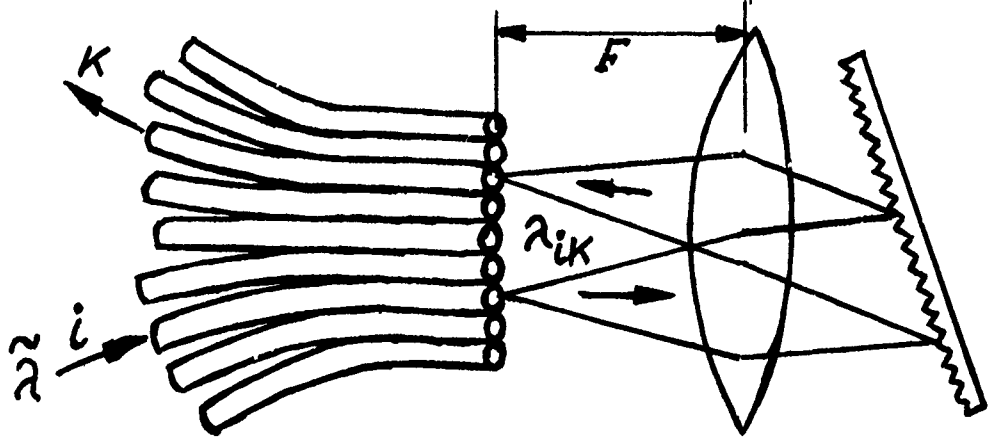

Fig. 1. Passive spectral commutator for star optical net with tunable abonent transmitters.

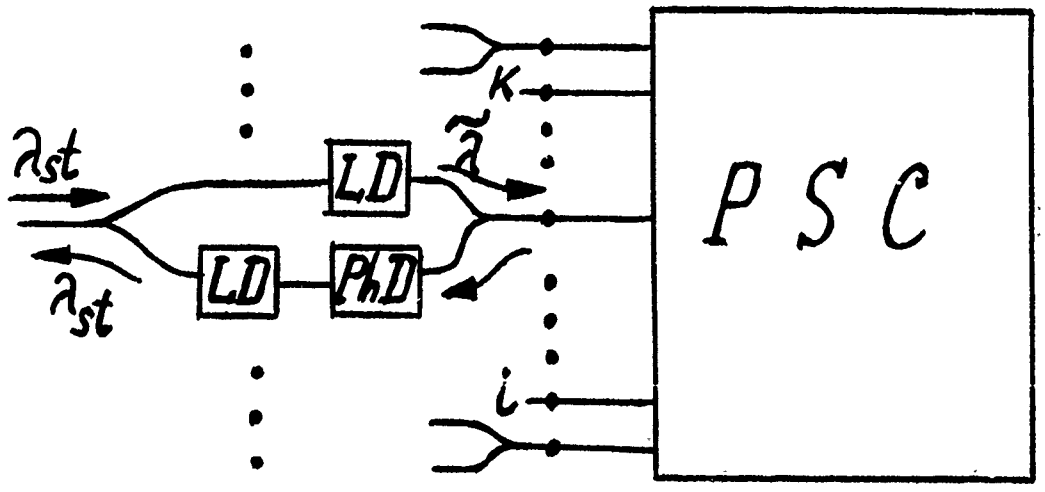

Fig. 2. Mini-star commutator structure with PSC inside for different architectures of usual and optical nets.

FRIDAY, MARCH 3, 1989

SALON E

8:30 AM–9:45 AM

FA1–FA4

PACKET SWITCHING SYSTEMS

Paul R. Prucnal, Princeton University, *Presider*

OPTICAL PROCESSING IN PHOTONIC SWITCHING SYSTEMS

Ikutaro KOBAYASHI
NTT Communication Switching Laboratories
3-9-11 Midori-cho Musashino-shi 180 JAPAN

BACKGROUND

Communications switching systems originated with electrically controlled mechanical switches, which formed a unique path determined by the number dialed. In response to the need for alternative paths, wired logic control and then stored program control were introduced. Later, the application of time-division-multiplexed transmission required the replacement of the sophisticated mechanical cross-bar switches with time-division switches.

Many structural changes were initiated by new demands and realized with new technology. Recently, the advanced features of optical technologies are expected to initiate the next generation of communication switching systems. These features include a proven immunity to induction, potential advantages of the optical frequency domain, and expected switching speeds superior to electrical switches. Of these features, the first is ready for practical use, the second can be demonstrated experimentally(1), and the third is currently under discussion(2).

DOES SWITCHING NEED OPTICAL PROCESSING?

Optical switches are suitable for high-speed signals because of their immunity to induction and their wide-bandwidth channels. However, their matrix size has not yet reached ten ports, and for time- and frequency-division systems, the available number of optically-multiplexed channels is also less then ten. Therefore, scale-up is the main problem to be overcome before optical switching can be used commercially (Fig.1).

Practical systems need about 1,000 channels for multiplexing. This number has been realized in current electronic time-division switching systems for low-speed channels, but is not yet available for high-speed channels. Optical switches can

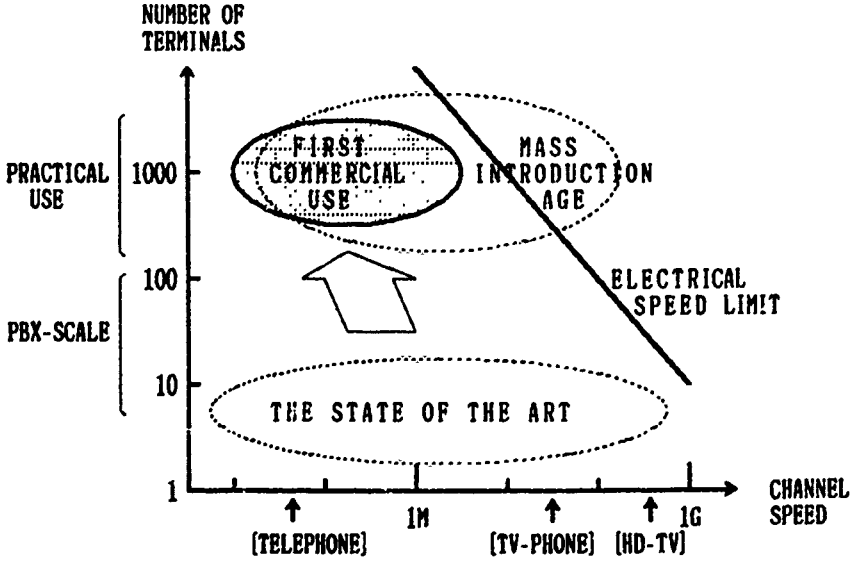

Figure 1 TARGET FOR PRACTICAL SWITCHING SYSTEMS

play an important role for high-speed-channel switching when the switches are scaled up to provide several tens of ports. For practical use, new technology, such as optical parallel processing, will be required to deal with many high-speed channels by compact detection/control circuits which match the switch structure and size.

For further extention to higher-speed switching, optically--controlled photonic switches are promising because they are not limited by the speed of electrical driving circuits. These switches would require high-speed optical logic circuits to drive themselves.

After such trial small-scale introductions, optical processing and logic circuits will gradually become popular and will trigger a basic structural change in communication switching systems. In the future, optical switching and processing will be integrated, and in time, their boundaries will vanish.

WHEN WILL IT BE NECESSARY?

In the next several years, the optical-switch advantages of immunity to induction and wide-bandwith of channels, will be applied to small, wideband PBX. This system, however, does not yet need optical processing because it requires only primitive optical switches, and has the same structure as the current system.

When an optical switch is scaled up, it will first be tested in a wideband multimedia switching system connected by light FDM over a fiber loop to each subscriber. To directly deal with light FDM signals, frequency-division switching will be required, and optical processing will be partially applied to the control circuits. This will hopefully be implemented by the end of 20th century.

Although not currently necessary, in the future, the advantages of optical logic and processing, such as high-speed, parallelism and immunity to induction, will be essential. Therefore, at the beginning of the 21st century, optical technologies will become the dominant part of systems, forcing changes in system structure.

WHAT FUNCTIONS ARE REQUIRED FOR OPTICAL PROCESSING?

The future functions of optical processing for communication switching systems are difficult to determine precisely. Within the frame work of the macro-trend toward parallel processing, which is response to the scale-up of switch size, the optical control of high-speed photonic switching and the integration of switching and control are areas, that could be targeted for future research.

Taking advantage of immunity, one impressive target would be for functional devices to be implemented in a size comparable to fiber-bundle diameter. A simple example of this would be a concentrator, which picks up all live lines among input lines and connects them to output lines. When live lines change, it must be assumed that they are also connected to output lines. The concentrator would have three essential functions: detecting the light-signal level, shifting the light-signal position, and connecting the light-signal to output fibers, the required

number of which is only a small percentage of the number of input fibers. Other examples would include the functions of call detection, switch control, etc..

The optical frequency domain will provide an opportunity to create new functions such as multiplexing of a large number of channels, new addressing methods, and new network structures, etc.. The essential components for these functions are frequency convertors, tunable frequency selectors and combiners. Each of these components have been realized experimentally but have not been merged into a single functional device that detects, re-allocates, and generates a set of signals in the optical frequency domain. Also, there are still no proposals for frequency-switching devices.

In addition to assembling integrated optical function devices, many essential optical circuits like oscillators, invertors, shift-registers, and synchronization circuits need to be developed. Also, to fully utilize high-speed switching, it is necessary to provide control circuits based on optical logic. One significant step has been made in this area so far. The operation of optical invertors, synchronization circuits, optical intensity oscillators(3), and shift registers(4) using laser-diodes has been demonstrated. With progress in optical logic devices and circuits, for example, a packet-switching circuit applicable to ATM switches will be designed using fully-optic components.

CONCLUSION

In optical logic and processing, speed is currently limited by electrical driving circuits, and optical interconnection stands as a big barrier to parallel processing. The optical switching field can offer some clues for overcoming these difficulties by providing simple examples applicable to near-future systems.

For interconnection, a hologram technique provides a method of uniformly converting an image when a particular rule, like Fourier Transform, is applied. It is, however, difficult to make up particular-pattern connections between images or signal sets, although these connections are required in practical systems. Optical switching offers useful and functionally simple examples, for example, a concentrator consisting of simple position shiftors.

In summary, the optical switching field can be very helpful in stimulating the evolution of optical processing. In addition, new challenges are developing in the use of the optical frequency domain, which will lead to the creation of new functional devices.

References

(1) H. Toba et al., Electronics Letters, Vol.14, pp.520-521, Aug. 1978.
(2) P. W. Smith, BSTJ, Vol.61, No.8, pp.1975-1993, Oct. 1982.
(3) K. Habara et al., ECOC'88, pp.167-170.
(4) T. Odagawa et al., IECE 1988 Autumn National Convention Record, C-166, p.C-1-48.

OPTICAL TECHNOLOGY APPLICATIONS TO FAST PACKET SWITCHING

Paola CINATO and Alfredo de BOSIO
CSELT-Centro Studi E Laboratori Telecomunicazioni,10148 Turin,Italy

1. INTRODUCTION

Fast Packet Switching (FPS) techniques can be applied to switch voice, data and video in an ATM network; information is packetized and each packet is assigned a label to route it through the network; layered semplified protocols are required to perform high speed. Many resources are devoted at present to FPS techniques and it is reasonable that, when the optical technology is mature, it will have to face with an ATM network. In this wake it is analyzed the utilization of the optical technology to realize an optical switching fabric in an FPS node.

2. OPTICAL FABRIC SWITCHING DELAY

In order to evaluate the maximum switching delay of the optical fabric, we will refer to the network model shown in figure 1.

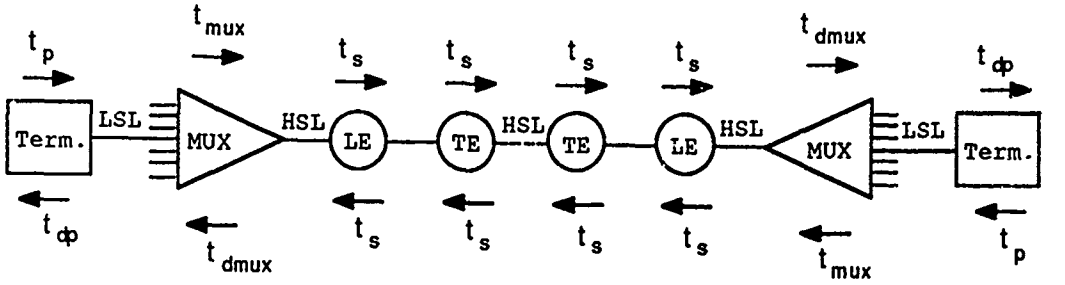

LSL= Low Speed Links TE = Trunk Exchange Term. = Terminal capable of generating
HSL= High Speed Links LE = Local Exchange packetized information

Fig. 1: FPS Network Model

Referring to this model, the total packet delay can be expressed as:

$$Td = Tp + Tmux + N*Ts + Tdmux + Tdp + Ttras$$

where Tp is the packetization delay, Tmux is the delay introduced by the queues at the multiplexer, Tdmux is the delay introduced by the demultiplexer, N*Ts is the delay introduced by N exchanges in a terminal-to-terminal path, Tdp is the delay introduced at the receiving terminal and Ttras is the propagation delay. Assuming a minimum packetization bit rate of 128 Kbit/s at terminal level, a speed of 2048 Kbit/s over the low speed links, a speed of 600 Mbit/s over the high speed links, a maximum MUX concentration ratio of Cmux=300 and a packet length Lp=2048 bit, we have: Tp=16ms, Tmux=1ms+3.4us*300=2ms. With N=15, Ttras=50ns (5 ns/m for 10000 Km), Tdp=0, Td=90ms, we obtain a maximum acceptable switching delay Ts=1.4ms.

3. OPTICAL FABRIC THROUGHPUT EVALUATION

To evaluate the throughput of the optical fabric, the following hypothesis are made:

- Services like videoconference, bulk data transmission etc., characterized by 2048 bit length packets, are handled by the optical

fabric; services like telephony and signalling, which require short packets are electrically handled.
- A local exchange is able to serve 40000 users in the average; 25% of the users generate packetized information traffic of 60 packet/s per user and are connected to MUXs.
With these hypothesis, and assuming a conventional traffic share between local and trunks exchanges, it can be shown that an optical fabric in a local exchange should be capable of switching 1.08 Mpacket/s, whereas an optical fabric in a trunk exchange should be capable of handling up to 1.5 Mpacket/s
Note that diffusive services traffic is supposed to be carried by a separate network and directly conveyed into the local exchanges' distribution network.

4. OPTICAL FABRIC CONTROL STRUCTURE

An hybrid solution with electrical control and optical switching seems the more realistic for the near future (see [1]). The control structure of the optical fabric can be centralized or distributed. A fully distributed optical structure would require optical input processors which, at present, are impossible to implement: therefore we will consider a distributed structure, with optical buffers, electrical input processors and two matrixes having the same structure, one electrical and one optical, as shown in figure 2 (patent pending).

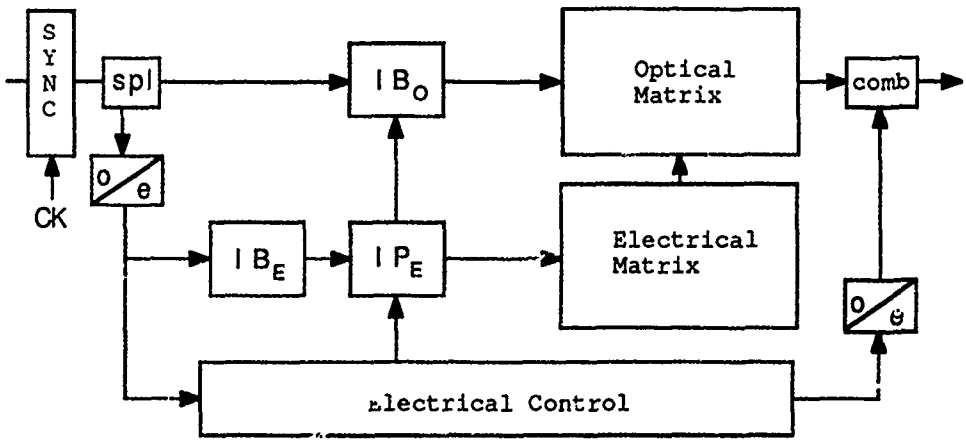

Fig. 2: Distributed Control Structure

5. OPTICAL MATRIX SETTING TIME AND DIMENSION EVALUATION

To evaluate the optical matrix setting time an optical fabric with synchronous strategy is considered. Figure 3 shows the switching matrix operation time diagram. We suppose that the optical matrix is based on a structure of s stages with self-routing capacity [2] and that the speed of the optical network is k times faster than the electrical one. Teset is the time spent setting the electrical network; the packets which succeed in coming out of the electrical network cause the transmission of acknowledge packets, which reach the input lines after a time Tack. During Tack also the optical network is set; this means that optical switching elements with a setting time Toset =< Tack are required. After input lines acknowledgement, the information packet is sent through the optical network in a time equal to Ttrasf. Assuming an electrical network

bit rate of 20 Mbit/s, an optical network bit rate of 600 Mbit/s, a packet length of 2048 bit, a packet header length of 32 bit, an electrical acknowledge packet length of 4 bit and operating in condition of low traffic (R=0.2 E), the network dimension, the network cycle and the optical matrix setting time versus the number of stages for different network topologies are obtained and shown in table 1. The same table shows also the applicability field of some of the most promising network topologies for optical switching.

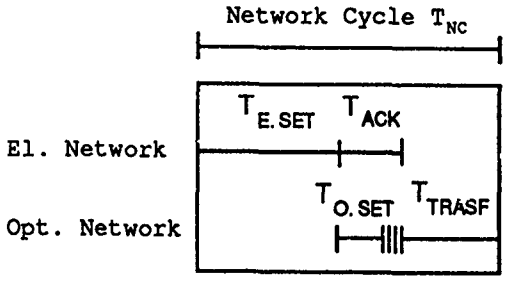

T_{NC}: network cycle (maximum admitted)
T_{OSET}: optical matrix setting time (maximum admitted)

Fig. 3: Switching Matrix Operation Time Diagram

s	N	T_{NC} (μs)	T_{OSET} (μs)	
6	43	5.8	0.5	Delta
10	46	6.2	0.7	
30	62	8.2	1.7	Bitonic Sorter + Omega
50	76	10.2	2.7	
100	114	15.2	5.2	
150	151	20.2	7.7	Shimoe
200	189	25.2	10.2	
250	226	30.2	12.7	
300	264	35.2	15.2	

Table 1: N, T_{NC}, T_{OSET} versus s

6. INPUT BUFFER EVALUATION

In order to have fully optical paths, optical buffers are considered in the switching model; as they are at present impossible to implement, they can be substituted for practical implementation with electrical ones, without affecting the model validity. The optical input buffer length can be estimated using the model proposed by Hui et al. [3], for non-blocking networks (e.g. Shimoe network or a sorting network followed by a Delta network) and random traffic conditions. Assuming a traffic of 0.2 E and a buffer overflow probability P(loss) < 10.E-6, we obtain an (optical) memory amount varying from 250 up to 3000 Kbit according to the network dimension.

7. FINAL REMARKS AND CONCLUSION

The basic idea followed in the electro-optical switching node model design is that, in order to accelerate the introduction of optical technology in the existing telecommunication network, an add-on strategy is required. Further studies have to be made on packet synchronization and packet header structure, on buffer dimension and blocking probability using simulation programs, as well as on detailed design of the controlling electrical architecture.

8. REFERENCES

[1] A.de Bosio, F.Melindo, Topical Meeting on Photonic Switching, Lake Tahoe, Mar. 1987.
[2] S.Thanawastien , IEEE Trans. on Comp., Vol C-30 N.8, Aug.1981
[3] J.Hui et al., IEEE JSAC, Vol.SAC-5, Oct. 1987.

PHOTONIC PACKET SWITCH USING OPTICAL BUFFER MEMORIES

S. Suzuki, H. Suzuki, K. Kasahara*, M. Fujiwara* and T. Takeuchi
C & C Systems Res. Labs. *Opto-Electronics Res. Labs.
NEC Corporation. 4-1-1 Miyazaki, Miyamae-ku, Kawasaki, 213 JAPAN

1. Introduction A packet switch, which can handle wide-bitrate-range data streams in an integrated manner, is expected to play an important role in future broadband networks. Although introduction of photonic technology to very high-speed packet switches has recently been proposed[1,2], these packet switches employ the photonic technology only in routing fabrics. The switches use electronic buffer memories, speed and density limit of which restrict packet switch performance. This paper proposes fully photonic packet switches using two kinds of optical buffer memories, which have potential of achieving higher performance than that of electronic buffer memories.

2. Photonic packet switch using fiber loop buffer memory The packet switch needs large amount of buffer memory to store many packet cells. Optical fiber delay line memories can store such extremely high-speed optical signals as 10-Gbps signals. However, because of their bulkiness, it is difficult to prepare many fiber delay lines to store many packet cells. Introduction of wavelength-division multiplexing is effective to solve this problem.

Figure 1 shows a basic optical fiber loop buffer memory. A wavelength tunable optical transmitter sends optical packet cells, having different wavelengths, $\lambda 1$ -λn, packet by packet, to a fiber delay line through a 2x2 optical coupler. The fiber delay line has a delay time equal to a packet cell transmission time. Output signals from the fiber delay line are split into two signals by the 2x2 optical coupler. One is led to the fiber delay line again. Therefore, wavelength-division multiplexed(WDM) packet cells circulate in this fiber delay line loop. A wavelength demultiplexer, optical gate switches and a wavelength multiplexer are inserted in the fiber delay line loop. By using optical gate switches with optical amplification function, as laser diode switches[3], closed loop optical loss of fiber delay line, including optical coupler, wavelength demultiplexer and multiplexer loss, can be compensated. Therefore, optical packet cells can circulate in the fiber delay line loop without attenuation. The other signal from the 2x2 optical coupler is led to a wavelength tunable optical receiver.This signal includes the same WDM packet cells as stored in the fiber delay line loop. The tunable optical receiver, using a tunable wavelength filter[4] or optical coherent detection technique, selects an arbitarary wavelength (λi) packet cell from injected WDM signals. If the wavelength λi cell was selected by the tunable optical receiver, the optical gate switch, amplifying the wavelength λi cell, is turned off during the cell transmission time to erase the wavelength λi packet cell. After that, the tunable optical transmitter can use wavelength λi again to enter another packet cell into the fiber delay line loop. In this way, this buffer memory can store upto n packet cells in a random-in/random-out manner using only one fiber delay line.

This buffer memory can be applied to various packet switches. Figure 2(a)(b)(c) shows some examples of m x m packet switches using the buffer memories as input buffer memories, output buffer memories and a shared buffer memory, respectively. Required number of wavelength n, calculated using M/D/1 model, are 10, 50 and 50+5m for the input buffer, output buffer and shared buffer switches, respectively, under the condition that switch input link utilization is 80 % and packet cell loss rate is less than 10^{-10}. The required n of the input buffer switch is reduced owing to multiple-cells simultaneous-

ly read out capability of the fiber loop memory. As a result, the input buffer switch can be put into practice based on today's WDM technology and can exchange several-Gbps packet cells. With future progress in WDM technology, output and shared buffer packet switches will be turned into reality.

3. Photonic packet switch using optical memory two-dimensional (2D) array

An optical memory 2D array has capability of achieving large-scale integration in small size. Moreover, the optical memory 2D array has massively parallel interconnection capability, based on free-space light beam propagation. Parallel operation in the buffer memory of the packet switch is very effective in achieving high total switch throughput.

Figure 3 shows an m x m photonic shared buffer packet switch using the optical memory 2D array. Input electronic packet signal, with cell length p, are led to an (m-column) x (p-row) shift register, latch and light source 2D array and converted to a p-bit parallel configuration by shift registers. Parallel signals are stored in latches during every cell transmission time. The m x p light source 2D array converts m-columns of p-bit parallel packet signals, stored in latches, to optical signals. Optical signals from the light source 2D array are distributed to a (d-column) x (p-row) optical buffer memory 2D array through a half mirror and holographic lens. Figure 4 shows an optical buffer memory timing chart. The first half of each memory cycle time, which is equal to the cell transmission time, is a write period. The write period is divided into m time-slots. In each time slot, one column of light source 2D array sends parallel optical signals to the optical memory 2D array and one column of optical memories, activated by a controller, the store optical signals. The latter half of the memory cycle time is a read period, which is also divided in m time-slots. In each time-slot, one column of optical memory 2D array sends parallel optical signals to an (m-column) x (p-row) photodiode, latch and shift register 2D array and one column of photodiodes, activated by the controller, convert optical signals to electric signals. These parallel electric signals are stored in latches and converted to a serial-bit configuration output packet cell by shift registers.

A VSTEP (Vertical-to-surface transmission electro-photonic device)[5,6] is suitable for this packet switch. The reason is that the VSTEP can be used as not only a low-switching-energy optical memory but also as a light source and photodiode. VSTEP switching energy can be reduced less than 0.01 pJ. Therefore, packet cell speed can reach 10 Gbps, on condition that m=8, p=552 (the cell length is 69 byte), d is 50+5m=90 to satisfy cell loss rate less than 10^{-10} for 80-% input link utilization, 1-mW light source output power and 6-dB free-space interconnection loss. A 90 x 552 VSTEP array will be integrated within 3 mm x 20 mm size. As a result, a 8 x 8 packet switch with 10-Gbps cell speed will be achieved in small size and an extremely high-capacity packet switching system will be fabricated using a multi-stage switching network. Moreover, introduction of wavelength tuning function into the optical memory makes it possible to change buffer memory m time-division operation, during every write/read periode, to wavelength-division operation. As a result, higher switch performance will be achieved using the same switching energy optical memory.

4. Conclusion Photonic packet switches, which can achieve extremely high cell speed, as 10 Gbps, using the WDM fiber loop buffer memory and the optical memory 2D array, were proposed. Introduction of WDM technology makes it possible to reduce amount of fiber delay lines dramatically. Massively parallel interconnected packet switch structure using the optical memory 2D array is effective to obtain high packet cell speed. These phtonic packet

switches will be able to achieve higher performance than packet switches using electronic buffer memories.

References

(1)K. Y. Eng GLOBECOM'87 47.2 (2)M. S. Goodman et al. ECOC'88 part 1, p. 255 (3)M. Ikeda IEEE J-QE-19, no. 2 1983 (4)T. Numai et al. ECOC'88 part 1 (5)Y. Tashiro et al. to be published in Appl. Phys. Lett. (6)K. Kasahara et al. Appl. Phys. Lett. 52(9), 29 Feb. 1988, p.679

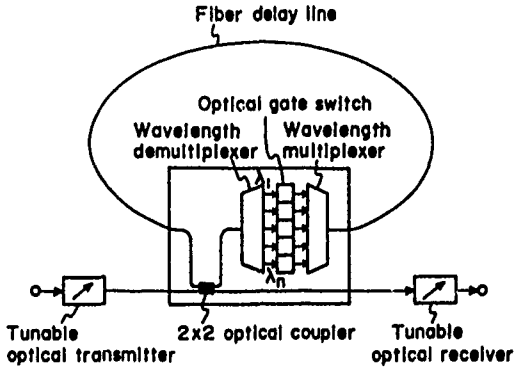

Fig 1. Basic fiber loop buffer memory

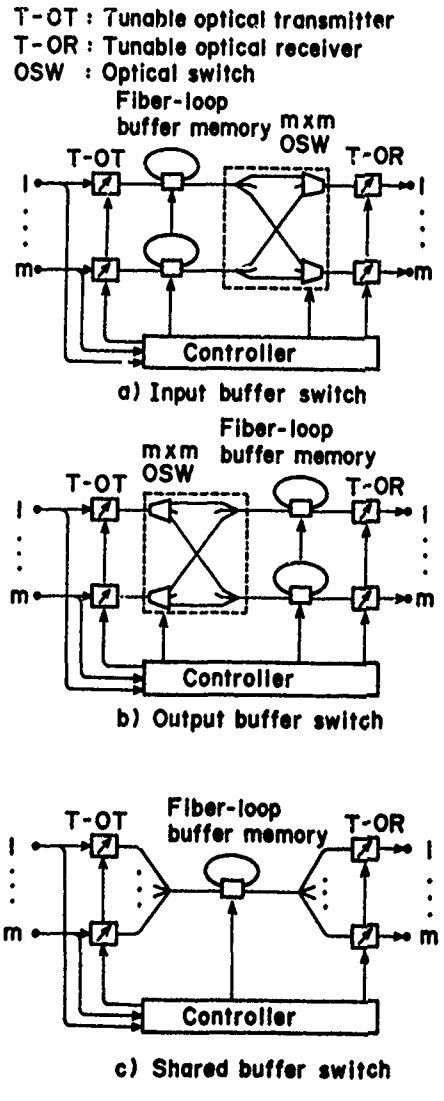

Fig.2 Photonic packet switch using fiber-loop buffer memory

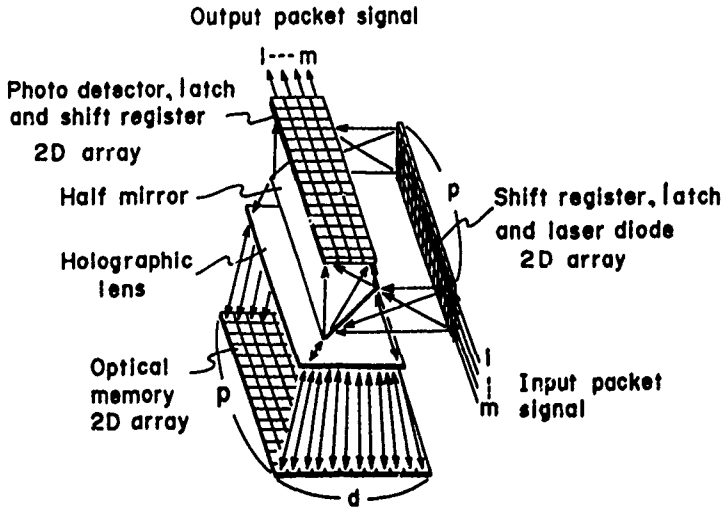

Fig. 3 Photonic packet switch using optical memory 2D array

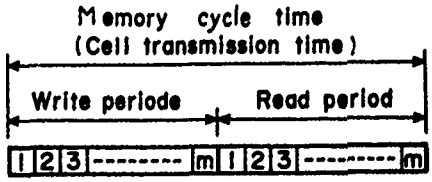

Fig. 4 Optical buffer memory timing chart

InP Based 4×4 Optical Switch Module and Its Application to ATM Switching

H. Inoue, T. Kato, Y. Sasaki, K. Ishida, K. Mizuishi and E.Amada

Central Research Laboratory, Hitachi Ltd.,
Kokubunji, Tokyo 185, Japan

S. Kashimura

Cable Research Laboratory, Hitachi Cable Ltd.,
Hitachi, Ibaraki 319-14, Japan

Introduction

Non-blocking N×N optical switch modules (OSM) are key components for future broadband communications. To realize large scale integrated OSMs, it is necessary to develop small-size optical switch units suitable for integration, and a precise alignment technique between a chip with an optical switch array(OSA) and single mode fibers. Recently, we reported an InP-based non-blocking 4×4 OSA with a novel structure (Single Slip Structure: S^3) for optical switch units[1] operating through carrier-induced refractive index change[2]. This OSA exhibited polarization-independent switching characteristics and features suitable for larger scale integration(only 8 mm long for 4×4 OSA). Here, we present experimental results obtained with the OSM being a packaged version of our 4×4 OSA. In assembling this OSM, a novel technique for aligning a single-mode fiber array with the OSA was developed. The fiber array was inserted into a Si attachment with a set of photolithographically defined pyramidal through-holes. This technique obviously has a much wider application and is suitable for precise alignment of a large number of fibers with other types of optical integrated circuits such as OSA.

The OSM will typically be applied to switching systems. In future networks, ATM(Asynchronous Transfer Mode) technique will play an important role in realizing flexible and economical broadband services. Therefore, we propose an ATM switch architecture using the OSA. Wide bandwidth and fast switching features of the optical switch can be successfully utilized to realize large capacity switching systems.

Optical Switch Module

Figure 1 shows a schematic view of the InP-based non-blocking 4×4 OSA fabricated by integrating 16 S^3 optical switch units. Every S^3 optical switch unit is composed of one X-cross element and two Y-branches incorporating carrier-injection regions. All waveguides are single-mode InGaAsP/InP ridge waveguides with X-crossing and Y-branching angles being 10° and 5°, respectively.

A schematic view of the proposed fiber array aligned by pyramidal through-holes(APT fiber array) is shown in Fig 2. Tapered fibers are maintained and aligned by a fiber attachment having truncated pyramidal through-holes. These through-holes are formed by anisotropic etching of a Si substrate. Since positioning of fibers is decided by a photolithography technique, less than 0.5-μm-precision alignment can be expected. Furthermore, this technique enables us to align all fibers by adjusting only two points of the fiber attachment, even if the fiber array has a 2-D structure. Once the fiber attachments are installed, all fibers can be fitted without any adjustment by inserting

the tips of tapered fibers into the pyramidal through-holes.Thus, the assembly process is also simplified.

Figure 3 shows a photograph of a fabricated non-blocking 4×4 OSM with permanently attached APT fiber arrays. Two Si fiber attachments (input and output) are settled on a Kovar plate using adhesive and solder. A set of tapered fibers is guided through conventional V-grooves, and inserted into the appropriate fiber attachment having truncated pyramidal through-holes. The fabricated OSMs are 15 mm wide, 10 mm high and 50 mm long.

Experimental Results

Light from a 1.3-μm-wavelength laser diode was coupled into each fiber to measure the fundamental switching and coupling characteristics of the fabricated 4×4 OSM for various injection currents to each S^3 optical switch. At 200 mA injection current, crosstalk reached -23.9 dB and minimum total insertion loss was 23.7 dB, including Fresnel reflection loss. The additional total insertion loss was only 1 to 2 dB compared with the results of one to one fiber coupling using the conventional alignment method.

ATM Switch Architecture using the Optical Switch Array

Application of the OSM to ATM switching systems is promising since it can offer a wide bandwidth more easily than electronic devices. Figure 4 shows a proposed ATM switch architecture using the OSM. Signals from 32 input ports are multiplexed into a 4.8 Gbps (150 Mbps×32) signal. The multiplexed signals are buffered electrically to avoid cell loss caused by instantaneous congestion. The buffer outputs are converted to optical signals and exchanged by the OSM according to cell header information. The optical memory controller (SW CONT) receives cell transmission requirements from the buffer memory controller (CONT) and decides which cells are transmitted to which output port. The SW CONT controls the OSM and serds permission signals to CONTs which have cells to be transmitted. This process is executed cell by cell and the ATM switching function is realized. At the output stage, the signal from the OSM is demultiplexed and sent to the output port according to the cell header.

In this architecture, the OSM exchanges multiplexed signals, enabling the OSM's wide bandwidth to be fully utilized and the number of interconnection cables to be reduced compared. Switching capacity is 19.2 Gbps in the system shown in Fig. 4. However a larger ATM switch can be realized by a large capacity OSM or cascade connection of OSMs.

Conclusion

The fabricated non-blocking 4×4 OSM with APT fiber arrays showed satisfactory switching and coupling characteristics. The novel fiber array attachment for aligning a large number of fibers by truncated pyramidal through-holes(APT fiber array) was proposed for large scale integrated optical circuits. An ATM switch architecture was also proposed as an application of the OSM to switching systems. The wide bandwidth of the OSM was successfully utilized and large switching capacity was easily realized.

References

1) H. Inoue, H. Nakamura, K. Morosawa, Y. Sasaki, T, Katsuyama and N. Cinone, IEEE J. Select. Areas Commun., J-SAC-6, 1262 (1988)

2) K. Ishida, H. Nakamura, H. Matsumura, T. Kadoi and H. Inoue , Appl. Phys. Lett., 50, 141

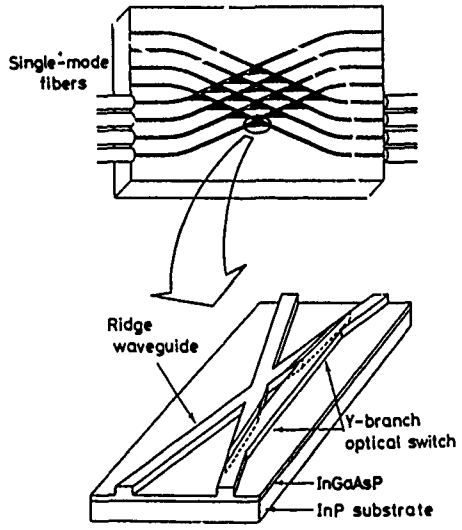

Fig. 1 Schematic view of InP based 4×4 optical switch array

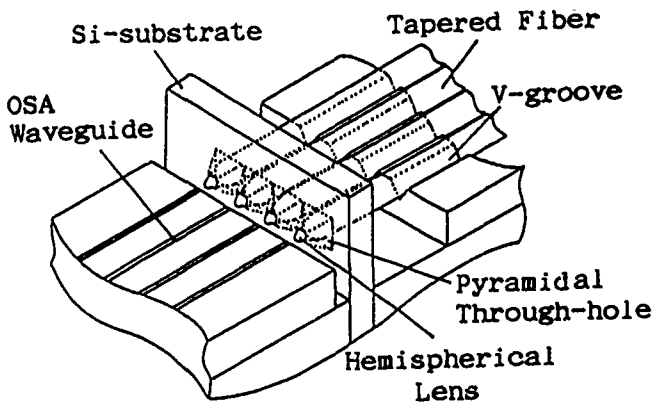

Fig. 2 Schematic view of a fiber array aligned to OSA waveguides

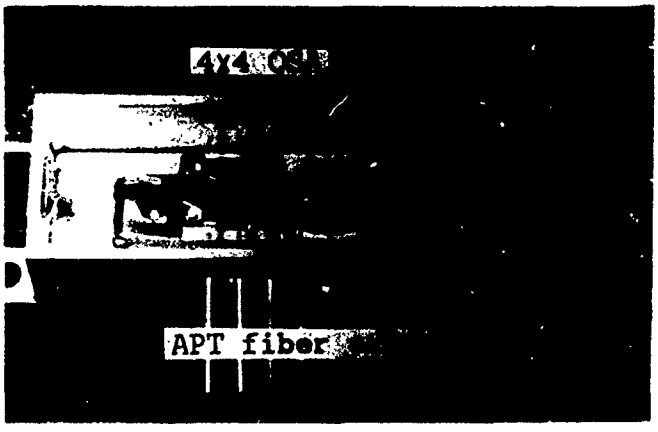

Fig. 3 InP based 4×4 OSM with APT fiber array

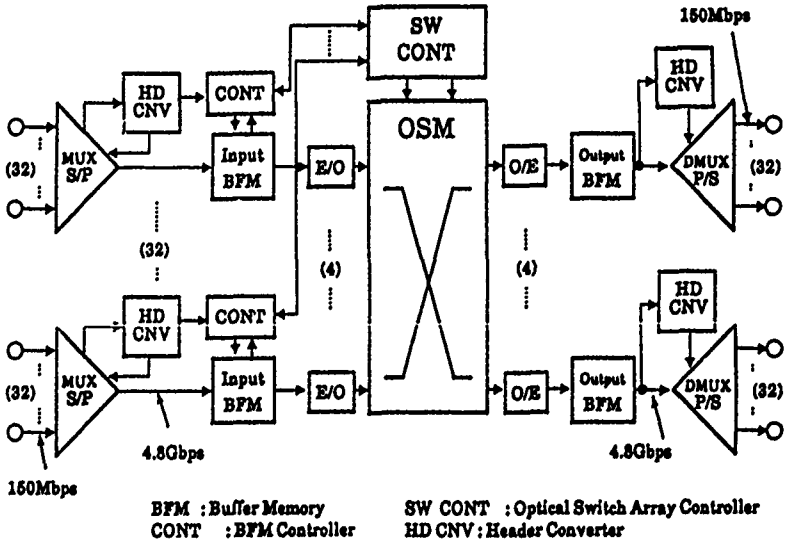

Fig. 4 ATM switch architecture using the OSM

NOTES

FRIDAY, MARCH 3, 1989

SALON D

9:45 AM–10:30 AM

FB1–FB4

POSTER SESSION: 2

An Optical Parallel Processor for Control of Photonic Switching Networks

Daniel J. Blumenthal
University of Pennsylvania
Department of Computer and Information Sciences
200 South 33rd Street, Moore Building
Philadelphia, PA 19104

Abstract

Photonic switching networks are currently limited in throughput and delay by the processing speed of the control system. A parallel optical processor is proposed which processes optical routing information for all switch inputs concurrently, allowing for simultaneous control of switching crosspoints. Improvements in throughput and delay are obtained through an architecture which utilizes the high interconnectivity and bandwidth of bulk optics and holographic optical elements (HOE). Control of an integrated-optic tree switch is given as example.

I. Introduction

Photonic switching networks provide a fabric for the routing of high-speed, wide-band optical information. A topic of current interest is the study of optical signal processing for switch control. Optical processing of routing information eliminates an electronic control bottleneck[1], resulting in lower delays and higher throughput [2].

Photonic switches are unique in their capability to pipe information through at rates compatible with that of the fiber-optic transmission medium. Several issues drive the requirement to increase the processing speed of photonic switch control; among them is a need to route information in real time, possibly on a bit-by-bit basis. Packet switching systems require the processing of a destination header in conjunction with the routing of data. The bit rate of header information will be limited by the bandwidth of control electronics, leading to a reduction in total throughput of the switching system [3]. The need to buffer data in order to compensate for processing speed is also at issue.

To date, optical control of a single switching node has been implemented [1,4-5]. Fiber-optic delay-line processors are employed to temporally encode and decode destination addresses. Recently, an architecture has been proposed to control the N^2 nodes of an optical crossbar switch[2]. The high interconnectivity of free-space optics allows for concurrent processing of all input channels in order to simultaneously set the switch crosspoints. The high temporal and spatial bandwidths of bulk optics and binary phase gratings results in lower delay and higher throughput for optical crossbar switching networks.

In this paper, a control architecture for more generalized switching structures (i.e. tree) is proposed. The high space-bandwidth product inherent in holographic optical elements (HOE) is utilized to map crossbar control information to a spatial equivalent corresponding to the crosspoint configuration of a switching network. Information is processed in parallel, allowing simultaneous control of all switch crosspoints. This architecture reduces processing delays to the order of free-space optical propagation times and processing times dictated by the method of encoding.

II. Single Node and Crossbar Control Architectures

An optical processing architecture for control of a single switching node has been proposed and demonstrated [1]. Temporally encoded destination information is processed by an optical pipeline processor in order to make an up or down routing decision at the node. Extension of this technique to control optical crossbar switches has been described using a parallel optical pipeline (POP) processing architecture [2]. Control information is extracted from data at the fiber-optic switch inputs and decoded in parallel using an array of optical pipeline processors. The output of the POP is a two-dimensional array of control signals corresponding spatially to the crosspoints of the crossbar switch.

III. Generalized Control Architecture

Switching networks other than the crossbar are desirable due to the reduced number of crosspoints (less than N^2) necessary to fully interconnect N inputs to N outputs. However, the control complexity increases from setting one crosspoint per connection (crossbar) to setting multiple crosspoints. Here the POP control architecture for crossbars is extended to these more general networks. As shown in Figure 1, the POP processor is utilized as an optical pre-processor which transforms temporally encoded routing information to a spatial representation. Each element in the POP output array represents the logical interconnection between input N and output M, based on routing requests at the switch input.

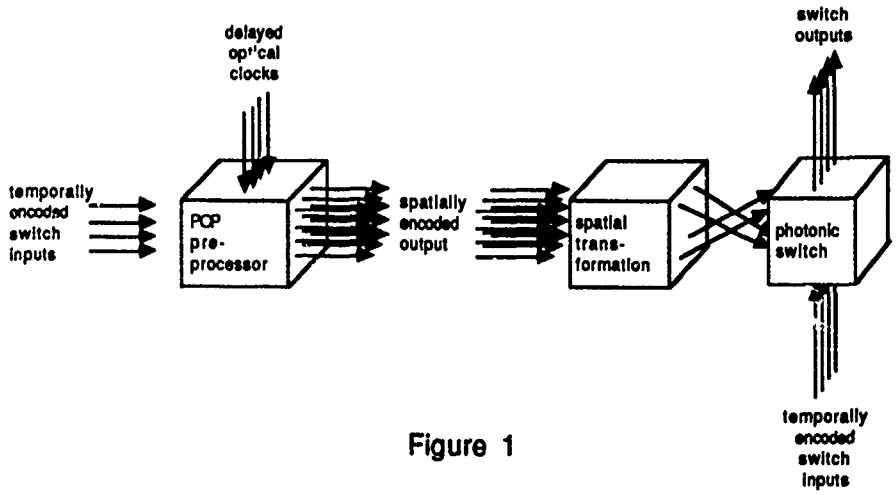

Figure 1

The output of the POP processor is termed the **control matrix** [2]. For optical pulse position encoding of the destination address [5], the control matrix is given by [2]:

$$\begin{bmatrix} \delta_{j1,1} & \delta_{j1,2} & \delta_{j1,3} & \dots & \delta_{j1,M} \\ \delta_{j2,1} & \delta_{j2,2} & \delta_{j2,3} & \dots & \delta_{j2,M} \\ \cdot & \cdot & \cdot & & \cdot \\ \delta_{jN,1} & \delta_{jN,2} & \delta_{jN,3} & \dots & \delta_{jN,M} \end{bmatrix}$$

where each element is a delta function operating on the encoded inputs and a synchronously delayed optical clock. Each element of the matrix is mapped to the appropriate crosspoints in the photonic switching network.

IV. Optical Implementation: Control of a Tree Switch

Integrated-optic switching networks such as the tree switch have been demonstrated [6]. As shown in figure 2, the control matrix is mapped to the switch using a HOE composed of many subholograms [7] specific to the switch architecture. To avoid blocking states of a switching network, transformation of the control signals may be done using a dynamically controlled HOE. The HOE fans-out each element of the control matrix to photodetectors and driving circuitry located at the appropriate crosspoints. Each crosspoint is biased in the up select state. An incident optical control signal switches the crosspoint to the down select state, routing the information to the requested output. An array of optical bistable elements[8] may be used to extend setup times for the routing of packets. The duration of the control process consists of the total free-space propagation delay in addition to the response time of bistable elements (sub-nanosecond). Figure 2 shows routing of input 4 to output 1 and input 3 to output 4.

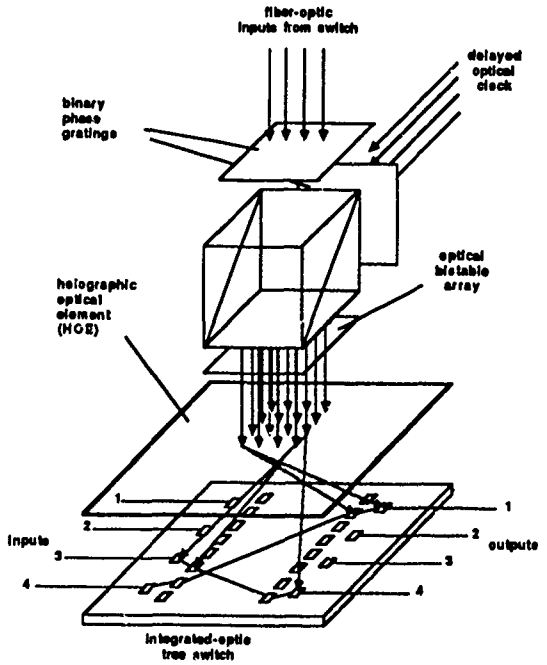

Figure 2

V. Summary

The throughput and delay of photonic switching networks is currently limited by the processing bandwidth of electronic control systems. Optical processing of routing information using free-space optics results in a control system with delay (sub-nanosecond) and throughput comparable with that of the photonic switching fabric. High-speed packet switching and other applications demanding real time control are possible given the performance of such a system.

References

[1] P.R. Prucnal, D.J. Blumenthal, and P.A. Perrier, *Opt. Eng.*, **26**, p. 473, 1987
[2] D.J. Blumenthal and L. Thylen, *ECOC*, Session 10, p. 268, 1988
[3] H.S. Hinton, *IEEE J. Selected Areas Comm.*, **6**, p. 1209, 1988
[4] D.J. Blumenthal, P.R. Prucnal, L. Thylen, and P. Granestrand, *Elec. Lett.*, **23**, 1987
[5] P.A. Perrier and P.R. Prucnal, *CLEO*, Anaheim, paper TuK2, 1988
[6] L. Thylen, *Journal of Lightwave Technology*, **6**, p. 847, 1988
[7] M.R. Feldman and C.C. Clark,*Proc. Top. Opt. Comp.*, Incline Village, paper ME2-1, 1987
[8] D.A.B. Miller *et. al.*, *Proc. Conf. Lasers Electro-optics*, San Francisco, p. 32, 1986

Characterization of High Speed Electrodes for $LiNbO_3$ Electro-Optic Switch Arrays

R. A. Nordin
*M. T. Ratajack**

AT&T Bell Laboratories
200 Park Plaza
Naperville, Illinois 60566-7050

1. INTRODUCTION

Electro-optic switching system applications that require fast reconfiguration rates (<1ns)[1] [2], must have electrodes constructed as transmission lines instead of lumped elements[3]. The coplanar strip (CPS) pattern is generally preferred (for z-cut $LiNbO_3$) for medium to large size array's, where routing congestion becomes important. The transmission line can be shunt terminated three ways. First it can be terminated on the optical substrate. The termination power and termination network surface area would be limited however. Second it can be terminated off of the substrate. This has the problem of limited routing flexibility and more area for I/O pads. Third the termination can be series distributed along the electrode length. The last case is the most advantageous not only for its ease of routing, but as will be shown requires less source power, termination power, and settling time. This leads to efficient and fast electrode structures. The distributed series termination resistance is simply implemented by keeping the electrode very thin (.3 μm), thereby increasing the conductor loss. This structure is referred to as an unterminated lossy transmission line[4] electrode. This paper describes the characteristics and the performance advantages of these lossy unterminated CPS electrodes.

2. ELECTRODE CHARACTERIZATION

CPS unterminated lossy electrode test patterns were fabricated on $LiNbO_3$ substrates. The electrode dimensions were 25μm width and 5 μm spacing. Thickness of .33 & .44 μm were used to determine conductor loss sensitivity to transmission line parameters. Two configurations of electrodes were made. One for two port measurements and used for transmission line parameter spectra extraction.The other for one port measurements and used for crosstalk and thermal measurements.

The electrodes were first characterized by measuring the input reflection and forward transmission scattering parameter spectra using an HP8510A network analyzer. The scattering parameter spectra can then be transformed into transmission line parameter spectra (complex characteristic impedance and propagation constant) by solving a system of four non-linear transcendental equations at each frequency. The results of this transformation, on four CPS electrodes are shown in Figure 1 (a) and (b). The high frequency characteristic impedance asymptotically approaches a real 30Ω and the phase velocity approaches 5.5 cm/ns. The dielectric material parameter spectra (dielectric constant and loss tangent) can then be determined, using the transmission line parameter spectra, by solving another set of equations at each frequency point. These experimental results match quite closely to theoretically simulated spectra. The simulated spectra is calculated from the CPS geometrical data and its dielectric properties. This is important because now we can simulate the CPS performance (as per section 3) with

* Current address: Department of Physics DePaul University, Chicago, Illinois 60614

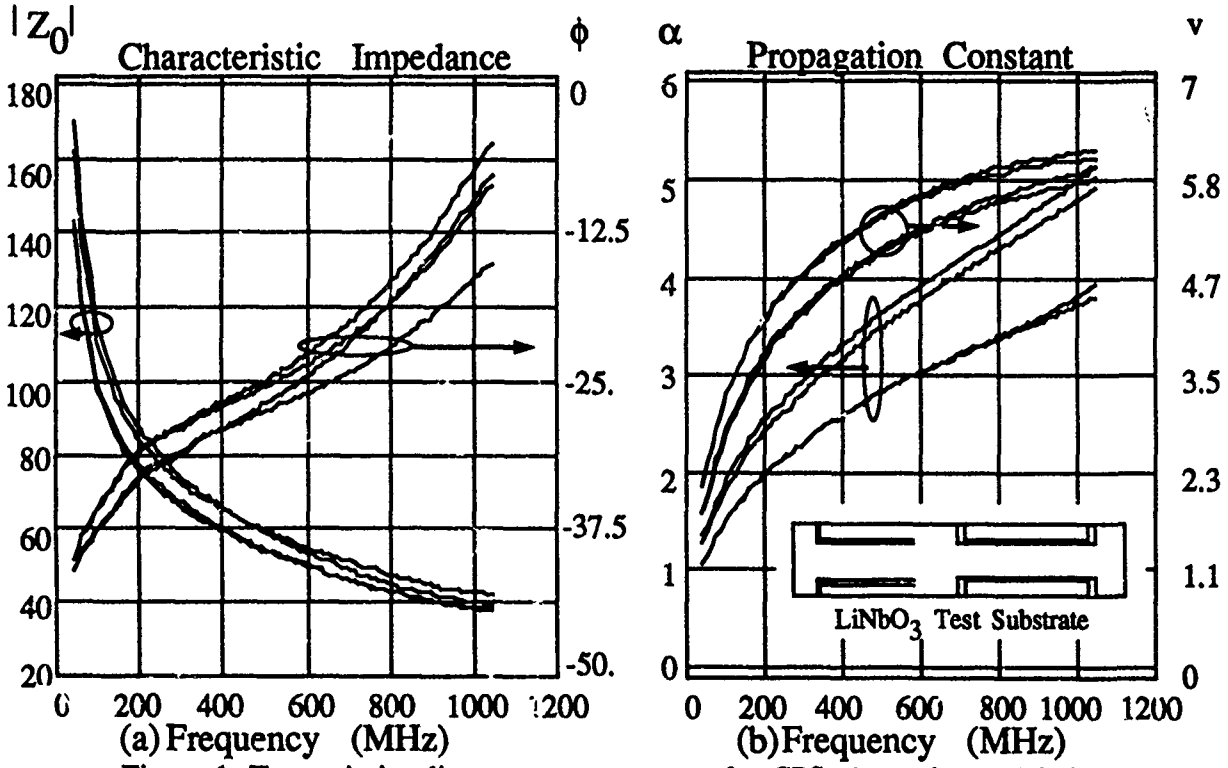

Figure 1. Transmission line parameter spectra for CPS electrodes on $LiNbO_3$

a great deal of confidence.

Electrode to electrode coupling (or crosstalk) was measured to be near -20 dB for parallel separated adjacent electrodes (see inset fig. 1b). Although this crosstalk preturbs the optical output signal by only -30dB with one interferring electrode, it may get worse with more electrodes. The crosstalk mechanism's are electro-magnetic and/or acoustical. The dominant mechanism (experimentally determined) was acoustical coupling, which was identified in the time domain. Mechanically damping the substrates may become an important issue as the switch size increases.

Power is dissipated along the length of the electrode heating the substrate, hence a temperature gradient can be measured. A 5 degree rise above ambient was measured, for a single electrode being driven with a 400MHz, 15 volt p-p signal. Although this at first seems small, $LiNbO_3$ is pyroelectric, and at a higher frequency and/or higher p-p signals this can become an important concern[5].

3. ELECTRODE PERFORMANCE

The performance of these lossy CPS electrodes (as simulated by their step response and required source power) are shown in Figure 2 (a) and (b). The step response of various unterminated electrodes (with and without a series source resistor) as well as terminated electrodes (with series load capacitor to reduce termination power) are shown. The unterminated CPS electrode with the series source resistor has the fastest settling time (as measured by the output reaching within 1% of the final value). This is faster than the unterminated electrode without a series source resistor for primarily two reasons: first the electrode has more loss (which means that reflections will be attenuated further), and secondly the series source resistor adds to the characteristic impedance of the electrode which then matches the 50

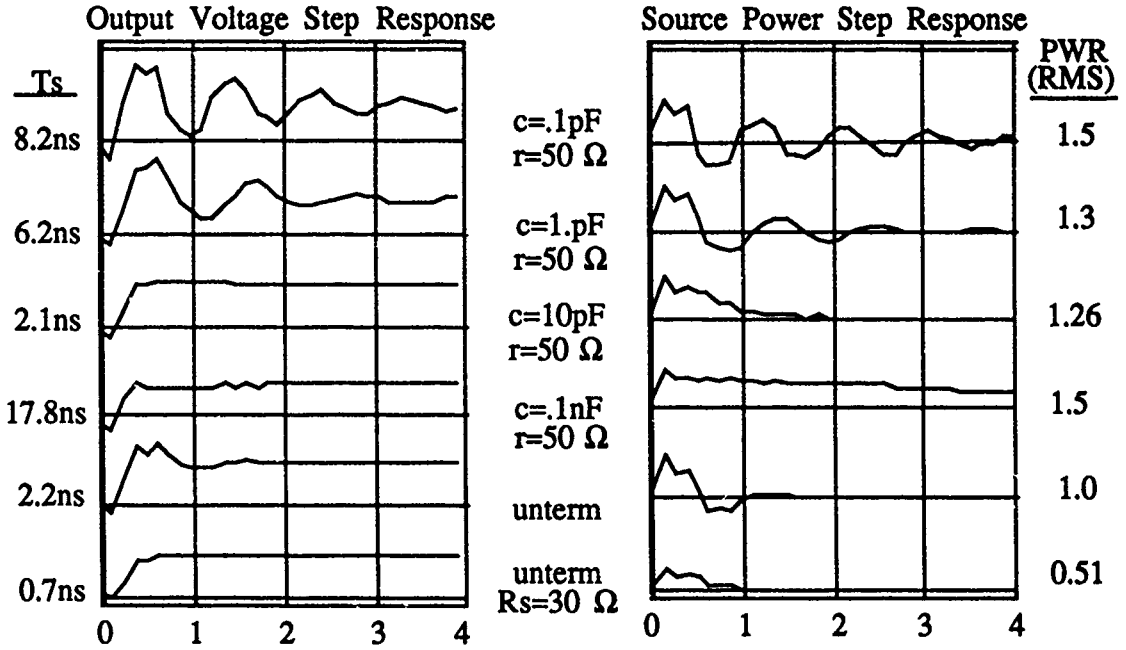

Figure 2. Simulated CPS electrode performance

ohm source impedance. Note that the unterminated electrodes have faster settling times than the terminated ones. This occurs for two reasons. First the series termination capacitance leads to matching and rc time constant problems. Secondly the characteristic impedance of any of these electrodes is not constant which leads to matching difficulties with resistance values (a matching network perhaps would be more suitable). Similarly, we see in Figure 2b that the power required from the source is minimized when the unterminated electrode with a series source resistor is utilized.

4. CONCLUSIONS

CPS unterminated lossy transmission line electrodes provide an efficient technique for fast reconfiguration rate electro-optic switch arays. These electrodes have been successfully fabricated on experimental Ti:$LiNbO_3$ switch arrays configured as a time-multiplexed switch.

REFERENCES

1. Erickson J.R. et al.,"A 1.7 Gigabit-per-Second, Time-Multiplexed Photonic Switching Experiment", Proceedings of the First Topical Meeting on Photonic Switching - 1987, pp.204-207.
2. Erickson J.R. et al.,"High-Speed Hitless Switching Using Ti:$LiNbO_3$", Submitted to Topical Meeting on Photonic Switching - 1989.
3. Becker R.A.,"Broadband Ti:$LiNbO_3$ Guided Lumped-Element and Traveling-Wave Interferometric Modulators",paper Tua2,IGWO'84
4. Ho C.W. et al.,"The Thin-Film Module as a High-Performance Semiconductor Package",IBM J. RES. Develop., vol 26,No.3, May '82,pp.286-96.
5. Giles C.R and Korotky S.K.,"Stability of Ti:$LiNbO_3$ Waveguide Modulators in an Optical Transmission System",1988 Technical Digest, Vol.5, paper ME5-1,IGWO pp.115-7.

All-Optical Signal Routing using Bistable Interferometers

G.S. Buller, S.D. Smith and A.C. Walker

Department of Physics, Heriot-Watt University,

Edinburgh EH14 4AS, Scotland, UK

Optically bistable Fabry-Perot etalons have been studied since 1979, fabricated in a wide range of semiconductors and organic materials[1,2]. Demonstrations of the potential applications of such devices have been mainly confined to optical parallel processing[3]. However, with increasing interest in signal routing, a number of schemes utilising optically bistable devices in such network have been studied[4,5].

At a previous meeting[6], we described a simple 1 x 2 all-optical spatial switch using a ZnSe nonlinear interference filter (NLIF)-based on an optothermal nonlinearity. In this demonstration, a NLIF was switched between reflecting and transmitting states. The purely optical control of these states and the subsequent latching action allowed high-frequency data to be passed in either direction with no electrical or mechanical intervention. The upper limit on the frequency of the data is set by the transmission bandwidth of the device (typically THz).

The optical control of such switches could be advantageous, especially if it can be utilised in a more complex routing network. We have designed and fabricated a demonstration 1 x 4 all-optical routing network based on the 1 x 2 switch[7]. The data path was encoded within the header pulses that preceded the high frequency data. This concept could be extended to form larger N x N nonblocking networks.

In the above experiments, single wavelength data was spatially

switched. In an optically bistable Fabry-Perot device (with a refractive nonlinearity), the interference peak is shifted in wavelength by an amount proportional to its initial detuning. Hence, if a bistable interferometer is switched from off-resonance to on-resonance by a source with wavelength λ_1, a second wavelength λ_2, initially on-resonance, will be switched in the complementary manner. In this way, it is possible to construct an optically controlled, wavelength exchange-bypass switch.

This was demonstrated using the outputs of two single-frequency GaAs laser diodes, at λ_1 and λ_2, incident upon a ZnSe NLIF with an external absorber[8]. The wavelength separation was $\sim$ 2 nm. The reflection characteristics for both wavelengths are shown in Figure 1.

When input λ_1 was held in the bistable region and slow ($\sim$ 10 ms) positive and negative pulses were applied, λ_1 latched into the lower and then the upper state and vice versa for λ_2. This is shown in Figure 2.

One of the problems in using optically bistable devices in many applications is the poor contrast often found (typically $\sim$ 3:1). We will describe a number of ways by which this may be improved, including a novel angle-dependent polarization switching effect which can be used to greatly increase the contrast of both optoelectronic and optothermal bistable etalon devices. The contrast levels that we have achieved, limited by the quality of the polarisation optics used, are typically $\geq$ 50:1. An example is shown in Fig. 3.

References

1. H.M. Gibbs, Optical Bistability: Controlling Light with Light (Academic Press, Florida, 1985).
2. P. Mandel, S.D. Smith and B.S. Wherrett, From Optical Bistability towards Optical Computing (Elsevier, Amsterdam, 1987).
3. S.D. Smith, A.C. Walker, F.A.P. Tooley and B.S. Wherrett, Nature 325, 27, (1987).
4. T. Venkatesan, P.J. Lemaire, B. Wilkens, L. Soto, A.C. Gossard, W. Wiegmann, J.L. Jewell, H.M. Gibbs and S.S. Tarng, Optics Letters, 9 297 (1984).

5. L. Zhang, R. Jin, C.W. Stirk, G. Khitrova, R.A. Athale, H.M. Gibbs, H.M. Chou, R.W. Sprague and H.A. McLeod, IEEE Selected Areas in Communication, Vol. 6, No. 7, p. 1273 (1988).
6. C.R. Paton, S.D. Smith and A.C. Walker, Photonic Switching, (Eds. T.K. Gustafson and P.W. Smith, Springer-Verlag, Berlin) p. 59 (1988).
7. G.S. Buller, C.R. Paton, S.D. Smith and A.C. Walker, Appl. Phys. Lett. (to be published)
8. A.C. Walker, Optics Commun. 59, 145 (1986).

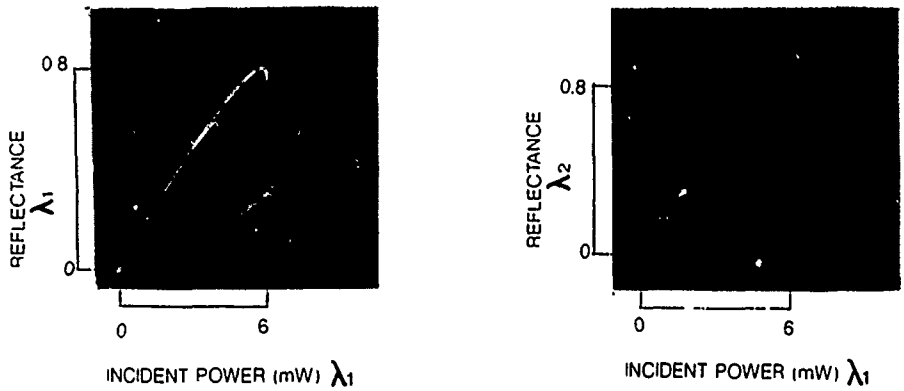

Fig. 1 Reflection characteristics for wavelengths λ_1 and λ_2.

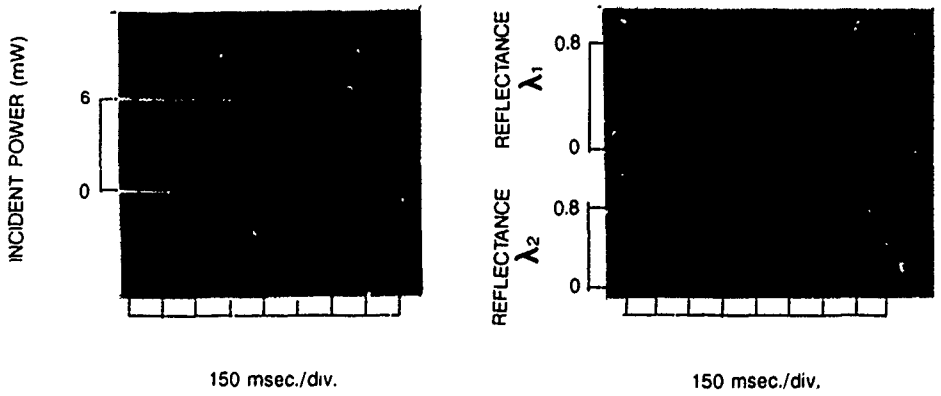

Fig. 2 Incident pulse train and corresponding reflection response for wavelengths λ_1 and λ_2.

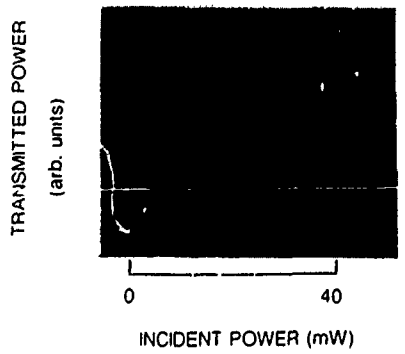

Fig. 3 High contrast optical bistability characteristic.

A self-routing optical switch using ring topology

S. F. Su and K. T. Koai
GTE Laboratories Incorporated
40 Sylvan Road, Waltham, MA 02254

I. Introduction

Packet switching is one of the basic switching techniques used in telecommunication switching systems. It has been commonly implemented by using conventional electronic technology. Input data are stored in the so called elastic memories and output to the designated destination according to the destination address at the header. With the increasing deployment of optical fibers in transmission systems and demand for variable bandwidth services, packet switching in the optical domain may be desirable for future switching systems.

Ring-based switch has successfully been developed for fast circuit switching using electronic technology [1]. On the contrary, due to a lack of optical digital devices, it was very difficult to develop an optical ring-based switch. However, the new photonic shift register [2] in conjunction with the recent progress in optical amplifiers has kept the hope of developing an optical switch alive. Here we propose a self-routing optical switch using ring topology. This switch is able to simultaneously route multiple optical packets according to the information imbedded in the headers.

II. General description

The basic structure of this optical ring-based switch is shown in Fig. 1. As indicated, all switch ports are ring connected. Each port consists of an input processor, a switch cell, an output decoder, and an output processor. The incoming and outgoing optical packets are serial, but all internal transfers are parallel.

The inputs to the switch are serial optical packets (packets of optical pulses) containing data, source identification, destination address, and flag bits. A variety of message formats may be chosen for the incoming packets. Different formats will require different designs for the switch but will not change the basic architecture of the switch. Here we use a simple, generic format just to show how the proposed switch works. We assume that an incoming optical packet consists of a header and data. They are organized as a sequence of optical bits. The header consists of source identification, destination address, and flag bits, which signal the start of a packet. For simplicity, we also assume that each packet is of the same length. A long message may contain a large number of packets.

The input processor converts the incoming serial optical bits in a packet into a number of parallel optical bytes, called switch words. Each switch word contains a header and a data field. Switch words from all input processors are synchronously loaded into the corresponding switch cell at the CLK3 rate. For an optical ring containing n ports, there are n switch words in the ring. The switch words shift around the ring and enter every output decoder at the CLK2 rate. The output decoder accepts or abandons the switch word by comparing the address carried by the switch word and the switch port address. If the addresses match, the switch word is transferred to the corresponding output processor where it is converted to a serial data stream and output to the destination.

III. Functional Design

Functional designs of the input processor, switch cell, and output decoder/processor are briefly described below. Detailed design will be elucidated during the presentation.

1. Input processor

As shown in Fig. 2, the input processor consists of four major sections: demultiplexing, serial-to-parallel conversion, optical memory, and loading control. The demultiplexing section separates the header from the data. The serial-to-parallel conversion section, which is made of optical serial-to-parallel converters, converts the serial bits to parallel bits and sends them to the optical memory section. The memory section, which is made of photonic shift registers, stores the parallel switch words. The loading control is responsible for timing and for proper loading of the switch words onto the ring-connected switch cell.

2. Switch cell

A switch cell, which is connected to an input processor and an output decoder, is basically a photonic shift register. It receives the new switch word from the input processor and erases the old one at a CLK3 pulse. At a CLK2 pulse, it shifts the switch word to the next switch cell and receives a new one from the preceding switch cell. At a CLK1 pulse, the optical pulse is shifted from Cell 1 to Cell 2 within the shift register. Figure 3 shows a single optical ring which consists of four switch cells. There are N optical rings in an optical ring-based switch, where N is the number of bits in a switch word. The delay in the ring itself depends on the speed of the photonic shift registers and the physical size of the ring. Using today's technology, the photonic shift register can run at a speed of several gigabits per second.

3. Output decoder and processor

Figure 4 shows a functional diagram of output decoder and output processor. The function of output decoder is to select or "gate" switch words destined for the selected output port. The output decoder compares the destination address carried by the switch word with the port address using optoelectronic gates. Switch words with the proper destination address are transferred to the output processor. The output processor maps switch words into optical packets and converts them into serial data streams.

IV. Performance estimates

Performance of the optical ring-based switch depends on the components and technology used in the switch. In general, switching speed of an optical ring-based switch is limited by the speed of the photonic shift registers and the processing speed of its output decoders and output processors. Using discrete components and hybrid integration technology, the switching speed of the optical ring-based switch is on the order of gigabytes (giga switch words) per second, which is about 10 times faster than that of the electronic ring-based switch. This speed can increase to tens of gigabytes per second when integrated optics and optoelectronic integrated circuits technologies are employed. The larger the switch words, the higher the throughput. Typical switch word size ranges from tens of bits to hundreds of bits. This indicates that the throughput of an optical ring-based switch is on the order of terabits per second.

V. References

1. J. Lenart, L. Jou, and S. F. Su, "A high-speed ring-based switching concept," Proceedings of ISS 1987, pp. 43-47, March 1987.

2. S. F. Su and K. T. Koai, "Photonic shift register," presented at 1988 OSA Annual Meeting, Santa Clara, Calif., Oct. 31 - Nov. 4, 1988.

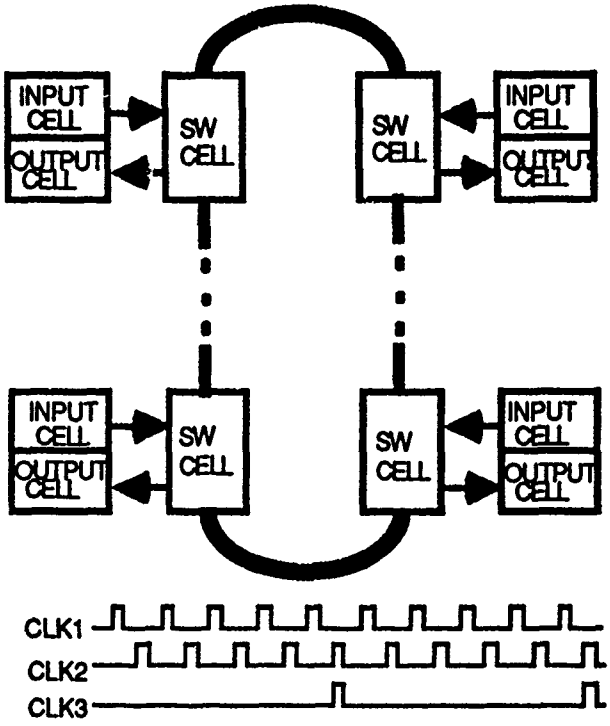

Fig. 1. Optical ring-based switch.

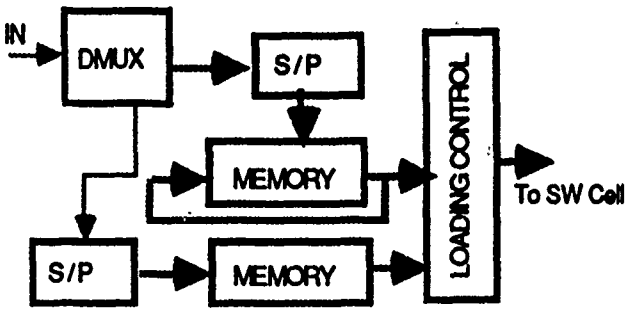

Fig. 2. Input processor.

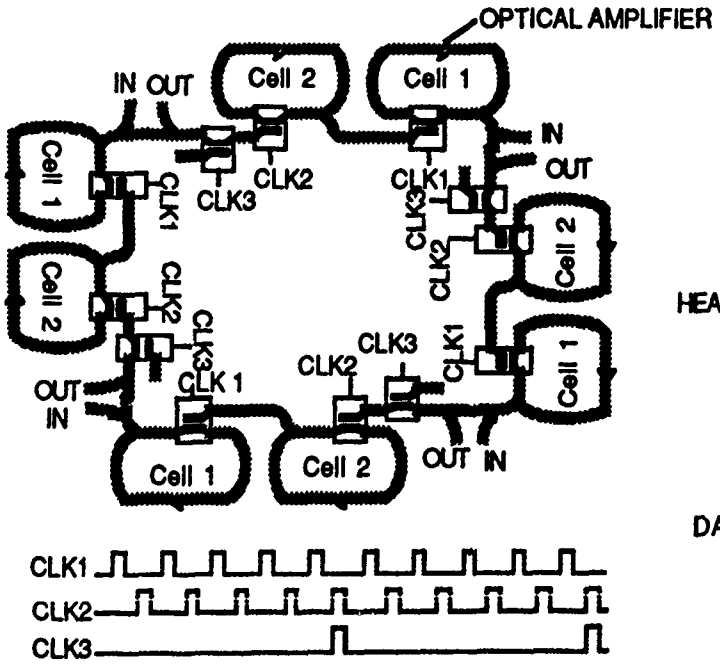

Fig. 3. An optical ring with four switch cells.

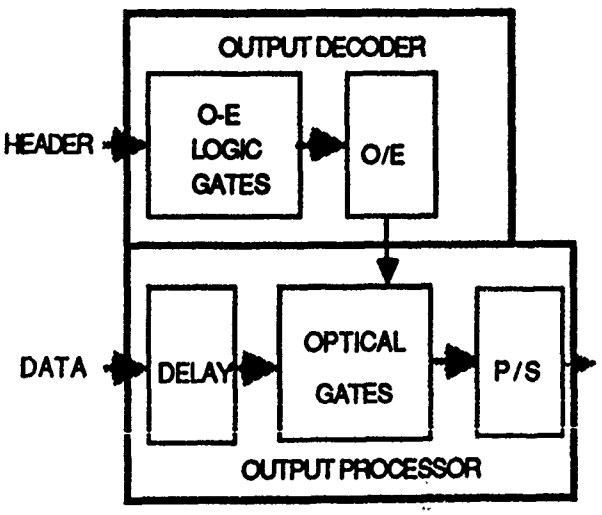

Fig. 4. Output cell.

NOTES

FRIDAY, MARCH 3, 1989

SALON E

10:30 AM–12:00 M

FC1–FC5

TIME-DIVISION SWITCHING SYSTEMS

T. Yasui, NTT Telecommunication Networks Laboratories, Japan, *Presider*

Time-Multiplexed Optical Systems

R. S. Tucker, G. Eisenstein, and S. K. Korotky

AT&T Bell Laboratories

Crawford Hill Laboratory

Holmdel, NJ 07733

Time-division multiplexing is used widely in electronic switching and transmission systems operating at low and moderate bit rates. At multi-gigabit per second rates, however, the bandwidth and switching speed of electronic devices become limiting factors and give rise to an electronic speed bottleneck. Optical time-division multiplexing (OTDM) eliminates these electronic devices from the key high-speed multiplexing operations and creates new opportunities in very high speed switching and transmission.

Optical time-division multiplexing and demultiplexing offers several attractive characteristics: (a) It enables very high bit rates to be achieved, while employing electronics with only moderate bandwidth; (b) it is a digital technology, which leads to an inherent compatibility between photonic switching and transmission systems; (c) it provides flexibility in the choice of the number of transmitter lasers; and (d) it offers the potential for full use of the zero dispersion wavelength in transmission systems. The potential of OTDM systems has been recognized for more than two decades [1-5]. However, it is only recently that system-level demonstrations of the technique have been reported [6-12]. These experiments have served to highlight some key aspects of the potential of OTDM such as very high bit rate transmission [11], high bit rate switching switching [12], and self-routing using optical processing [10].

This paper surveys recent progress in optical time-division multiplexing for very high bit rate transmission and switching systems. The required characteristics of key devices will be

described, with particular emphasis on mode-locked and gain-switched lasers for picosecond pulse generation, optical switches for data encoding, multiplexing, and demultiplexing, and optical amplifiers for compensation of system losses. System architectures for transmission and switching systems will be described and methods for timing and clock recovery will be reviewed. Performance limitations due to crosstalk will be explained.

REFERENCES

1. T. S. Kinsel and R. T. Denton, Proc. IEEE., **56**, 146 (1968)
2. F. S. Chen, IEEE J. Quantum Electron.,**QE-7**, 24, (1971)
3. M. Thewalt, IBM Technical Disclosure Bulletin, **24**, 2473 (1981)
4. A. Alping, T. Andersson, R. Tell, and S. T. Eng, Electron. Lett.,**18**, 422 (1982)
5. S. K. Korotky, G. Eisenstein, R. C. Alferness, J. J. Veselka, L. L. Buhl, G. T. Harvey, and P. H. Read, J. Lightwave Technol. **LT-3** (1985)
6. P. R. Prucnal, M. A. Santoro, S. K. Sehgal, and I. P. Kaminow, Electron. Lett., **22**, 1218 (1986)
7. R. S. Tucker, G. Eisenstein, S. K. Korotky, U. Koren, G. Raybon, J. J. Veselka, L. L. Buhl, B. L. Kasper, and R. C. Alferness, Electron. Lett., **23**, 208, (1987)
8. G. Eisenstein, R. S. Tucker, U. Koren, and S. K. Korotky, IEEE J. Quantum Electron. **QE-22**, 142 (1986)
9. L. C. Blank, E. G. Bryant, A. Lord, J. M. Boggis, and W. A. Stallard, Electron. Lett. **23**, 977 (1987)
10. P. R. Prucnal, D. J. Blumenthal, and M. A. Santoro, Electron. Lett., **23**, 629 (1987)
11. R. S. Tucker, G. Eisenstein, S. K. Korotky, L. L. Buhl, J. J. Veselka, G. Raybon, B. L. Kasper, and R. C. Alferness, Electron. Lett., **23**, 1270 (1987)
12. S. K. Korotky, D. A. Herr, T. O. Murphy, J. J. Veselka, A. Azizi, R. W. Smith, and B. L. Kasper, Conf. on Optical Fiber Communications, Houston, Texas, Feb. 1989

An Experimental 512 Mbps Time-division Photonic Switching System

T. Shimoe, S. Kuroyanagi, K. Murakami,
H. Rokugawa, N. Mekada, and T. Odagawa

FUJITSU LABORATORIES LTD.
1015 Kamikodanaka, Nakahara-ku, Kawasaki 211, Japan

1. Introduction

Broadband switching systems offering high-quality video services must operate at high speeds and photonic switching is highly promising for overcoming the many problems limiting switching speeds. This paper describes our experimental photonic time-division switching system. We have developed a system using high-speed and thermally stabilized optical memory and optical switch modules.

2. System configuration

The experimental system can switch four 128 Mbps full-motion color video signals for 512 Mbps operation.

Figure 1 is a block diagram of the system. Four video channels are multiplexed onto a 512 Mbps highway in a bit-interleaved form and sent to a time switch. The time switch consists of a 1 X 4 write optical switch, four optical memories, and a 4 X 1 read optical switch. The signals in the input highway are sequentially written to the optical memories, where time slot #i is stored in the #i optical memory during the frame, and then randomly read out to the output highway according to the controller's instructions.

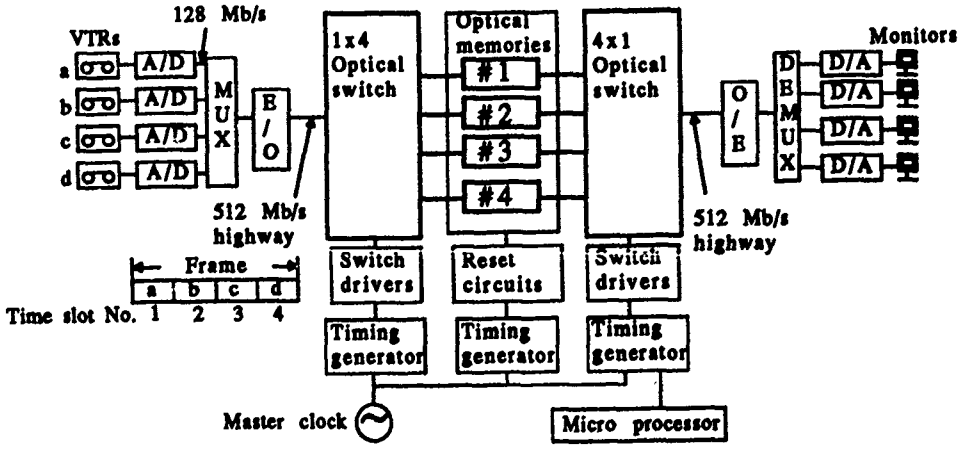

Figure 1 Experimental system configuration

3. Optical devices

The key devices in the system are bistable laser diodes with tandem electrodes used as optical memories and Ti:$LiNbO_3$ waveguide switches.

3.1 Optical switch modules

For the 1 X 4 / 4 X 1 optical switches, three 2 x 2 directional couplers are integrated in the tree structure shown in Figure 2.

For high-speed switching, traveling-wave electrodes are used. So, less than 200 ps switching is obtained by GaAs FETs drive.

For thermal stabilization, a Si layer with an appropriate resistivity between the SiO_2 buffer layer and electrode is formed[2]. This structure reduces thermally-induced drive voltage shift to less than 0.1 V/°C by uniform surface-charge distribution. In the optical switch module, a polarization maintaining fiber is permanently attached to the switch chip through a ruby bead. This reduces the thermally-induced loss deviation[3].

3.2 Optical memory modules

The main feature of the bistable laser diodes is the embedded semi-insulating InP current blocking layer[4] shown in Figure 3. This structure decreases the response time to less than 150 ps. In the optical memory modules, fibers are permanently attached to the bistable laser diode with lenses. Coupling losses are 4 to 6 dB at the input ports and 7 to 9 dB at the output ports.

For wavelength stabilization, the optical memory modules use external Peltier devices to prevent operating condition deviations. This is especially important as the coincident wavelength with the light source can reduce switching power -5 dBm at 512 Mbps.

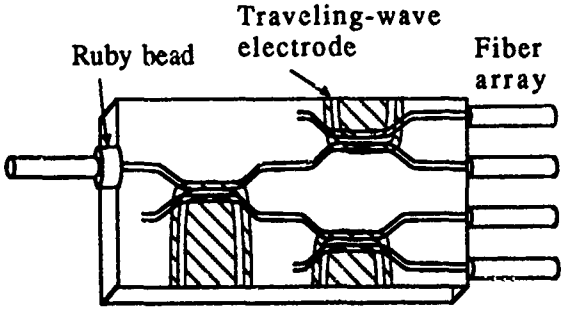

Figure 2 1x4 optical switch

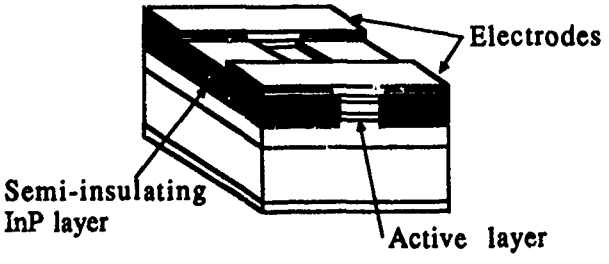

Figure 3 Bistable LD

4. Experimental results

Figure 4 shows the experimental system, which is composed of a rack for the switching system and four video sources and TV monitors. The rack is 1.5 m high, with 3 shelves for the video codecs and control circuits, the optical switching network, and a micro-processor. All switching circuits are installed in the same rack.

Video quality is Adequate. To provide enough input power to the bistable memories, a 10 dBm high-power VSB laser diode is used as the light source. Figure 5 shows the output highway waveform. The 3 dB deviation at the bistable memory outputs are made uniform at the connectors between the optical memories to avoid error rate degradation at the optical receiver. A 10^{-9} bit error rate is obtained in the worst-case path.

Figure 4 The experimental system

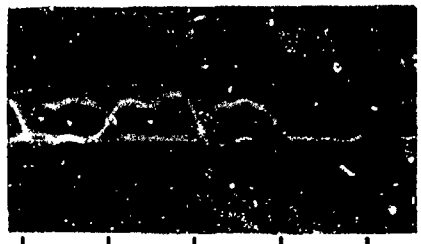

Figure 5 Output optical waveform

5. Conclusion

An experimental time-division photonic switching system has been demonstrated. Stable 512 Mbps switching was established in a practical environment. All optical modules are rack mounted with the electronics circuits.

Acknowledgement

The authors wish to express their appreciation to Dr. H. Takanashi for his encouragement and guidance. The authors also wish to thank members of the FUJITSU LABORATORIES Communication and Space Division and the Electron Devices Division.

References

[1] S. Suzuki et al., *IEEE J. of Lightwave Technol. vol. LT-4, no. 7*, 1988.
[2] I. Sawaki et al., *CLEO'86, paper MF2*, 1986.
[3] N. Mekada et al., *IGWO'88 to be presented*, 1989.
[4] M. Kuno et al., *Appl. phys. Conf., 29T-ZH-7*, 1987, *(in Japanese)* .
[5] T. Odagawa et al., to be presented *SSDM'88*, 1988.

Demonstration of a self-clocked optical time-slot interchanger

Philippe A. Perrier, Paul R. Prucnal, Michel W. Chbat

Department of Electrical Engineering
Princeton University
Princeton, NJ 08544

1. Introduction

Three classes of switches have been investigated in the optical domain: wavelength-division (WD), space-division (SD) and time-division (TD).

WD switches are attractive because of their potentially high throughput. Their development is however still at an early stage due to the lack of wavelength converters.

In SD switches, a matrix of crosspoints is used to connect any of the input ports to any of the output ports. As the number of ports increases, the complexity of the switch increases correspondingly, and ultimately limits the size of the switch that can be fabricated.

Larger photonic switching systems can be implemented by cascading SD switches and TD switches (also referred to as time-slot interchangers (TSI)). In TD switching, the time-multiplexed optical input data stream is first demultiplexed and the data in each time slot is written into an optical memory. Switching is accomplished by sequentially reading out the stored data in any desired order [1].

Few optical TD switches have been proposed [2,3,4]. In this paper, a novel optical TSI implementation is presented.

2. Previous proposals

Optical implementations of NxN TSIs have used integrated-optic 1xN and Nx1 switch matrices as optical write and read gates, respectively [2,3,4]. Fiber-optic delay-lines and bistable laser diodes (BLDs)[2,3] have been used as optical memories. Implementations of photonic TD switches with architectures analogous to their electronic counterparts seem to have, however, several shortcomings. Implementing optical memories with fiber-optic delay-lines necessitates 2N delays if all possible time slot permutations are required. Reentrant delay-lines can reduce this number to N at the expense of amplification [3]. On the other hand, BLDs can store only one bit of information at a time. To store B bits per time slot with BLDs would therefore require BxN memory elements.

3. Proposed TSI Architecture

A block diagram of the proposed optical TSI is shown in Fig. 1. It consists of a high-speed serial-to-parallel demultiplexer, that serves as a write gate, and of a bank of programmable optical delays, used as memory elements.

The optical data input to the TSI consists of time-multiplexed channels forming a frame of length T (A frame of data is also depicted in Fig. 1.). Each frame is divided into N+1 time slots, denoted 0 through N, of duration t. The 0^{th} slot is always occupied by a reference pulse, each of the remaining slots 1 through N contains one bit of data. The demultiplexer consists of N cascaded 1x2 photonic switching elements, labeled 1 through N, and of a gating controller. The incoming signal is loaded into the demultiplexer as in a shift register. Upon detection of the reference pulse at the controller, each time slot is located at the input of its corresponding switching element. The controller generates a gating pulse of duration t which simultaneously sets all switching elements in the cross-state. Each time slot is routed to the switched output of the switching element, thus achieving the required demultiplexing.

The demultiplexed pulses simultaneously enter the bank of N programmable optical delays. Each optical delay shifts the pulse to a new time position. A fiber-optic summer multiplexes the delayed pulses and the reference pulse, appropriately retarded, to yield a time slot interchanged version of the initial input sequence.

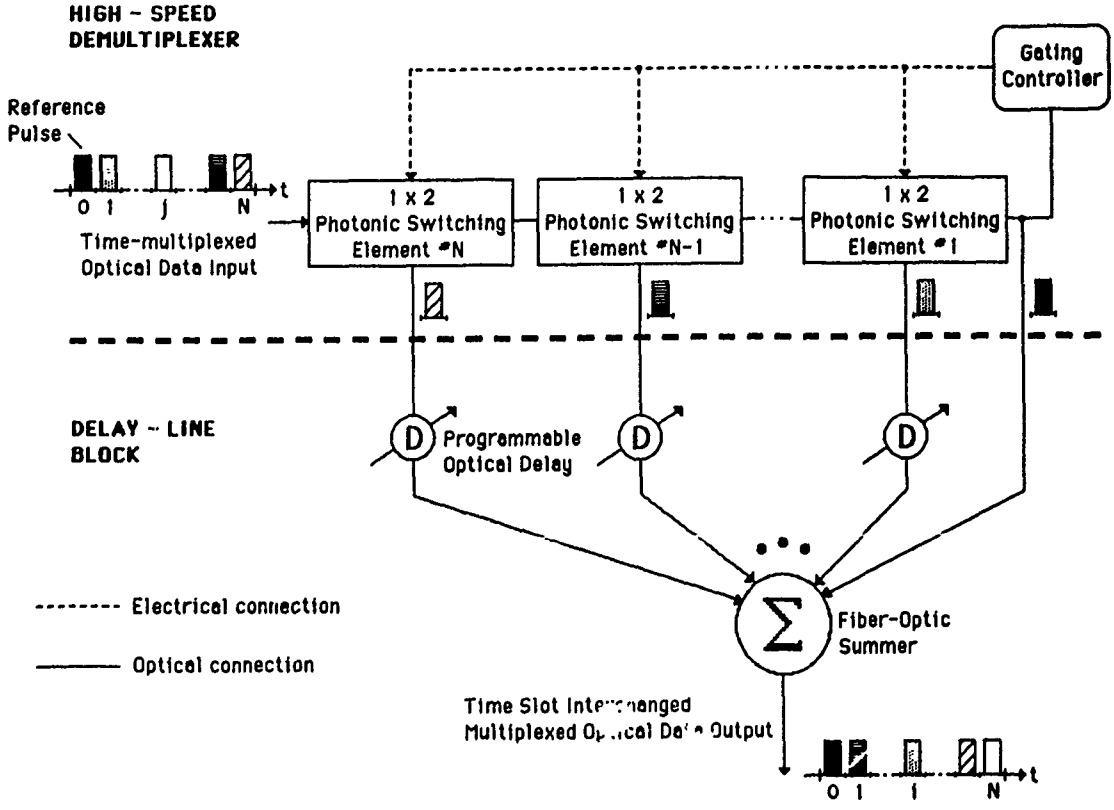

Fig.1: Block Diagram of the Optical Time-slot Interchanger

4. Features of the proposed TSI

The proposed TD switching architecture has several advantages over previously demonstrated TSIs. First, sending a reference pulse with the data, together with the shift-register design configuration, simplifies the demultiplexing function. This self-clocking capability allows high-speed demultiplexing without the need of an external control. Second, the self-clocking capability also makes the TSI operation asynchronous since no external clock is required. Third, the multiplexing function is achieved passively in the summer, eliminating the need for an active read gate.

The setting of each delay is a low-speed function compared to the demultiplexing, which has to be done within time t. Indeed, the reconfiguration of the time slot arrangement has to be performed in a time less or equal than T which corresponds to the time it takes to load a frame into the demultiplexer.

Finally, simultaneous demultiplexing allows an optimized number of only N delay-lines to perform all possible permutations of the initial sequence.

The serial configuration of the demultiplexer results in a non-uniform attenuation of the demultiplexed time slots. Time slots closer to the reference pulse undergo a larger attenuation than time slots further away since they travel through a larger number of photonic switching elements.

In this talk, an experimental demonstration will be reported and ways to compensate for the non-uniform attenuation will be discussed.

References

1. M. Schwartz, Telecommunication Networks: Protocols, Modeling and Analysis, Addison-Wesley Publishing Co., 1987.

2. H. Goto, K. Nagashima, S. Suzuki, M. Kondo, and Y. Ohta," Optical time-division digital switching: an experiment," 6th topical meeting on Optical Fiber Communication, Digest of technical papers, paper MJ6, pp. 22-23, New Orleans, LA, 28 February-2 March, 1983

3. S. Suzuki, T. Terakado, K. Komatsu, K. Nagashima, A. Suzuki, and M. Kondo, "An experiment on high-speed optical time-division switching," Journal of Lightwave Technology, Vol. LT-4, No. 7, pp. 894-899, 1986

4. R.A. Thompson and P.P. Giordano, "An experimental photonic time-slot interchanger using optical fibers as reentrant delay-line memories," Jounal of Lightwave Technology, Vol. LT-5, No. 1, pp. 154-162, 1987

Efficient Clock Distribution in a High-Speed Time-Multiplexed-Switched Optical Network

S.K. Korotky and A. Azizi

AT&T Bell Laboratories
Crawfords Corner Road
Holmdel, NJ 07733
(201) 949-5576

Time-multiplexed-switched (TMS) optical networks can serve to provide broadband communications among a number of high-capacity digital terminals, such as public branch exchanges (PBXs), central office switches, and computers. As such, recently they have been receiving increased attention [1-6]. The central element in these networks is a high-speed optical hub switch that reconfigures on a regular basis to route traffic in the form of blocks of data among the terminals. Depending on the nature of the traffic, a variety of switch architectures are suited to both arbitrary [2,3] and scheduled [1,4-6] interconnection patterns. The latter effectively provide virtual circuit interconnections among all the terminals on the network. Experimental demonstrations of an 8×8 dilated-Benes architecture with ~2 ns switch reconfiguration time [3] and a 4×4 banyan architecture with ~250 ps switch reconfiguration time [5] based on Ti:$LiNbO_3$ directional couplers have been reported. To take advantage of the short guardbands that are possible and keep system overhead low, a means of clock distribution is required. Here we describe and demonstrate an efficient method of clock distribution suitable for attaining bit-synchronization of local networks. We present experiments to show that the local clock oscillator of a 4 Gb/s terminal of a TMS network can be locked to the switch master clock located 5 km from the terminal.

The logical interconnections we wish to implement in a four-terminal TMS network [5] are depicted in Fig. 1. Each terminal is connected to the optical TMS hub switch via fibers to form a broadband network. A master clock is used to define the frames and time-slot positions of the switch and hence the network, as described previously [5]. This clock must also be conveyed to the terminals to ensure that the duration of the time-slots transmitted by the terminals are identical to the time-slots allocated by the switch. In addition, the terminal may use the clock in the decision circuit of its receiver. A variety of means may be used to distribute the clock from the master clock at the switch location to the terminals. For example, the clock may be distributed over a distinct network, as we have previously done [5], or over a separate wavelength over the same fiber as the data. These approaches require many additional devices, however. (Note, we assume the geographic extent of the network is not so great that wander of the distributed clock, which might be caused by significant temporal variations in the temperature differentials across the network or laser wavelengths, is a concern.)

In Fig. 2 we illustrate a novel and efficient method of clock distribution that requires essentially only the addition of a set of optical modulators to the data network. This set of modulators, one for each terminal, may be integrated onto the same substrate(s) constituting the hub switch. The optical modulators are used to impress a continuous-wave low-amplitude tone onto the optical data signals, which originate at the terminals, *without an optical-to-electrical conversion* as they traverse the switch location. For the non-return-to-zero (NRZ) coded digital data signals used by the network [5], the clock tone is best placed at the clock frequency, where little rf power exists in the data signal. Thus, for the present 4 Gb/s links, the clock tone is placed at 4 GHz. As Ti:$LiNbO_3$ traveling-wave electrooptic modulators are capable of high-speed modulation with low drive power and low insertion loss, we use them here. To attain the highest possible efficiency (i.e. minimum excess insertion loss) for the clock modulators, they are operated in an unconventional mode. Normally, the

electrooptic intensity modulators are dc-biased to near the point of 50% optical transmission to attain the most linear optical replica of the drive signal [7]. This mode of operation, however, introduces an excess insertion loss of 3 dB over the inherent waveguide loss of the modulators. We instead choose to bias the modulators for 100% transmission, thereby incurring negligible excess loss. At this operating point, the optical output of the modulator is a local maximum as a function of the applied voltage. Thus, the effect of the modulator is nonlinear and, in particular, causes a frequency-doubling of the modulating signal.

The experimental arrangement used to demonstrate these concepts is illustrated in Fig. 3. As indicated, the terminal's transmitter and receiver are intended to operate at nominally 4 Gb/s and take their clock from the terminal's local oscillator. A two-way, 1.3 μm wavelength, single-mode fiber link of effectively 5 km connects the terminal to the switch location. There the light is passed through the clock modulator, which is driven by a synthesizer that serves as the master clock. As described above, the clock modulator is biased so as to frequency-double the master clock signal. The synthesizer is therefore operated at 2 GHz to place the 4 GHz clock signal on the lightwave. The modulation depth was $\sim$1%, corresponding to an excess loss of $\sim$0.1 dB. From the output of the clock modulator, the composite optical signal is routed back to the terminal's receiver. At the receiver a portion of the data signal is routed to an electrical phase-lock-loop (PLL), which permits the local voltage-controlled-oscillator to be locked to the master clock tone. The data signal from the receiver and the clock signal are connected to a test set to measure the bit-error-rate. In Fig. 4 we show the rf spectrum of the output of the receiver in the neighborhood of 4 GHz. With the master clock turned off, a remnant of the local oscillator clock, which has relatively large phase noise when free-running, is observed, Fig. 4a. When the master clock is turned on, the PLL was observed to pull the local oscillator frequency to the master clock tone as seen in Fig. 4b. Under this condition, a BER of $< 10^{-9}$ was obtained for a received optical power of $\sim$-20 dBm.

In summary, we have proposed and experimentally demonstrated an efficient method of clock distribution to achieve timing synchronization of an optical TMS local area network with multi-gigabit/second throughput. We are grateful to C.A. Burrus, A.H. Gnauck, D.A. Herr, G. Raybon, and R.S. Tucker for their assistance, T.O. Murphy and R.W. Smith for the modulators, and B.L. Kasper for the receiver.

REFERENCES

[1] K. Habara and K. Kikuchi, Electron. Lett. 21, 631 (1985).

[2] J.R. Erickson, R.A. Nordin, W.A. Payne, and M.T. Ratajack, in *Tech. Dig. 1st Top. Meet. Photonic Switching*, Incline Village, 1987, paper FD2.

[3] J.J. Veselka, T.O. Murphy, D.A. Herr, J.E. Watson, M.A. Milbrodt, K. Bahadori, M.F. Dautartas, C.T. Kemmerer, D.T. Moser, and A.W. Schelling, in *Tech. Dig. Conf. on Opt. Fiber Comm.*, Houston, 1989.

[4] U. Mukherji and H.V. Jagadish, in *Tech. Dig. Globecom*, Santa Clara, 1988.

[5] S.K. Korotky, D.A. Herr, T.O. Murphy, J.J. Veselka, A. Azizi, R.W. Smith, and B.L. Kasper, in *Tech. Digest Conf. on Opt. Fiber Comm.*, Houston, 1989.

[6] R.A. Thompson, contribution this conference.

[7] S.K. Korotky, G. Eisenstein, A.H. Gnauck, B.L. Kasper, J.J. Veselka, R.C. Alferness, L.L. Buhl, C.A. Burrus, T.C.D. Huo, L.W. Stulz, K. Ciemiecki Nelson, L.G. Cohen, R.W. Dawson, and J.C. Campbell, J. Lightwave Technol. LT-3, 1027 (1985).

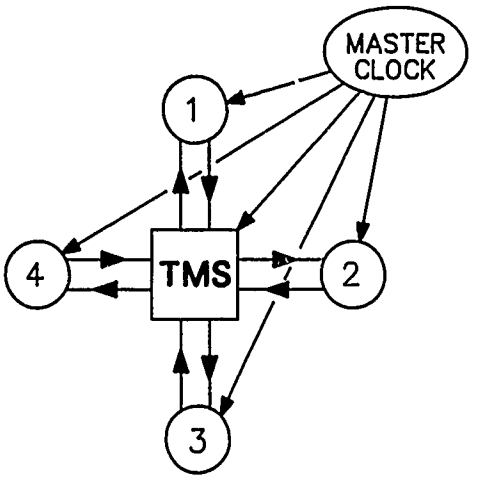

Fig. 1: Schematic of a four-terminal TMS network showing the logical data and clock connections

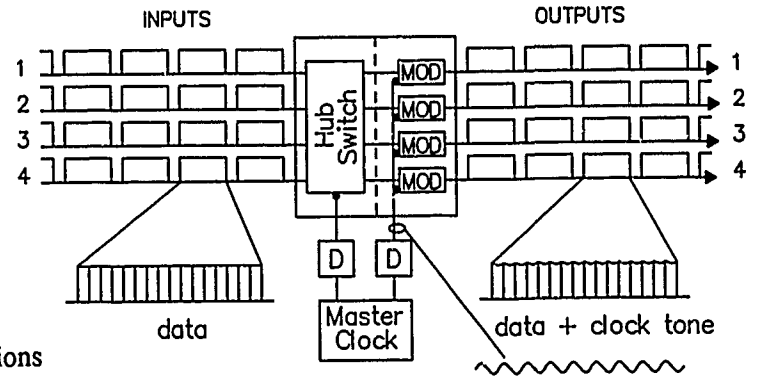

Fig. 2: Illustration of an efficient clock distribution scheme

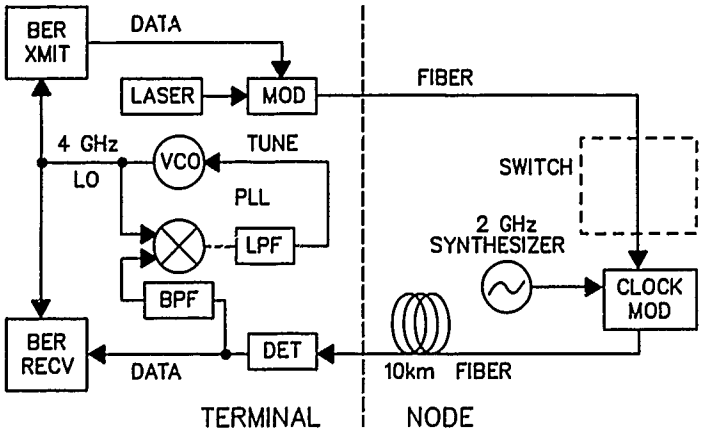

Fig. 3: Experimental arrangement to demonstrate clock distribution technique

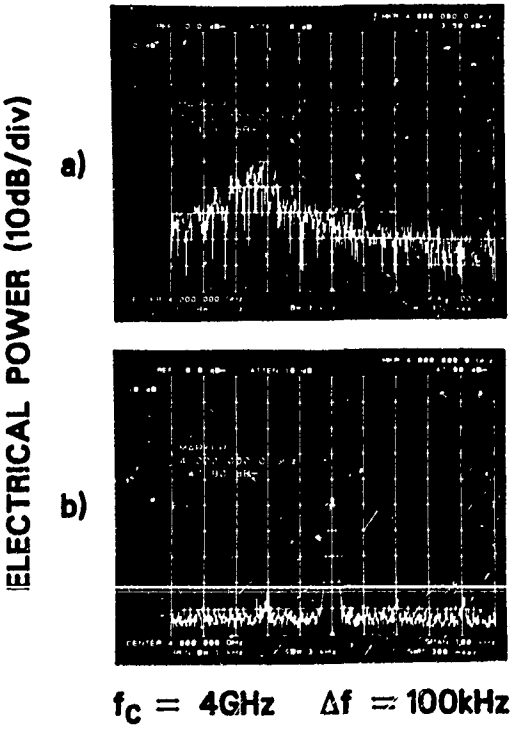

Fig. 4: RF spectrum of received data channel in the neighborhood of 4 GHz clock frequency
a) master clock off, local oscillator free running
b) master clock on, local oscillator phase-locked

Experiments on optical drop/insert function using bistable laser diodes for optical access nodes

S. Masuda, N. Fujimoto, H. Rokugawa, K. Yamaguchi, and S. Yamakoshi

Fujitsu Laboratories LTD.
1015, Kamikodanaka, Nakahara-ku, Kawasaki 211, Japan

1. Introduction

The next generation photonic network will need a new architecture for signal access between the optical data highway and terminals or subscribers at the optical level. This architecture must support broadband imformation services, such as motion video signals. Optical signal access using a $LiNbO_3$ optical switch has been tried[1], but the device requires a high operation voltage. Therefore, simple optical semiconductor devices with smaller operating energies are needed. In this paper, we present a prototype photonic access node using bistable lasers with a direct optical drop/insert function which can access the optical data highway without O/E and E/O conversion.

2. Principle of optical data latch

For optical direct access to an optical data highway, we used InP optical bistable laser diodes (BSLDs) with tandemelectrodes[2] as optical data latches. A BSLD has two current inputs, I1 and I2, which control its hysteresis and threshold characteristics. When I1 is fixed, a BSLD has two stable states, "H" and "L", while I2 is at an adequate value Ib (Fig. 1(a)), and it has a threshold within the optical input, Pin (Fig. 1(b)). Suppose the optical data stream comes into the BSLD, as shown in Fig. 1(c). It is set to the "H" state by the optical input beyond the threshold Pth (data bit "2" in Fig. 1(c)). And it is reset by a current pulse within the frame duration. To set the BSLD for a particular optical data bit as described above, an optical frame pulse superimposed on the data pulse is needed. In this way, only the desired data can be latched as the output of BSLD (Fig. 1(d)). We call this effect optical sampling memory (OSM) .

3. Experiments

3-1. BSLD modules

The BSLD's optical data latch operation basically stands on its hysteresis characteristic, and the hysteresis characteristic depends severely on its temperature. Therefore we made BSLDs into modules to help stabilize their temperature and optical coupling conditions. Figure 2 shows the optical setup in the BSLD module. Optical coupling between the BSLD and optical fibres is achieved with GRIN rod lenses at both cleaved surfaces of the BSLD. The entire body of the module is mounted on a thermoelectric heat pump which includes a temperature sensor. The temperature of the module is stabilized with a PID controller within $\pm 0.02^{\circ}C$.

3-2. Experimental setup

Figures 3(a) and (b) show the experimental setup for the optical data drop and insert functions. The bit rate of the optical data highway is 50 Mbit/s (RZ), and the degree of multiplexing is four. Optical memory operation drastically changes according to the relationship of optical data and BSLD wavelengths[2]. So the optical data/frame wavelengths are kept constant by controlling the temperature of optical source LD modules. In insert operation (Fig. 3(b)), the optical data to be inserted is divided from the highway electrically by data divider before the data E/O. Then it is transmitted by a separated E/O in a 12.5 Mbit/s RZ-pattern, on which the optical frame pulse is superimposed, and is fed to the BSLD.

3-3. Results

Optical input/output waveforms during drop and insert operation are shown in Fig. 4. In Fig. 4(a) we can see 12.5 Mbit/s RZ optical data is dropped out of the 50 Mbit/s data highway, and in Fig. 4(b) 12.5 Mbit/s optical data is duty-converted and inserted into the 50 Mbit/s highway. The bit error rate characteristics of the optical data latch output for drop and insert are shown in Figs. 5(a) and (b). Good performance with a bit error rate of less than 10^{-9} is achieved. The allowable deviation of the optical data power was narrower in the drop case to keep the error rate less than 10^{-9}. We think this is due to the difference in signal sequence between drop and insert.

4. Conclusion

The first optical data drop/insert function was achieved using bistable laser diodes as optical data latches. This is a key function for direct data access to the optical data highway, applying optical signal processing technology.

Acknowlegement

The authors wish to thank Dr. H. Takanashi and Dr. T. Nakagami for their guidance and encouragement.

References

[1] L. C. Blank et al., "Demonstration of optical drop-insert for accessing 2.24 Gbit/s optical transmission systems directly at the 140 Mbit/s level," Technical digest of ECOC'88, vol.1, pp.463-466, 1988.

[2] T. Odagawa et al., "All optical flip-flop operation of bistable laser diode," Extended abstracts of the 20th (1988 International), Conference on solid state devices and materials, Tokyo, D-5-1, pp. 331-334, 1988.

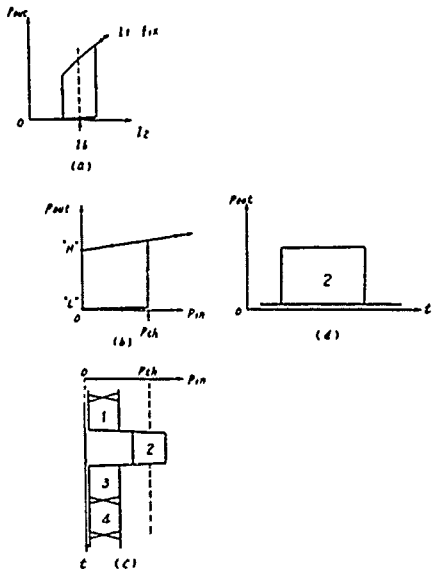

Fig. 1 Principle of the optical data latch

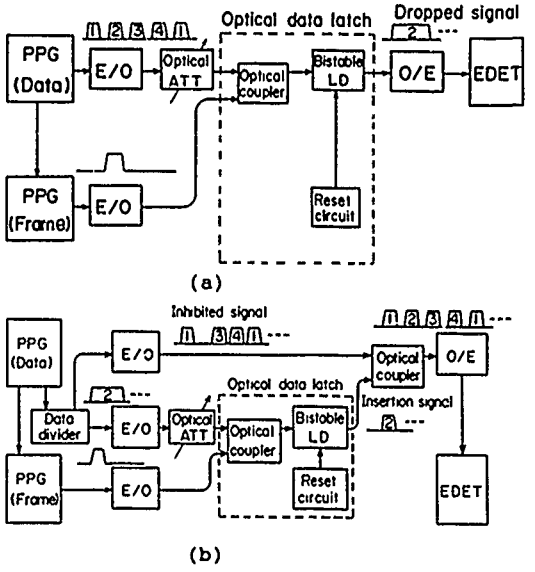

Fig. 3 Experimental setup for (a) Optical drop and (b) Optical insert

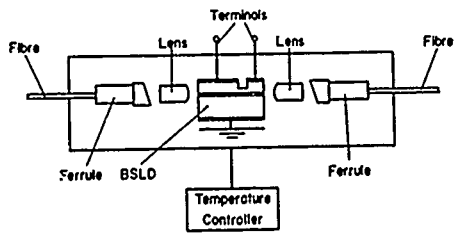

Fig. 2 Optical setup in a BSLD module

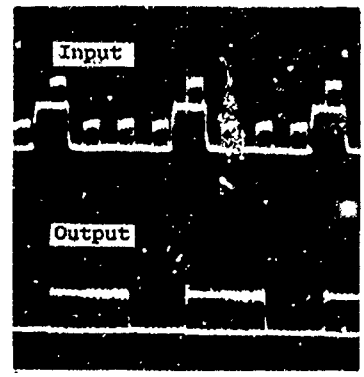

(a)

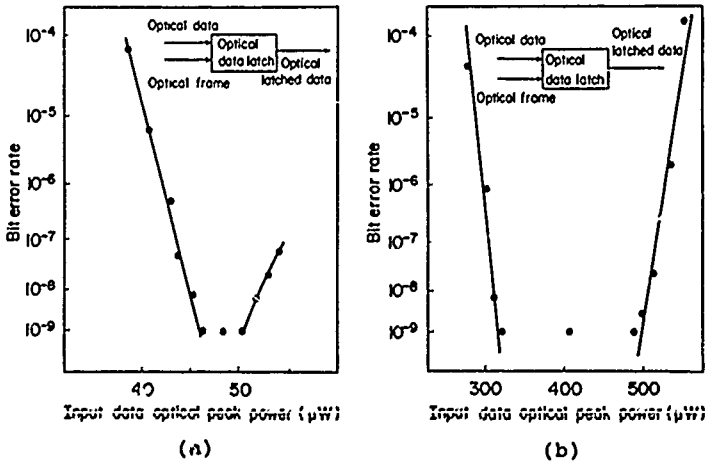

Fig. 5 Optical data latch bit error rate characteristics for (a) drop and (b) insert

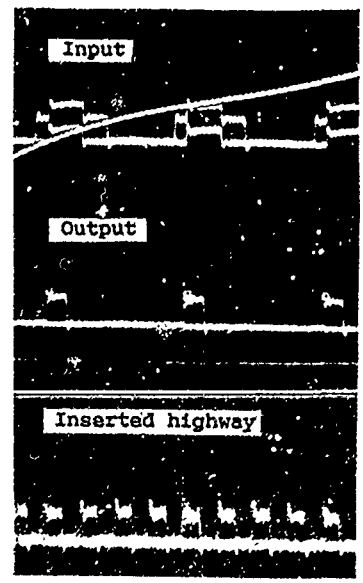

(b) H:20ns/div

Fig. 4 Optical input/output signal waveform for (a) drop and (b) insert

NOTES

FRIDAY, MARCH 3, 1989

SALON E

1:30 PM–3:15 PM

FD1–FD6

SEMICONDUCTOR DEVICES

R. I. MacDonald, Alberta Telecommunications Research, Canada, *Presider*

Bistable Laser Amplifiers as Optical Memories/Regenerators in Photonic Switching Systems

M J Adams

British Telecom Research Laboratories
Martlesham Heath
Ipswich IP5 7RE
England

Introduction

There is growing interest worldwide in the potential applications of diode laser amplifiers for all-optical logic, switching, wavelength conversion, pulse-shaping, and other aspects of signal processing. Two types of device are currently under study, corresponding to two different physical mechanisms of operation. In the first type the dispersive nonlinearity at wavelengths close to the band-gap is utilised to produce switching and bistability between two different states of transmission. In the second type the device consists of two or more sections, each with its own electrical contact, and the switching arises as a consequence of the absorptive nonlinearity when some sections are driven close to lasing threshold and the others receive little or no current. The advantages of the former device type are its ready availability and low switching energy (of order femtojoules), although it suffers from a marked sensitivity to the wavelength of the optical input. By comparison, the two-section device shows good tolerance to input wavelength and can give significantly higher contrast ratios between the 'off' and 'on' states. In the present contribution recent progress made with these two device types will be reviewed with reference to potential applications as memories, switches and regenerators in photonic switching systems.

Single-section (dispersive) amplifiers

For wavelengths close to the band-gap, the refractive index in a diode laser varies with the injected carrier concentration at a rate of order 10^{-20} cm^3 for both GaAs ($\lambda = 0.8$ μm) and InGaAsP ($\lambda = 1.3$ or 1.5 μm) devices. When the laser is biassed just below threshold and used as an amplifier, the input optical signal can saturate the material gain and thus reduce the carrier concentration. The resultant change in refractive index, and hence in optical path length, is sufficient to cause nonlinear changes in transmission as a result of the shift of resonant wavelength with respect to the wavelength of the optical input. For 1.3 μm [1] and 1.5 μm [2] quaternary amplifiers, bistability in the optical output/input characteristics occurs at input powers of around 1 μW, and the switching repetition rate is limited by the carrier recombination time which is about 2 ns [3,4].

The nonlinear response of the dispersive amplifier has been used to demonstrate an optical AND gate with a contrast ratio of 5:1 [5], and by a further extension of this idea, all-optical signal regeneration of a 140 Mb/s data stream has been realised [6]. In the latter experiment, an optical clock waveform generated by a tunable laser source was combined with the data stream from a DFB laser and coupled into an amplifier. The peak power of the clock was arranged to lie just below the bistable threshold of the amplifier. When the data is low a slightly amplified clock pulse appears at the output; when the data is high the output jumps to a higher level which is insensitive to the data power. Thus the key functions of a regenerator have been achieved, namely pulse-shaping and retiming. However, the retiming relies on the provision of an optical clock, whereas the recovery of a timing signal from a data stream alone would be a more desirable target [7]. At the time of writing the only claim to clock recovery in an all-optical regenerator has relied upon SEED devices within an electrically and optically powered circuit at a data rate of 5 kb/s [8].

The optical regeneration experiments reported by Webb [6] demonstrated another novel feature, namely the ability to translate the wavelength of a data stream to a new wavelength as determined by the clock signal wavelength. The case where a data stream at one wavelength is switched by a control signal at another wavelength has been demonstrated by Kawaguchi et al [9]. Using signal and control beams derived from DFB lasers at 1.5315 μm and 1.5460 μm, a high speed switching experiment in a 1.5 μm laser amplifier has been reported using an 800 Mb/s pulse pattern [10]. The sensitivity to temperature and current shown by an uncoated amplifier can be reduced by the use of AR-coated facets, and a two-wavelength switching experiment using 1.5 % reflectivity facets has been performed [11]. For the two-wavelength configuration, depending upon the initial detuning of the optical data signal, both normal (anticlockwise) and reverse (clockwise) hysteresis loops have been achieved in the signal output power as a function of the control input power [9]. This opens up the possibility of operation of an amplifier to perform the NOT, NOR and NAND gate functions. It has also been proposed [12] that these functions might be achieved by using the reflected signal from an amplifier with single-wavelength operation.

Two-section (absorptive) amplifiers

In this device, as first proposed by Lasher [13] in 1964, the top contact is divided into two sections, one of which is driven with sufficient injected current to be just below lasing threshold, whilst the other receives only a small bias current, if any. In the OFF state, light emitted from the first section is absorbed in the second section, and optical output is thus suppressed. If the loss in the second section can be saturated by the creation of sufficient electron-hole pairs, then optical output can occur either by amplification of an input optical signal, or by lasing action, usually at a different wavelength to that of the optical input. As a consequence, the optical output versus optical input can show strongly nonlinear and bistable behaviour, depending on the drive currents applied to each section and on the wavelength of the input signal [14]. Bistability can also occur in the graph of optical output versus current injected into the amplifying section, even in the absence of an optical input. Recent experiments on two-section amplifiers have demonstrated nonlinear switching for input powers as low as -51 dBm, with minimum repetition time of 700 ps and a maximum gain of 26 dB [15].

Two-section bistable lasers have been used as memory elements in a high-speed optical time-division switching system [16,17]. In this application, $LiNbO_3$ directional coupler switch matrices were used as read/write gates for the bistable lasers. Four 64 Mb/s digitally encoded colour video signals were time-multiplexed and directed to the memory elements in turn by the optical write gate. Then the optical read gate was used to read out the signals stored in the memories in any desired sequence. Thus time-switching on the time-multiplexed optical highway at 256 Mb/s was accomplished [17].

Another application of absorptive bistability in laser amplifiers is to tunable wavelength conversion for optical wavelength-division switching networks. The principle employed is to control the emission wavelength of the emitted light by the incorporation of a grating whose effective pitch can be changed by injecting carriers and thus altering the active layer refractive index. Multielectrode DFB laser amplifiers have been used for this purpose [18,19], and a tunable range of 3 nm achieved [19]. A similar structure has also exhibited optical tristability, including spectral bistability, controlled either electrically or optically [20]. In this case the output wavelength can be either one of the two dominant resonant modes of the DFB. By using the spectrally resolved output from the device, AND, OR, NAND, NOR, INVERT, XOR and memory operations have been observed [20].

Conclusion

The physics and applications of single-section (dispersive) and two-section (absorptive) amplifiers have been reviewed. It is clear that early demonstrations of applications as memories and regenerators in photonic switching systems have indicated the scope for future work. In particular attention has been drawn to the requirement for a means of all-optical clock recovery in signal regeneration, and to the breadth of possibilities in wavelength-division switching networks. These and other opportunities for innovation should ensure a continuing evolution in the field of bistable laser amplifiers.

References

1. W. F. Sharfin and M. Dagenais, Appl. Phys. Lett. 46, 819 (1985).
2. H. J. Westlake, M. J. Adams and M. J. O'Mahony, Electron. Lett. 21, 992 (1985).
3. M. J. Adams, IEE Proc. J, Optoelectron. 132, 343 (1985).
4. H. J. Westlake, M. J. Adams and M. J. O'Mahony, Electron. Lett. 22, 541 (1986).
5. W. F. Sharfin and M. Dagenais, Appl. Phys. Lett. 48, 1510 (1986).
6. R. P. Webb, Opt. and Quantum Electron. 19, S57 (1987).
7. M. J. O'Mahony, presented at ECOC 87, Helsinki, Finland (1987).
8. C. R. Giles, T. Li, T. H. Wood, C. A. Burrus and D. A. B. Miller, Electron. Lett. 24, 848 (1988).
9. H. Kawaguchi, H. Tani and K. Inoue, Optics Lett. 12, 513 (1987).
10. K. Inoue, Electron. Lett. 23, 921 (1987).
11. G. Groβkopf, R. Ludwig, R. Molt, H. G. Weber and S. B. Zhang, Appl. Phys. B 45, 171 (1988).
12. M. J. Adams, Opt. and Quantm Electron. 19, S37 (1987).
13. G. J. Lasher, Solid State Electron. 1, 707 (1964).
14. H. Kawaguchi, Opt. and Quantum Electron. 19, S1 (1987).
15. I. W. Marshall, M. J. O'Mahony, D. M. Cooper, P. J. Fiddyment, J. C. Regnault and W. J. Devlin, presented at IQEC, Tokyo (1988).
16. Y. Odagiri, K. Komatsu and S. Suzuki, presented at CLEO'84, Anaheim, California (1984).
17. S. Suzuki, T. Terakado, K. Komatsu, K. Nagashima. A. Suzuki and M. Kondo, J. Lightwave Technol. LT-4, 894 (1986).
18. H. Kawaguchi, K. Oe, H. Yasaka, K. Magari, M. Fukuda and Y. Itaya, Electron. Lett. 23, 1088 (1987).
19. S. Yamakoshi, K. Kondo, M. Kuno, Y. Kotaki and H. Imai, presented at OFC'88, New Orleans (1988).
20. M. Jinno, M. Koga and T. Matsumoto, Electron. Lett. 24, 1031 (1988).

Optical flip-flop operation of a bistable laser diode using one-wavelength light signals

T. Odagawa, and S. Yamakoshi
Fujitsu Laboratories, Atsugi
10-1, Morinosato-Wakamiya, Atsugi 243-01, Japan

1. Introduction

Bistable laser diodes(BSLDs) are useful as optical memories and optical logic devices. They are usually set by optical pulses and reset by electrical pulses. For all optical signal processing, it is indispensable to reset the BSLDs by light injection.

Inoue *et al* reported an optical reset method of the BSLDs using the beat vibration between the injected light and the lasing light of the BSLDs [1]. In the method, the frequency difference between two light pulses must be smaller than the life time of carriers in a saturable absorption region(typically several ns). Therefore the injected light wavelength must be tuned to the lasing wavelength of the BSLD precisely. Recently we reported another optical reset method using a gain-quenching phenomenon, in which the injected light wavelength does not need to be tuned to the lasing wavelength, and demonstrated all optical flip-flop operation of the BSLD [2]. In the report, the wavelength of the reset light was different from that of the set light, and two light sources were necessary.

In this paper, we demonstrate optical flip-flop operation of the BSLD using only one-wavelength light signals.

2. Experiments

2.1 Experimental condition

Figure 1 shows a schematic structure of the BSLD we used. The active region is embedded with semi-insulating InP layers. I_1 and I_2 are the currents in gain region 1 and 2. Turn-on current I_{1on} = 6.5 mA, and turn-off current I_{1off} = 4.6 mA in the condition of I_2 = 28 mA. In the following experiments, a bias current I_1 was set at 4.9 mA. Under this condition, lasing wavelength is 1.302 μm.

2.2 Wavelength dependence of optical set and reset characteristics

The mechanism of the optical reset method using gain quenching is as follows. Because the saturable absorption region is pumped by the lasing light, the light injection whose wavelength is slightly longer than the lasing wavelength of the BSLD, decreases the carrier densities not only of the gain regions but also of the saturable absorption region. Thereby it decreases the net gain of the lasing mode and stops the lasing [2].

First, we investigate the wavelength dependence of the threshold light intensity necessary to set or reset the BSLD in a static condition. Figure 2 shows the experimental results. Arrows show the resonant wavelength in the EL or lasing state. In the BSLD, they are different from each other, because the carrier density of the active layer changes between the two states. And the threshold set light intensity has minima near the resonant wavelength in the EL state, but the threshold reset light intensity has minima near the resonant wavelength in the lasing state. There are two kind of wavelength regions, that is, the set-able wavelength regions and reset-able wavelength regions. Light in a set-able wavelength region, can set the BSLD but can't reset it. And light in a reset-able wavelength region, can reset it but can't set it.

However, the situation may change at the boundary areas which divide the set-able wavelength regions and the reset-able wavelength regions. There is a possibility to set and reset the BSLD by one-wavelength signals.

2.3 Optical set and reset operation with one-wavelength light

We investigated, in a dynamic condition, if one-wavelength light in the boundary area can set and reset the BSLD. To operate the BSLD with one-wavelength light signals, we changed the set and reset light signals in it's intensity or it's pulse width. Figure 3 shows the experimental results of the flip-flop operation of the BSLD with one-wavelength light signals. The wavelength of the injected light was at the boundary area(1.30826μm). In figure 3 (a), the intensity of set and reset light pulse are 30 μW and 170 μw. In figure 3 (b), the pulse width of the set light and that of reset light are 10 and 50 ns. In both cases, making the energy of the reset light be larger than that of the set light, we can operate the BSLD with one-wavelength light signals .

3. conclusion

We demonstrated the optical flip-flop operation of the BSLD with only one-wavelength light signals which have different intensity or pulse width.

Acknowledgements

We thank T. Sanada, K. Wakao, K. Kondo and T. Sakurai for useful discussions and the continuous encouragement.

References

(1) K. Inoue, and K. Oe, "Optically triggered off-switching in a bistable laser diode using a two-electrode DFB-LD," Electron. Lett. , vol.24, pp. 512-513, Apr. 1988.

(2) T. Odagawa, T. Sanada, and T. Yamakoshi, " All optical flip-flop operation of bistable laser diode," Extended abstracts of the 20th Conference on Solid State Devices and Materials, D-5-1, pp. 331-334, 1988

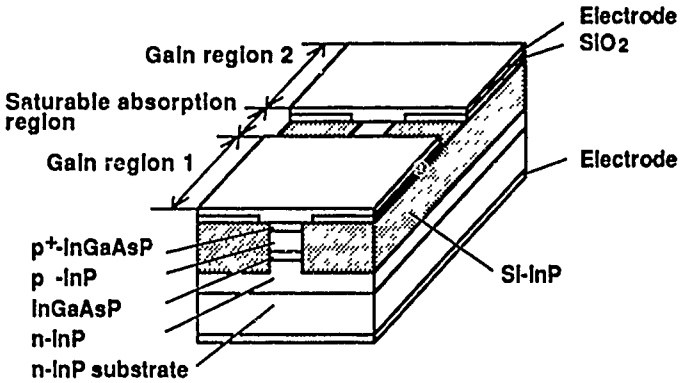

Fig. 1 Structure of BSLD

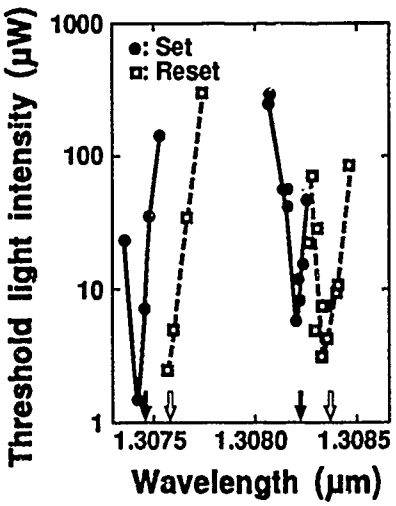

Fig. 2 Threshold light intensity necessary to set and reset the BSLD.Black and white arrows show the resonant wavelengths in the EL state and in the lasing state.

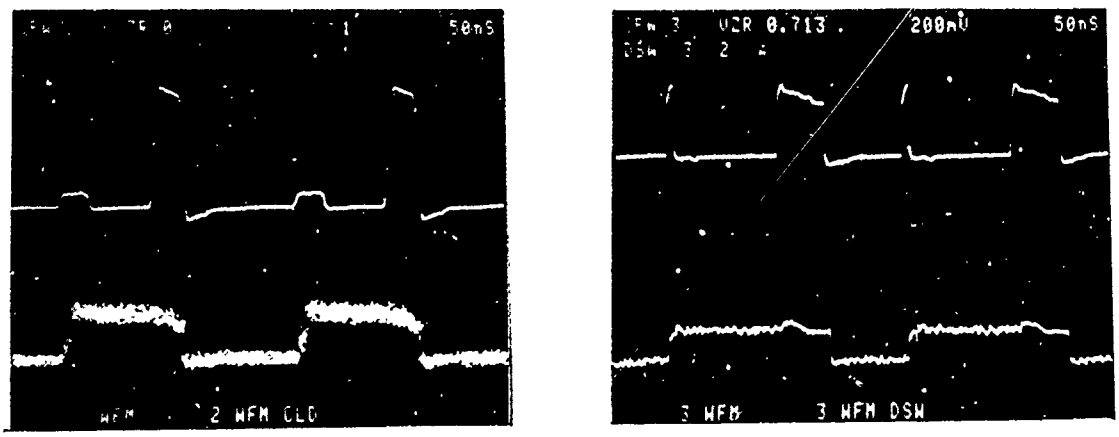

50 ns/div.

(a)

50 ns/div.

(b)

Fig. 3 Flip-flop operation of the BSLD. (a) Set pulses(30μW) and reset pulses(170μW) have different intensity. Their pulse width is 30 ns. (b) Set pulses (10 ns) and reset pulses(50 ns) have different pulse width. Their intensity is 380μW. In both cases, upper traces are set and reset optical signals, and lower are the light output of the BSLD.

EFFECT OF ABSORBER POSITION IN BISTABLE InGaAsP LASERS

Ulf Öhlander and Olof Sahlén

Institute of Optical Research and Department of Physics II
Royal Institute of Technology
S-100 44 STOCKHOLM
SWEDEN

Laser diodes with saturable absorbers [1], [2] are among the most interesting nonlinear and bistable elements studied so far for telecommunication purposes. They have been used to demonstrate time-multiplexing [3] and pulse regeneration [4]. Subnanosecond switching times with subpicojoule optical input pulses have been reported [5]. However, despite their merits, their physical behaviour is only partially understood. Since they consist of several sections, having very different injection levels before switching-on, such lasers show a richer variety in behaviour than ordinary semiconductor lasers. It has, for instance, been shown experimentally [6] and theoretically [7] that a too long absorber section causes the bistability to disappear in two-section lasers, a phenomenon which can be understood on the basis of bandgap-renormalisation in the gain-section [6].

We present detailed measurements on the hysteresis width, threshold current, lasing and luminescence wavelengths and carrier redistribution during switching as a function of current bias into the absorber in a three-section 1.3 μm Etched-Mesa Buried-Heterostructure laser. We find a large difference between placing the absorber at the end facet or in the middle of the laser. We also report on the new phenomenon of two-stage switching in such lasers. The results presented are important for optimising such lasers in telecommunication applications.

Figure 1 shows a schematic drawing of the structure used. The lasers were fabricated by Ericsson Components AB. The total length was 400 μm, and there were three separately contacted sections. The relative lengths of the three contacted sections 1, 2 and 3 were measured in a microscope and found to be 154 μm, 103 μm and 103 μm respectively, with 20 μm long unconnected, separating segments. The visual measurements were supported by measurements of the differential resistance when the sections were biased above threshold. The dark resistances between the sections were about 500 Ω.

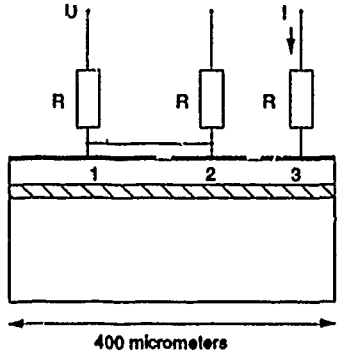

Figure 1. Inhomogenously pumped InGaAsP laser. Sections 1, 2, 3 are independently connected, with R = 47 Ω resistors. Both section 2 or 3 as well as 2 + 3 can be used as absorber. When two sections are used as gain sections, as in the figure where 1 + 2 are gain sections and section 3 absorber, they are electrically connected after the 47 Ω resistors, to assure that the injected current densities are equal. The section used as absorber was operated with an additional, large resistor (50 kΩ) in series with a voltage supply, to guarantee that it was current-controlled.

In Figures 2a and 2b we show the hysteresis width and lasing threshold, respectively, as functions of the injected current into the saturable absorber. Different curves in these figures correspond to the cases when section 3 was used as absorber (sections 1 and 2 connected and acting as gain section), when section 2 was used as absorber (sections 1 and 3 connected and acting as gain section) and sections 2 and 3 connected and acting as absorber (section 1 acting as gain section). Great care was taken to assure that thermal effects did not affect the results. We used low duty-cycles, and were able to reproduce the results when using even lower duty-cycles.

When sections 2+3 were operated as an absorber, the laser was not bistable for any current injected into the absorber. Instead it showed differential gain. The threshold was high as seen in Figure 2b. This is consistent with findings on two-section lasers [6]: a too long absorber imparts the bistability. This is contrary to simple single-mode, mean-field theory, but consistent with more elaborate models [7].

Sections 2 and 3 were almost identical with respect to measured length and measured differential resistance. One could thus have guessed that it should not matter which one of them is used as absorber. We see on the contrary that the difference is very large: When section 2 was used as absorber the threshold was much higher and the hysteresis width much larger for negative or slightly positive currents injected into the absorber. For large positive absorber currents, the threshold currents became almost identical and the hysteresis vanished. This difference between having the absorber in the middle or at an end facet has also been observed in another, similar laser.

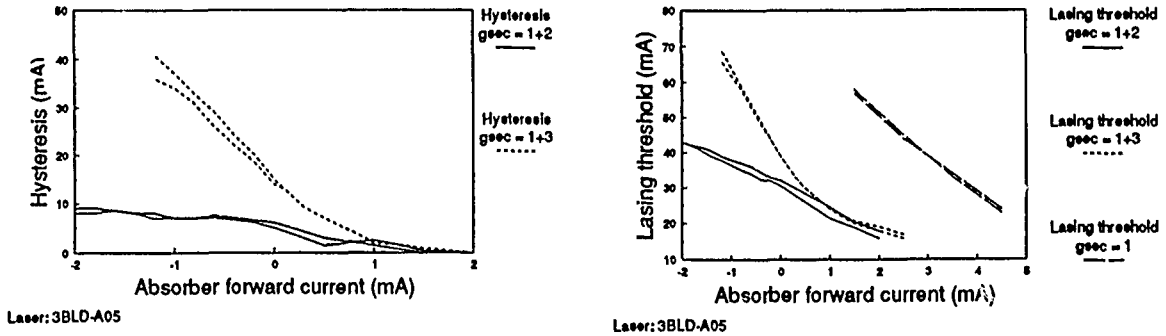

Figure 2a (left) and 2b (right) showing hysteresis width ΔI = Ion - Ioff and lasing threshold Ion as functions of injected current into the absorber. Two curves are shown for each case, corresponding to two different measurements on the same laser (proving the results to be reproducible). The labels correspond to different biasing conditions, for instance gsec=1+2 means that sections 1 and 2 were connected to act as gain section and section 3 was used as saturable absorber.

Figure 3 shows the measured luminescence peak (measured just below the threshold current) and lasing wavelengths. We see several interesting features: When a large negative current was injected into the absorber, the luminescence peak was at high photon energies due to the high carrier density needed to have a sufficient gain to reach lasing. The lasing wavelength was longest when sections 2+3 were used together as a long absorber, consistent with our previous [6] explanation of why bistability is not seen in lasers with too long absorbers, since in this case the injected current to overcome the losses is high enough to induce sufficient bandgap renormalisation to force the laser to turn-on in the transparency region of the absorber. When section 2 was operated as absorber alone (and hence the hysteresis largest), the lasing wavelength was shortest. The luminescence peak wavelength was considerably shorter when the middle section (2) was used as absorber than when the end facet section (3) was used as absorber. Thus higher gain is required to switch on when the middle section is used as absorber.

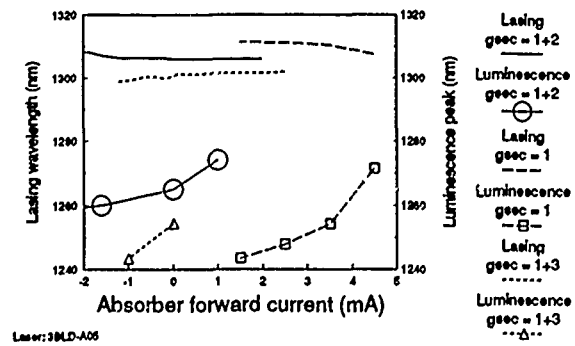

Figure 3a (left). Measured wavelength of luminescence peak (for a current slightly below threshold) and lasing, as functions of injected absorber current. All luminescence spectra were recorded by measuring the light emitted from section 1.

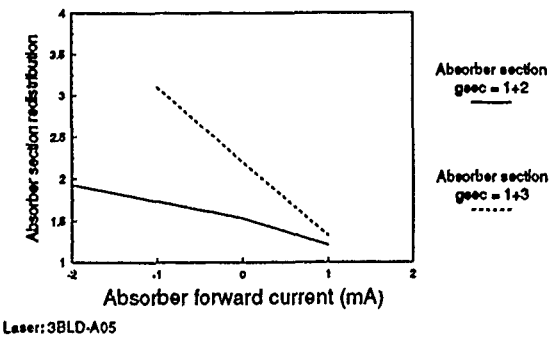

Figure 4. The parameter K (as defined in text) versus current injected in the absorber. K is an approximate measure of carrier redistribution upon switching.

Figure 4 shows the parameter $K = \exp[(V_g - V_f)/2V_T]$ versus absorber current, where V_f is the voltage measured over the absorber section before switching on, and V_g the corresponding voltage after switch on. The difference $V_g - V_f$ was measured by taking advantage of the critical slowing-down effect, well known in bistable devices: A long rectangular pulse was applied to the gain section, with an amplitude very slightly exceeding the threshold, so that the critical slowing down was many hundred of nanoseconds. This allowed the difference $V_g - V_f$ to be measured (for identical injection conditions). The parameter K is an approximate value of the carrier

redistribution when switching (the carrier density decreases in the gain section and increases in the absorber section). We see that K decreased monotonically when the laser became less bistable, and that the redistribution was largest when the middle section (2) was used as absorber.

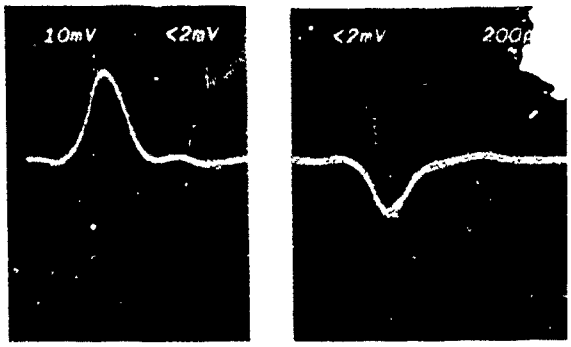

Figure 5. Fast electrical set (left) and reset (right) of the bistable laser, biased with a DC current to the middle of the hysteresis loop. Sections 1, 2 and 3 were DC biased with currents of 25, 0.26 and 19 mA, respectively. The laser was set and reset by injecting positive and negative pulses, respectively, of an amplitude of 0.35 V superposed on the DC bias with the help of a high-frequency bias tee.

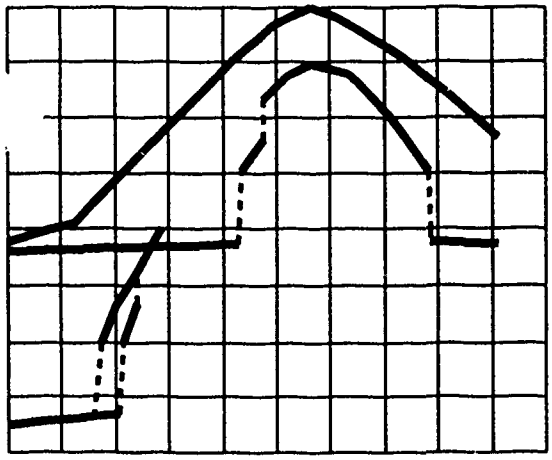

Figure 6. Two-stage switching when the middle section was used as absorber. The device first switched to a meta-stable intermediary level, and later, if the current was increased, to a second level with 10 nm shorter lasing wavelength. (The upper and middle trace show the gain current and light output as functions of time, respectively, and the bottom figure shows the output light as function of input gain section current.)

The results presented in Figures 2 - 4 are all consistent with each other. This is to our knowledge the first report on a systematic investigation on the behaviour of three-section lasers when the position of the absorber section is altered. We have found that when the middle section was used as absorber the threshold current and hysteresis width were larger, as well as the carrier density in the gain section before switching. Also the carrier redistribution was larger in this case We believe that a full theoretical analysis of the phenomena reported on here would require both the electric coupling and the multi-mode character of the device to be considered.

We have also done an experiment where the laser was DC biased to the middle of the hysteresis loop, and short positive and negative electrical pulses were injected into the absorber section to respectively switch-on and switch-off the laser. Figure 5 shows the detector-limited (70 ps rise time, 200 ps fall time) response of the laser. We have not performed a systematic variation of the electric pulse energy, but for those amplitudes which we have used no difference in switching speed between using section 2 or 3 as absorber has been seen.

Finally we show in Figure 6 the phenomenon of two-stage switching which we have observed when section 2 was used as absorber and the injected absorber current was in the interval from +0.3 to +1.5 mA. The laser first switched on to a level characterised by a long lasing wavelength. When the gain section current was increased 2-3 mA, the device switched to a higher level, but now lasing at about 10 nm shorter wavelength. This phenomenon was only seen when the absorber was in the middle of the laser. (When plotting Figure 3, we used the shorter wavelengths corresponding to the highest branch).

In conclusion, we have found a large difference between placing the absorber in the middle or at the end facet of a three-section InGaAsP 1.3 μm bistable laser.

This work was supported by Ericsson Telecom, Ericsson Components and the Swedish Natural Science Research Council (NFR).

---

[1]H. Kawaguchi and G. Iwane, Electron. Lett., **17**, 167, 1981.

[2]C. Harder, K. Y. Lau and A. Yariv, IEEE J. Quant. El., **QE-18**, 1351, 1982.

[3]S. Suzuki, T. Terakado, K. Komatsu, K. Nagashima, A. Suzuki and M. Kondo, J. of Lightwave Techn., **4**, 894, 1986.

[4]L. W. Marshall, M. J. O'Mahony, D. M. Cooper, P. J. Fiddyment and J. C. Regnault, presented at International Quantum Electronic Conference, Tokyo, 1988.

[5]U. Öhlander, P. Blixt and O. Sahlén, accepted for publication in Applied Physics Letters.

[6]U. Öhlander, O. Sahlén and L. Ivarsson, J. Appl. Phys., **62**, 2203,1987.

[7]M. C. Perkins, R. F. Ormondroyd and T. E. Rozzi, IEE Proc. Part J, **133**, 283, 1986.

Travelling Wave Semiconductor Laser Amplifiers for Simultaneous Amplification and Detection: Systems Experiments

Mats Gustavsson, Lars Thylén, and Anders Djupsjöbacka
Ericsson Telecom AB, S-126 25 Stockholm, Sweden

Anders Karlsson
Department of Microwave Engineering and Fibre Optics,
Royal Institute of Technology, S-100 44 Stockholm, Sweden

Introduction

Semiconductor laser amplifiers (SCLAs) have received considerable attention in recent years due to the potential of employing them as simple repeaters in fibre optic links for single- or multichannel, coherent or wavelength multiplexed information; as optical preamplifiers and in local area network type applications to compensate for insertion and power splitting losses, see e.g. [1], [2].

However, the versatility of the amplifier would be significantly increased if the amplifier could also perform detection. This will permit this single device to perform a variety of functions such as simultaneously tapping and amplification of the data on a high speed fibre optic data bus, cf. [3], surveillance of input power and error rate in a repeater application and use for signal extraction, self routing and feedback stabilization in photonic switching networks. The detection properties of semiconductor laser diodes have been treated by several authors, e.g. Alping et al. [4] investigated the signal registration characteristics of a GaAlAs BH/BOG laser for local area networks. They also performed a transmission experiment at 100 Mbit/s, using the amplifier as a tapping terminal while simultaneously obtaining a 3.5 dB net fibre to fibre gain. The comparatively low amplification was compensated for by a large input signal (0.32 mW). Also, the FP mode of operation that was used is not practical for systems usage; the travelling wave amplifier is preferred for reasons of gain, output power and insensitivity to wavelength and temperature and also responsivity in the detector mode of operation. In reference [5] we reported experimental results on simultaneous detection and amplification in such a near travelling wave SCLA, in terms of responsivity measurements. However, to evaluate systems performance it is necessary to perform bit error rate (BER) measurements. Also, it is important to establish the bandwidth of the detector mode of operation.

In this paper, we report BER measurements for detected and amplified signals as well as bandwidth measurements.

Theory

The small signal characteristics of the SCLA detector can be described by a linearization of spatially independent rate equations, resulting in an electrical equivalent circuit [5], from which it follows that the frequency response is limited by the spontaneous recombination time. The equivalent circuit can be used to calculate the signal to noise ratio, from which one can show that the sensitivity of the detector mode of operation is roughly comparable to a PIN-FET detector at data rates around 0.5 Gbit/s and for cavity gains around 25 dB.

Experimental Results

Figure 1 shows a block diagram of the experimental arrangement. A tunable 1.3 μm external cavity semiconductor laser is used as a narrow linewidth source for the transmitted signal. The light from the source is launched into a polarization maintaining fibre and a polarization preserving fibre optic coupler gives the possibility of monitoring the power coupled into the semiconductor laser amplifier, which is an antireflection (AR) coated 1 mm long 1.3 μm BH-laser with residual facet reflectances of 0.07 %. The BER test is carried out by amplitude modulation of the external cavity laser light by an AR coated Ti:$LiNbO_3$ Mach Zehnder external modulator. To minimize coupling losses, light is coupled into and out of the laser amplifier by tapered lensed optical fibres.

The transmission experiment was performed at 150 Mbit/s with a modulated coupled input optical power of 14 μW to the SCLA detector. For a cavity gain of 18.5 dB, giving a fibre to fibre gain of 8.5 dB, the detector responsivity was 64 mV/mW_{in}. At the SCLA detector receiver the detected signal was electrically amplified 58 dB and a twelve bit sequence, 000111010011, was transmitted at a BER less than 10^{-9}. These experimental results are the best ones reported to date for this mode of operation of the SCLA. Figure 2 shows an example of a received eight bit pattern. Comparisons between experimental and theoretically calculated sensitivities will be presented at the conference. Employing an electrical network analyzer, the frequency characteristics shown in figure 3, were obtained.

Conclusions

We have theoretically and experimentally analyzed the systems performance of a near travelling wave semiconductor laser amplifier for simultaneous amplification and detection. BER's below 10^{-9} were found for the detection function at data rates below 150 Mbit/s, and with a fibre to fibre amplification of 8.5 dB. (For the simultaneously amplified signals, these bit error rates can be achieved at multi gigabit rates; we experimentally demonstrated 2 Gbit/s.) In comparison with the reported amplifier, calculations predict a factor of 2 increase in detection bandwidth for a 300 μm amplifier, at a 25 dB cavity gain. The mode of operation of the amplifier device we report here significantly increases the utility of laser amplifiers in photonic transmission and switching systems.

The authors gratefully acknowledge K. Bergvall for the AR coating work, L. Atternäs for providing the external cavity laser and L. Gillner for the laser amplifier model with computer program.

References

[1] L. Thylén, P. Granestrand, A. Djupsjöbacka, *Optical Amplification in Switching Networks,* Proc. 1st Topical Meeting on Photonic Switching, 1987.

[2] M. J. O'Mahony, *Semiconductor Laser Optical Amplifiers for Use in Future Fiber Systems,* J. Lightwave Technol., vol. LT-6, pp. 531-544, 1988.

[3] L. Thylén, A. Djupsjöbacka, M. Janson, W. Döldissen, *Integrated-Optic Device for High-Speed Databuses,* Electron. Lett., vol. 21, pp. 491-493, 1985.

[4] A. Alping, B. Bentland, S. T. Eng, *100 Mbit/s Laser Diode Terminal with Optical Gain for Fibre-Optic Local Area Networks,* Electron. Lett., vol. 20, pp. 794-795, 1984.

[5] M. Gustavsson, A. Karlsson, L. Thylén, *A Travelling Wave Semiconductor Laser Amplifier for Simultaneous Amplification and Detection,* Proc. 10th Topical Meeting on Integrated and Guided Wave Optics, 1989.

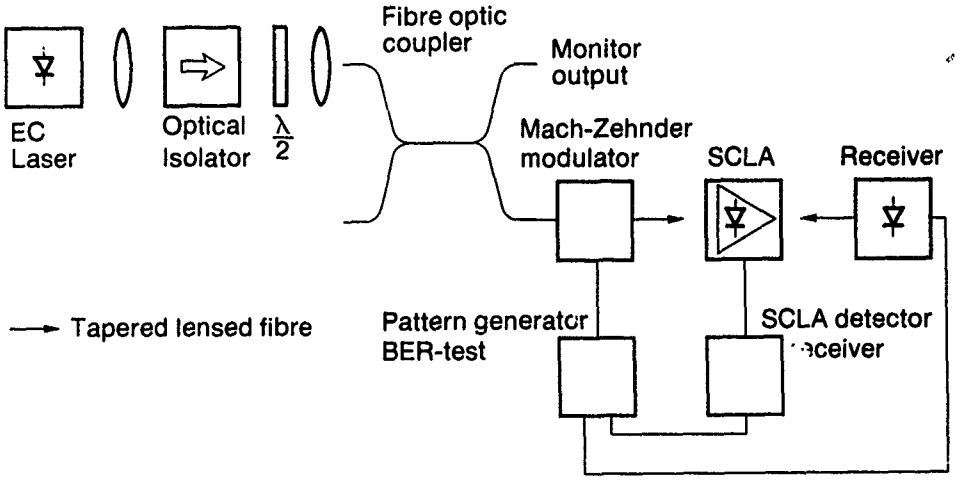

Figure 1. Experimental arrangement.

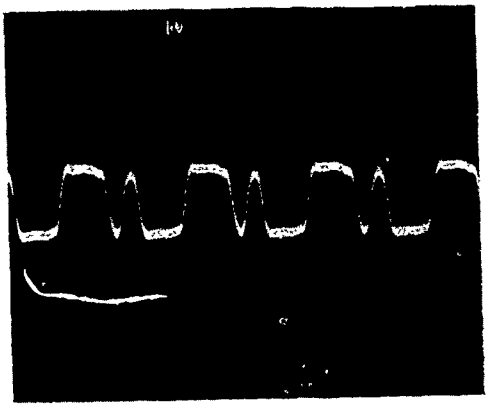

Figure 2. An eight bit pattern at the SCLA detector receiver output.
The data rate is 150 Mbit/s, NRZ.

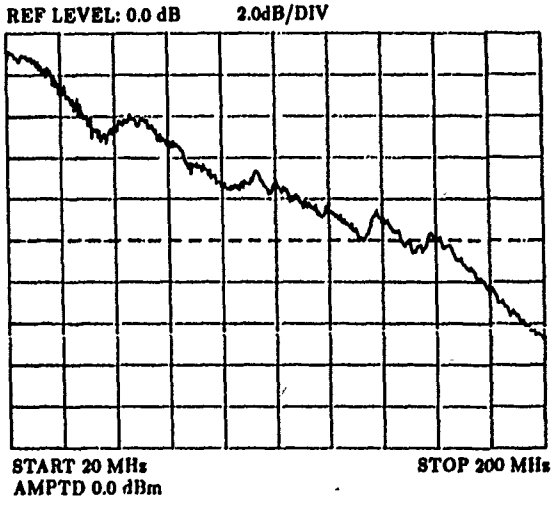

Figure 3. Frequency characteristics of the SCLA detector.

Compact InGaAsP Quantum Well Electro-Optic Waveguide Switch

J. E. Zucker, K. L. Jones, M. G. Young, B. I. Miller, and U. Koren
Room 4F-319, AT&T Bell Laboratories, Holmdel, New Jersey 07733

Semiconductor optical waveguide switches are critical elements in photonic integrated circuits for optical signal processing and optical communications. In large-scale applications where many devices must be fabricated on a single wafer, it is essential to minimize the length of each switch. Bulk semiconductor waveguide switches based on the linear electrooptic effect typically have lengths on the order of a millimeter. This size is due to the smallness of the linear electrooptic coefficient r. In GaAs- and InP-based compounds at wavelength λ=1.55 μm and applied field E= 10 V/μm, the length needed to acheive a π phase change $l_\pi=\lambda/(2n_0^3 r_{41}E)$ is ~1.3 mm. Directional coupler switches require coupling regions at least $\sqrt{3}$ larger than l_π. In this paper we demonstrate a semiconductor electro-optic directional coupler switch with device length under 600 μm. We achieve switching in short lengths by making use of the large excitonic electrorefraction associated with the quantum confined Stark effect in InGaAsP quantum wells [1]. Quantum well waveguide switches also have a unique advantage in that they can be designed to provide optimum device performance at a specific wavelength. In particular, control of the bandgap through quantum well thickness and InGaAsP composition allows us to maximize optical phase modulation while minimizing absorption loss and intensity modulation at 1.55 μm, a wavelength of interest for optical fiber communications.

Devices were fabricated from a p-i-n waveguide structure grown by organo-metallic vapor phase epitaxy. Ten InGaAsP/InP quantum well layers are centered in the 1.135 μm thick intrinsic core region. The 85 Å thick wells are formed from InGaAsP and the InP barriers are 250 Å thick. Strip-loaded directional couplers are formed by wet chemical etch of the upper InP cladding layers. A schematic of the switch is shown in Fig. 1. Both the electrical and the optical fields are confined under the ribs. Switching characteristics are determined by end-fire coupling TE-polarized light from a 1.55 μm semiconductor diode laser into the device via a microscope objective. The input ports of the switch are laterally separated by 20 μm. IR TV cameras monitor the near-field output intensity pattern as well as the the input face of the switch, to ensure good input coupling. Bias voltages are applied between one arm of the coupler and the substrate, such that the field is along the 001 direction normal to the quantum well layers. Reverse breakdown voltages for individual ribs are 25 - 30 V at 1 μA.

Figure 2 shows the photocurrent spectrum as a function of reverse bias voltage for a large-area p-i-n diode formed from the same wafer as the switch. The clear red-shifting of the ground state excitonic peak with voltage indicates that we have high-quality quantum wells with low impurity concentration in the intrinsic part of the diode. These spectra illustrate electroabsorption features which are desirable for a quantum well electro-optic phase modulator utilizing the quantum confined Stark effect: first, large red-shifting of excitonic absorption above the bandedge, which produces a large positive change in refractive index at the below-gap wavelength of operation [1], and second, negligible absorption and electroabsorption at the wavelength of operation.

Figure 3 shows the output near-field intensity pattern of a switch with a 570 μm long coupling region. At 0 V bias to the input guide (on the right), maximum power transfer to the coupled guide (on the left) occurs. Optical switching is acheived by reverse biasing the input guide, causing an index change in that side and destroying the phase match condition for coupling. Light then emerges from the input channel. At -12 V, the relative output power from the coupled guide is reduced to 56 percent, and at -22 V most of the light (76 percent) emerges from the right channel. Since the output cleave is located in the strong coupling region of the switch, there is still significant overlap of the modes and this somewhat limits the measured extinction ratios.

In summary, we have demonstrated the first application of excitonic quantum well electrorefraction to a directional coupler switch. The device operates at 1.55 μm and is composed of InGaAsP/InP, the most promising material system for monolithic integrated optics in the wavelength range 1 to 1.6 μm. The fabrication techniques used here are extremely simple and improvements in device performance can be easily effected. For example, switching voltages will be reduced by at least a factor of three by decreasing the thickness of the intrinsic region. Finally, it is important to note that these switches are operated under reverse bias and that there are no dopants in the quantum wells. Thus, unlike switches which employ current injection [2] or doped quantum wells [3], we avoid both the speed limitations imposed by carrier recombination times and absorption losses associated with carriers in the quantum wells.

REFERENCES

[1] J.E. Zucker, I. Bar-Joseph, B. I. Miller, U. Koren, and D. S. Chemla, Appl. Phys. Lett. January 1989.

[2] K. Ishida, H. Nakamura, H. Matsumura, T. Kadoi, and H. Inoue, Appl. Phys. Lett. 50,141 (1987).

[3] K. G. Ravikumar, K. Shimomura, T. Kikugawa, A. Izumi, S. Arai, Y. Suematsu, K. Matsubara, Electron. Lett. 24,415 (1988).

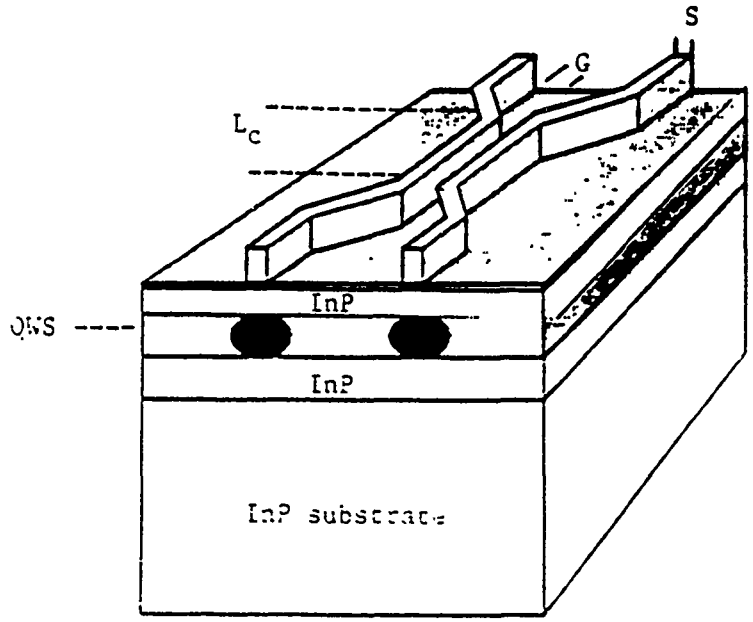

[1] Schematic of strip-loaded directional coupler. QW=quantum well region, rib width S=2 μm, gap G=2.5 μm, length of coupling region=L_c.

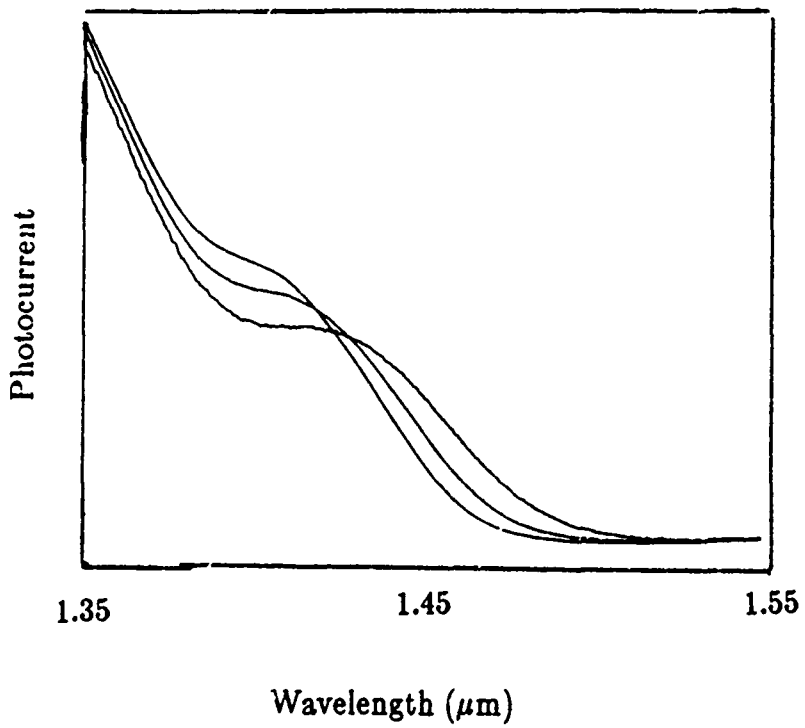

[2] Photocurrent spectrum at 5, 10 and 15 V reverse bias.

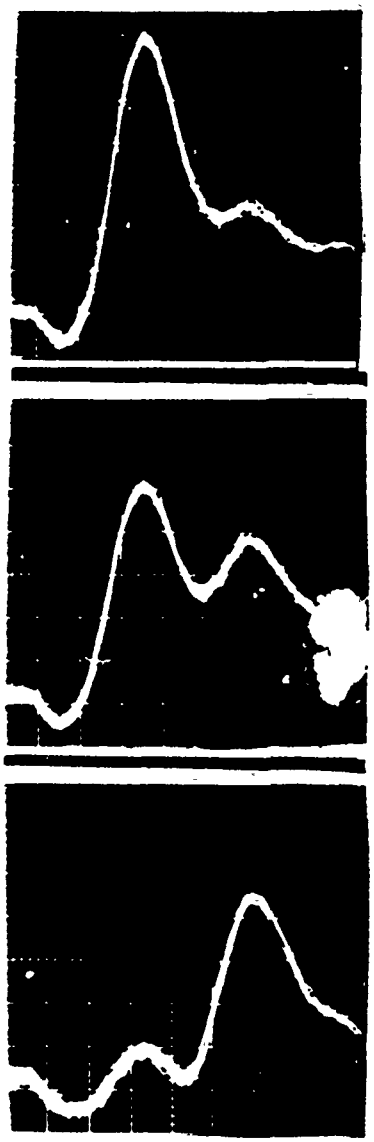

[3] Near-field intensity pattern of switch output monitored by IR video system. L_c=570 μm. Bias is applied to the input side (on the right): top, 0V; middle, -12 V; bottom, -22 V.

HIGH GAIN OPTICAL TRANSISTOR RESISTANT TO PUMP INSTABILITY

A.A.Maier
Institute of General Physics, Moscow, USSR

Self-switching of light in nonlinear systems with unidirectional distributely-coupled waves (UDCW) (predicted in [1-4] for the whole class of such systems) consists in a sharp change of the ratio of output intensities of waves caused by a slight intensity change of one of the input waves. A new class of optical transistors based on this effect was first suggested in [1,5]. The UDCW are well known [1,3]: waves in tunnelly coupled optical waveguides (TCOW); waves with two orthogonal polarizations in an optical waveguide (TE, TM-waves) or in a crystal; unidirectional waves under Bragg diffraction in a periodic structure and so on. For the particular case of launching of light into one of identical TCOW the self-switching of light was also predicted independently in [6]. Equations [1]:

$$\begin{cases} i\beta\frac{\lambda}{\pi}\frac{dA_0}{dz} + KA_1\exp(i\Delta z2\pi/\lambda) = -\theta_0|A_0|^2A_0 \\ i\beta\frac{\lambda}{\pi}\frac{dA_1}{dz} + KA_0\exp(-i\Delta z2\pi/\lambda) = -\theta_1|A_1|^2A_1, \end{cases} \qquad (1)$$

(where $\Delta=\beta_1-\beta_0$, $\beta=(\beta_0+\beta_1)/2$) for amplitudes ($A_j=\beta_j\exp(i\varphi_j)$) describe light self-switching not only in TCOW, but also in other systems with UDCW for which the corresponding equations are similar to (1), differ from them only slightly in the nonlinear part and can be easily reduced to (1) by a trivial substitution.

Solution of (1) for the general case when the both waves ($j=0,1$) are fed in the system with an account of the nonidentity of UDCW ($\Delta\neq0$, $\theta_0\neq\theta_1$) has the form [7]:

$$J_{11}=\frac{(J_a+J_dP/Q)+(J_dP/Q-J_a)cn(\tilde{s},r)}{1+P/Q+(P/Q-1)cn(\tilde{s},r)}\,,\quad J_{01}=R_0+R_1-J_{11}\,, \qquad (2)$$

where $J_j=I_j/I_M$ are normalized intensities, $I_M=8K/|\theta_0+\theta_1|$ is critical intensity, $I_j=|A_j|^2$, $J_j(z=0)=R_j$, $J_j(z=1)=J_{j1}$, $I_j(z=0)=I_{j0}$, $I_j(z=1)=I_{j1}$, $\Psi=\varphi_1-\varphi_0+\Delta z2\pi/\lambda$, $\Psi_0=\Psi(z=0)$, $\tilde{s}=s+F(\gamma,r)\cdot n$, $n=\pm1$, $s=2\sqrt{PQ}\,L$, $L=2\pi Kl/\lambda\beta$, $\gamma=2\mathrm{arcctg}[Q(J_a-R_1)/P(R_1-J_d)]^{1/2}$, $r^2=1-r_1^2=r^2=[(J_a-J_d)^2-(P-Q)^2]/4PQ$, $P^2=(J_a-J_b)(J_a-J_c)$, $Q^2=(J_d-J_b)(J_d-J_c)$, J_a,J_b,J_c,J_d are the roots of equation $-(J-R_1)^2(R_0-\Delta/2-J)^2-(J-R_1)(R_0-\Delta/2-J)\sqrt{R_0R_1}\,\mathrm{sign}(\theta_s)\cos\Psi_0+R_0(J-R_1\cos^2\Psi_0)/4-J(J-R_1)/4=0$, $\Delta=\zeta+2(\theta_d/\theta_s)(R_0+R_1)$, $\zeta=\mathrm{sign}(\theta_s)\Delta\beta/K$, $\theta_s=(\theta_0+\theta_1)/2$, $\theta_d=(\theta_1-\theta_0)/2$,

$n=\pm1$ is determined by the sign of $\sin\Psi_0$.

For identical UDCW ($\Delta=0$, $\theta_0=\theta_1=\theta$) [3]:

$$J_{0,1;1}=(R_0+R_1)/2\pm\sqrt{D}\,cn(\tilde{s},r),$$

where $s=2L\sqrt{D_+-D_-}$, $\gamma=\arccos[(R_o-R_1)/2\sqrt{D_+}]$, $r_1^2=1-r^2=D/(D_+-D_-)$, $D_\pm=[(R_o+R_1)^2-(1\pm\sqrt{D})^2/4]/4$, $D=16R_oR_1-8\sqrt{R_oR_1}\,\mathrm{sign}(\theta)\cos\Psi_o+1$.

Self-switching arises when $\exp(\tilde{s})\gg 1$ and $r\approx 1$ (that is $|r_1|^2\ll 1$) or, more exactly, when $|r_1|^2\lesssim 16\exp(-\tilde{s})$.

Let's assume R_o is pump, R_1 is small variable signal: $R_1\ll R_o$. Conditions of self-switching are reduced to $\exp(L)\gg 1$ and $R_o\approx 1$ ($\delta\equiv 1-R_o$, $|\delta|\ll 1$) or, more exactly, $|\delta+\Delta|\lesssim 8\exp(-L)$. Then at

$$R_1=R_{1M}^{(j)}=[4\exp(-L)-m(\delta+\Delta)/2-\varepsilon/2]^2\cos^{-2}\Psi_o \qquad (3)$$

(where $m=\mp 1$ corresponds to $j=0,1$; $|\varepsilon|\ll|\delta|$; $\cos^2\Psi_o\sim 1$) we have $J_{11}=\max\approx R_o$, $J_{01}=\min\approx 0$ (if $j=0$, $m=-1$) or $J_{11}=\min\approx 0$, $J_{01}=\max\approx R_o$ (if $j=1$, $m=1$).

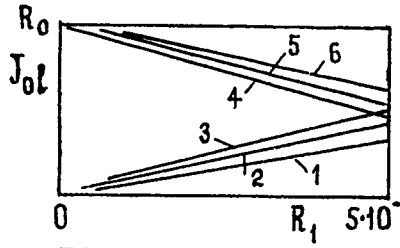

Fig.1. $L=2\pi$;
1-3: $m=1$, $\Psi_o=0$;
4-6: $m=-1$, $\Psi_o=\pi$;
1,6: $\varepsilon=-0.001$;
2,5: $\varepsilon=0$;
3,4: $\varepsilon=0.001$

Let's assume $R_{1M}^{(j)}=0$. Then under $m\cos\Psi_o>0$ and $\varepsilon=0$ a signal with $R_1\sim R_{1max}\sim[3\exp(-L)]^2\ll 1$ has to be amplified linearly (see Fig.1) with amplification coefficient (gain of optical transistor):

$$k_s=\partial I_{01}/\partial I_{10}=\partial J_{01}/\partial R_1\sim m\cos^2\Psi_o\exp(2L)/25, \qquad (4)$$

which is much higher (in $\sim\exp(L)/3$ times) than in the case [2] when the pump and the signal are fed in the system as the same wave ($R_1=0$). For instance with $L=2\pi$ and $\cos^2\Psi_o=1$, $\varepsilon=0$, according to (4) we have $k_s\sim 10^4$ whereas in the case [2] we have only $\partial I_{01}/\partial I_{00}\sim\exp(L)/8\sim 70$. Under $R_{1M}^{(j)}=0$ with $\varepsilon>0$ at small $R_1\lesssim R_{1max}$ $|k_s|$ is even greater than that with $\varepsilon=0$.

If $R_{1M}^{(j)}=0$ and $\varepsilon=0$, $R_1\sim R_{1max}$, then amplification of variation of pump intensity is estimated by $\partial I_{01}/\partial I_{00}\sim(\exp(L)/8)\sqrt{R_1/R_{1max}}$. Thus at $\cos^2\Psi_o\approx 1$ the signal variation changes output radiation power in $\gtrsim(\exp(L)/3)\sqrt{R_{1max}/R_1}$ times stronger than the same power variation of the pump. So the requirement on the stability of the pump power for this optical transistor is in $\gtrsim(\exp(L)/3)\sqrt{R_{1max}/R_1}$ times less than in the case [2].

[1]. A.A.Maier. Kvantov. Elektron., 9, 2296 (1982). [2]. A.A.Maier. Kvantov. Electron., 11, 157 (1984). [3]. A.A.Maier. Izv. AN SSSR, Ser. Phys., 48, 1441 (1984). [4]. A.A.Maier. Kratk. soobsch. po fizike, FIAN, No 12,20 (1984). [5]. A.A.Maier. USSR Inventor's Certificate No 1152397 (1982). [6]. S.M.Jensen, IEEE J. Quantum Electron. QE-18, 1580 (1982). [7]. A.A.Maier. Preprints of Inst. of Gen. Phys. No 153, No 351, Moscow (1987); Opt. Eng. Journal of SPIE, to be published.

FRIDAY, MARCH 3, 1989

SALON E

3:45 PM–5:30 PM

FE1–FE6

SPACE-DIVISION SWITCHING

S. S. Cheng, Bellcore, *Presider*

HDTV PHOTONIC SPACE-DIVISION SWITCHING SYSTEM USING 8X8 POLARIZATION INDEPENDENT LiNbO3 MATRIX SWITCHES

S. Suzuki, H. Nishimoto*, M. Iwasaki**, S. Kajitani*, M. Kondo*
M. Shikada*, M. Ashibe** and F. Akashi
C&C Systems Res.Labs. *Opto-Electronics Res.Labs. **C&C Infor.Tech.Res.Labs.
NEC Corporation, 4-1-1 Miyazaki, Miyamae-ku, Kawasaki 213 JAPAN

1. Introduction A photonic space-division switching system guarantees transparent connection between two optical transmission media, and hence, it can provide various broadband services simultaneously, including high-definition TV (HDTV). NEC has already reported 32-line photonic space-division switching systems[1,2] using 8X8 $LiNbO_3$ matrix switches. In these systems, however, optical polaization-maintaining fibers were used as subscriber lines, owing to polaization dependency in LiNbO3 matrix switches. This paper reports the first 8X8 polarization-independent $LiNbO_3$ matrix switches and an advanced photonic space-division switching system using these switches. The system can use ordinary optical single-mode fibers as subscriber lines, and provide HDTV distribution as well as TV phone switching services.

2. Polarization independent 8X8 matrix switch The first strictly non-block 8X8 polarization independent matrix switch has simplified tree structure and consists of four 4X4 polarization independent matrix switches[3], four 1x2 switches and four 2X1 switches, as shown in Fig. 1. For this matrix switch, a polarization independent directional coupler switch element driven by uniform 4β was chosen considering its low switching voltage. The directional coupler has 8 μm waveguide width and 6 μm gap. On the other hand, 10 μm bend waveguide width, which was greater than that of the directional coupler, was adopted to reduce the bending loss. Fiber to fiber insertion loss, crosstalk level and switching voltage are 8-13 dB, less than -15 dB and 90 volt, respectively.

3. System design The 32-line photonic switching network, shown in Fig. 2, are devised for providing both TV phone and HDTV distribution services. A 3-stage switching network, which is a blocking network and requires reduced number of matrix switches, is used to provide TV phone services. However, in HDTV distribution services, non-blocking connection has to be guaranteed. Therefore, 4-channel HDTV signals are led to the 3rd-stage switches through a 1X8 external optical splitter to distribute the signals to multiple subscribers up to 32 without any blocking.

Figure 3 shows an 8X4 polarization independent matrix switch for 3rd-stage switches, which must guarantee point-to-multi point connectivity to provide HDTV distribution services. Therefore, a passive splitter/ active selector structure[4,5] 4X4 matrix switch, whose loss is less than 15 dB, is integrated with a 4X4 matrix switch for TV phone services, whose loss is less than 9 dB.

4. Experiment Part of the photonic switching network, shown in Fig. 2, has been made and used to distribute HDTV signals and to exchange 100-Mbps TV phone signals. The HDTV analog signal from a camera or VTR is encoded to 32.4-Mbps 19-parallel digital pulse streams by a TCI (Time Compressed Integration) encoder[6]. These parallel signals are scrambled and converted to a 780-Mbps serial signal including frame synchronization bits. The 780-Mbps

signal is converted to an optical signal by an electro-optical converter (E/O). The optical signal is distributed through an optical splitter and the 3rd-stage switch, and it is converted to an electric signal again, using an opto-electronic converter (O/E). This signal is converted to parallel digital signals and descrambled. Finally, these digital signals are converted to analog HDTV signals by a TCI decoder and sent to an HDTV monitor.

Output power of the E/O was 0 dBm. Optical loss of the external splitter, using fiber couplers, and 3rd-stage switch were 10 dB and 13 - 15 dB, respectively. The 10 - 12 dB levels were obtained as system margins with several meter-optical fiber subscriber lines. Therefore, it can be concluded that 6 - 8 dB system margins with 2-Km subscriber lines are possible. These values are practical enough for real application. As for TV phone services, total insertion loss of the 3-stage switching network was 28 - 33 dB. Output power of the E/O in a TV phone terminal was 2 dBm. The 9 -14 dB levels were obtained as system margins with several-meter fibers. Therefore, 5 - 10 dB system margins with 2-Km subscriber lines are expected.

Figure 4 shows a photograph of the experimental switching network. Owing to polarization independence of matrix switches, tape fibers can be attached to switch modules and optical wiring is simplified. A photograph of the HDTV switching demonstration display is shown in Fig. 5.

5. Conclusion A photonic space-division switching system was fabricated using 8X8 polarization independent $LiNbO_3$ matrix switches. The switching system is successfully operating in distributing HDTV signals and exchanging TV phone signals, which are transmitted through ordinary single-mode fibers. Therefore, the photonic space-division switching system using $LiNbO_3$ matrix switches taked a step forward for practical use.

References (1)S.Suzuki et al. OFC/IOOC'87 WB4 (2)T.Sawano et al. GCOM'87 51.5
(3)H. Nishimoto et al. Electron. Lett., vol. 23, p. 1167, 1988
(4)R. E. Spanke, IEEE J-QE-22, No. 6, June 1986, P. 964
(5)K. Habara et al., Electron. Lett., vol. 21, P.631, 1985
(6)M. Ashibe et al., 2nd HDTV Workshop

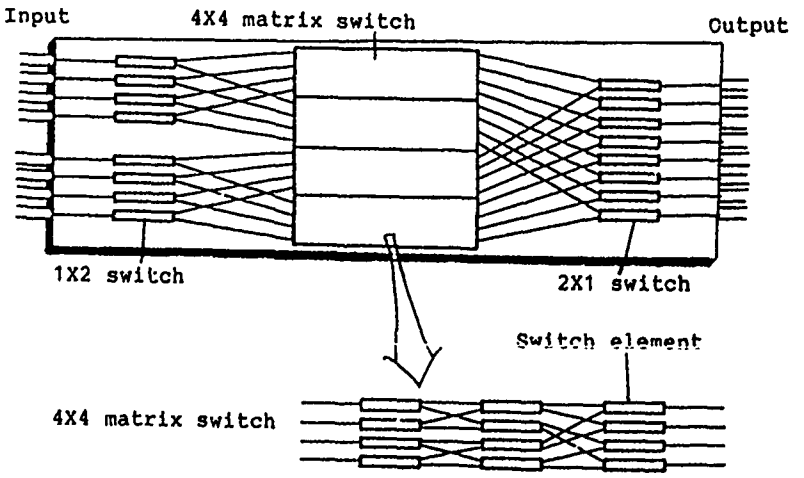

Fig. 1 Polarization independent 8X8 matrix switch

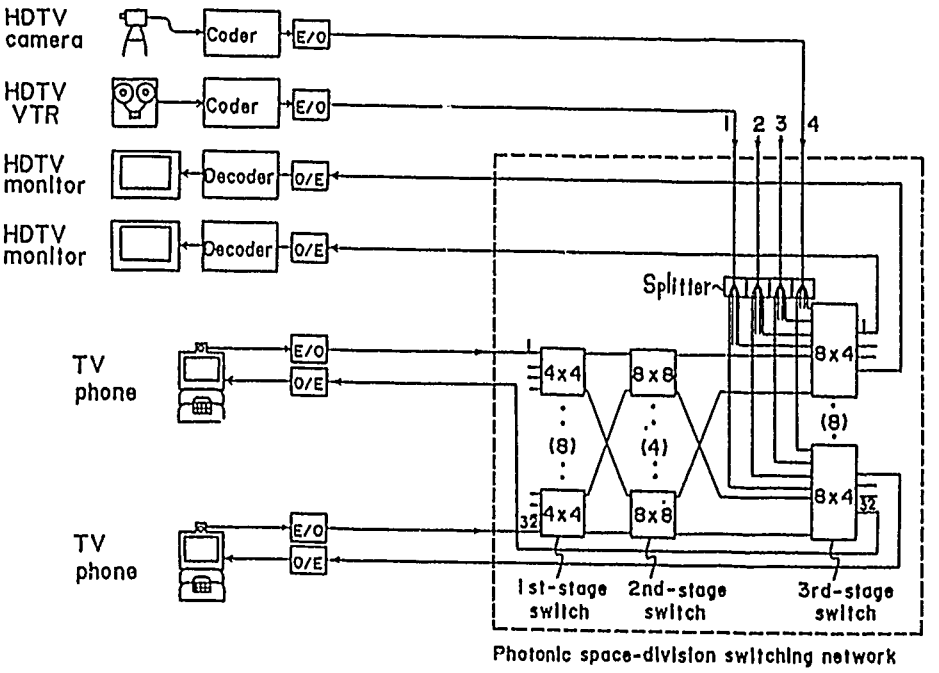

Fig. 2 Photonic switching system block diagram

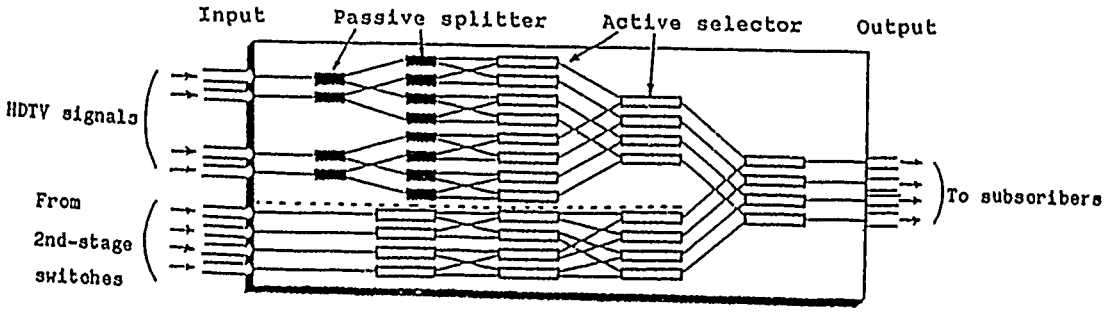

Fig. 3 Polarization independent 8X4 matrix switch for 3rd-stage switches

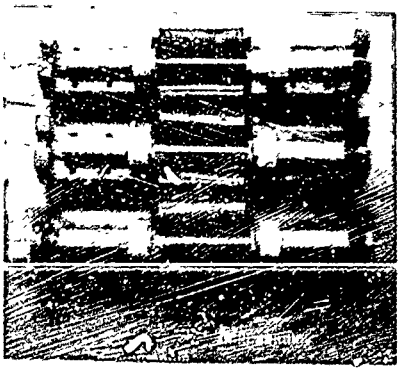

Fig. 4 Experimental photonic switching network

Photonic switching system

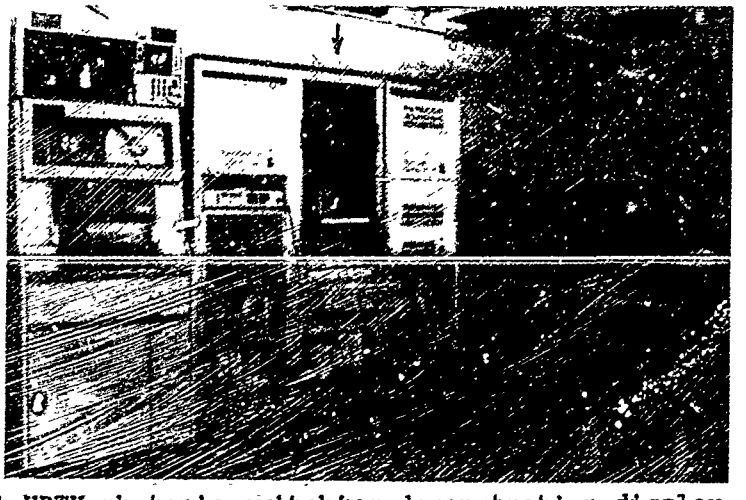

Fig. 5 Experimental HDTV photonic switching demonstration display

Systems Experiments with a Packaged 4x4 Polarization Independent Switch Matrix

Per Granestrand and Lars Thylén
Ericsson Telecom
S-126 25 Stockholm
Sweden
Tel +4687196738

Björn Stoltz and Jan-Erik Falk
Ericsson Components AB
S-164 81 Stockholm Sweden

INTRODUCTION

Integrated optics space switch arrays have received much attention in recent years due to their ability to route information practically irrespective of its frequency contents and coding format ("frequency and code transparency"), in marked contrast to electronic switches[1]. Several polarization dependent switch arrays have been demonstrated : crossbar switches [2,3] as well as lattice[4] and tree[5] structures; recently duobanyan structures[6,7].

For polarization independent switches, only sizes up to 4x4 have been reported[8,9]; polarization independent switches are in general characterized by a voltage length product which is at least 3 times that of polarization dependent switches. The polarization independent switches allow interfacing to standard single mode fibers and greatly increases the scope for systems applications in switching as well as transmission.

In this paper we report a systems experiment with a packaged polarisation independent 4x4 switch matrix[8]. Bit error rate measurements are carried out for 2 Gb/s input signals; the performance is studied for varying optical powers through the matrix as well as with an interfering 34 Mb/s signal from a commercially available system, which is interfering with the 2 Gb/s signal by deliberately increasing the crosstalk in the signal path.

EXPERIMENTAL SET UP

Fig 1 shows the setup for the experiment. The 1.3 μm CW laser signal is modulated at a 2 Gb/s rate by an external modulator (Mach-Zehnder modulator) and connected to one of the matrix inputs. The matrix is controlled by a computer via a control interface in which the serial stream of digital data defining the state of the matrix is converted to the pertinent electrode voltages. The 2 Gb/s-signal is routed to one of the outputs and is then detected, amplified and fed to a BER-test equipment. The bit pattern is a pseudo random pattern of length 2^{15}-1. Through another path in the matrix a 34 Mb/s disturbing signal (alternating one's and zero's) is led giving crosstalk in the 2 Gb/s-stream. The crosstalk was varied by partial switching of two of the crosspoints in the matrix to investigate the effect of the crosstalk on the system performance. Fig 2 shows a photo of the packaged matrix. The matrix package is a sandwich construction of alumina and printed circuit board for interfacing to the electronic control system. Standard single mode fiber were attached to the $LiNbO_3$-chip by using UV-curing acryl at the chip edge and at a secondary support. Additionally, a strain release was used at the package wall.

RESULTS OF SYSTEMS MEASUREMENTS

Data for the packaged matrix: The insertion loss of the packaged matrix was measured for all 16 input-output combinations. For the TE-mode the average loss was 10.7 dB with a standard deviation of 1.3 dB and for the TM-mode the average was 10.4 dB, standard deviation 1.4 dB. These rather high loss figures are probably due to insufficient substrate quality, which deviates from previous batches. The crosstalk was fully characterized (288 measurements) giving crosstalk of less than -35 dB with equal excitation in the TE- and TM-polarizations. The switch voltage of a crosspoint, defined as the maximum voltage shift when switching between cross- and bar-state (all six electrodes shifted) has an average of 50 Volts for the 24 switches (crosspoint length 4.3 mm).

In fig 3 results of BER-measurements are shown. The curve to the left corresponds to transmission from the transmitter directly to the reciever. The next curve corresponds to the case where the signal is routed through the matrix, with the disturbing 34 Mb/s signal switched off and with the disturbing signal at an average of -57 dBm (this corresponds to the normal crosstalk of the matrix). No difference was seen between these two cases, however a penalty of approximately .5 dB relative the first curve was encountered. The third curve corresponds to a disturbing signal level of -27.5 dBm, corresponding to -10(-11) dB crosstalk. Only a degradation of approximately 1 dB of the reciever sensitivity results even for this large crosstalk. Fig 4 shows the eye-diagram for 2 Gb/s transmission through the matrix with a BER of $<10^{-11}$.

SUMMARY

We have demonstrated high speed (2 Gb/s), low bit error rate transmission through a 4x4 packaged polarization independent switch matrix, connected to standard single mode fibers. The influence on transmission quality of inserting the matrix was very small. The influence on BER of the 2 Gb/s channel by an interfering 34 Mb/s video channel, introduced into the 2 Gb/s bit stream by deliberately increasing the switch array crosstalk, was also examined. Further data, including more comprehensive BER measurements will be reported. Stability will be discussed. This work was partially carried out within the RACE OSCAR project.

REFERENCES

1. T Iwama et al, "4x4 OEIC Switch Module Using GaAs Substrate", J. Lightwave Technol., 1988, Vol. 6, pp772-778

2. P Granestrand et al, "Strictly nonblocking 8x8 integrated optical switch matrix", Electron. Lett., vol 22, (1986), p 816

3. S Suzuki et al, "32-line optical space division switching system", Proc OFC/IOOC '87, (1987), paper WB4

4. D Hoffmann et al, "Low-loss, rearrangeably non-blocking 4x4 switch matrix module", Proc 12th Euro. Conf. Optical Commun., (1986), p 167

5. G A Bogert, "4X4 $Ti : LiNbO_3$ switch array with full broadcast capability", Proc OSA Topical Meeting on Photonic Switching, (1987), paper ThD3

6. M A Milbrodt et al, "A tree-structured 4x4 switch array in Lithium Niobate with attached fibers and proton exchanged polarizers", Proc OSA Top Meet Integrated and Guided Wave Optics, (1988), MF9

7 H Okayama et al, " Optical switch matrix with simplified nxn tree structure", Proc OSA Top Meet Integrated and Guided Wave Optics, (1988), MF10

8. P Granestrand et al, "Tree-structured polarization independent 4x4 switch matrix in $LiNbO_3$,Electron. Lett. Vol 24(1988), p1198

9. H Nishimoto el al, "Polarization independent $LiNbO_3$ 4x4 matrix switch ", ibid, p1122

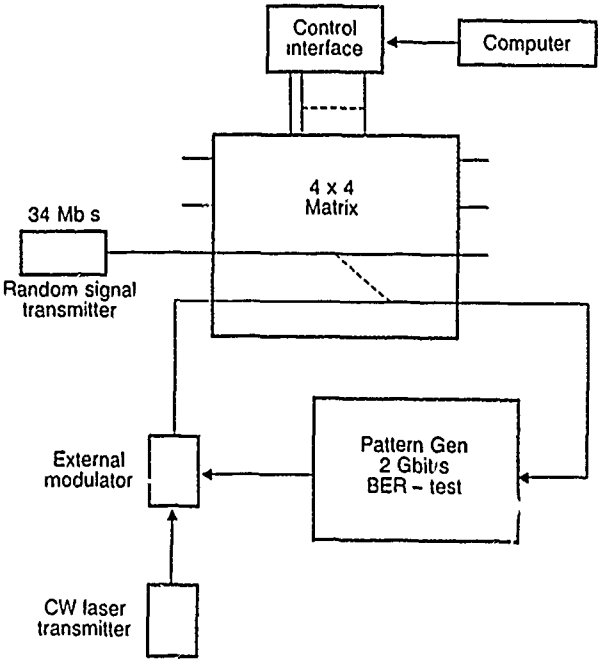

Fig 1. Experimental set-up for BER-measurements.

Fig 2.Packaged 4x4 switch matrix with ordinary single mode fibers and connectors.

Fig 3. BER as a function of average input power to the reciever for different cases: transmitter-reciever back to back, transmission through the matrix and transmission with a disturbing signal present.

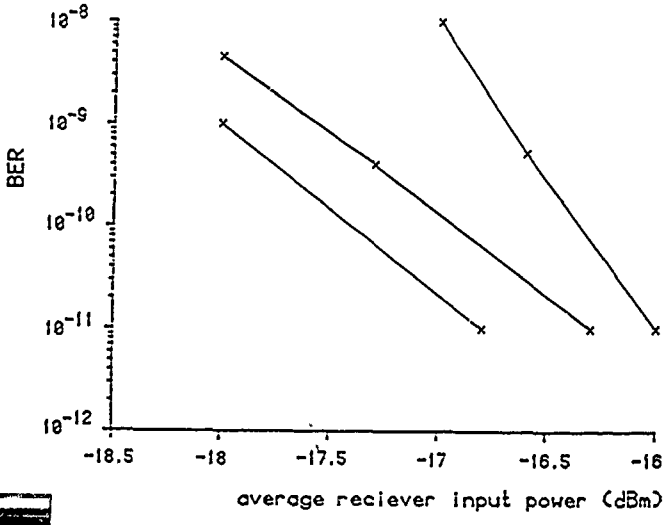

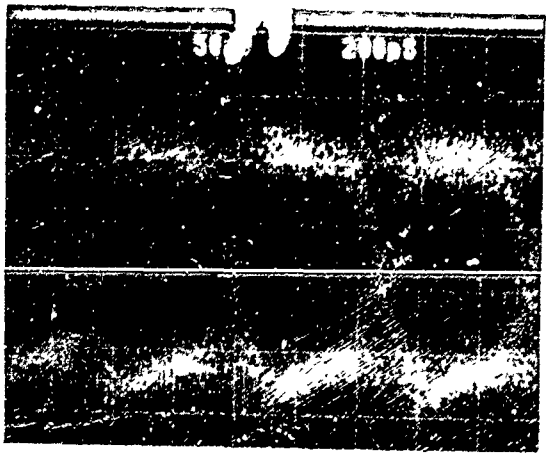

Fig 4. Eye-diagram for transmission of a 2 Gb/s pseudo random pattern through the matrix.

Comparison of Linear and Reflective 4x4 Ti:LiNbO3 Switch Arrays

P.J. Duthie, M.J. Wale and I Bennion
Plessey Research Caswell Ltd
Allen Clark Research Centre, Caswell, Towcester,
Northants, NN12 8EQ, UK

Recently several alternative architectures for integrated optical switch arrays have been investigated experimentally using the Ti:LiNbO3 material system [1,2,3,4]. All these architectures lead to chips with very large length/width ratios, owing to the large radius of curvature required for low-loss Ti:LiNbO3 waveguides, all require separate optical fibre interfaces at the input and output facets. A reflective switch architecture [5] relaxes the first constraint, allowing more effective use of substrate area, and permits a single fibre array to be used for both input and output, thereby potentially reducing assembly costs and providing a more convenient package. We have fabricated small 4x4 switch array modules to compare the reflective and linear architectures.

Both the reflective and the linear devices employ X-propagating titanium indiffused waveguides in Z-cut lithium niobate. The patterned metal, 7um wide by 750A thick, was diffused for 10 hours at 1050 degrees C, to make waveguides suitable for operation at 1.3um wavelength with TM polarisation. Aluminium electrodes were deposited over a 2500A SiO2 buffer layer. In order to reduce electrical interface and control complexity, only one live connection was provided to the reverse delta-beta electrodes, rather than the two connections required to access both uniform and reverse delta-beta states of the switch.

The device layouts of the linear and reflective arrays are shown in figure 1 and figure 2 respectively. The length of the arrays is determined by the bending radius (40mm), the switch gate length (6mm) and the crossover angle (6 degrees). These parameters were chosen on the basis of earlier experiments to yield low loss, drive voltage and crosstalk. For the reflective array, the reflectors are formed by electro-optically tunable 3dB reflective couplers, shown in figure 3. For convenience, the reflective couplers were identical to the switching gates in the matrix. The various contributions to the total length in each design are summarised in table 1 : the linear array is 62mm in length, whereas the reflective array is 53mm. This can be reduced to 48 mm if the electro-optic coupler tuning is replaced by passive tuning - either by suitable directional coupler design, or by passive trimming of the coupling length [6].

The single-pass insertion losses of the two designs were measured with respect to a York VSOP type HB1250 fibre without a reflector in either case. For the linear array, the reflection-corrected loss varied between 5.5 and 6.5dB according to path, corresponding to a propagation loss of 0.7dB/cm and an excess loss compared to a straight waveguide of between 1 and 2dB for the array. For the reflective array, the propagation loss was again 0.7dB/cm, and the excess loss for the array varied between 2 and 5dB. The additional path-dependent loss corresponds to the loss of the waveguide crossovers and may be reduced by using crossovers optimised for low loss. The average operating voltage and crosstalk values of the two designs are compared in table 2. It can be seen that the voltages for the two designs are

comparable, despite the linear design being nearly 30% longer than a reflective design where passive reflectors are used. The length advantage of the reflective design can be used either to reduce switch operating voltages, or to increase the size of switch array which can be integrated on a single substrate.

The switch chips were glued to a copper carrier and wire bonded to a printed circuit board for connection to the electrical controller. The optical interface employed polarisation maintaining fibres (York VSOP type HB1250) oriented in silicon V-groove arrays.

In summary, we have compared linear and reflective Ti:LiNbO3 switch arrays and shown that a reduction in length and interface complexity can be obtained by adopting a reflective architecture.

We would like to acknowledge the assistance of R Gibbs, J Hendy, E Hindson, F Randle and M Owen in the fabrication of these devices. This work was part-funded by the Commission of the European Communities under the RACE programme.

References

1. L. McCaughan and G. Bogert, '4x4 Ti:LiNbO3 integrated optical crossbar switch array', Appl. Phys. Lett.,47, 1985, pp348-350
2. R. A. Spanke, 'Architectures for large non-blocking optical space switches', IEEE J. Quantum Electron., QE-22, 6, pp964-967
3. M. Kondo et al, '32-element integrated low-crosstalk LiNbO3 4x4 optical matrix switch',IOOC-ECOC 85, pp361-364
4. P. J. Duthie and M. J. Wale, 'Rearrangeably non-blocking 8x8 guided wave optical switch', Electron. Lett., 24, 10, pp594-596
5. P. J. Duthie, M. J. Wale and I. Bennion, 'A new architecture for large integrated optical switch arrays', Proceedings of the first topical meeting on photonic switching, Incline Village, USA, 1987, pp146-150
6. O. Mikami et al, 'Phase tuning in optical directional couplers by photostructural effect of chalcogenide glass film', Appl. Phys. Lett., 31, 1977, pp376-378

	LINEAR ARRAY	REFLECTIVE ARRAY
Couplers	7x6mm = 42mm	4x6mm = 24mm
Connections	6x1.3mm = 8mm	3x4mm = 12mm
Inputs	2x6mm = 12mm	1x6mm = 6mm
Reflective Couplers	nil	11mm
Total	62mm	53mm
Total with passively tuned reflectors	62mm	48mm

Table 1 : Comparison of linear and reflective switch array lengths

	Linear array	Reflective array
V cross	14V	15V
V bar	34V	31.5V
V switch	20V	16.5V
Crosstalk	20dB	23dB

Table 2 : Comparison of linear and reflective switch operation

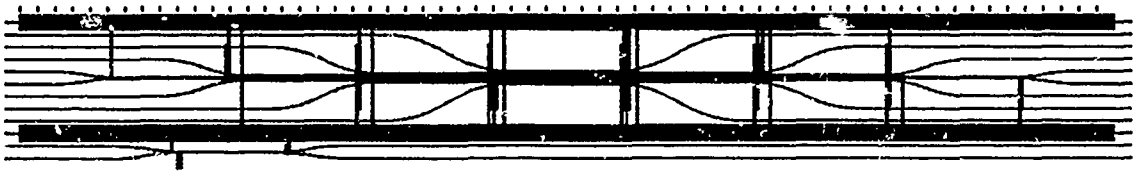

Figure 1 : linear array

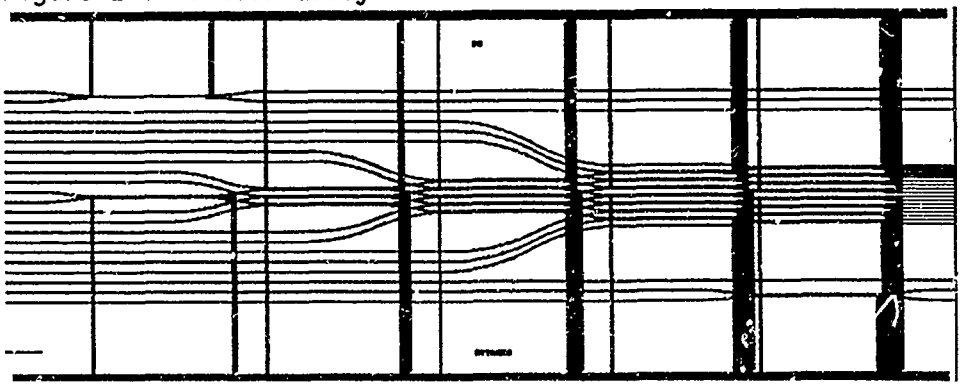

Figure 2 : Reflective array

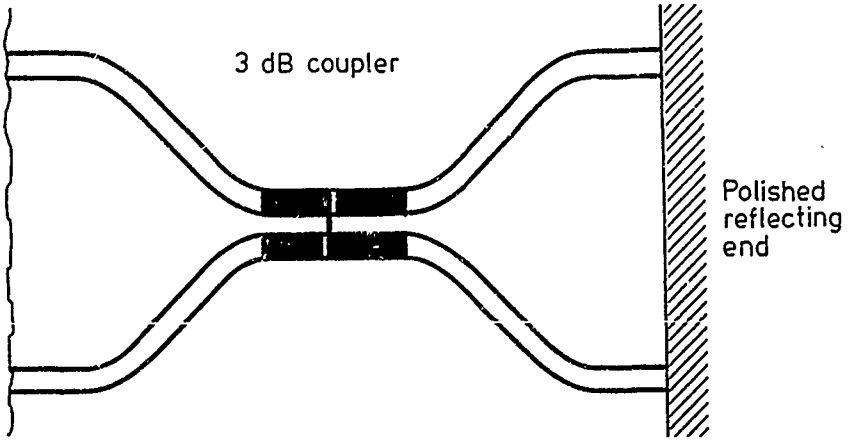

Figure 3 : Reflector design employed in this work

Small-Size, Low-Crosstalk GaAs/AlGaAs Electro-Optic Directional Coupler Switches with Alternating Δβ for Long Wavelength Matrix Switches

K. Komatsu, M. Sugimoto, A. Ajisawa and A. Suzuki
Opto-Electronics Research Laboratories, NEC Corporation
4-1-1 Miyazaki Miyamaeku, Kawasaki 213, JAPAN

There has been a growing interest in optical switches made of III-V semiconductor compounds for photonic switching systems, because of their large scale integration capability and their ability to be integrated with other semiconductor devices, such as optical amplifiers and electronic circuitry. A GaAs/AlGaAs electro-optic directional coupler (EODC) is attractive as a switch element for integrated matrix switches, because of its low absorption loss at long wavelength region (λ=1.3~1.55μm), fast switching speed, low electric power consumption and wavelength independent operation capability. Recently, extremely low loss passive GaAs/AlGaAs waveguides, with 0.15 dB/cm propagation loss [1] and a GaAs/AlGaAs EODC with submillimeter device length [2], have been reported. Although these results encourage us to study on GaAs/AlGaAs EODC matrix switches, the coupling length controlability problem still remains to be solved. Since the coupling length control becomes more difficult, as device size becomes smaller, solving this problem is essential to allow GaAs/AlGaAs EODC to realize integrated matrix switches, in which coupler length is fixed.

This report describes small size GaAs/AlGaAs EODC switches, with complete switching of light without a requirement for an exact device length (L) to coupling length (l_0) ratio by using the alternating Δβ technique [3]. Devices have been acheived with crosstalk as low as −16 dB, 16 V switching voltage at λ= 1.3 μm, and 0.8 dB propagation loss.

A drawing of the GaAs/AlGaAs EODC with alternating Δβ is shown in Fig. 1. The 2mm device length was chosen to realize a 4×4 matrix switch with less than 10 mm device length. Relatively thin GaAs guiding layer, 0.2 μm thick, and relatively high Al composition ratio, 0.5, in AlGaAs cladding layers were chosen to obtain high electric field and strong overlap between electric and optical fields. The p^--AlGaAs cladding layer is inserted between the p^--GaAs guiding layer and the p-AlGaAs top cladding layer, in order to maintain each individual waveguide electrically independent. Here, the thickness for each layer was designed to give single-mode conditions up to 3 μm waveguide width at λ= 1.3 μm, when rib etching reaches the p-AlGaAs - p^--AlGaAs interface (i.e. when etch depth t = 0.8 μm).

The 2 mm-long p-side electrodes are divided into two equally long (1 mm-long) sections, as shown in Fig. 1. So, the asynchronism of $\Delta\beta$ with equal magnitude, but reversal sign, can be introduced. In the single step $\Delta\beta$ reversal EODC, like the configuration indicated in Fig. 1, both⊗-state and ⊖-state are always available, if L/ι_o value ranges from 1 to 3 [3]. So, an exact L/l_o ratio is not required in this configuration, unlike the requirement for a uniform $\Delta\beta$ configuration.

EODCs with various waveguide widths (w = 2~3.5 μm) and various waveguide distances (d = 1.5~2.5 μm) were fabricated on an MBE (Molecular Beam Epitaxy) grown wafer by using conventional photolithography technique and Cl_2 RIBE (Reactive Ion Beam Etching).

Switching characteristics for the EODC, with w=2 μm, d=2 μm, and t=0.9 μm, are shown in Fig. 2. Both⊗-state and ⊖-state are obtained at V = 13 V and V = 29 V, respectively, under the alternating $\Delta\beta$ operation, as shown by the solid lines. On the other hand, under uniform $\Delta\beta$ operation, complete switching can not occur, as indicated by the broken lines in Fig. 2, because L/l_o is not an odd integer. In this device, measured coupling length was 0.90 mm. Measured crosstalk values for the⊗-state and ⊖-state are −14 dB and −15 dB, respectively, under alternating $\Delta\beta$ operation. Propagation loss was evaluated by measuring the finesse of the Fabry-Perot waveguide resonators, formed by cleaving two opposite ends of waveguides [1]. Measured propagation loss was 0.8 dB/2 mm, which is coincident with calculated free-carrier absorption in the p- AlGaAs and n- AlGaAs cladding layers. Absorption loss calculation indicates that further layer structure optimization could reduce the propagation loss. Switching bandwidth, measured by a [illegible]t frequency technique [4], was 1.6 GHz, which is also coincident with the 1.8 [illegible]ated value.

Switching characteristics for another EODC with w =2.5 μm, d = 1.5 μm and t = 0.9 μm, are shown in Fig. 3. Since coupling length in this device is 0.73 mm, and then L/l_o is close to 3, switching occurs even under uniform $\Delta\beta$ operation. However, alternating $\Delta\beta$ operation gives better crosstalk than uniform $\Delta\beta$ does, as shown in Fig. 3. Measured crosstalk value for the⊗-state and ⊖-state are −16 dB and −15 dB, respectively, under the alternating $\Delta\beta$ operation.

In conclusion, excellent switching characteristics for small size GaAs/AlGaAs directional couplers have been obtained, without the requirement for precise device dimension control, by using alternating $\Delta\beta$ technique. The results help to realize low-loss, high-speed GaAs/AlGaAs EODC matrix switches for long wavelength.

References

[1] E. Kapon et al: Appl. Phys. Lett., 50, pp. 1628-1630, 1987

[2] H. Takeuchi et al: Electron. Lett., 22, pp. 1241-1243, 1986
[3] H. Kogelnik et al: IEEE J. Quantum Electron., QE-12, pp. 396-401, 1976
[4] S. Uehara : Appl. Opt., 17, pp. 68-71, 1978

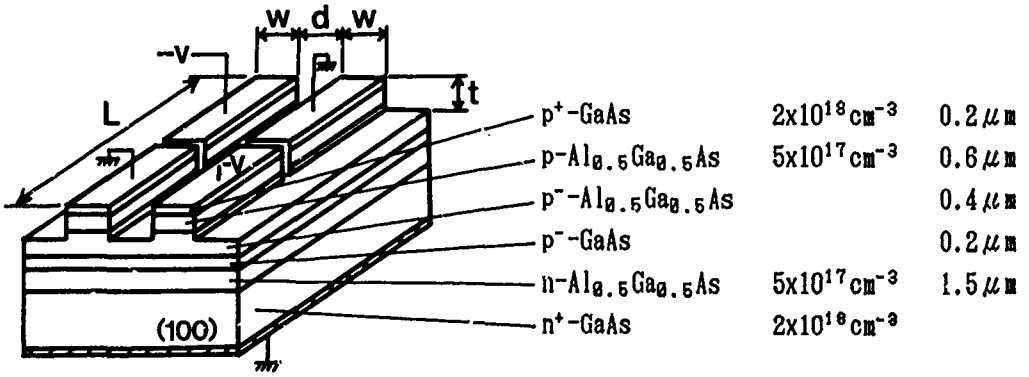

Fig. 1 GaAs/AlGaAs electro-optic directional coupler switch with divided electrodes for alternating $\Delta\beta$.

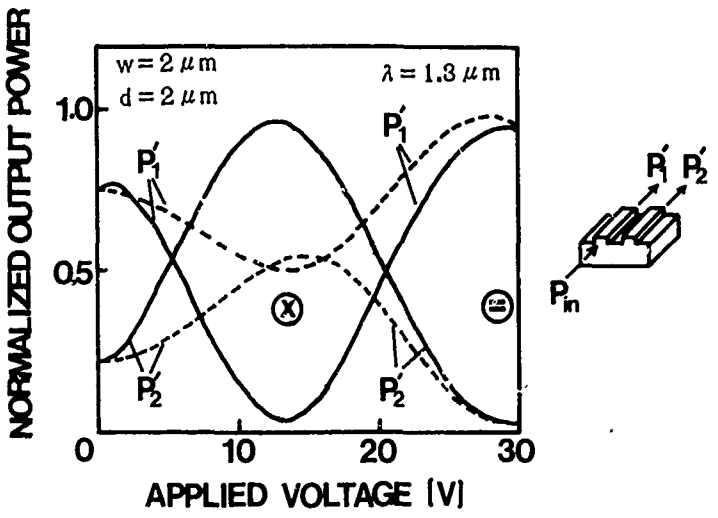

Fig. 2 Measured switching characteristics for an EODC with w=2 μm, d=2 μm and t=0.9 μm.

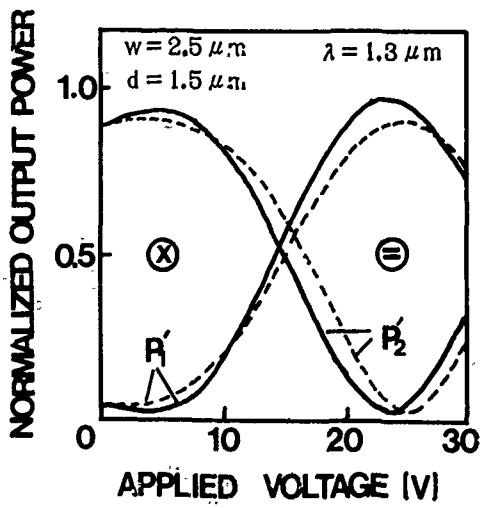

Fig. 3 Measured switching characteristics for an EODC with w=2.5 μm, d=1.5 μm and t=0.9 μm.

Switch Matrix with Semiconductor Laser Amplifier Gate Switches: A Performance Analysis

Mats Gustavsson and Lars Thylén
Ericsson Telecom AB, S-126 25 Stockholm, Sweden

Introduction

Integrated optics space switches have attracted considerable attention in recent years [1], [2] due to their ability to switch (route) information in a practically frequency and code transparent fashion, making them a natural extension of the optical transmission medium, the fibre. Important applications in the future transport network (optical crossconnect etc) are envisioned. This frequency transparency is to a large extent shared by semiconductor laser amplifiers (SCLAs) [3]. In addition, these amplifiers can offset the losses that plague matrices based on "passive" switching mechanisms, such as electro-optical or plasma, whether they are implemented in $LiNbO_3$ or semiconductors. Thus, in a proposed structure according to figure 1, the SCLAs can be used for space switching [4], implementing an optical SDS and, if the time switching feature is used, for STM or ATM switching, with the appropriate electronic interfaces.

The use of SCLAs as switch points further enables nonoptical [5] means for feedback stabilization of output power, under varying input polarization [6], and, to a degree, wavelengths and input power. Furthermore, the simultaneous detection and amplification properties [5] can be used for self routing of data packets by attaching headers to the packets and introducing suitable guard bands. In addition, the transmission can be surveilled. The switch of figure 1 can thus be viewed as constituting an intelligent, multifunctional switching fabric with a variety of systems applications.

This paper presents detailed calculations, based on the formalism of references [7] and [8] for such switch matrices of the tree structure based on SCLA gate switches. Attainable matrix sizes are given in terms of required signal to noise ratio (SNR), waveguide losses and for different input power levels; taking the optical bandwidth into account for a given data rate, while requiring that the insertion loss of the matrix be 0 dB.

Theoretical Model

According to the matrix architecture of figure 1, light losses for the worst case signal path as a function of propagation distance are given by

$$
\begin{aligned}
L(x) \;=\; & \alpha_W[xH(x)-(x-x_{tot})H(x-x_{tot})] + 3\sum_{j=1}^{\mathrm{ld}N} H\Big(x-[N-1-\sum_{i=1}^{j}2^{i-1}]\frac{s}{\theta}\Big) + \\
& L_M H\Big(x-[(N-1)\frac{s}{\theta}+\frac{N}{2}(\frac{N}{2}-1)\Delta]\Big) + L_M H\Big(x-[(N-1)\frac{s}{\theta}+\frac{N}{2}(\frac{N}{2}-1)\Delta+N(N-2)s]\Big) + \\
& 3\sum_{j=1}^{\mathrm{ld}N} H\Big(x-[\frac{N^2}{2}\Delta+N(N-2)s+(N-1+\sum_{i=1}^{j}2^{i-1})\frac{s}{\theta}]\Big).
\end{aligned}
$$

Here, the terms on the right hand side originate from waveguide losses (loss coefficient α_W), power splitting losses due to the 3 dB splitters and the two mirrors in the signal travelling path, each of which introduces a loss L_M. The number of matrix inputs and outputs is denoted by N, the total propagation distance by x_{tot} and the Heaviside step function by H.

Since the incoming optical signal might be rather weak (it should be possible for an optical signal with a power on the order of 1 μW to pass the matrix), an SCLA at the matrix input amplifies the signal. A sufficient number of SCLAs are then placed in each signal path to meet the requirement of a total insertion loss of 0 dB. With increasing waveguide losses the magnitude of optical amplification of course increases, resulting in a larger variance of the number of output photons and thereby a larger degradation of the SNR. Therefore, it is important to analyze which waveguide losses are tolerable for a given matrix size and

information bandwidth while retaining a good signal quality, defined in terms of a certain SNR at the matrix output. The analysis, based on the formalism of references [7] and [8], takes into account signal shot noise, spontaneous emission shot noise, beat noise between signal and spontaneous emission, beat noise between spontaneous emission components and signal excess noise.

Computational Results

Figure 2 shows the required number of SCLAs in the signal propagation path for a 32×32 matrix when the maximum SCLA gain is 20 dB. Acceptable waveguide losses for three different matrix sizes (8×8, 16×16, 32×32) and two noise bandwidths (10 nm, 40 nm) are presented in figure 3. The calculations shown include two optical input power levels, 1 μW and 10 μW, and the information bandwidth is 1 GHz for all cases. Now, consider the case of a 32×32 matrix with an input power of 1 μW and the 40 nm noise bandwidth. It can be seen from figure 3 that with the requirement of an SNR better than 20 dB at the matrix output, the waveguide losses must not be greater than about 1 dB/cm, which is a reasonable demand on waveguide fabrication. In this case three laser amplifiers are needed in the signal path. Having a larger input power of 10 μW, an SNR of better than 30 dB can be achieved at the matrix output for the noise bandwidth of 40 nm if the waveguide losses are less than about 7 dB/m. Note that no optical filtering has to be employed.

Conclusions

Detailed calculations have indicated the feasibilty to make SCLA tree structure switch matrices up to 32×32 in size with an output SNR of 20 dB, and an optical input power of 1 μW for 0 dB insertion loss; at a data rate of 1 GHz and without optical filtering. Clearly, the fabrication of such matrices will be dependent upon progress in semiconductor processing. Further, these matrices would be wide bandwidth (> 1 THz), imply relaxed requirements on waveguide fabrication, where the reasonable loss requirements increase yield and flexibility in waveguide fabrication. The use of SCLAs also enables implementing, in a nonoptic way, polarization independence and reduced sensitivity to wavelength and input power variation. Finally, the simultaneous amplification and detecting properties of the amplifiers can be used for self routing of data packets.

Extensive simulation results as well as implementation aspects will be discussed. Preliminary results on integrated amplifiers and passive waveguides will be presented. We acknowledge discussions with M. Janson.

References

[1] P. Granestrand, B. Stoltz, L. Thylén, K. Bergvall, W. Döldissen, H. Heinrich, D. Hoffman, *Strictly Nonblocking 8 × 8 Integrated Optical Switch Matrix,* Electron. Lett., vol. 22, pp. 816-818, 1986.

[2] S. Suzuki, M. Kondo, K. Nagashima, M. Mitsuhashi, K. Komatsu, T. Miyakawa, *Thirty-two-line Optical Space-Division Switching System,* Proc. Optical Fiber Communication Conference, 1987.

[3] M. J. O'Mahony, *Semiconductor Laser Optical Amplifiers for Use in Future Fiber Systems,* J. Lightwave Technol., vol. LT-6, pp. 531-544, 1988.

[4] M. Ikeda, O. Oiiguchi, K. Yo.nino, *Monolithic LD Optical Matrix Switches,* Proc. 13th European Conference on Optical Communication, 1987.

[5] M. Gustavsson, A. Karlsson, L. Thylén, *A Travelling Wave Semiconductor Laser Amplifier for Simultaneous Amplification and Detection,* Proc. 10th Topical Meeting on Integrated and Guided Wave Optics, 1989

[6] A. Ellis, D. Malyon, W. A. Stallard, *A Novel All Electrical Scheme for Laser Amplifier Gain Control,* Proc. 14th European Conference on Optical Communication, 1988.

[7] K. Shimoda, H. Takahasi, C. H. Townes, *Fluctuations in Amplification of Quanta with Application to Maser Amplifiers,* J. Phys. Soc. Japan, vol. 12, pp. 686-700, 1957.

[8] Y. Yamamoto, *Noise and Error Rate Performance of Semiconductor Laser Amplifiers in PCM-IM Optical Transmission Systems,* IEEE J. Quantum Electron., vol. QE-16, pp. 1073-1081, 1980.

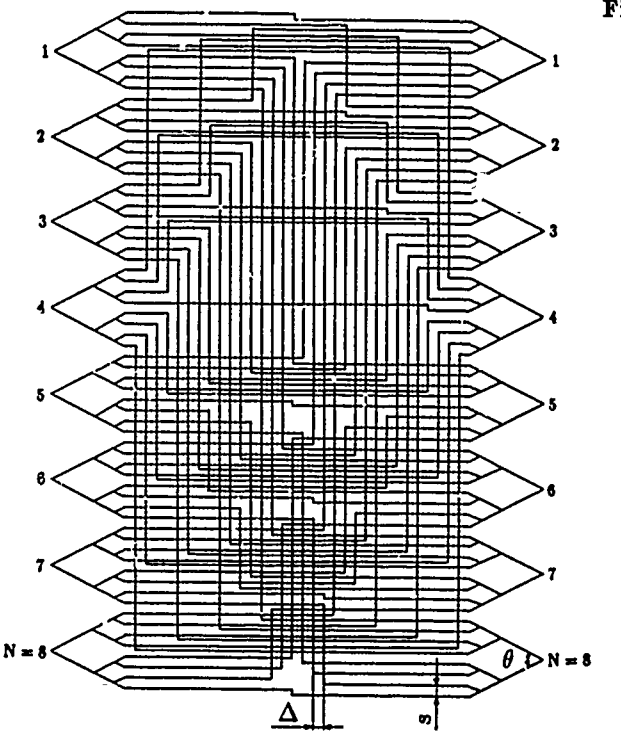

Figure 1. Matrix structure. Here, an 8×8 matrix is shown as an example. The geometrical parameters are defined in the figure. SCLA gate switches are placed in the signal paths (not shown). At two positions in each path the light changes propagation direction 90° which is achieved by employing e.g. mirrors.

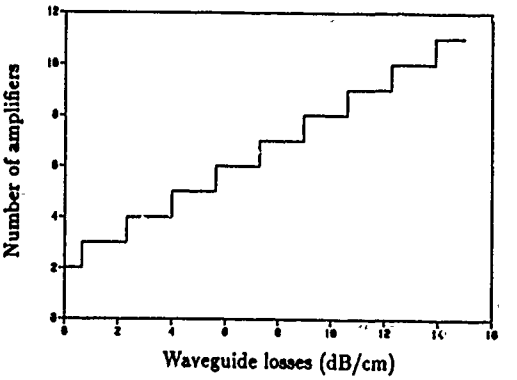

Figure 2. Number of required amplifiers in the worst case signal path of a 32×32 matrix for 0 dB insertion loss, as a function of waveguide losses. Maximum SCLA gain is 20 dB, L_M = 1 dB, and the geometrical parameters are $\Delta = 20\ \mu$m, $s = 60\ \mu$m and $\theta = 4°$.

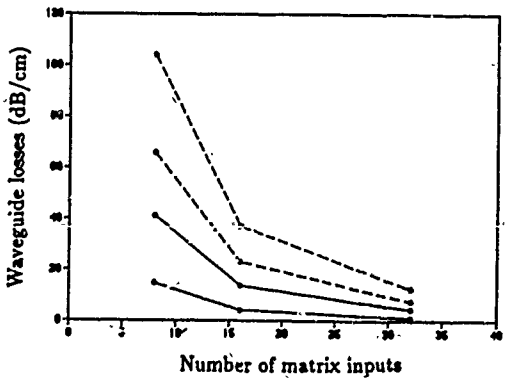

Figure 3. Allowed waveguide losses, for specified output SNRs, as a function of matrix size. The solid lines represent 1 μW input power with a required 20 dB output SNR for noise bandwidths of 10 nm and 40 nm, respectively. The broken lines represent 10 μW input power with a required output SNR of 30 dB for noise bandwidths of 10 nm and 40 nm, respectively.

A LINEAR TORSION-HINGED DEFORMABLE MIRROR DEVICE FOR OPTICAL SWITCHING

R. Mark Boysel, T. Gus McDonald, and Jeffrey B. Sampsell
Texas Instruments Incorporated
Central Research Laboratories
Dallas, Texas 75265

SUMMARY

We have designed and built a long linear deformable mirror device (DMD) spatial light modulator (SLM) suitable for free-space or optical fiber switching. Texas Instruments has developed an evolving family of deformable mirror devices including both linear and area array devices.(1,2,3) All of the devices have in common an aluminum mirror suspended by thin cantilever or torsion hinges over an air gap, thereby forming a capacitor with the underlying electrode. When a voltage is applied to the electrode, the grounded mirror is electrostatically attracted to it.

The DMD we report on consists of a linear array of mirrors with torsion hinges suspended over a 5.4 micron air gap. The chip contains elements of several designs, all of which are bistable. That is, the underlying electrode structure allows the reflecting elements to be tipped in either direction. In this paper we describe the performance of a 2 mil square element rotated by 45 degrees to the chip axis and hinged at opposing corners (Figure 1a). The mirrors are spaced 10 mils apart for optical isolation and to permit easy alignment to optical fibers. Although the elements can be operated in an analog fashion, for switching applications it is preferable to apply a voltage sufficient to fully deflect the mirror. This voltage is geometry dependent, varying with air gap width, electrode area, and hinge dimensions. The reflecting elements described here have a maximum deflection angle of approximately 8.5 degrees and a full-deflection voltage of 21 volts. Other mirror geometries permitting even larger deflections are on the chip and are being characterized.

Figures 1b and 1c compare two reflecting elements one deflected and one undeflected. Figure 1b is a bright field micrograph of the elements. The light reflected from the deflected pixel is thrown out of the aperture of the 10X objective used to take the photograph, so it appears dark. Figure 1c is a dark field photomicrograph of the same two elements. This time the light reflected off the deflected element enters the objective. The resulting flare in the photo indicates that the dynamic range available with a single mirror exceeds that of the film. Figure 1d is an interference micrograph of the deflected element at a higher magnification. (The 11 micron tip to tip deflection of the mirror exceeds the depth of focus of the microscope, but the interference fringes can still be discerned on half the mirror.) The wavelength of the illumination is 5400 A, so one interference fringe corresponds to 2700A. The approximately 20 fringes along the center to tip distance of the deflected element indicate 5.4 microns of deflection, which corresponds to 8.7 degrees, or full deflection.

In order to measure the switching efficiency of the DMD, we

used an acoustooptic light modulator operating at two frequencies (1.000 GHz and 1.005 GHz) to split a laser beam into two beams which are then focused onto reflecting elements 10 mils apart. The light is then reflected back through a beamsplitter onto a CCD camera (Fig 2a). The resulting image is shown in Figure 2b. If one element is then deflected, the light is thrown out of the optical system and the resulting CCD image is shown in Figure 2c. The line of video through the peaks can be displayed on an oscilloscope for both elements undeflected and for one pixel delflected (Figure 2d). (The intensity of the RF at the higher frequency is reduced to emphasize the excision of the larger lower frequency signal.) Measurements of the dyanmic range made in this fashion are limited by the dynamic range of the CCD detector. We have measured the ratio of the light intensity in the on state to that in the off state using a photomultiplier tube to be approximately 2600:1, a dynamic range of 34 dB in optical power. A frequency excision application of this free-space optical switching capability is currently under development. Frequency excision is better accomplished through the use of the contiguous 2 mil mirrors on the chip which allows a five-fold increase in frequency sensitivity over that achievable with 10-mil mirror spacing.

The free space switching system has excellent contrast ratio, but it is too large for fiber optic switching applications such as fiber optic interconnects. An alternative method of using the DMD for optical fiber switching is shown in figure 3. A bifurcated fiber has a transmitter on one leg and a receiver on the other. Light exiting the central fiber is imaged by a microlens onto the reflecting element of the DMD. If the element is flat (solid line), the incident light is reflected back through the same microlens, coupled back into the fiber, and detected at the receiver. However, if the reflecting element is deflected (dashed line), the light is reflected out of the acceptance angle of the microlens and is incident on a stop allowing no light back to the receiver. For optimum switching the deflection angle of the reflecting element should be just slightly greater than the NA of the optical system.

A switch of this type has been demonstrated using 50/125 multimode fiber with a NA of 0.2. A laser diode at 1.3 micron wavelength was used as the light source. The NA of 0.2 requires a mirror deflection angle of 11.5 degrees for optimum switching. Although the deflection angle of the DMD elements was about 8.5 degrees, less than the optimum angle,a switching contrast of 11.5 dB was obtained. That is, all but seven per cent of the available light was deflected out of the system. This seven per cent can be accounted for by the limited swing of the DMD element, reflection at the fiber/air interface, and optical feedthrough at the bifurcation.

Further work is underway to improve the switching contrast with other fiber/optical arrangements using both bifurcated and non-bifurcated fibers. Additionally, a DMD with a larger deflection angle is being designed specifically for fiber switching. A DMD-based four-by-four fiber optic crossbar switch is currently under development.

Acknowledgements.

We wish to thank Doug Weaver for the free-space switching data and Mark Reed for device processing and packaging, and to acknowledge Larry Hornbeck, Jim Florence, and Richard Gale for useful discussions and advice.

References:

1. L.J. Hornbeck and W.E. Nelson, "Bistable Deformable Mirror Device", OSA 1988 Technical Digest Series 8,107 (1988).
2. J.M. Florence and R.O. Gale, "Coherent Optical Correlator Using a Deformable Mirror Device Spatial Light Modulator in the Fourier Plane", Applied Optics 27,2091 (1988).
3. W.R. Wu, R.O. Gale, L.J. Hornbeck, and J.B. Sampsell, "Electro optical Performance of an Improved Deformable Mirror Device", SPIE Proceedings 825,24 (1987).

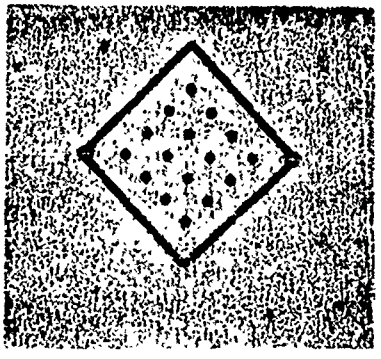

Fig.1a Pixel detail.

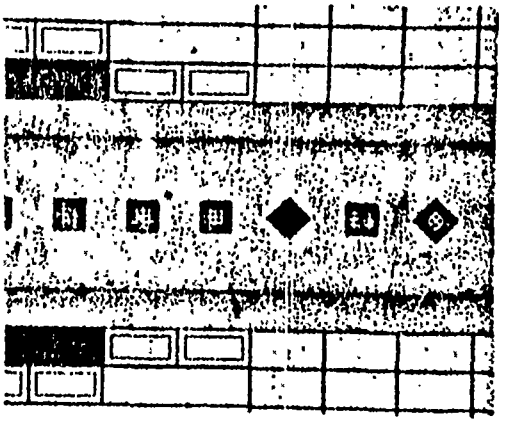

Fig.1b Bright field pixel operation.

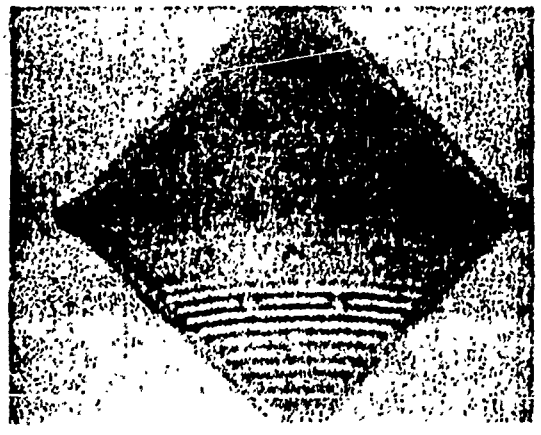

Fig.1d Interferometric detail of deflected pixel.

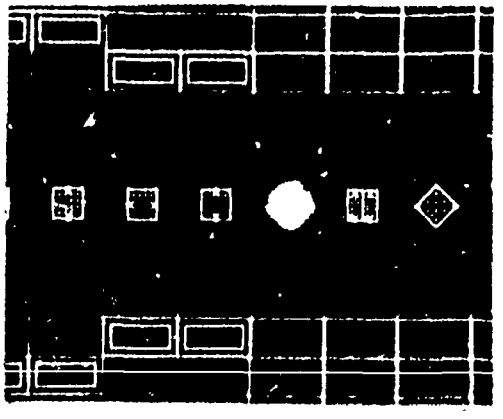

Fig.1c Dark field pixel operation.

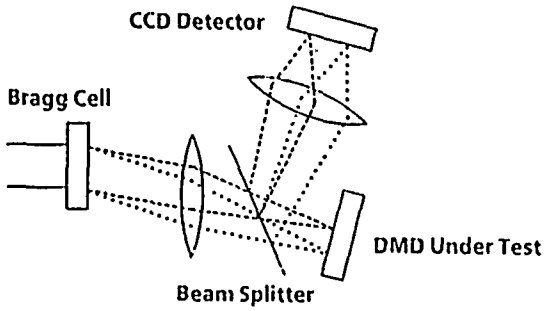

Fig.2a Dynamic range test set up.

Fig.2b CCD image of both pixels on.

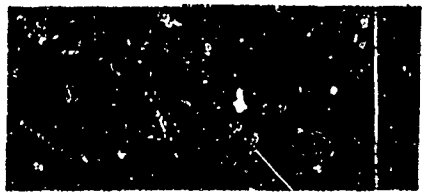

Fig.2c CCD image with one pixel off,

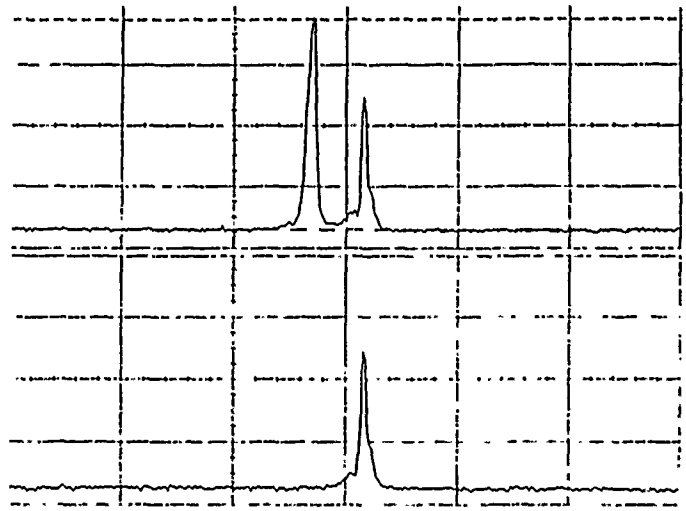

Fig.2d Oscilloscope trace of CCD outputs for Figs 2b and 2c.

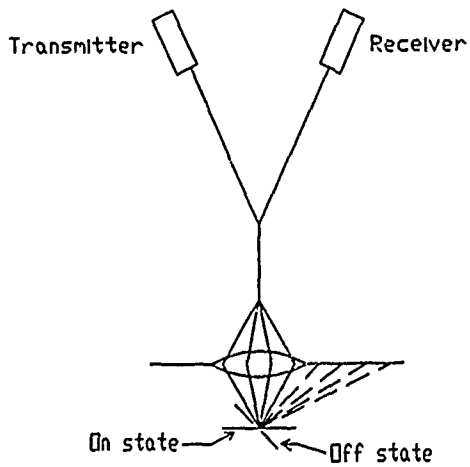

Figure 3. Optical fiber switch using a bifurcated fiber and a DMD.

KEY TO AUTHORS, PAPERS AND PRESIDERS

Adams, M. J. — FD1
Ajisawa, A. — FE4
Akashi, F. — FE1
Amada, E. — FA4
Anderson, R. V. — ThE3
Andrejco, M. J. — ThA3
Arent, D. J. — ThB4
Asher, S. — ThB4
Ashibe, M. — FE1
Azizi, A. — FC4

Banwell, T. C. — ThC4
Bennion, I. — FE3
Berthold, J. E. — WA1
Blumenthal, Daniel J. — FB1
Borghs, G. — ThB4
Boyd, G. D. — ThD4
Boysel, R. Mark — FE6
Brackett, Charles A. — ThE1
Buller, G. S. — FB3

Camlet, J. V. — ThE3
Capron, B. A. — ThB3
Cassidy, S. A. — ThE4
Chbat, Michel W. — FC3
Cheng, S. S. — ThC4, FE
Chirovsky, L. M. F. — ThC5, ThD4
Cinato, Paola — FA2
Cunningham, Jack — ThD5

D'Asaro, L. A. — ThC5, ThD4
Davison, A. S. — ThA4
de Bosio, Alfredo — FA2
Derstine, M. W. — ThB3
Dianov, E. M. — ThE6
Djupsjobacka, Anders — FD4
Drury, D. R. — ThB2
Duthie, P. J. — FE3

Ebeling, K. J. — ThB5, ThD1
Eisenstein, G. — FC1
English, J. H. — ThD2
Erickson, J. R. — ThE2

Falk, Jan-Erik — FE2
Fiddy, M. A. — ThB2
Fouckhardt, H. — ThA3
Fujimoto, N. — FC5
Fujiwara, M. — ThE5, FA3

Giglmayr, J. — ThC3
Giordano, P. P. — ThE3
Goodman, J. W. — WAA, WAA3
Gossard, A. C. — ThD2
Granestrand, Per — FE2
Gustavsson, Mats — FD4, FE5

Hackbarth, T. — ThD1
Hammer, J. M. — ThD6
Hanna, M. — ThB4
Harvey, M. G. — ThB4
Hayes, R. — ThB4
Healey, P. — ThC2, ThE4
Hendricks, H. D. — ThD6
Heritage, J. P. — ThA1
Hinton, H. S. — WAA4
Holm, D. A. — ThB3
Huang, P. C. — ThC4
Hughes, J. — ThB1
Huisman, R. F. — ThE2
Hunter, J. J. — ThB1

Iltaif, A. — ThB1
Inoue, H. — FA4
Ishida, K. — FA4
Itoh, M. — ThE5
Iwasaki, M. — FE1

Jenkins, B. Keith — ThC1
Jewell, J. L. — ThD2
Jones, K. L. — FD5

Kajitani, S. — FE1
Karlsson, Anders — FD4
Kasahara, K. — FA3
Kashimura, S. — FA4
Kato, T. — FA4
Koai, K. T. — FB4
Kobayashi, I. — FA1
Komatsu, K. — FE4
Kondo, M. — FE1
Koren, U. — FD5
Korotky, S. K. — ThA2, FC1, FC4
Kowalsky, W. — ThB5, ThD1
Kuroyanagi, S. — FC2
Kuznetsov, A. A. — ThE6

Leaird, D. E. — ThA3
Lentine, A. L. — ThC, ThC5, ThD4
Livescu, Gabriela — ThD5

MacDonald, R. I. — FD
MacKenzie, H. A. — ThB1
Maier, Alex A. — FD6
Majerfeld, A. — ThB4
Major, K. D. — ThE2
Masuda, S. — FC5
Matson, R. — ThB4
McCall, S. L. — ThD2
McCormick, F. B. — ThC5
McDonald, T. Gus — FE6
McGoldrick, E. — ThD3
Mekada, N. — FC2
Midwinter, J. — WAA
Miller, B. I. — FD5
Miller, David A. B. — WAA2, ThD, ThD4, ThD5
Miyakawa, T. — ThE5
Mizuishi, K. — FA4
Murakami, K. — FC2

Nakagami, T. — ThA
Nefjodov, S. M. — ThE6
Nishimoto, H. — FE1
Nishio, M. — ThE5
Nordin, R. A. — ThE2, FB2
Numai, T. — ThE5

Odagawa, T. — FC2, FD2
Oh, E. G. — ThB4
Ohlander, Ulf — FD3

Pankove, J. I. — ThB4
Parsons, Nick — WA2
Perrier, Philippe — FC3
Port, M. — ThB5
Prucnal, Paul R. — WA4, FA, FC3

Ratajack, M. T. — FB2
Reith, L. A. — ThC4
Rejman-Greene, M. A. Z. — ThD3
Rokugawa, H. — FC2, FC5
Ronaldson, D. — ThB1

Sahlen, Olof — FD3
Saifi, M. A. — ThA3
Salehi, J. A. — ThA1
Sampsell, J. B. — FE6
Sasaki, Y. — FA4
Scherer, A. — ThD2
Scott, E. G. — ThD3
Shikada, M. — FE1
Shimoe, T. — FC2
Shimosaka, N. — ThE5
Silberberg, Y. — ThA3
Sizer, Theodore II — ThD5
Smith, D. W. — ThE4
Smith, Peter — WA, ThA3
Smith, S. D. — FB3
Stephens, W. E. — ThC4
Stern, M. — ThA1
Stoltz, Bjorn — FE2
Su, S. F. — FB4
Suda, D. — ThB4
Sugimoto, M. — FE4
Suzuki, A. — FE4
Suzuki, H. — FA3
Suzuki, S. — ThE5, FA3, FE1
Szmyd, D. M. — ThB4

Takeuchi, T. — FA3
Thompson, R. A. — ThE3
Thylen, Lars — WA3, ThE, FD4, FE2
Tu, C. W. — ThD4
Tucker, R. S. — FC1

Veach, R. S. — ThE2
Veselka, J. J. — ThA2
Voevodkin, G. G. — ThE6
Vogel, Nick — WA2

Wale, M. J. — FE3
Walker, A. C. — FB3
Walker, N. P. — ThB2
Weiner, A. M. — ThA1, ThA3
White, I. H. — ThA4
Whitehead, Nigel — WA2
Wicklund, Goren — WA2

Yamaguchi, K. — FC5
Yamakoshi, S. — WAA1, FC5, FD2
Yasui, T. — FC
Young, M. G. — FD5

Zucker, J. E. — FD5

PHOTONIC SWITCHING

POSTDEADLINE PAPERS

MARCH 1-3, 1989
SALT LAKE CITY, UT

THURSDAY, MARCH 2, 1989, POSTER PRESENTATION, 9:45AM-10:30AM:

PD1
Room Temperature Electroabsorption and Switching in GaAs/AlGaAs Superlattice. P. W. Goossen, I. Bar-Joseph, J. M. Kuo, K. F. Lam, D. A. B. Miller and D. S. Chemla. AT&T Bell Laboratories. We report room temperature observation of Wannier-Stark localization in a GaAs/AlGaAs superlattice and show large modulation and self electro-optic effect over a wide spectral range.

THURSDAY, MARCH 2, 1989, POSTDEADLINE SESSION - ORAL PAPERS:

EACH ORAL PAPER WILL BE GIVEN
8 MINUTES PRESENTATION, 2 MINUTES DISCUSSION

PD2, 8:00PM-8:10PM
Thermally Stable, Optically Bistable AlGaAs Etalon with a Silver Combined Mirror and Heat Sink, E. Masseboeuf, INPG, France; O. Sahlen, U. Olin, Royal Institute of Technology, Sweden; N. Nordell, M. Rask and G. Landgren, Swedish Institute of Microelectronics, Sweden. Room-temperature, low-power and nanosecond switching of bistable AlGaAs etalons with silver mirror/heat sinks, which are thermally stable for half a second, is reported.

PD3, 8:10PM-8:20PM
Vertical Cavity Single Quantum Well Laser, J. L. Jewell, AT&T Bell Laboratories; K. F. Huang, National Chiao Tung University, China; K. Tai, Y. H. Lee, R. J. Fischer, S. L. McCall, A. Y. Cho, AT&T Bell Laboratories. Pulsed and cw optical pumping produce lasing in MBE-grown etalon with 80 Å active material length of In0.2Ga0.8As. Estimated absorptions at threshold are ~12fJ/um2 and ~7uW/um2.

PD4, 8:20PM-8:30PM
Multiple Quantum Well Asymmetric Fabry-Perot Etalons for High-Contrast, Low Insertion Loss Optical Modulation, M. Whitehead, G. Parry, A. Rivers, University College London, United Kingdom; J. S. Roberts, University of Sheffield, United Kingdom. We propose an asymmetric Fabry-Perot cavity modulator, containing quantum wells, to achieve high contrast (>10dB) with less than 3dB insertion loss at ~5-10V bias. Preliminary experimental results are presented.

PD5, 8:30PM-8:40PM

Cascadable Optical Logic Module Using Symmetric Self-Electrooptic Effect Devices, M. E. Prise, R. E. LaMarche, N. C. Craft, M. M. Downs, S. J. Walker, L. A. D'Asaro and L. M. F. Chirovsky, AT&T Bell Laboratories. We describe an optical module which uses arrays of symmetric self electro-optic effect devices (S-SEEDs) to perform cascadable optical logic and describe its performance.

PD6, 8:40PM-8:50PM

A Novel Two Dimensional Perfect Shuffle Network, M. G. Taylor, J. E. Midwinter, University College London, United Kingdom. We will introduce a two dimensional network, a pipeline of two dimensional perfect shuffle interconnections and layers of square 'super exchange' modules.

PD7, 8:50PM-9:00PM

An Opto-Electronic Dynamic Random Access Memory (DRAM) Cell Utilizing a Three Terminal N-Channel Self-Aligned DOES Device, G. W. Taylor, D. L. Crawford and J. G. Simmons, AT&T Bell Laboratories. An opto-electronic DRAM cell is implemented with an N-channel self-aligned DOES in a three terminal configuration. The cell operates with one polarity and achieves XY selectivity with the inversion channel contact and the optical input/outputs.

PD8, 9:00PM-9:10PM

Fiber Polarization Rotation Switch Based on Modulation Instability. C. E. Soccolich, M. N. Islam, AT&T Bell Laboratories. We demonstrate an ultrafast, all optical, active fiber polarization rotation switch based on modulation instability operating near 1.5um, exhibiting contrast ratios up to 40:1 and small signal gains up to 40dB.

PD9, 9:10PM-9:20PM

Optically Controlled Bistable Switching Element Based on Electro-Optic Feedback, J. A. Cavailles, M. Erman, LEP, France. We describe an optically controlled bistable switching device based on a SEED-type electro-optic feedback in a vertical coupler containing Multiple Quantum Wells material.

PD10, 9:20PM-9:30PM

An FDM Coherent Optical Switch Experiment with Monolithic Tunable Lasers Covering a 1,000 GHz Range, F. S. Choa, M. Santoro, T. L. Koch, W. W. Snell and J. Stone, AT&T Bell Laboratories. We report results of an FDM coherent optical switch experiment with monolithic tunable lasers covering 1,000 GHz at 700 Mb/s and with a novel tuned, balanced coherent receiver, establishing feasibility for a 125x125 switch.

PD11
Analytic Expressions for Switching Irradiances of Bi-and Multistable Nonlinear Fabry-Perots, H. Thienpont, I. Van de Voorde, I. Verbesselt, I. Veretennicoff, Vrije Universiteit Brussel, Belgium. Analytic expressions are proposed, allowing accurate determination of the commutation irradiances of nonlinear Fabry-Perots and bringing forward new tools for device characterization and optimization.

PD12
A Novel Light Modulator and Optical Transistor for the Far Infrared Region: A Proposal for a Modulable Mirror, Maarten Kuijk, Roger Vounckx, Vrije Universiteit Brussel, Belgium. It is shown that the reflection properties of two-dimensional electron gases in III-V semiconductors can be used to build picosecond far infrared switches and invertors.

PD13
Reduced Waveguide Intersection Losses for Large Tree Structured Ti:LiNbO3 Switch Arrays, T. O. Murphy, AT&T Bell Laboratories; F. Hernandez-Gil, Telefonica, Spain; J. J. Veselka, S. K. Korotky, AT&T Bell Laboratories. Using the Beam Propagation Method, geometries have been found which lower losses in the waveguide intersections required of tree-structured Ti:LiNbO3 switch arrays. We fabricated these geometries and measured a reduction in attenuation as high as 50%.

Room Temperature Electroabsorption and Switching in GaAs/AlGaAs Superlattice

K.W. Goossen, I. Bar-Joseph, J.M. Kuo, R.F. Kopf, D.A.B. Miller and D.S. Chemla
AT&T Bell Labs, Holmdel, NJ

Quantum well (QW) based optoelectronic devices have been rapidly evolving in the last few years. The observation of the quantum confined Stark effect, which gives an absorption edge red shift with an applied electric field[1], was followed by numerous device demonstrations, especially reverse - biased p-i-n diode light modulators at both near infra-red and longer wavelengths[2]. It was also shown that the same structure can function as an optical logic switching gate, the self-electro-optic device (SEED)[3].

Bleuse et al. have recently predicted that interesting behavior should occur when an electric field is applied in the growth direction of a superlattice (SL)[4], a structure with thin barriers between the QWs[5]. Because of the potential drop across the SL the resonant tunneling process is turned off and the delocalized SL electronic wave function becomes localized. The manifestation of this phenomenon, which is called Wannier-Stark localization, is a change of the absorption edge from a broad line shape, associated with the delocalized conduction miniband, to a sharp QW-like excitonic shape, associated with the localized state. The position of the new absorption edge with field is at approximately the center of the broad miniband absorption edge without field. It corresponds therefore to an effective blue shift of the absorption edge. The field needed to localize the electrons is given by $F_{loc} \approx \Delta/ed$ where Δ is the miniband width and d is the superlattice period. At smaller fields a formation of a Stark ladder and steps in the absorption spectrum was predicted. These steps are caused by absorption from a hole state, which localizes at very low fields, to electron states in adjacent wells. They are separated by $n\times(eFd)$, where F is the electric field and n is an integer index. Correspondingly, absorption from a hole state into the nearest well are labeled as ± 1 and so forth. These steps should shift linearly with the fields away from the main absorption peak which is direct in real space.

These predictions were fully confirmed in GaAs/AlGaAs SL using low temperature photoconductivity,[6] photoreflectivity[7] and resonant Raman[8] measurements, and in InGaAs/InP SL using transmission measurements[9]. In this paper we study this effect at room temperature using both photo-conductivity and transmission measurements. We report the first room temperature observation of Wannier-Stark localization. We show that a large modulation can be obtained over a substantial spectral range and demonstrate the operation of a blue-shift SEED.

The sample was grown on an n+ GaAs substrate followed by a 1.3 μm $Al_{0.3}Ga_{0.7}As$ n doped layer. The intrinsic region is composed of a 100 period superlattice of undoped 30 Å GaAs wells and 30 Å $Al_{0.3}Ga_{0.7}As$ barriers. Two buffer layers of 500 Å undoped $Al_{0.3}Ga_{0.7}As$ separate the superlattice at both the n and the p sides. Then 0.5 μm p doped and 0.3 p^+ doped $Al_{0.3}Ga_{0.7}As$ layers were grown, followed by a 1000 Å GaAs p^+ contact layer. The wafer was processed to form square mesas of $200\times200\mu m^2$. It was then bonded and epoxied to a sapphire substrate using transparent epoxy, and a large hole was etched through the GaAs substrate to the AlGaAs which acted as a stop etch layer.

The photocurrent spectra under electric field at room temperature are shown in Fig. 1. The transition from a broad to a sharp absorption edge is evident. As the voltage is increased the Stark ladder peaks -1 and -2 are clearly observed and they shift linearly with the voltage away from the 0 peak. Also observed is the formation of a sharp exciton at the 0 peak. Comparing the results at 0 and 10 V shows a net "blue shift" of the absorption edge, with some residual absorption below the high field edge, originating from the -1 and -2 peaks. This residual absorption decreases only slightly beyond 10 V.

Simulations of the absorption are in a qualitative agreement with these results. Although the heavy holes are strongly localized in one period for fields larger than $\approx 2\times10^3$V/cm , electrons only become strongly localized for fields larger than $\approx 8\times10^4$V/cm , which is approximately the field at which the central peak becomes dominant in the spectra. The simulations also show, however, that the electron wavefunction is not fully localized in one period even at these fields, confirming the experimental observation that there is still residual absorption at high voltages for the -1 and -2 peaks.

At high fields, when both electrons and holes are localized, the optical transitions show clear excitonic enhancement, reminescent of that seen for quasi-2D excitons in QW structures. However, for transitions other than the direct (0) transition, the centroid of the electron wave function is spatially separated from the hole wave function, so that we observe a reduced correlation.

At low fields the excitonic features significantly decrease, until at 0 V they hardly exist. The built-in field across the junction is $2.7X10^4$V/cm. At such a field the holes are localized while the electrons are not, so that the excitons are easily ionized.

We determined the actual absorption changes with field by applying a square-wave voltage modulation between 0 V and a certain reverse bias V, and measuring the corresponding transmission changes with a lock-in. Figure 2 shows such a spectrum for V=-10 V. The large transmission increase near 750 nm corresponds to the blue-shift of the absorption edge. The negative peak at 730 nm is due to the QW exciton formed at high fields, and the one at 770 nm is due to residual absorption from the -1 Stark ladder transition.

The complex changes of the absorption spectrum with field cause the differential transmission spectra to be much different at lower values of V. This is reflected in the nonlinear behavior of the modulation response with field, shown in Fig. 3 for 750 nm. There is a slow increase until V=5 V, where the response increases sharply. Above 10 V there is again a slow increase. The value of $\Delta T/T_0$ for 15 V, which is 0.37, corresponds to $\Delta alpha = 7700 cm^{-1}$. It can be projected then that a 1 μm SL structure would yield a 2:1 modulation ratio for V=-20V. The sharp rise at medium voltages could be exploited to generate a large modulation for a small voltage swing.

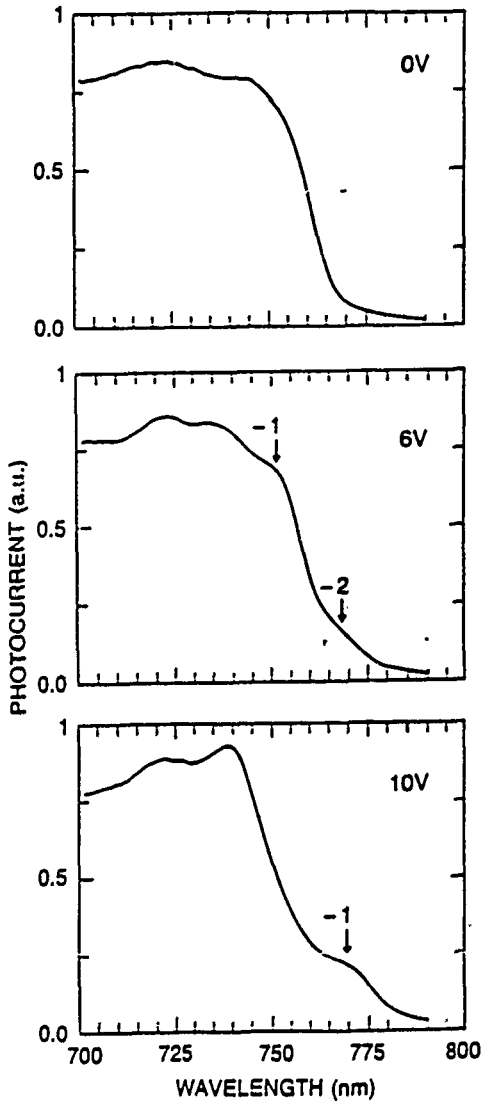

Figure 1: Room temperature photocurrent spectra for 0, 6, and 10 V.

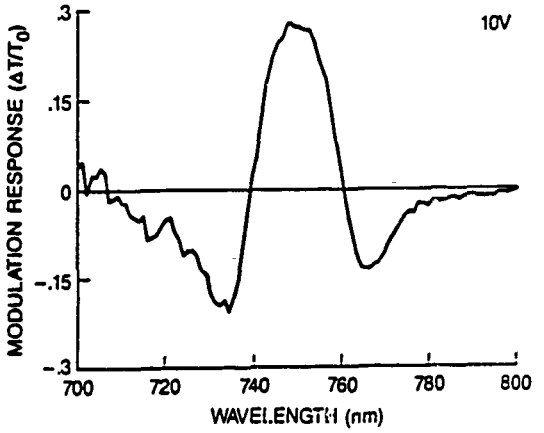

Figure 2: Modulation response ($\Delta T/T_0$) as a function of wavelength for a square wave modulation between 0 V and -10 V (T_0 is taken to be the transmission at 0 V).

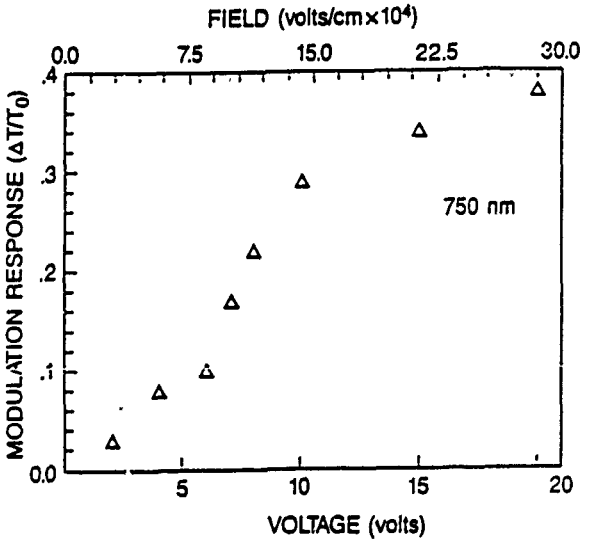

Figure 3: Response ($\Delta T/T_0$) for a square wave between 0 V and the voltage of the ordinate.

The decreased absorption near 750 nm yields a decrease in the photocurrent and therefore a negative differential resistance. This behavior can be used to construct a logic element, similar to the self electro-optic device (SEED), which is based on a blue shift[10] rather then the red shift associated with the quantum confined Stark effect. We connected the SL diode in series with a silicon photodiode which when illuminated with white light acted as a current source load. We used a tungsten lamp and a 0.22 m SPEX spectrometer as a monochromatic illumination source for the SL diode. Figures 4a and 4b shows the bistable behavior for different wavelengths and voltages, respectively. It can be seen that bistability is obtained over a wide spectral range and is almost constant between 745 and 755 nm. Clear bistability is observed at 8 V and there is not much change beyond 15 V.

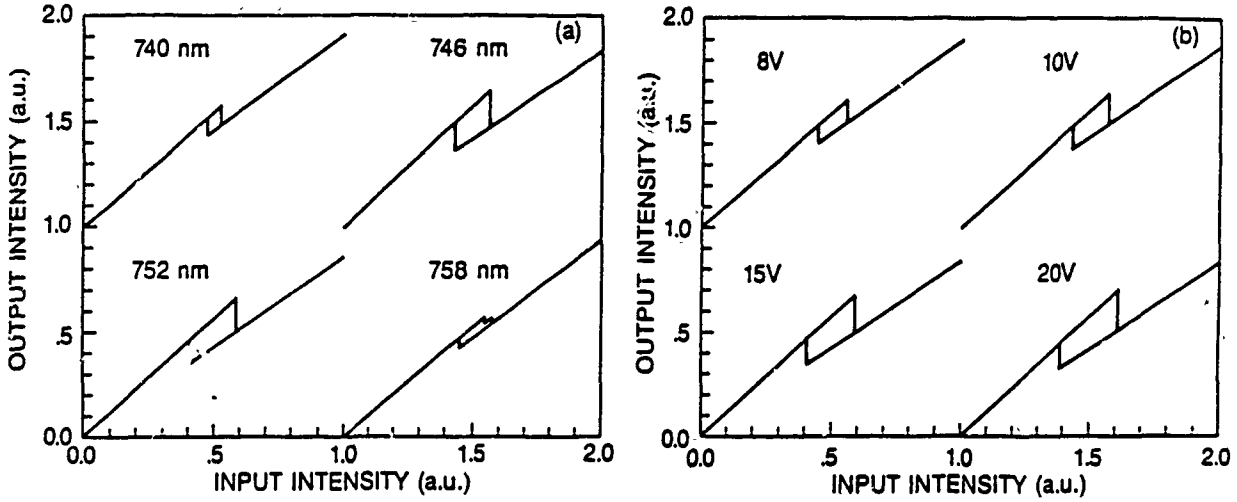

Figure 4: Output intensity vs. input intensity for (a) several wavelengths and (b) several voltages.

One potential advantage of these structures compared to QW modulators is that it may be easier to sweep carriers out of the structure because of the lower effective barriers for tunneling and thermionic emission. This may reduce problems resulting from saturation and space charge build-up due to holes accumulation, that can prevent high power operation of modulators and high speed operation of SEED's. The superlattice electroabsorption may also give a larger usable spectral bandwidth because it relies less on sharp exciton resonances.

References

[1] D.A.B. Miller, D.S. Chemla, T.C. Damen, A.C. Gossard, W. Wiegmann, T.H. Wood and C.A. Burrus, Phys. Rev. B 32, 1043 (1985).

[2] T.H. Wood and C.A. Burrus, D.A.B. Miller, D.S. Chemla, T.C. Damen, A.C. Gossard and W. Wiegmann, IEEE J. Quantum Electron. QE-21, 117 (1985), U. Koren, B.I. Miller, T.L. Koch, G. Eisenstein, R.S. Tucker, I. Bar-Joseph and D.S. Chemla, Appl. Phys. Lett. 51, 1132 (1987).

[3] D.A.B. Miller, D.S. Chemla, T.C. Damen, T.H. Wood, C.A. Burrus, A.C. Gossard and W. Wiegmann, IEEE J. Quantum Electron. QE-21, 1462 (1985).

[4] J. Bleuse, G. Bastard and P. Voisin, Phys. Rev. Lett. 60, 220 (1988).

[5] L. Esaki and R. Tsu IBM J. Res. Dev. 14, 61 (1970).

[6] E.E. Mendez, F. Agullo-Rueda, and J. M. Hong Phys. Rev. Lett. 60, 2426 (1988).

[7] P. Voisin, J. Bleuse, C. Bouche, S. Gaillard, and C. Alibert, Phys. Rev. Lett. 61, 1639 (1988).

[8] F. Agullo-Rueda, E.E. Mendez and J. M. Hong, Phys. Rev B (Rapid Commun.), 38, 12 720 (1988).

[9] J. Bleuse, P. Voisin, M. Allovon and M. Quillec, Appl. Phys. Lett. 53, 2632 (1988).

[10] D.A.B. Miller, Appl. Phys. Lett. 54, 202 (1989).

THERMALLY STABLE, OPTICALLY BISTABLE AlGaAs ETALON WITH A SILVER COMBINED MIRROR AND HEAT SINK

E. Masseboeuf (*), O. Sahlén, U. Olin, N. Nordell (**), M. Rask (**) and G. Landgren (**).

Institute of Optical Research and Department of Physics II, Royal Institute of Technology, S-100 44, STOCKHOLM, SWEDEN

(*) Permanent address: Laboratoire d'Electromagnetisme Microonde et Optoelectronique, INPG, Grenoble, France.

(**) Swedish Institute of Microelectronics, P. O. Box 1084, S-164 21 KISTA, SWEDEN.

1. Introduction.

Bistable étalons of GaAs and related materials have been extensively studied for use in parallel optical processing. The devices studied so far are not well suited for applications, since they are not thermally stable. We have developed a theoretical model which allows the optical and thermal properties to be simultaneously optimised. In this paper we report on experiments with nonlinear AlGaAs étalons, designed with that model, that are thermally stable for half a second, optically bistable with 10 mW input power, and rely on the electronic nonlinearity with switching times of about 10 ns. The devices have been fabricated with argon ion sputtering followed by deposition of a three micrometer thick silver layer which acts as a combined heat sink and high reflecting mirror.

2. Background.

A common problem with nonlinear semiconductor devices relying on a plasma induced fast nonlinearity is that the electronic effect is counteracted by a slow thermal nonlinearity, caused by heating due to non-radiative recombination of holes and electrons. One such device is the bistable étalon of GaAs [1], where the competition between electronic and thermal nonlinearities lead to regenerative pulsations [2] if the device is left in the ON state for many microseconds. The operating wavelength also depends on the thermal load and hence on the duty cycle. From the practical point of view this is not acceptable: It must be possible to operate them with arbitrary bit patterns and at arbitrary duty cycles without any changes in the transfer characteristics due to heating.

Improvements have recently been reported concerning the thermal properties of AlGaAs étalons operating in reflection with epitaxial Bragg reflectors as mirrors. 200 µs thermal stability in optically bistable mode [3] and several ms stability in differential gain mode [4] have been reported. However, the devices were not truly thermally stable.

3. Fabrication of étalons.

Our new devices have been fabricated starting from a MOVPE-grown structure, consisting of a 20 period buffer superlattice (5 nm GaAs / 5 nm AlAs) first grown on a GaAs substrate, followed by 0.5 µm AlAs, an 18-period Bragg reflector of alternating AlAs/$Al_{0.1}Ga_{0.9}As$ quarter-wave layers designed for 830 nm, 50 nm $Al_{0.3}Ga_{0.7}As$, a 2.5 µm $Al_{0.06}Ga_{0.94}As$ nonlinear spacer layer, 0.5 µm $Al_{0.3}Ga_{0.7}As$ and a final 5 nm GaAs cap layer.

Pieces were cut from the wafer and put in a vacuum chamber. The cap and about half of the $Al_{0.3}Ga_{0.7}As$ layer were removed by argon ion sputtering. Without breaking the vacuum, a 3 µm silver layer was subsequently evaporated. The devices were then soldered with indium to a copper mount, plane polished to less than a few fringes. The In thickness was less than 20 µm. The substrate was removed by grinding and selective etching.

The resulting étalon consisted of the nonlinear $Al_{0.06}Ga_{0.94}As$ layer between the back silver mirror and the front epitaxial Bragg reflector. The crucial step is to get a high reflectance at the semiconductor - metal interface and at the same time good sticking of the silver to the semiconductor structure. Several other methods, such as evaporating thin "glue" layers of Ti or Cr failed, due to reduced reflection.

4. Thermally stable, optically bistable operation.

Figure 1 shows bistable switching in reflection of such an étalon, at 842 nm (at room temperature), with a 140 μs long input pulse. It was carefully checked that the switching was due to the electronic nonlinearity, both by examining the (negative) sign of the nonlinearity, and the switching speed (about 10 ns). Figure 2 shows switching of the same device with a 1000 times longer pulse (140 ms), without any change in sample position, ambient temperature, operating wavelength or average duty cycle. The oscilloscope settings are identical in Figures 1 and 2 when recording the input power - reflected power hysteresis loop. It is seen that no regenerative pulsations occur, that the device is truly bistable even on this long time scale and that the hysteresis loop is almost identical to the one with a short input pulse.

Figure 3 shows the input power - reflected power characteristic for a 50 μs long input triangular pulse, with low and high duty cycles. The two curves are almost identical, with the same oscilloscope settings and without any change of other operating parameters than the duty cycle.

5. Comparison with theory.

The devices have been fabricated on basis of a recent theoretical study of heat flow and thermal optimisation of GaAs étalons [5]. We have developed a numerical model which makes it possible to solve the coupled, nonlinear system of the wave equation (including diffraction), carrier diffusion equation and heat equation in steady-state, for an arbitrary layered metal - semiconductor - dielectric structure, with proper boundary conditions at each interface. To model the optical nonlinearity we have implemented the carrier- and temperature dependent plasma theory of Banyai and Koch [6].

Results from that study clearly points to the necessity to avoid all thermal barriers between the nonlinear spacer layer and the heat sink, and to use a mirror with highest possible thermal conductivity (silver has 9 times larger thermal conductivity than GaAs). One must avoid thick layers of AlGaAs, which has much lower thermal conductivity than the binary constituents. The calculations predict less than 1 K temperature rise in the structure which we have fabricated, which proves to be sufficient to avoid regenerative pulsations. This is a factor 2-3 lower than in conventional all-epitaxial étalons without metal mirror/heat sink, which are not thermally stable.

The method which we have presented here is suitable for fabrication of large arrays of bistable elements, in which case forced cooling should be applied to the back of the silver layer (which, if required, could easily be made thicker by electroplating or other methods). The results should also be applicable to other materials and other types of nonlinear semiconductor devices.

---

1. H. M. Gibbs, Optical Bistability: Controlling Light with Light, Academic Press, New York 1985.

2. J. Jewell, H. M. Gibbs, S. S. Tarng, A. C. Gossard, W. Wiegmann, Appl. Phys. Lett., 40, 291 (1982).

3. O. Sahlén, E. Masseboeuf, N. Norrell, M. Rask, G, Landgren, Appl. Phys. Lett., 53, 1785 (1988).

4. R. Kuszelewicz, J. - L. Oudar, J. C. Michel, R. Azoulay, Appl. Phys. Lett., 53, 2138 (1988).

5. U. Olin and O. Sahlén, submitted to Optics Letters.

6. L. Banyai and S. W. Koch, Z. Phys. B, 63, 283 (1986).

20 microseconds / division

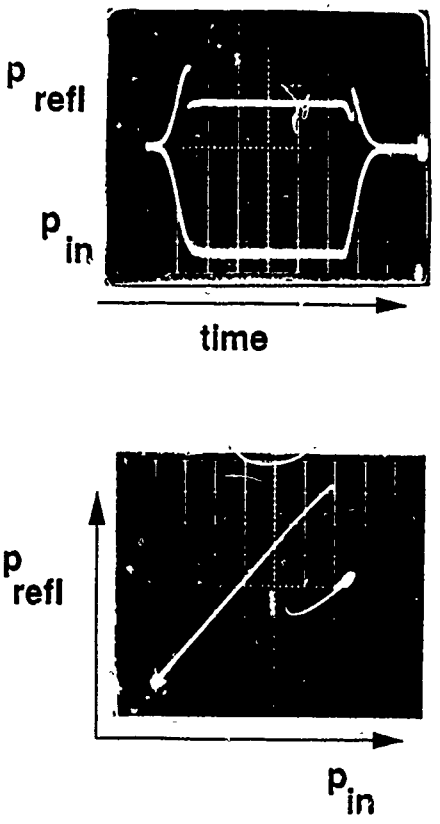

FIGURE 1

20 milliseconds / division

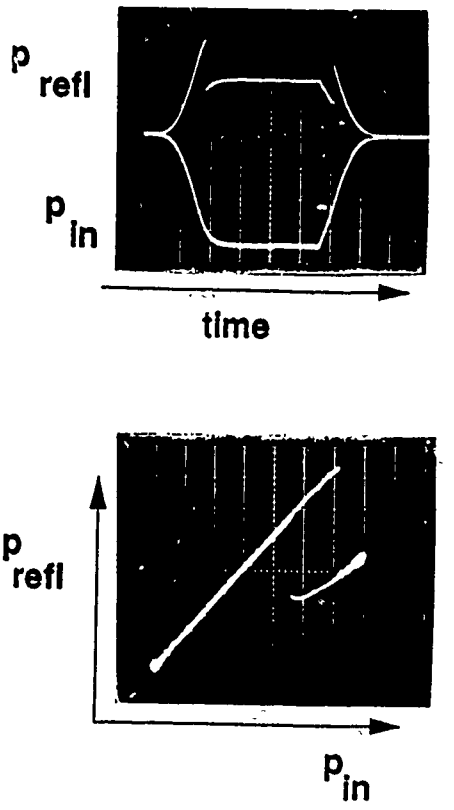

FIGURE 2

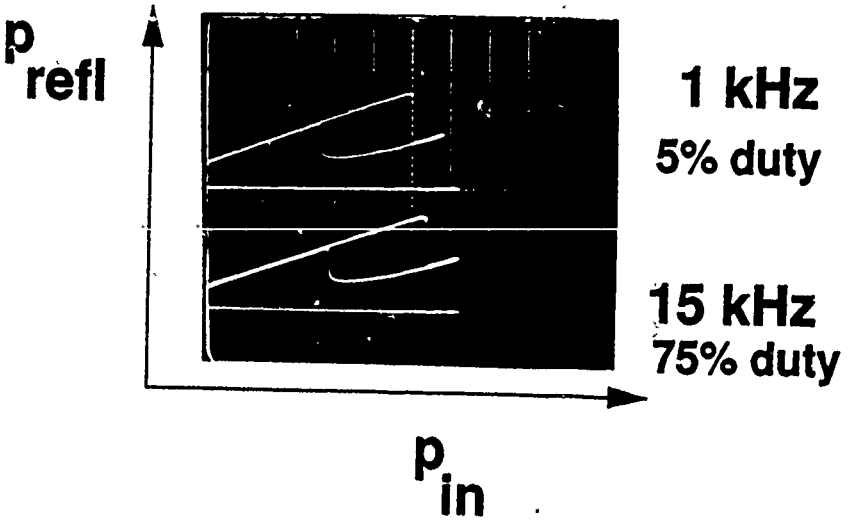

198

FIGURE 3

Vertical Cavity Single Quantum Well Laser

J.L. Jewell, K.F. Huang[a], K. Tai[b], Y.H. Lee,
R.J. Fischer[b], S.L. McCall[b], and A.Y. Cho[b]

AT&T Bell Laboratories, Rm. 4G-520, Holmdel, NJ 07733 U.S.A.

We report room-temperature pulsed and cw lasing at 980 nm in an optically-pumped vertical cavity structure grown by molecular beam epitaxy (MBE) containing a single quantum well (SQW) of $In_{0.2}Ga_{0.8}As$. Limited gain due to the extremely short active material length of 80 Å implies that losses due to absorption, scattering and mirror transmission are extremely low. Pulsed excitation yielded a threshold with an estimated absorbed average energy density in the spacer ~ 12 fJ/μm^2, implying a carrier density in the SQW about 4 times the density for "transparency" of about 1.3×10^{12} cm^{-2}. In cw experiments the estimated average absorbed power density at threshold was ~ 7 μW/μm^2 and the internal slope efficiency was ~ 33 %. The carrier densities per QW are similar to those in previous multiple QW lasing experiments. The very low energy and power densities here are the result of reducing the number of wells to just one, and increasing finesse to a high enough level to permit lasing.

The MBE-grown structure is shown in Fig. 1. All layers are nominally undoped. The bottom mirror is designed to be more transmissive so more than half the light should exit into the substrate. The InGaAs SQW should be elastically strained since it is well below the critical thickness of ~ 200 Å. GaAs/AlAs resonators with $In_xGa_{1-x}As$ QW are interesting for optical device applications since the typical operating wavelengths of 950-1000 nm are almost as short as for GaAs QW, yet the GaAs substrates are transparent.

The unetched wafer was pumped through the top mirror by a synchronously-pumped mode-locked dye laser emitting ~ 10 ps pulses tunable from about 900-920 nm. The beam was focused by a 5× microscope objective. We also used an unmodulated cw dye laser to pump at 860 nm. Pulsed measurements were carried out with the pump wavelength in two regions where the mirror reflectivity was low about 860 (880) nm which is above (below) the GaAs bandgap energy. With the pump photon energy above the GaAs bandgap energy, the top mirror absorbed about 80% of the incident energy. The spacer absorbed ~ 23% of the light which had transmitted through the top mirror and the rest was absorbed in the bottom mirror and substrate. Thus, neglecting reflections, the absorption in the spacer was only ~ 4.6% of the incident beam. The carriers generated must then cool and be trapped in the InGaAs QW. This pumping efficiency is still much larger than a similarly estimated ~ 1.6% absorption in the QW only, due to pumping below the GaAs bandgap. The incident energy required for lasing was about 2.7 times larger with below-gap than for above-gap pumping, thus our calculations are consistent. Both calculations tend to overestimate the carrier density in the lasing region of the QW since many carriers are generated outside the lasing area and a significant number of them will be in the GaAs barriers. For cw operation we use the ~ 4.6 % pump efficiency since the pump is above the GaAs bandgap. Possibilities of multiple reflections which might enhance the pump efficiencies were extensively investigated and compared with experimental variations in the incident pump energy when changing the pump wavelength. The results indicate that any such possible enhancement would be of a factor much less than two.

Fig. 2 shows an output/input characteristic with a threshold of 100 pJ incident or ~ 4.6 pJ absorbed in the spacer (above the GaAs bandgap). Minimizing the threshold required *defocusing* the pump beam from its minimum spot size, due to finesse and area requirements imposed by the small gain and mirror structure. We estimate a maximum gain-length product

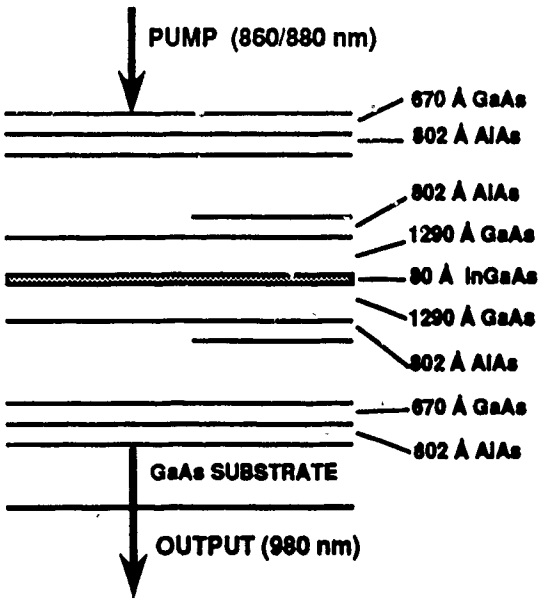

Figure 1. Schematic of the MBE-grown SQW resonator.

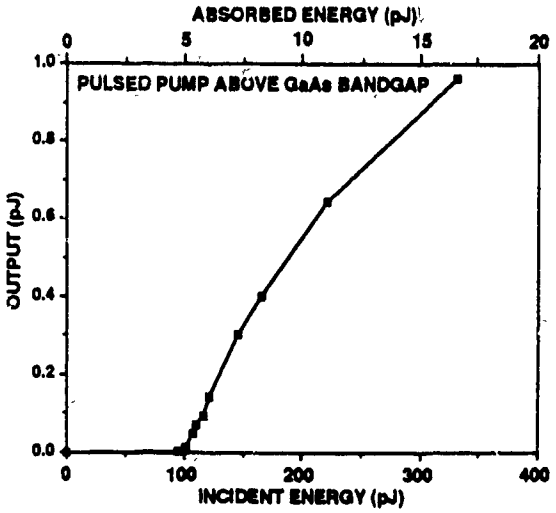

Figure 2. Output through the bottom mirror vs. incident input and estimated absorbed input for pulsed pumping at 860 nm.

of 3×10^{-3} for the SQW, thus the cavity losses must be smaller than $\sim$0.3 %. The calculated mirror reflectivities are both above 99.9% neglecting diffraction losses. Because there are no waveguiding structures (e.g. microresonators) such small loss cannot be attained in a small diameter. For a cavity loss per pass of $\sim$ 0.002 the SQW etalon needs about 430 μm^2 area which is larger than the diffraction limit of the focused pump beam. Thus we expect lower thresholds when carriers are directly injected into the optimum area by defocusing. The actual area of the lasing region for Fig. 2 was calculated by measuring the angular divergence of the output beam, and was about 400 μm^2 for the whole lasing region. Thus the absorbed energy density averaged over the lasing area is <12 fJ/μm^2 creating an average carrier density $\sim 5 \times 10^{12}$ cm^{-2}. Even if all the carriers fell into the SQW, the density was only $\sim$4 times that required for transparency. It is quite possible that less than half this density actually existed inside the SQW. The data indicates a $\sim$14 % internal single-face slope efficiency which is higher than for previous lasers pumped by picosecond pulses. Pumping below the GaAs bandgap at 880 nm yielded a threshold of 270 pJ incident, or $\sim$4.3 pJ absorbed. Our estimates of the absorbed energies for above and below gap pumping are thus consistent to <7 %.

Other interesting effects were seen when we focused the pump beam more tightly. A high density of carriers is generated in an area too small to permit lasing as discussed above. However if enough of them are created, over a period of time they will diffuse outward eventually filling a sufficiently large region and if their density is still high enough, lasing should occur. It should have a reduced output however due to carrier losses during this diffusion time. This is exactly what we see. Fig. 3 shows that this delay can be more than 1 ns. It also shows a $\sim$150 ps minimum delay between the pump pulse and the output pulse. Since the cavity buildup time is only $\sim$10 ps and the carriers are trapped[11] in the well in $\sim$6 ps, we attribute this delay to the gain build-up time of the low-gain high-reflectivity cavity. The $\sim$150 ps delay was essentially constant with input energies ranging from $\sim 1.2\times$ to $>4\times$ threshold.

Continuous pumping yielded results consistent with the pulsed experiments. Fig. 4 shows a $\sim$45 mW cw threshold incident on the device, or about 2 mW of the 860 nm pump absorbed. The lasing area was $>300\ \mu m^2$ so $<7\ \mu W/\mu m^2$ was absorbed. The internal slope efficiency was $\sim$33 %, much larger than in the pulsed case. This may be largely due to more efficient use of the carriers in cw operation, and loss mechanisms in the pulsed case such as recombination during the 150 ps delay.

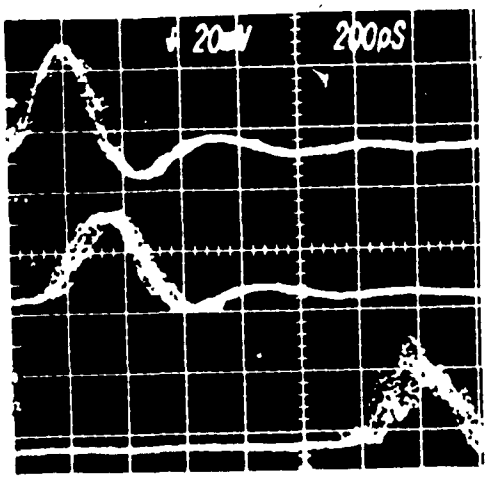

Figure 3. Triple exposure (all at 200 ps/div) showing the times of the pump pulse (upper), minimum-delay output (middle), greatly-delayed and reduced output (lower). The pulse widths on the oscilloscope indicate the response of the avalanche photodiode. The large >1 ns delay results from focusing the pump beam too tightly.

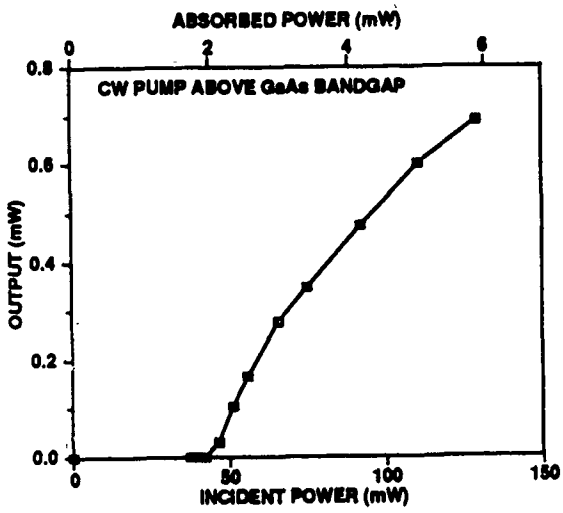

Figure 4. Output (bottom mirror) vs. incident input and estimated absorbed input for cw pumping at 856 nm.

Thermal effects did not appear to play any important role, probably because the lasing wavelength is far from the absorption band of GaAs. By using an acousto-optic modulator we were able to observe lasing in the absence of heating. The threshold actually *decreased* slightly, <5 %, when the device heated up. This is likely due to some thermal lensing created by the temperature gradient. With 40 mW average power incident above the GaAs bandgap (10 kW/cm^2) the laser heated enough to change its peak wavelength by $\sim$5 Å.

In conclusion we have demonstrated room-temperature lasing in a vertical cavity SQW resonator under both pulsed and cw optical pumping. Gain limitations of the 80 Å active material length place an *upper* limit of the cavity losses due to absorption, scattering and mirror transmission at less than $\sim$0.003 per pass in the MBE-grown resonator. This was achieved in the strained $In_{0.2}Ga_{0.8}As$ system where the substrate is transparent at the lasing wavelength of $\sim$980 nm. Since the active material thickness is well inside the quantum size regime, this SQW etalon represents the smallest quantum thickness of active material attainable. The large area of $\sim 400\ \mu m^2$ can be reduced considerably by forming microresonators. Resulting devices should have very low energies. It will be important to determine how small a microresonator can maintain such a high finesse since the required energy (or current for electrical pumping) is proportional to the cross-sectional area divided by finesse. A 1-μm diameter SQW microlaser electrically pumped would have a current threshold $<10\ \mu A$ if cavity losses and surface recombination are kept low.

Multiple Quantum Well Asymmetric Fabry-Pérot Etalons for High-Contrast, Low Insertion Loss Optical Modulation.

M.Whitehead, G.Parry and A.Rivers,
Department of Electronic and Electrical Engineering,
University College London, London WC1E 7JE, U.K.

J.S.Roberts,
Department of Electronic and Electrical Engineering,
University of Sheffield, Sheffield S13 3JD, U.K.

INTRODUCTION:

Multiple quantum well (MQW) optical modulators have been shown to offer improved performance over devices based on bulk semiconductors. For a simple transmission modulator operating at normal incidence one can typically obtain a contrast of 3dB [1,2], with about 10V bias across 1μm of GaAs quantum wells. Improved contrast ratios can be achieved in two ways, the first being the use of thicker MQW active layers [3], the second method being the introduction of high reflectance layers into the structure to effectively increase the optical path length to a double [4] or multiple traversal in a high-finesse Fabry-Pérot (F-P) cavity [5,6]. Devices demonstrating contrasts of up to 10dB have so far suffered from large insertion losses [3,4] due to background absorption, and/or have required bias voltages of 17-25V [3,5,6], which are disadvantageous when considering the integration of modulators with VLSI circuits for optical interconnects. High finesse devices so far have been designed to use the electro-refractive effect in MQWs. However, the effect of background absorption is very difficult to avoid or compensate for, which means that the devices have to operate at wavelengths well away from the excitonic absorption edge in order to maximise contrast. Thus the modulating effect of electro-refraction is somewhat diminished.

In this paper we propose an *asymmetric* F-P cavity modulator (AFPM), with low front reflectivity and high back reflectivity, which by resonant MQW *electro-absorption* may achieve better than 20 dB contrast and less than 3dB insertion loss at 10-12V bias. With adaptations to the basic structure the AFPM should provide 10-15dB contrast with as little as 5V bias voltage.

DESCRIPTION OF DEVICE OPERATION:

By a simple manipulation of the equations governing the spectral response of an absorptive F-P cavity it is possible to determine the amount of absorption required to bring the reflectivity at resonance to zero - the closer to zero the higher the possible contrast. With cavity front and back reflectivities R_f and R_b, absorption α and absorber (MQW) thickness d, we find:

$$\alpha d_{R=0} = 0.5 \ln (R_b/R_f) \quad \text{.....(1)}$$

which, for $R_f = 0.30$ and $R_b = 0.95$, gives us $\alpha d \approx 0.58$. Using the electro-absorptive properties of MQWs it should be possible to increase αd from a value close to zero to satisfy the above condition. Furthermore, in the limit of zero absorption, the resonant reflectivity for the asymmetric cavity remains high at ≈0.83. Thus we have the means of achieving high contrast modulation without incurring high insertion loss. By using electro-absorption and operating close to the absorption edge the device makes optimum use of the field-induced effects in MQWs. The construction of the device is less complex than previous resonant modulators as only one multilayer reflector stack need be grown and the front reflectivity is simply and accurately defined by the semiconductor:air interface.

The response of the proposed device has been simulated using a model which combines the electro-absorptive and electro-refractive properties of a 100Å GaAs well/100Å $Al_{0.3}Ga_{0.7}As$ barrier MQW structure with standard F-P equations. The method is described in detail elsewhere [7]. Figure 1 shows the calculated biased and unbiased spectra for a device with $R_f = 0.3$ and $R_b = 0.95$, and 12V bias across 1.2μm of MQWs. In this case the cavity length has been optimised so as to give the maximum contrast for <3dB insertion loss. At 862.8 nm the contrast is more than 23dB (230:1) and the insertion loss ≈2.6dB.

The high contrast region has a FWHM of ≈2nm. Just as for high-finesse symmetric F-P structures, the cavity thickness must be accurately controlled to optimise the contrast; if the resonant wavelength is too close to the absorption edge then insertion loss increases significantly; if too far away, higher biases are required to push the absorption to longer wavelengths, at which it may no longer be strong enough to meet the critical αd condition. The effect on contrast of varying the device cavity length at a fixed bias voltage is illustrated in figure 2. As cavity length varies, the wavelength of maximum contrast varies accordingly The device parameters are the same as for figure 1. The wavelength range represents ≈400Å change in cavity length. Better than 10dB contrast for <3dB loss is obtained over ≈7nm.

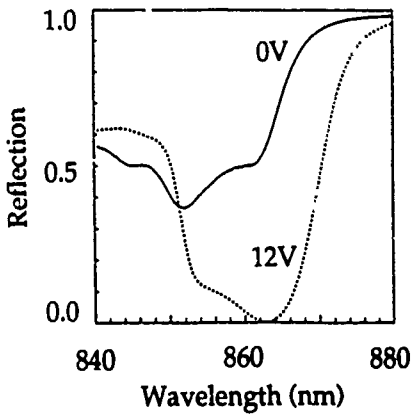

Fig.1 (left):
Calculated on:off reflection spectra for AFPM (R_f=0.30, R_b=0.95) with 1.20μm of MQW and 12V bias. Cavity length is set to make device operate at 862.8nm.

Fig.2 (right):
Variation of contrast and insertion loss with operating wavelength for AFPM as in fig.1.

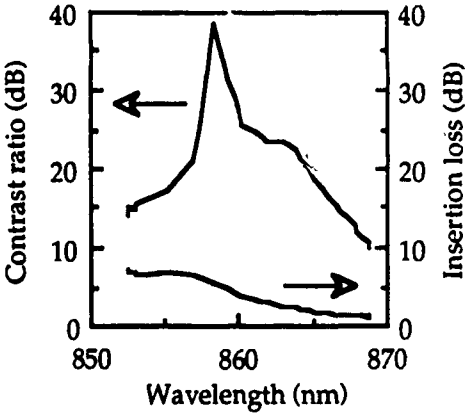

EXPERIMENTAL RESULTS:

Epitaxial integration of a back reflector stack within the MQW p-i-n structure would be the most suitable way of fabricating the AFPM. However, in order to demonstrate the basic operating characteristics of the device, we have modified existing MQW p-i-n transmission modulators [2] by applying a highly reflective gold coating to the back surface, leaving the natural semiconductor:air reflectivity at the front. This provides a thin asymmetric cavity (<3μm) close to the specification above. The MQW structure was grown by MOVPE and contained 50 x 90Å GaAs quantum wells with 60Å $Al_{0.3}Ga_{0.7}As$ barriers. The complete structure was in no way optimised, however the reflectivity modulation which was achieved was a significant improvement on previous results in terms of contrast per volt. Figure 3 shows the on:off spectra for the optimum bias of 7.6V. At 861nm the contrast is 6dB (4:1) and the insertion loss ≈2.4dB. Resonant reflective modulators containing 80-100 quantum wells, which have given contrasts up to 9dB [5,6], have required more than twice the bias of the AFPM.

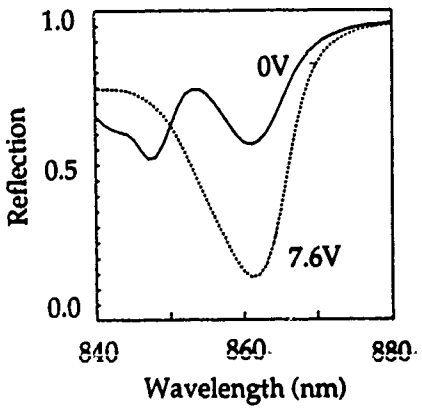

Fig.3 (left):
Measured on:off reflection spectra for test AFPM at optimum bias.

Fig.4 (right):
Simulation of the on:off characteristics for test AFPM. Cavity length is set so that the resonance is the same distance from the MQW absorption peak as in fig.3.

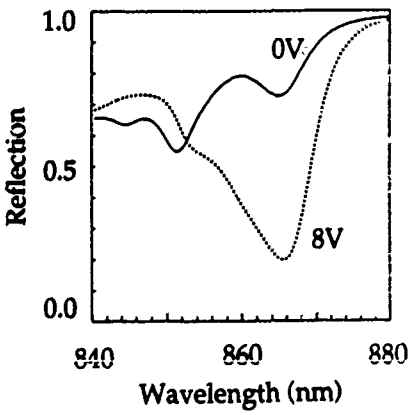

We find very good agreement between the experimental results and the modelled response of our test structure, which is displayed in figure 4. The contrast achieved is limited by there being insufficient MQW material in the cavity to satisfy eq.1, coupled with the F-P resonance being slightly too far away from the MQW absorption edge. The insertion loss at the resonant wavelength is higher than calculated, probably due to the absorption tail being underestimated.

OPERATION AT LOWER VOLTAGES:

It has been suggested that MQW modulators would be an attractive interface device for optical interconnects between large scale electronic processors. We have carried out further simulation to determine the prospects for an AFPM operating at no more than 5V bias, this being compatible with existing CMOS. To obtain more than 10dB contrast at such low bias voltages it is necessary to decrease the MQW layer thickness, whilst increasing the cavity finesse slightly by raising the front reflectivity to ≈0.45. Thus a front mirror would have to be integrated with the basic AFPM structure. The results are shown below in figure 5.

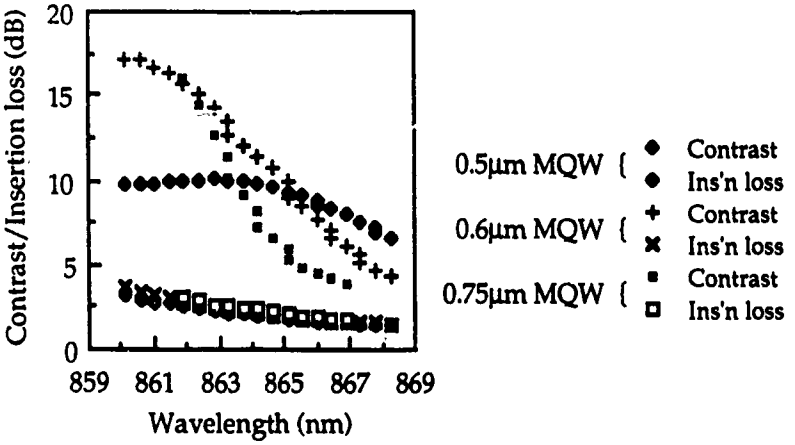

Fig.5:
Simulated performance of the modified AFPM with R_f=0.45, R_b=0.95, operating at a fixed 5V bias, with different MQW thicknesses.

With the bias voltage fixed at 5V, the field across the MQW region falls with increasing thickness. For 0.5μm of MQWs, the field is high enough to induce a significant shift of the absorption edge, and so the contrast remains quite uniform over the range, although the reduced αd factor means that it does not climb above 10dB. For thicker MQW regions there is only an improvement of the contrast at wavelengths close to the absorption edge, where the reduced electric field still has effect. The fall-off in contrast becomes more rapid with increasing MQW thickness (decreasing field). We note also that the loss is fairly insensitive both to operating wavelength and MQW thickness.

REFERENCES:

[1] Wood T.H., Burrus C.A., Miller D.A.B., Chemla D.S., Damen T.C., Gossard A.C. and Wiegmann W., "High-speed optical modulation with GaAs/GaAlAs quantum wells in a *p-i-n* diode structure", *Appl. Phys. Lett.* , 1984, **44**, pp.16-18.

[2] Whitehead M., Stevens P., Rivers A., Parry G., Roberts J.S., Mistry P., Pate M. and Hill G., "Effects of well width on the characteristics of GaAs/AlGaAs multiple quantum well electroabsorption modulators", *Appl. Phys. Lett.* , 1988, **53**, pp.956-958.

[3] Hsu T.Y., Wu W.Y. and Efron U., "Amplitude and phase modulation in a 4μm-thick GaAs/AlGaAs multiple quantum well modulator", *Electron. Lett.*, 1988, **24**, pp.603-604.

[4] Boyd G.D., Miller D.A.B., Chemla D.S., McCall S.L., Gossard A.C. and English J.H., "Multiple quantum well reflection modulator", *Appl. Phys.Lett.* , 1987, **50**, pp.1119-1121.

[5] Simes R.J., Yan R.H., Geels R.S., Coldren L.A., English J.H., Gossard A.C. and Lishan D.G., "Electrically tunable Fabry-Perot mirror using multiple quantum well index modulation" *Appl. Phys. Lett.* , 1988, **53**, pp.637-639.

[6] Lee Y.H., Jewell J.L., Walker S.J., Tu C.W., Harbison J.P. and Florez L.T., "Electrodispersive multiple quantum well modulator", *Appl.Phys. Lett.* , 1988, **53**, pp.1684-1686.

[7] Whitehead M., Parry G. and Wheatley P., "An investigation of étalon effects in GaAs-AlGaAs multiple quantum well modulators", *IEE Proceedings*, 1989, **136**, Pt.J (Optoelectronics), pp.52-58.

A Cascadable Optical Logic Module using Symmetric Self-Electrooptic Effect Devices

M. E. Prise, R. E. La Marche, N. C. Craft, M.M. Downs and S. J. Walker
AT&T Bell Laboratories
Holmdel, NJ 07733

L. A. D'Asaro and L. M. F. Chirovsky
AT&T Bell Laboratories
Murray Hill, NJ 07974

We demonstrate an optical module which will be used to implement an optical digital switching fabric [1], using symmetric self electro-optic effect devices (S-SEEDs) as the logic gates and laser diodes as the optical power supply. Provision for the required inputs and outputs, a method for presetting the S-SEEDs and a split and shift interconnection are implemented. We demonstrate the operation of a 7×3 array of S-SEEDs, and show both the switching of each device with an external input, and the simultaneous presetting of the entire array by modulating a single laser.

The use of S-SEEDs as optical logic gates [2] , the conditions on the optical power supply beams and methods for obtaining the power supply beams has been discussed [3]. The fabrication of arrays of S-SEEDs has been reported [4], the architecture of an optical digital processor based on arrays of optical logic gates with simple interconnects between them has been presented [5], and the operation of an optical shift register using a single array of S-SEEDs demonstrated [6]. The optical system described here is very similar to that necessary to implement a scheme for free space opto-electronic interconnections [7].

We have previously described a scheme for the operation of arrays of optical logic devices which allows the input of an array of power supply beams , two arrays of signal beams (which would come from the previous array of devices via a simple interconnection such as a split and shift), and the output of an array of beams (the reflected power supply array) [8]. The module described here uses the same technique of beam combination using polarizing beam splitters, wave plates and patterned reflectors which minimize the loss of power or optical resolution of the imaging system. Dammann (binary phase) gratings are again used for the array generation [9].

As has been preciously discussed [3] in order to use an S-SEED as a logic gate, each of the two modulators must be supplied with the same optical power. In [3] we suggested using a grating to split the beam from one laser into two equal beams, one for each modulator and then use another grating to distribute these two equal beams to all the other modulators. Here we use two lasers, (one for each modulator) of a single S-SEED and then use a single grating to distribute these two beams to all the S-SEEDs in the array. This has two significant advantages over our previous scheme.

First this method doubles the available optical power (two lasers rather than one) and second we can use one of the lasers to preset the devices (thus avoiding chromatic abberation problems). In order to use these devices as logic gates, they must be set to a given state between logic operations. Using an array of beams at another (shorter) wavelength, as the preset has been suggested. We initially tried this, but could not reconcile two following, opposing optical system constraints. Our imaging system suffers from chromatic aberrations making it difficult to focus arrays of beams with significantly different wavelengths on the device array at the same time. It is also difficult to make polarization insensitive dichroic beam splitters.

The optical layout is shown in Figure 1. LD1 and LD2 are both laser diodes capable of producing

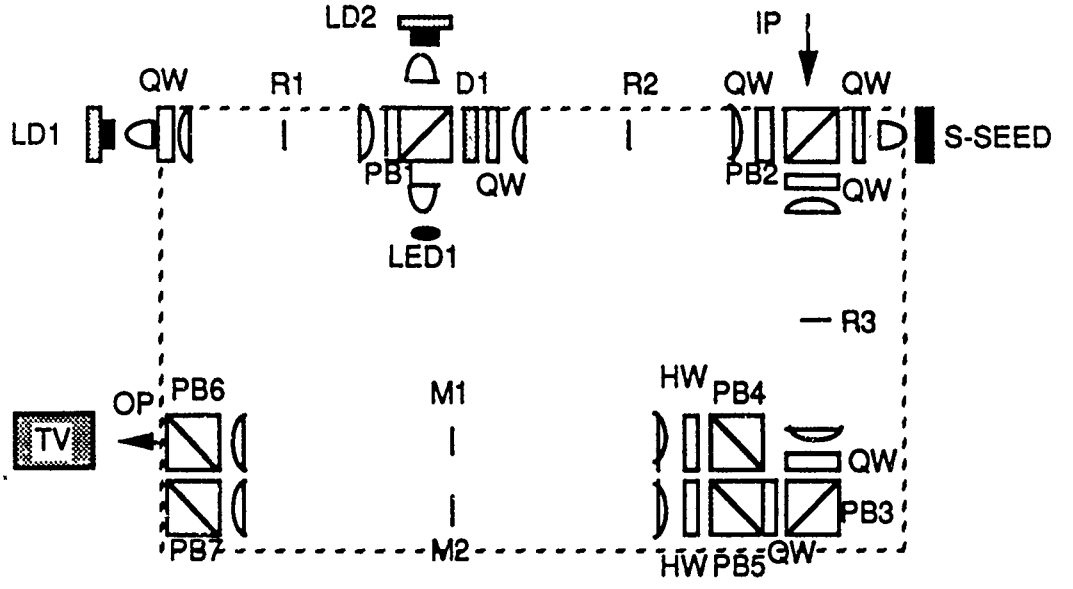

Figure 1: Optical layout with the dashed line showing what is include on the aluminium plate.

up to 25mW at a wavelength of 850nm. LED1 is a light emitting diode with an output centered around 850nm which is used for illumination. The S-SEED array has been described by [4]. QW are quarter wave plates and HW are half wave plates.

LD1 and LD2 are used to provide the optical power to the array of S-SEEDs. The outputs of LD1 and LD2 are combined at reflector R1 which is a knife-edge arranged so that the beam from LD1 is transmitted through it and the beam from LD2 is reflected at it. The spacing between the two beams is adjusted so that they are imaged onto the two modulators of a single S-SEED on the array. The beams are then split up at the grating D1. This is a Dammann (binary phase) grating with periods in the vertical and horizontal directions such that it distributes the two beams to all 21 devices on the S-SEED array. These beams are then relayed to PB2 and focused down onto the S-SEED array. R2 and R3 are reflector arrays and are used feed the input arrays, which come in through input port IP, onto the device array as described in [8].

The output, which is the reflected power supply beam array, is then relayed to PB3 where it is split into two (orthogonal polarizations), one array is relayed through M2 and the other array through M1. Masks M1 and M2 can be used to customize the interconnect. The arrays are then re-combined at PB6 and imaged onto the camera. PB7 is adjusted so that one of the arrays is shifted by one S-SEED period from the other, thus implementing a split and shift interconnect. The HW plates rotate the polarizations so recombination is possible at PB6. The optical system is designed so that the output at OP can be fed directly into the input IP of another identical module thus giving cascadable optical logic. We can also view the device array using the TV at polarization beamsplitter PB3 by slightly rotating QW to allow some of the light through PB3.

The entire arrangement, (excluding the diode lasers, collimators and the array of S-SEEDs), is contained on an aluminium plate which is 14in × 12in. The optical components are positioned using steel pins located by a numerically controlled milling machine. We found that using this technique makes optical

alignment much easier than using individual components on an optical bench. The accurate positioning of components means we can examine the performance of our our system using optical ray tracing software. We also found the system to be very stable and we found that we could take out and replace parts of the system without disturbing the overall system alignment.

Two experiments were carried out using this module.

The two laser diodes were adjusted so that equal powers were obtained (about 5 μW per S-SEED). Voltage was then applied to the S-SEED array. All the S-SEEDs went into definite logic states, that is one modulator was in a high reflectivity state while the other was in the low reflectivity state or vice-versa. The contrast between these reflectivities is about 4:1 at the wavelength we used, thus the output from each S-SEED appeared as a bright and dark spot on the TV monitor. By alternatively clocking the lasers, the states of all the devices on the array were switched simultaneously, demonstrating the required preset. For the operation of the S-SEEDs as logic devices one of the lasers can be turned on during the preset cycle, which occurs after the readout cycle during which the two lasers are on.

In the second experiment all the devices, were set in the same logical state and the beam from another laser diode operating at 850nm was fed in from IP through PB2, reflected off R3 and then imaged onto the S-SEED array. By moving this beam from one modulator to another we can switch the logical states of all the 21 S-SEEDs on the array. A video tape was made of both experiments.

In conclusion we have shown, that using a custom mechanical mounting system, it is possible to provide the necessary uniform optical power to arrays of S-SEEDs in order to use them as optical logic gates. We have also demonstrated a simple scheme to preset all the devices. We are attempting to use these techniques to build a cascadable optical digital system and we think better optical design will allow us to make future modules more compact.

References

[1] M. Murdocca and T. Cloonan, submitted to *Applied Optics*

[2] A. L. Lentine, D. A. B. Miller, J. E. Henry and J. E. Cunningham, *Conference on Lasers and Electro-optics 1988*, paper TUE4

[3] N. C. Craft and M. E. Prise,*Topical Meeting on Optical Computing 1989*,TuI29

[4] L. M. F. Chirovsky, L. A. D'Asaro, C. W. Tu, A. L. Lentine, G. D. Boyd, David A. B. Miller,*Topical Meeting on Photonic Switching 1989*, ThD4

[5] M. J. Murdocca , N. Streibl, A. Huang and J. Jahns, "Algorithmic Design Technique for a Free-Space Regularly Interconnected Digital Optical Computer", *Applied Optics*, 27, (9), 1651

[6] F. B. McCormick, A. L. Lentine, L. M. F. Chirovsky, L. A. D'Asaro,*Topical Meeting on Photonic Switching 1989*, ThC5

[7] A. Dickinson and M. E. Prise,*Topical Meeting on Optical Computing 1989*,TuB3

[8] M. E. Prise, M. M. Downs, F. B. McCormick, S. J. Walker and N. Streibl, *Optical Bistability IV* edited by W. J. Firth et al., published by Les Editions de Physique 1988

[9] H. Dammann and K. Gortler, *Optics Communications*,3,312-315,1971

A NOVEL TWO DIMENSIONAL PERFECT SHUFFLE NETWORK

M G Taylor
J E Midwinter

Department of Electronic and Electrical Engineering,
University College London,
Torrington Place,
London. WC1E 7JE
United Kingdom.

Introduction

Some of the most important optical computing systems which have been proposed are like the one in figure 1 : a pipelined sequence of perfect shuffle interconnections feeding into layers of adjacent binary i/o processing modules. A variety of parallel tasks can be performed by such a processor, the most important of which is to act as an N to N switch [1-3]. In this case each module is set to either exchange or bypass the pairs of data channels. The perfect shuffle interconnection is implemented using either bulk or holographic optics [4-5], and the exchange/bypass modules can be directional couplers [6] or an optoelectronic integrated circuit [7], to make a very powerful hybrid system.

In this paper we will introduce the two dimensional network of figure 2. This network is a pipeline of two dimensional perfect shuffle interconnections and layers of square 'super exchange' modules. The operation of the network is derived from its one dimensional counterpart, and the new processor does exactly the same task as the old one. Distributing the processing in two dimensions has two compelling advantages: a vast increase in the parallelism available, and the ability to build a given size of switch in a much more compact form. Also the optical implementation in the 2D case is possibly easier than in the linear case.

The 1D and 2D perfect shuffles

To understand the operation of the new network the mathematics of the perfect shuffle must be considered. The cleaving and interleaving transformation of the ordinary perfect shuffle (figure 3) can be expressed as a rotation of each port's address written in binary. For 64 elements this is

$$abcdef \rightarrow bcdefa$$

where a to f are *0*s and *1*s.

The 2D perfect shuffle [4] is a transformation of a square array comprising a horizontal followed by a vertical perfect shuffle, and it can be generated with a simple optical arrangement. The binary representation involves the twin rotation of the column and row addresses:

$$(jkl, pqr) \rightarrow (klj, qrp)$$

The four ports which meet at a module after being 2D shuffled are those which differ only in the least significant bits of the column and row addresses, bits j and p in the expression above. It was noted by Lin et al [8] that it might be possible to build a permutation network from multistages of 2D perfect shuffles and 4x4 local redirectors, but those workers were unable to provide any algorithm to control such a network. Here we will show how such an N to N switch can be constructed by reference to the equivalent N:N linear network.

The 2D perfect shuffle network

Figure 4 shows a sorting network, and is given simply as an example of a one dimensional perfect shuffle network. Telephony lines with destinations from 1 to 8 enter at the left hand side; arrowed modules divert the line with the higher destination number to the port indicated, and the empty modules always bypass. The signals arriving at the right hand side are correctly ordered. The workings of the network are described in Knuth [9], but need not concern us here.

Consider carefully two adjacent stages of a perfect shuffle sorter like that of figure 4 but with 64 lines. Port *abcdef* is shuffled to *bcdefa*, where the exchange/bypass module can 'fix' the final bit, that is route the data to *bcdefA* where *A* can be *0* or *1*. The next shuffle-module stage moves the channel to *cdefAB*, so it has a choice of four outputs to emerge from the two stage unit.

Let us examine the effect of picking up the ports of this unit and moving them in space according to the rule

$$abcdef \rightarrow (\text{column } bdf, \text{ row } ace)$$

Two perfect shuffles taken together, which is written in 1D notation as

$$abcdef \rightarrow cdefab$$

becomes under the mapping rule

$$(bdf, ace) \rightarrow (dfb, cea)$$

which is a single 2D perfect shuffle. The routing which was done by the relevant binary modules is

$$(dfb, cea) \rightarrow (dfB, ceA)$$

which corresponds to *cdefAB* under reverse mapping, and so can be performed by one of the new four way modules. The simple mapping rule above is crucial to realising the new networks, as it enables us both to prove that a 2D switch can be built, and to determine the functionality required of the super exchange modules.

One of the super exchange modules performs the operations of four of the old modules, in the topology of figure 5. It is readily deducible which the four modules are through the mapping rule, and so the function of the new module is completely specified. By dividing the whole of the shuffle network into pairs of stages and converting them in turn into a 2D format, an entire 2D routing network can be built up.

Sorted output

A two dimensional shuffle network which is constructed starting from the linear shuffle network of figure 4 will do the same function as that processor - rearrange the parallel communication lines. It is worth noting that since the new modules make decisions in order to sort the output into what would be the correct order for the flat network, the final square array of destination numbers does not appear to be naturally ordered. An 8x8 matrix as ordered by a 2D network is shown in figure 6.

This apparent 'scrambling' of lines is not important because it occurs in a wholly deterministic way. If there is a situation where formal ordering is required, then either the decision making of the modules or the destinations can be modified to compensate.

Summary and Conclusions

This paper has provided an introduction to 2D networks. A single type of two dimensional perfect shuffle network has been described, but it should be apparent that other perfect shuffle networks [1-2] can be readily mapped into a 2D format. It will be shown in reference 10 how to construct a two dimensional network in the general case. The motivation for 2D rather than 1D networks is clear - the number of parallel channels which can be accommodated rises from N to N^2, and the packaging becomes more tractable.

Acknowledgements

We would like to thank Peter Healey for helpful discussions. The work was supported by the UK Science and Engineering Research Council and by British Telecom.

References

[1] D. H. Lawrie, IEEE Trans. Comp. **C-24(12)** p1145 (1975).
[2] C.-L. Wu, T.-Y. Feng, IEEE Trans. Comp. **C-30(5)** p324 (1981).
[3] H. S. Stone, IEEE Trans. Comp. **C-20(2)** p153 (1971).
[4] A. W. Lohmann, Appl. Optics **25(10)** p1543 (1986).
[5] K.-H. Brenner, A. Huang, Appl. Opt. **27** p135 (1986).
[6] P. Granestrand et al, Electron. Lett. **22(15)** (1986).
[7] J. E. Midwinter, IEEE Proc. J **134(5)** p261 (1987).
[8] S.-H. Lin et al, SPIE **752** p209 (1987).
[9] D. E. Knuth, "Sorting and Searching," Addison-Wesley (1973).
[10] M. G. Taylor, J. E. Midwinter, to be pubiished.

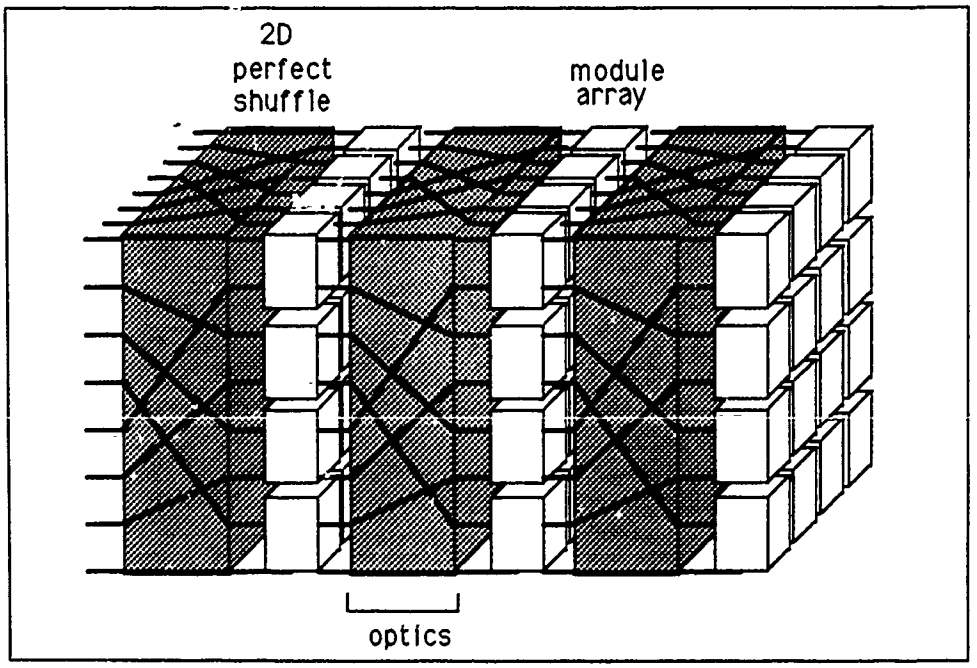

Figure 2. A general 2D perfect shuffle network.

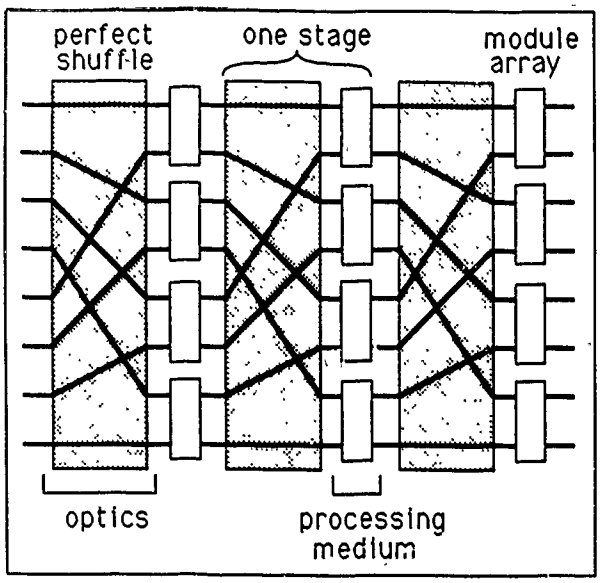

Figure 1

1	2	5	6	17	18	21	22
3	4	7	8	19	20	23	24
9	10	13	14	25	26	29	30
11	12	15	16	27	28	31	32
33	34	37	38	49	50	53	54
35	36	39	40	51	52	55	56
41	42	45	46	57	58	61	62
43	44	47	48	59	60	63	64

Figure 6

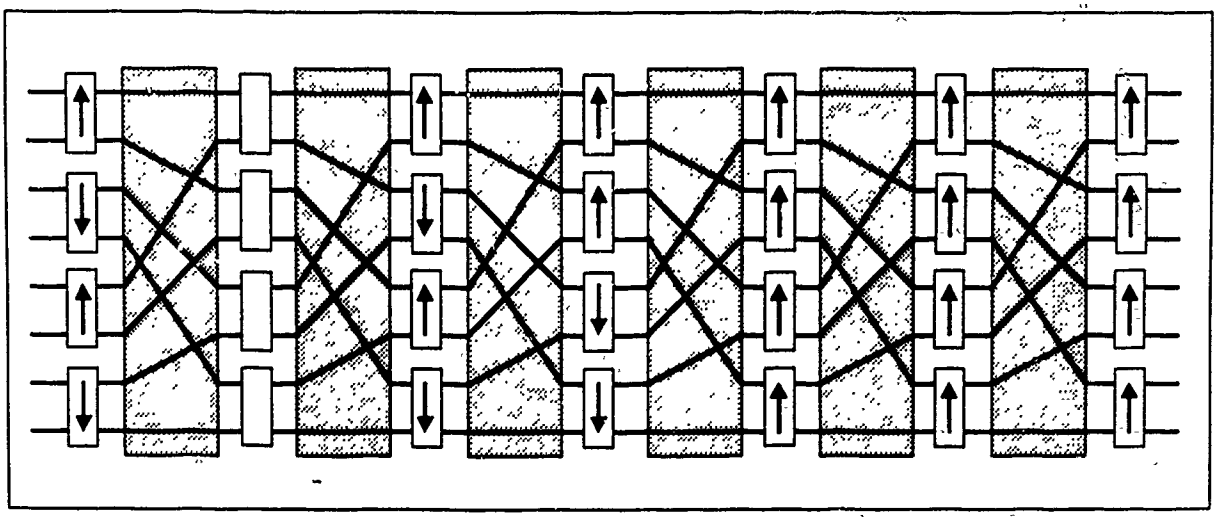

Figure 4. A perfect shuffle sorting network.

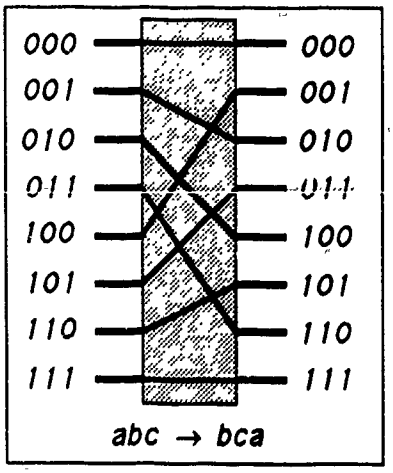

Figure 3

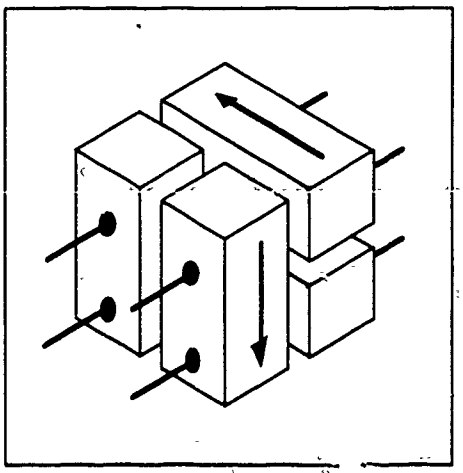

Figure 5

An Opto-Electronic Dynamic Random Access Memory (DRAM) Cell Utilizing a Three Terminal N-Channel Self-Aligned DOES Device

G. W. Taylor, D. L. Crawford and J. G. Simmons

AT&T Bell Laboratories

Holmdel, NJ

The Double Heterostructure Opto-Electronic Switch (DOES) device has been demonstrated as a three terminal [1] opto-electronic bistable switch having high and low conduction states with and without optical emission respectively and which can be switched on and off by both an optical and an electrical input signal. The third terminal permits xy addressing of the cell in a manner very similar to the Dynamic Random Access Memories (DRAMS) of silicon technology. Currently in electronic dynamic memories, the limitations on performance and density arise from the minimum ratio of cell to bit line capacitance (i.e. stored cell charge) that will still allow reliable sensing. Using the optical output of the DOES relieves this constraint because it is an active element whose output can be increased to the limits of the device power.

We describe a memory cell which uses a self-aligned DOES and a single polarity of bias. The storage is dynamic in nature and utilizes the electronic stored charge to maintain the device on state. The above attributes, together with its inherent compatibility with a new family of opto-electronic integrated circuits [2], suggest the three terminal DOES might form the basis of a new memory technology in III-V material systems.

THE MEMORY CELL

The DOES device is shown in cross-section in Fig.1. The device is an N-Channel device grown by .

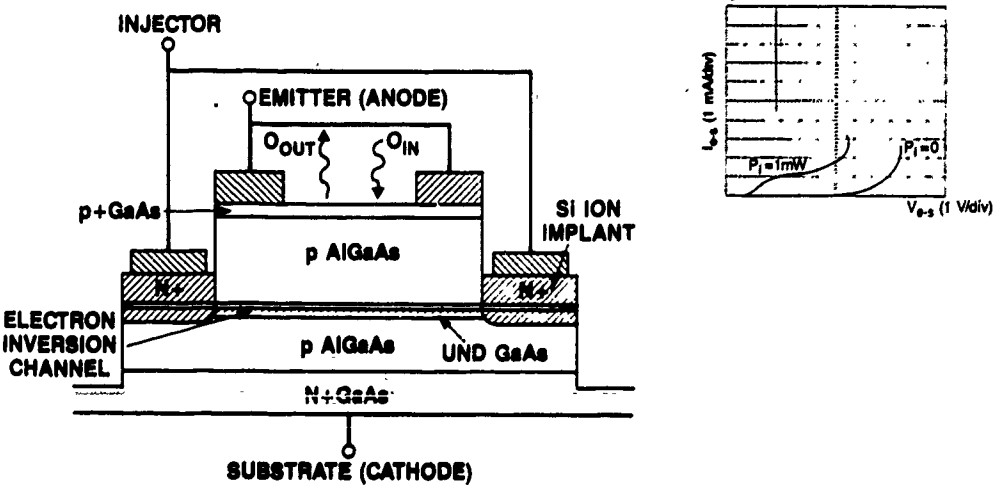

Figure 1 Cross-sectional view of a double heterostructure opto-electronic switch (DOES) for an optical dynamic memory element.

molecular beam epitaxy. The fabrication sequence discussed previously [3] allows formation of the third terminal (injector) by ion implantation as a contact to the electron inversion channel. The IV characteristics of the DOES are also shown in Fig. 1 (inset) for the case of two different light intensities. Switching occurs when the device is biased as shown and an optical signal applied. The d.c. switching voltage, V_S, of these devices after processing was 8V, with no injector input. An injector input of 0.2 ma reduces V_S to 5V.

The turn-on and turn-off time using the channel contact has been measured to be about 8ns for these devices [3]. The DOES is operating as an LED for the demonstration here to allow emission and absorption perpendicular to the surface. When optically triggered, the turn-on time is about 5ns, being limited by the RC delay time. In Fig. 2 the DOES is depicted as a memory cell.

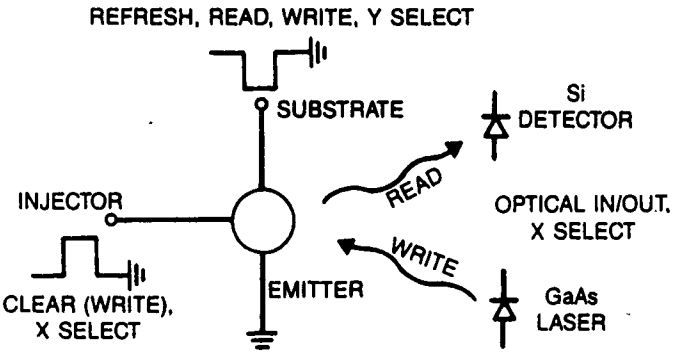

(b)

Figure 2 Opto-electronic circuit configuration of the DOES device as an optical dynamic memory cell.

The emitter (anode) is grounded, the injector and the optical output of the DOES perform the x select function and the substrate terminal and optical input to the device perform the y select function.

The basic functions of the cell are demonstrated by the waveforms in Fig. 3a (from top to bottom) of the injector reset pulse, the optical input pulse and the current flowing in the device as sensed across a 50Ω load between the emitter and ground. In Fig. 3b the injector reset pulse (top) is shown together with the optical input (bottom) and the substrate waveform (middle) to illustrate the dynamic storage mechanism. Note that the injector pulses are positive to turn the DOES off and the substrate pulses are negative to turn the DOES on. The write, read and store sequences are described as follows. Writing into the cell is a two-step operation. First a positive pulse of 2.8V is applied to the x select (injector) which removes charge from the inversion channel and puts the DOES into a high impedance state (the zero state). Then a pulse of 3.5V, which has been reduced from 8V by the $\frac{dV}{dt}$ effect is applied to the y select (substrate) and at the same time the desired data is delivered to the cell optically. If an optical pulse is present, the DOES is switched to the low impedance state (the one state) and a "one" is written; if the pulse is absent, the DOES remains off and a "zero" is written. Note that in the data in Fig. 3, the optical input/y select combination actually occurs before the reset pulse. However, the net effect is the same. During the read operation, the y select line (substrate) is pulsed to 3.5V alone. If the DOES is on (low impedance), an optical pulse will be produced but if it is off, no optical pulse will be produced. The optical output of the device would be sensed selectively in the x direction by means of another DOES device; however, for convenience it is sensed here electrically across the 50Ω emitter resistor.

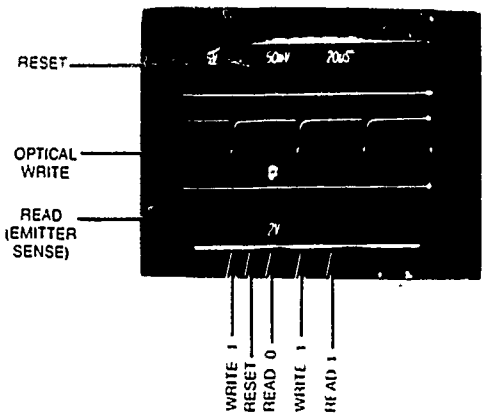

Figure 3a Waveforms illustrating optical memory cell operation. From top to bottom the pulses are injector input pulse (2V/div), optical input from GaAs laser (50mV/div at detector), device output through a 50Ω emitter resistor (50mV/div).

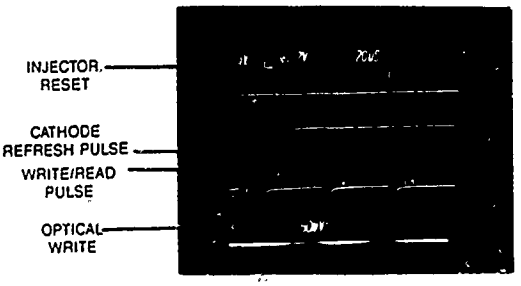

Figure 3b Waveforms illustrating refresh operations. From top to bottom; injector input (2V/div) substrate waveform with superimposed refresh (5V/div) and optical input (optical pulse peak power = 6mW).

In summary, a new configuration of the DOES device as a dynamic memory cell in a self-aligned N-Channel technology has been demonstrated. The DOES has shown a unique capability for dynamic refresh with potentially very long refresh times. Also the extension to high density dynamic arrays as an integrated circuit appears feasible.

[1] G. W. Taylor, R. S. Mand, J. G. Simmons, and A. Y. Cho, Appl. Phys. Lett., Vol. 50, No. 6, pp 338-340, 1987.

[2] G. W. Taylor, D. L. Crawford, P. A. Kiely, S. K. Sargood, P. Cooke, A. Izabelle, T. Y. Chang, B. Tell, M. S. Lebby, K. Brown-Goebeler, J. G. Simmons, Device Research Conf., 1988, paper IV B-1.

[3] D. L. Crawford, G. W. Taylor, P. Cooke, T. Y. Chang, B. Tell and J. G. Simmons, Appl. Phys. Lett., to be published.

Fiber Polarization Rotation Switch based on Modulation Instability

C.E. Soccolich and M.N. Islam
AT&T Bell Laboratories
Holmdel, NJ 07733

We demonstrate a Modulation Instability based Polarization Rotation Switch (MIPRS) operating near 1.5 μm, exhibiting contrast ratios up to 40:1 and small signal gains up to 40dB. Optical fiber switches are important for ultrafast, all optical, serial applications such as multiplexers/demultiplexers, and for ultrafast modulation of large signals. All fiber switches eliminate bottlenecks from slow electrical to optical interfaces and offer such advantages as: femtosecond response times, long interaction lengths and low power requirements, and a mature fiber technology foundation.

In the MIPRS, pulses from a mode-locked color center laser (CCL) are gated through a length of fiber by a low power, cw light signal from a semiconductor laser (SCL) ($1\mu W \leq P \leq 400\mu W$). The experimental setup is shown in Fig. 1. The CCL pump beam and SCL signal beam are simultaneously coupled into a 500 meter length of single-mode, non-polarization preserving, dispersion shifted fiber. To compensate for birefringence in the fiber, a quarter waveplate is used at the output of the fiber to linearly polarize the emerging pump beam. This is followed by a polarizer adjusted to null the fiber output while the SCL is blocked. The SCL which is at a slightly shifted frequency from the pump, induces modulation instability (MI) [1,2], causing the quasi-cw wave to break up into a train of solitons. We find that MI causes a net rotation of the output polarization from the fiber permitting some fraction of the energy to pass the polarizer.

The small signal gain and on:off contrast ratio shown in Fig. 2 demonstrate the usefulness of the MIPRS as a switch. Gain as high as 10^4 is achieved at low powers, and decreases with increasing signal power due to saturation caused by pump depletion and Raman or soliton self-frequency shift (SSFS) effects [3]. On the other hand, the on:off contrast ratio increases with increasing SCL signal power since the net output power increases while the pump leakage at the null is nearly constant. For the current experiment we expect the speed of response to be approximately 1 psec. However, we are still far from the ultimate speed of response set by the material, which is about 6 fsec. for fused silica. The speed of response of this device is limited by the MI gain bandwidth [1], calculated to be 960 GHz, which is a function of the pump power and fiber parameters. For example, if we operate closer to the zero dispersion point of the fiber or increase the pump power, the gain bandwidth increases.

We attribute the large gains observed in the MIPRS to the generation of upper and lower sideband frequencies centered around the pump wavelength combined with the wavelength dependence of the beat length L_b [4]. Since our fiber length is $500L_b$, a slight shift in the wavelength will have a noticeable difference in the polarization at the output. Fig. 3 shows the output spectrum of the device for a pump power of 5W and signal power of 318 μW. The gains after the polarizer for the individual components are: $G(\omega_0-6\pi f) = 28$, $G(\omega_0-4\pi f) = 95$, $G(\omega_0-2\pi f) = 1.4 \times 10^3$, $G(\omega_0) = 672$, $G(\omega_0+2\pi f) = 476$, $G(\omega_0+4\pi f) = 56$.

In summary, we have demonstrated an active, ultrafast polarization rotation switch in an optical fiber near 1.5μm with contrast ratio as high as 40:1, up to 40dB of small signal gain, and an anticipated 1 psec speed of response. MI induces rotation of the initially nulled polarization through wavelength dependent beat length. Also, since ordinary non-polarization maintaining, single mode fiber is used, the fiber length can be increased to $L = 1/\alpha$, further reducing the power requirements.

We thank N. Bergano for providing the fiber.

REFERENCES

[1] A. Hasegawa and W.F. Brinkman, IEEE J. Quantum Electron. **QE-16**, 694 (1980).

[2] K. Tai, A. Hasegawa and A. Tomita, Phys. Rev. Lett. **56**, 135 (1986).

[3] M.N. Islam, S.P. Dijaili and J.P. Gordon, Opt. Lett. **13**, 518 (1988).

[4] I.P. Kaminow, IEEE J. Quantum Electron. **QE-17**, 15 (1981).

FIGURES

1. Schematic of experimental apparatus.
2. Performance of MIPRS as a function of SCL signal power, (P_{CCL}=4.5 W, τ=75*psec*, f =832*GHz*); a) Net device gain (*Device output/SCL power in the fiber*); b) Contrast ratio (P_{on}/P_{off})
3. Spectrum of device output, (P_{CCL} = 5 W, P_{SCL} =318μW).

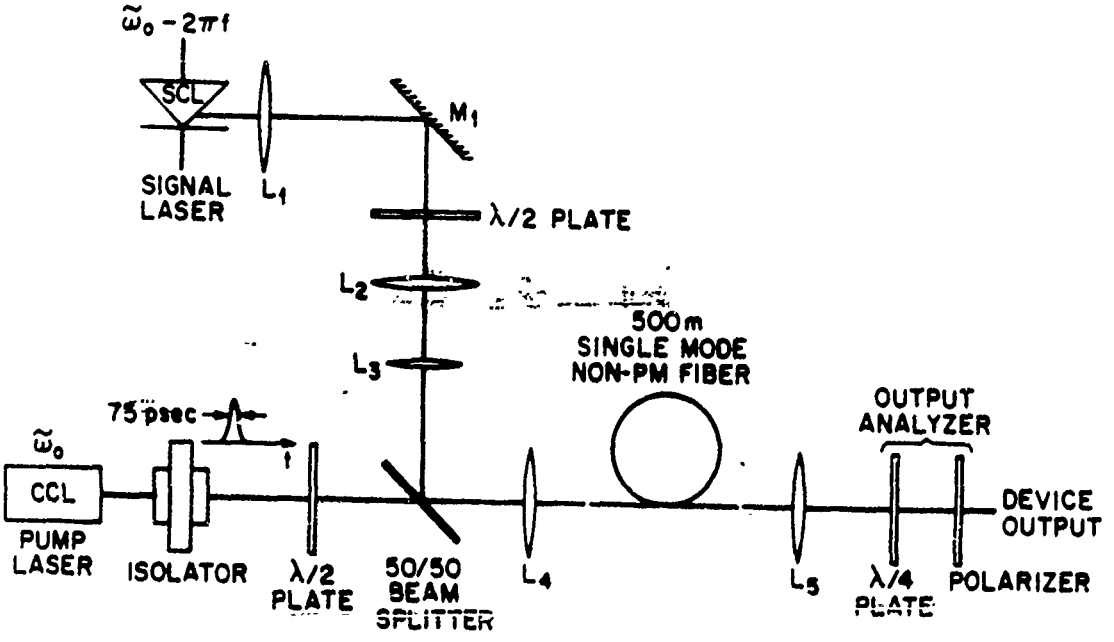

Figure 1.

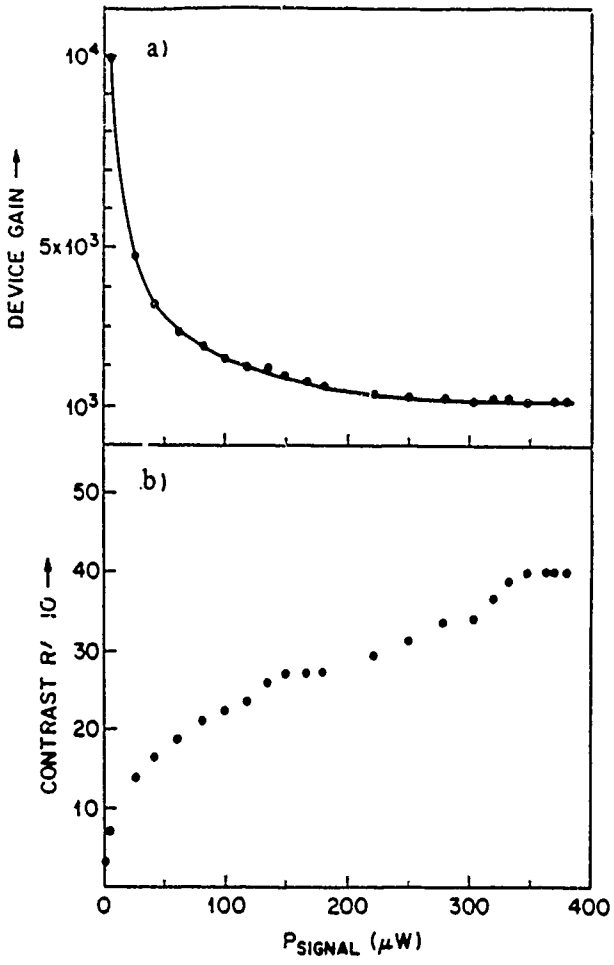

Figure 2.

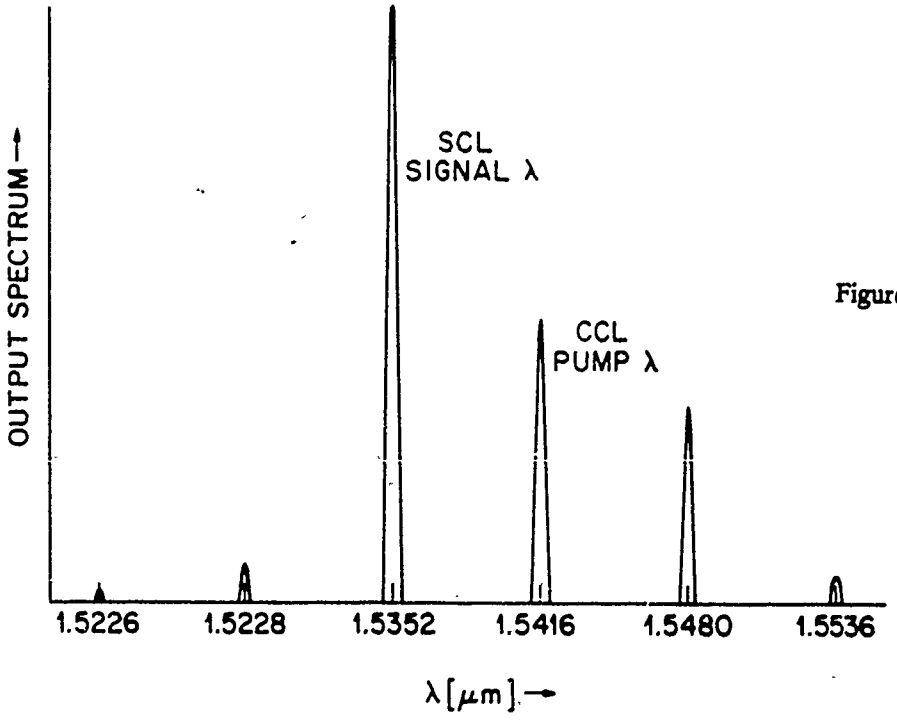

Figure 3.

Optically Controlled Bistable Switching Element based on Electro-Optic Feedback

J.A. Cavaillès and M. Erman .

Laboratoires d'Electronique et de Physique appliquée (LEP)[1]
3 Avenue Descartes, 94451 LIMEIL-BREVANNES CEDEX, France

Optically controlled switching devices provide interesting functionality in optical communications and optical computing . Several systems, based on non-linear coupling phenomena have recently been described /1-3/ . In these works, the non-linear response of Multiple Quantum Wells (MQW) material is exploited to change the state of a directional coupler in order to achieve switching . Among these structures, 'vertically' arranged couplers deserve particular attention, since they allow short coupling lengths in cunjunction with low crosstalks .

In this work, we demonstrate the possibility to obtain optically controled bistable switching, using an external electrical feedback in a way very similar to the case of SEED devices /4/ . We consider a 'vertical' directional coupler in which one of the guides is a MQW material, imbedded in the intrinsic region of a p-i-n junction, this junction beeing connected to an external electrical circuit. Principle of operation can be briefly described as follows : One injects light in the non-MQW guide; a power transfer between guides occur because of optical coupling .The amount of power in the MQW depends upon its optical characteristics, which are known to be strongly influenced by a transverse electric field . Acting as a detector the MQW will generate a photocurrent which will be proportional to absorbed light intensity. Feedback from the external electrical circuit enables optical control of the state of the coupler : injected power influences photocurrent, which changes the p-i-n bias, modifying the optical parameters in the MQW thus changing the path followed by the light .

We study the structure shown on figure 1 . It consists in two slab waveguides sequentially grown on a GaAs substrate . The lower guide (guide 1) is a GaAs/GaAlAs double heterostructure waveguide . The upper guide (guide 2) core is a 100 Å x 100 Å $GaAs/Ga_{0.7}Al_{0.3}As$ MQW and forms the intrinsic region of a p-i-n junction . Other parameters are indicated in the figure.

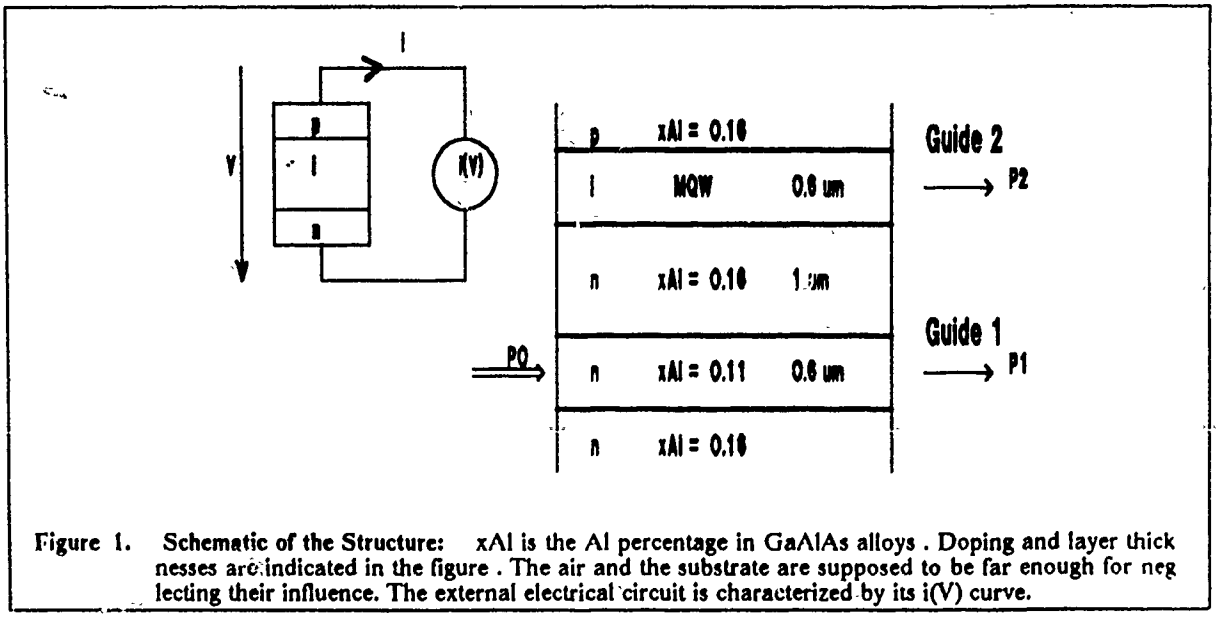

Figure 1. Schematic of the Structure: xAl is the Al percentage in GaAlAs alloys . Doping and layer thicknesses are indicated in the figure . The air and the substrate are supposed to be far enough for neglecting their influence. The external electrical circuit is characterized by its i(V) curve.

[1] LEP : a Member of the International Philips Research Organization

The structure is designed so that, when no reverse bias is applied, both guides are identical . We have taken into account the fact that the refractive index in MQW is ~ 1% higher than in the equivalent GaAlAs alloy /5/. The photon energy is fixed 30 meV below the zero-field first heavy-hole excitonic transition energy. The absorption is neglected in all layers exept in the MQW.

In this first approach, the influence of the electric-field,F, on the optical properties of the MQW has been modellized in a semi-quantitative way :

- The absorption is computed assuming gaussian lineshape and taking into account Stark shift of the exciton and field-induced electron- hole wavefunctions overlap changes as calculated using a standard tunneling resonance technique . This approximation is only valid below the exciton energy : we restrict ourselves to relatively low fields so that the Stark shift does not exceed the initial detuning (30 meV).
- The refractive index changes variations are taken as $\Delta n = 5.10^{-13}F^2$ (F in V/cm), in accordance with published data /6/.

For a given value of the bias V, we determine the guided modes of the structure taking the absorption into account and solving the associated ***complex*** eigenvalue problem in the TE polarization. We suppose that initially (at z = 0),light is injected in guide 1. The optical field distribution at any point along the propagation, E(x,z), is then determined using the modal decomposition of the initial field on the two modes which propagate in the structure. Power in both guides is computed from overlap integral between eigenmodes of the isolated guides with the actual field. The photogenerated current in the MQW region is computed assuming a unit quantum efficiency. The responsivity of the device, S, is defined as the photocurrent/incident power ratio.It is given by

$$S = \frac{I}{P_0} = \frac{e}{E} \quad \frac{\alpha}{P_0} \int_0^L \left(\int_{x1}^{x2} E^*(x,z)E(x,z)dx \right) dz \qquad [1]$$

where I is the photocurrent, x1 and x2 are the limits of the intrinsic region of the p-i-n junction, α is the absorption in the MQW, L is the length of the device, E is the photon energy and e the electronic charge. In the following it is supposed that the device is cleaved at the zero-field coupling length, which is around 288 μm.

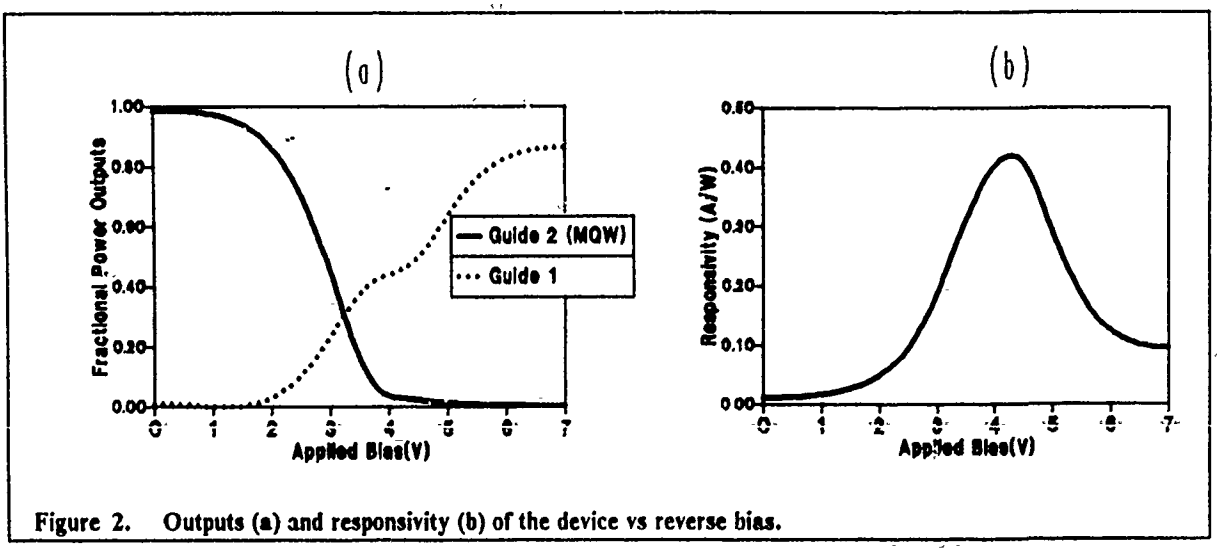

Figure 2. Outputs (a) and responsivity (b) of the device vs reverse bias.

Figure 2 shows the fractional outputs in both guides as well as the responsivity of the device plotted against the reverse bias, V, applied to the p-i-n diode. On fig. 2 (a), it is clearly seen that increasing the bias induces switching from cross- to parallel-propagation, with good predicted crosstalks (-20 dB and -30 dB respectively). The responsivity curve of fig. 2 (b) goes through a maximum, since it is given by the product of the

absorption in the MQW (which increases with V) with the amount of power in guide 2 (which decreases with V).

As far as the external electrical feedback circuit is concerned, we will consider the case of a constant current load for which one has $i(V) = i_0$ for V < V_0 and $i(V) = 0$ for V > V_0 with V_0 = 7 V. The bias point of the system is determined by:

$$S(V) = i(V)/P_0 \qquad [2]$$

The number of solutions for [2] depends upon the value of i_0/P_0 in the following way : if i_0/P_0 is greater than the maximum responsivity of the system one has $V = V_0$ and the switch is in the parallel state. If i_0/P_0 is smaller than $S(V_0)$ the only stable state is in the low bias region and the switch is in the cross-state. Between these two extremes, the system is bistable. Bistable switching can thus be obtained in a very versatile way: i.e. either electrically (changing i_0) or optically (changing P_0). As an example, figure 4 shows power outputs from both guides when the incident power P_0 is varied, while i_0 is kept constant. Since the relevant parameter is P_0/i_0, units on both axes of figure 4 are scaled to i_0 . As a consequence, switching powers can be adjusted by changing i_0. Ultimate performances are , however, limited by the p-i-n diode dark current. For a ~ 300 μm X10 μm device, the value of this parameter should be well below 1 μA, so that switching powers below 50 μW are predicted.

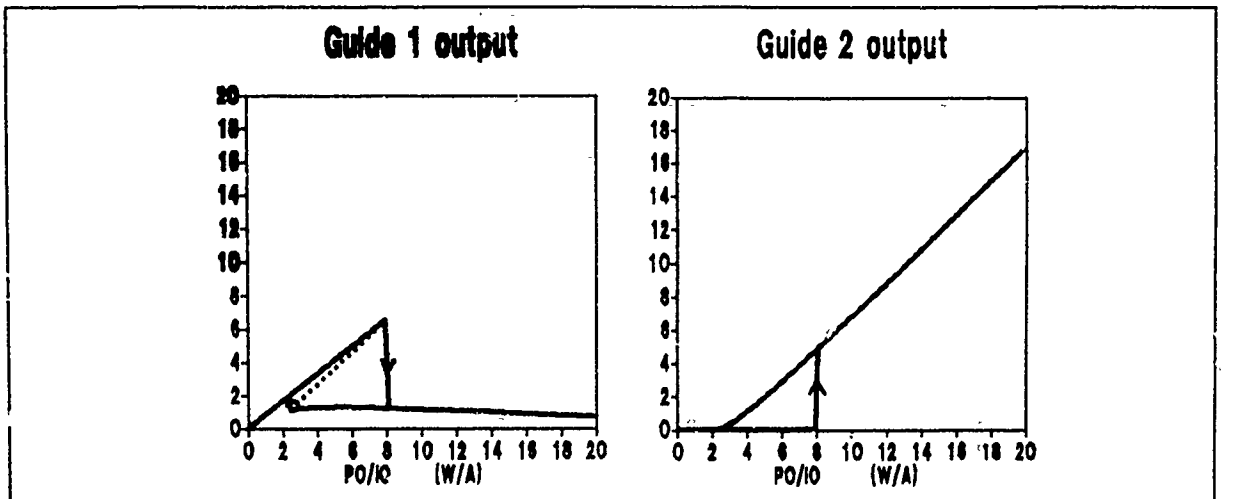

Figure 3. Outputs as a function of incident power: Powers are in arbitrary units. Dashed points correspond to unstable states.

Aknowledgements: We aknowledge partial financial support from the EEC within the 1033 RACE (OSCAR) program.

References:

1. M. Cada,R.C. Gauthier,B.E. Paton and J.M. Glinski, Appl. Phys. Lett. ,*51*(10),(1987),713
2. P. Li Kam Wa,J.E. Sitch,N.J. Mason,J.S. Roberts and P.N. Robson, Electron. Lett.,*21*,(1985) 26
3. P.R. Berger,Y. Chen,P. Bhattacharya,J. Pamulapati and G.C. Vezzoli, Appl. Phys. Lett.,*52*(14), (1988) 1125
4. D.A.B. Miller,D.S. Chemla,T.C Damen,T.H. Wood,C.A. Burrus,A.C. Gossard and W. Wiegmann. IEEE J. Quant. Electronics,*QE-21*,9, (1985) 1462
5. G.J. Sonek,J.M. Ballantine,Y.J. Chen,G.M. Carter,S.W. Brown, E.S. Kosteles and J.P. Salerno, IEEE J. Quant. Electronics, *QE-22*,7,(1986) 1015
6. J.S. Weiner,D.A.B. Miller and D.S. Chemla, Appl. Phys. Lett.,*50* (13), (1987) 842

An FDM Coherent Optical Switch Experiment With Monolithic Tunable Lasers Covering a 1,000 GHz Range

K. Y. Eng, M. Santoro, T. L. Koch, W. W. Snell* and J. Stone*
AT&T Bell Laboratories, Crawfords Corner Road, Holmdel, N. J. 07733
*AT&T Bell Laboratories, Crawford Hill Laboratory, Holmdel, N. J. 07733

I. Introduction

Considerable progress has been made in coherent optics for local network applications whereby a star coupler is used to combine various Frequency-Division-Multiplex (FDM) channels from the inbound lines for broadcasting onto each of the outbound lines [1-3]. Many practical challenges in such FDM networks (e.g. synchronization, control of the FDM comb, polarization maintenance etc.) can be minimized when we shrink the entire network inside a "box" so as to build an optical switch capable of cross-connecting many high-speed circuits carried in multi-Gb/s fibers [4]. We describe here results of an on-going experiment aimed at exploring the technical feasibility of this approach, and our laboratory demonstration is believed to be the first one done with *monolithic* tunable lasers covering 1,000 GHz at 700 Mb/s and with a novel tuned, balanced coherent receiver design, yielding a potential switch size as large as 125×125.

II. Experiment and Results

A conceptual block diagram of an FDM optical line-rate switch is shown in Fig. 1 where the arrangement of fixed transmitter/tunable receiver facilitates broadcasting and multicasting in the switch.

The experimental set-up is depicted in Fig. 2 where three transmitting laser signals (two closely spaced and one far apart) are summed in a 4×4 star coupler. One of the star coupler outputs is connected to a coherent tunable receiver which can receive any of the three transmitting signals. Another output is connected to a fiber Fabry-Perot (FP) filter (FSR = 13.8 GHz) providing a reference frequency comb for stabilizing the input laser frequencies [5,6]. The transmitting lasers are each dithered with a slightly different frequency for the purpose of channel identification. The frequency locking circuits can resolve dithering frequencies as close as 10 Hz apart, and the frequency locking system can support at least 1,000 channels.

The three single-mode transmitting lasers are all two-contact MQW DBR types, each tunable over ≈1,000 GHz in the 1.5 μm region [7]. The lasers were biased to produce a 0 dBm output into the isolators. One isolator was used for each laser (isolation > 30 dB, 0.5 dB insertion loss). A 2×2 titanium diffused lithium niobate waveguide switch element was used as an external modulator providing on/off modulation. While the modulators could operate up to 3 Gb/s, our experimental data rate was limited to 700 Mb/s because of restricted receiver bandwidth as well as the broad LO laser linewidth. In our laboratory demonstration, the two widely tuned lasers (F_1 and F_3) were locked to channels separated by ≈600 GHz, and the in-between one (F_2) could be positioned just one channel away (13.8 GHz) from F_1 or in any channel between F_1 and F_3. Light power from the modulators was coupled into fibers at -16 dBm leading to the polarization adjusters and the star coupler. The star coupler was wavelength independent and had an excess loss of 0.5 dB.

A block diagram of the coherent receiver is shown in Fig. 3. This is a novel design using a tuned, balanced technique without equalizing circuits. The signal and LO are combined in a fiber coupler and directed onto two photodetectors in a balanced configuration. An inductive T-matching network is used to bring the detected (IF) signal through a tuned bandwidth of 1 GHz centered at 4 GHz to an FET. A frequency locking circuit is also included to adjust the LO frequency to maintain the detected IF signal centered at the tuned passband (4 GHz). The LO used was another two-contact MQW DBR tunable laser supplying about -4.6 dBm into the fiber coupler. It was tunable over 1,000 GHz overlapping the frequency arrangment of Fig. 3 in our experiment. Therefore, any one of the three laser signals could be received. At 600 Mb/s, we measured a receiver sensitivity (signal power at the fiber coupler input) of -42 dBm for a BER of 10^{-10}, and at 700 Mb/s, the receiver sensitivity dropped to -38 dBm for the same BER probably due to the excessive linewidths of the signal and LO lasers ($\approx$70 MHz each) causing spillover outside the tuned receiver bandwidth. Further increase of bit rates to 800 Mb/s seemed possible but more work was required before reliable measurements could be reported. Prior to this system experiment, the receiver was tested to 1 Gb/s with an external cavity laser as LO for a measured sensitivity of -42.5 dBm at a 10^{-9} BER.

Based on our experimental experience of using tunable receivers with sensitivity of -38 dBm at 700 Mb/s, and a practical capability of launching -16 dBm into the star coupler input, a power margin of 26 dB is available to account for the star coupler splitting and excess losses. This implies that sufficient power margin exists for implementing a 125$\times$125 switch (at 700 Mb/s). The tuning range of the LO can easily support 125 channels with a channel spacing of 8 GHz.

III. Conclusions

We have described an on-going experiment using monolithic tunable lasers to explore the technical feasibility of building an FDM optical switch on a star coupler architecture. In our laboratory demonstration, three transmitting lasers were frequency locked onto peaks of a fiber FP filter providing the reference comb. These lasers were the monolithic MQW DBR type capable of tuning over a 1,000 GHz range and thus could be positioned in any of the designated channels within their tuning range. A coherent receiver using another monolithic MQW DBR tunable laser as the LO was used to recover any of the three transmitted signals. We measured receiver sensitivity of -42 dBm at 600 Mb/s and -38 dBm at 700 Mb/s, both at a BER of 10^{-10}. From these measurements, we concluded that a 125$\times$125 optical switch using this design technique could be feasible with state-of-the-art tunable lasers.

REFERENCES

[1] R. A. Linke, "Coherent Frequency Division Multiplexed Networks," *OFC '89.*
[2] L. G. Kazovsky et al., "Multichannel Coherent Lightwave Technology," *ICC '88.*
[3] P. S. Henry, "Very-High-Capacity Lightwave Networks," *ICC '88.*
[4] K. Y. Eng and M. Santoro, paper submitted for publication.
[5] J. Stone and L. W. Stulz, "Pigtailed High-Finesse Tunable Fibre Fabry-Perot Interferometers With Large, Medium and Small Free Spectral Ranges," *Electronics Letters,* 16 July 1987.
[6] B. Glance et al., "Densely spaced WDM coherent network," *OFC '88.*
[7] T. L. Koch et al., "High Performance Tunable 1.5 μm InGaAs/InGaAsP Multiple-Quantum-Well Distributed-Bragg-Reflector Lasers," *Appl. Phys. Lett.,* September 1988.

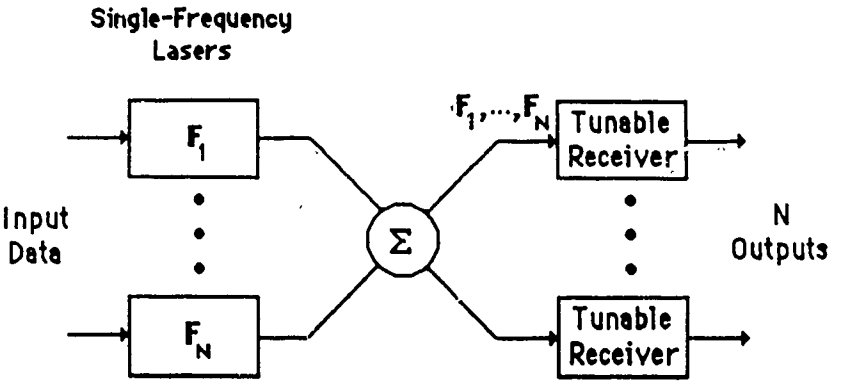

Figure 1: An NxN FDM Optical Switch Architecture

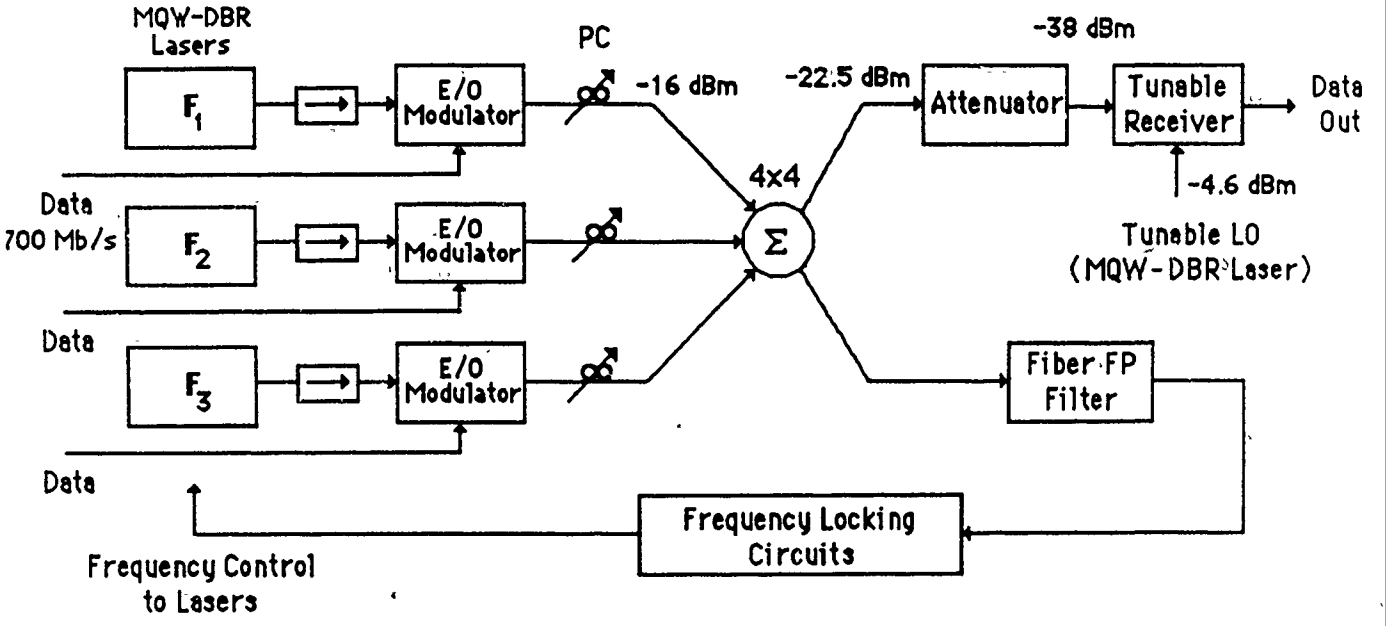

Figure 2: Experimental Set-up

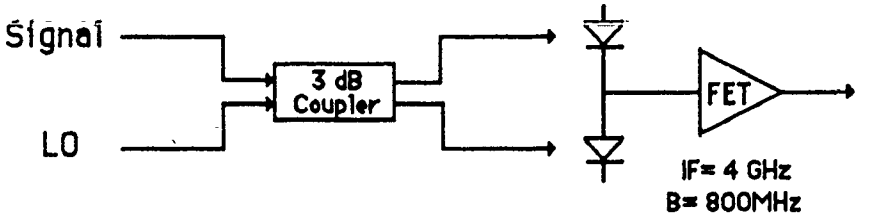

Figure 3: A Tuned, Balanced PIN-FET Receiver

Analytic Expressions for Switching Irradiances of Bi-and Multistable Nonlinear Fabry-Perots

H. Thienpont, I. Van de Voorde, I. Verbesselt, I. Veretennicoff

Vrije Universiteit Brussel, Applied Physics Department (TONA-TW)

Pleinlaan 2, B-1050 Brussel Belgium.

In search of devices that ultimately will allow for the design of digital optical information processors, one's intention, among other things , is to optimize the steady state behaviour of a promising device : the non linear Fabry-Perot (NLFP).
This steady-state behaviour can be described by hysteresis contrasts C_H, relative hysteresis widths W_H and hysteresis transmissions T_H, as far as the bistable and the multistable regions are concerned. These three factors in their turn are essentially determined by the different up- and downswitching irradiances, characterizing the device.
It is thus crucial to be able to determine these up- and downswitching irradiances in a fast and accurate way, for different device parameters.
Instead of calculating the commutation irradiances numerically, which is tedious and computer time consuming due to the transcendental character of the equations (1) and (2), we will bring forward a set of concise analytical expressions allowing for an accurate and straightforward determination of the up- and downswitching irradiances, I_{up} and I_{down} respectively.
Our technique, based on eliminating the transcendental character of (1) and (2) , consists in approximating the Airy curve (1) by a set of parabolas with an upward and a downward curvature in the vicinity of up- and downswitching points respectively. This is shown in Fig. 1. Once the analytic expressions for the parabolas are known, we can easily obtain the coordinates of the commutation points, leading to I_{up} and I_{down}.

$$\tau = \frac{1}{1 + \frac{4R}{(1-R)^2}\sin^2(\gamma I_{eff} + \delta)} \qquad (1)$$

$$\gamma I_{eff} = \frac{3}{2}\frac{\omega \chi^{(3)}}{n_o^2 c}\sqrt{\frac{\mu_o}{\varepsilon_o}}\,\tau\, I_{in}\frac{(1+R)^2}{(1-R)} \qquad (2)$$

The analytic formulas, allowing to calculate I_{up} an I_{down} are very concise and easy to use. They offer an accuracy of less than 5% error over the entire range of device parameters, such as detuning, reflection coefficients, finesse, etc., in comparison with the real values, as shown in Fig. 2. This error is minimized down to 0.2% after applying a parameter estimation method in order to improve the parabolic fit of the

Airy curve. We will also discuss the validity of these equations in the high finesse approximation.
We will apply these expressions to examine the influence of several device parameters such as thickness, reflection coefficients and detuning, on the value of the commutation irradiances and on the device characteristics C_H , W_H and T_H . This allows for a fast optimization of the bistable as well as of the multistable operating domains. An example is given in Fig. 3.
We will conclude by illustrating this new technique and the accuracy of the resulting expressions with two applications. First we will determine quantitatively the behaviour of the switching irradiances of NLFPs which are adressed by obliquely incident laser beams [1] and who have different states of linear polarization [2]. Second we will show -again quantitatively- the impact of the supplementary non linearities, appearing in the reflection coefficients, in case of thin non linear films [3].

1)H. THIENPONT, J. DANCKAERT, I. VERETENNICOFF,D. JÄGER and F.FORSMANN
Steady state operation of a non-linear Fabry-Perot for oblique incidence : Polarization and Beam angle dependence
Optical Bistability IV, Aussois, 23-25/3/88. Journal de Physique Colloque C2-137-C2-141, Supplément au no 6, Tome 49,juin 1988 .

2)H. THIENPONT, L. PEIRLINCKX, M. SMEDTS and I. VERETENNICOFF
Finesse switching : an alternative intensity independent commutation mechanism.
Proc.of the O.S.A./IEEE Topical Meeting on Optical Computing :Optical Computing '88, Toulon (France), sept 88 .

3)J. DANCKAERT, H. THIENPONT, I. VERETENNICOFF, M. HAELTERMAN and P. MANDEL
Self-Consistent Stationary Description of a Nonlinear Fabry-Perot.
Accepted for publication in Optics Communications,.jan 89 .

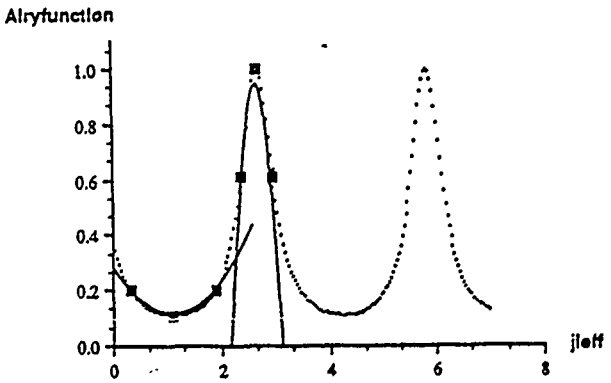

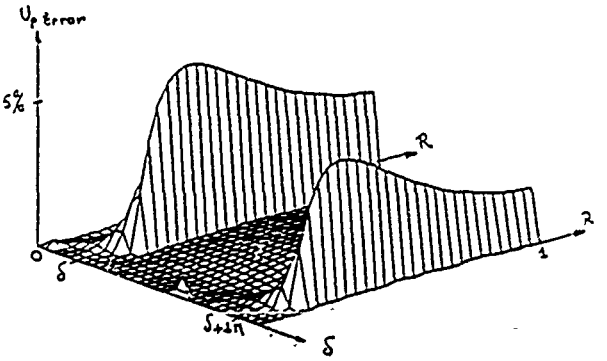

Fig. 1(left) shows the technique to eliminate the transcendental character of the NLFP equations, using a parabolic approximation of the Airy curve.
Fig. 2a (right) depicts the error of the upswitching irradiance as a function of the reflection coefficients of the interfaces R and the detuning δ . We used here the formula for I_{up} that was derived from a parabolic approximation before the parabola fit was optimized using parameter estimation theory. Notice that the maximum error does not exceed 5%.

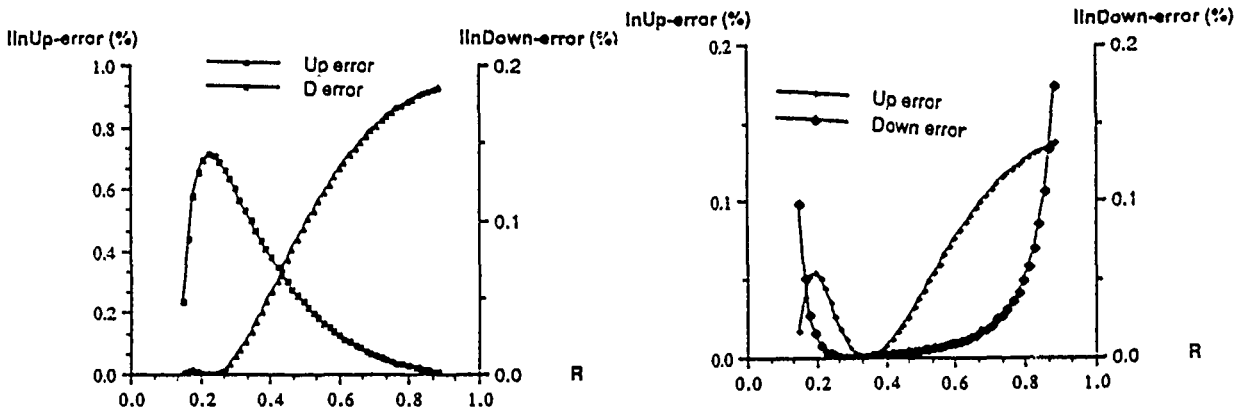

Fig. 2b shows the error of the up- and downswitching intensities before optimizing the parabola fit. Here we used a Silicon etalon with a fixed thickness D= 480 microns and a wavelenght of a Nd: YAG laser : 1.06 microns.
Fig. 2c shows the reduction of the error for I_{up} and I_{down} after parameter estimation.

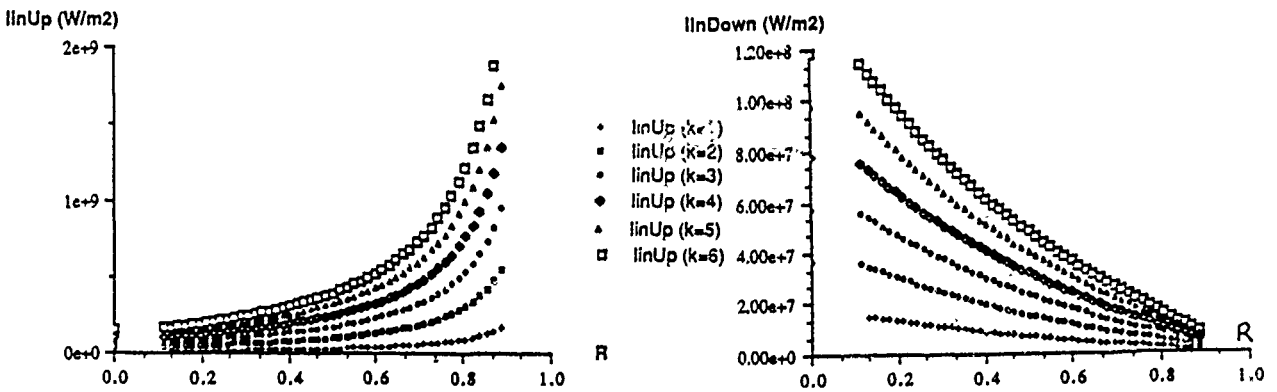

Fig. 3 a and b display the calculated values of up- and downswitching irradiances for different bi- and multistable loops as a function of the reflectioncoefficients. Here k is a parameter that determines the order of appearance of I_{up} (respectively I_{down}) for increasing values of irradiance.

A novel light modulator and optical transistor for the far infrared region : a proposal for a modulable mirror.

Maarten Kuijk & Roger Vounckx

Vrije Universiteit Brussel, Applied Physics Department (TONA-TW)

Pleinlaan 2 1050 Brussels

Belgium

Summary.

Recently, a new device has been proposed [1] in which the reflection properties of an electron gas are modulated in order to perform such functions as modulation and transistor action. The idea is to guide the light in an integrated waveguide which has lower or equal refractive index than the substrate. The confinement of the light is achieved through the use of an electron gas mirror in-between the waveguide and the substrate. By changing e.g. the density or the effective mass of the electrons the confinement, hence the output can be modulated.

The problem however with using electrons as a mirror is that a very high density gas with sufficient thickness is generally required to obtain good reflectance. At first sight, the resulting small Debye length (i.e. small with respect to the total thickness of the electron gas) excludes all possible modulation.

Yet, a rigorous model, directly derived from first principles, shows that a window exists in which sufficient reflectivity can be combined with sufficient modulation depth to yield practical devices. This model describes the reflection, absorption and transmission properties for electro-magnetic waves of a free electron gas embedded in a dielectric (e.g. a semiconductor) which is itself sandwiched between two other dielectrics (e.g. waveguide and substrate). The most important feature which is revealed is the difference between TE and TM incidence. Although in general for the same electron density the TE incidence is better reflected than the TM one, there is a peak in the reflection for TM at an electron density such that the plasma frequency of the electron gas matches the frequency of the light. Figure 1 shows the reflection coefficient of an electron gas in InSb (500 Å thick) versus electron density for TM polarization (wavelength of 10.6 μm).

Since the plasma frequency is determined by the effective mass and the density of the electrons only, the search for practical devices does not any longer imply a search for as high and as thick as possible electron gases (which cannot be depleted by an electric field anyway), but rather a search for the lowest effective mass combined with the right electron density. The losses (reflection ≠ 1) are minimal with highest electron mobility and highest

227

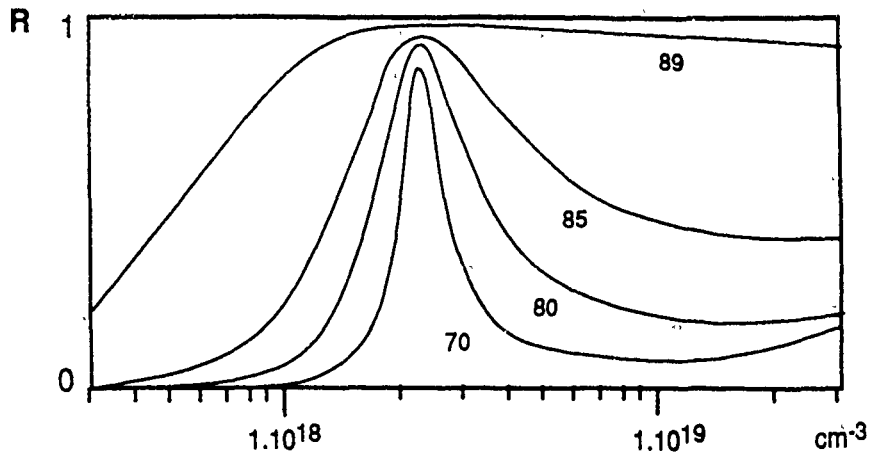

Figure 1 : R versus electron density in InSb for TM polarization (for several angles of incidence), maximum reflection occurs at 2.2×10^{18} cm^{-3}. $m_{eff} = 0.0145\ m_0$, thickness = 500 Å, μ = 80 000 $cm^2/V.s$.

Two classes of devices can take advantage of the TM polarization resonance : electro-optical ones in which the output is modulated by an electric field and all-optical ones in which the creation of extra electron-hole pairs e.g. by, say, band gap absorption switch the reflection coefficient to the low state. It should be noted that the TM peak is in fact very narrow (a mere factor of two to three in electron density) and is ideally suited for switching devices and invertors.

A common problem to both the electro-optic and the all-optical devices is caused by the absorption and transmission losses. Since these are closely linked to the electron mobility, the use of modulation doped heterojunctions [2] as in the electronic HEMT [3] seems appropriate. The problem of the extremely small thickness of the resulting two-dimensional electron gases (2DEG) can be overcome by the use of multiple barrier heterojunctions. Since the maximum depletion depth of an electron layer with densities in the 10^{18} - 10^{19} cm^{-3} region is of the order of a few hundred angströms, a first "optimized structure" for a light modulator is proposed as shown in figure 2 : a double barrier structure yields a total electron thickness of 500 Å, whereas the use of the same material for waveguide, electron gas carrier and substrate minimizes parasitical reflection.

The structure shown here is in the AlAs-GaAs system although the calculations reveal that about $7 \times 10^{18} cm^{-3}$ carriers are needed at high reflectivity : this is above the limit of what can be obtained today by modulation doping in this system. Yet, a demonstration prototype can more easily be built in these materials, since it is "standard III-V technology". However, it is clear that practical devices are in need of more suitable materials. Pseudo-morphic heterojunctions of AlAs-InGaAs or AlAs-InGaSb e.g. combine a larger conduction band discontinuity (which can produce higher electron densities) with a much lower electron effective mass. A very promising lattice-matched system is CdTe-InSb (figure 1) or

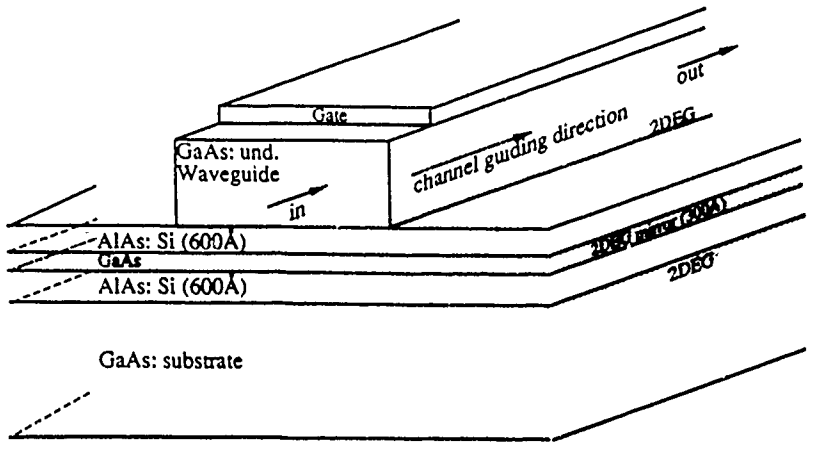

Figure 2 : "Optimized" light modulator structure for 10.6 μm wavelength in the AlAs-GaAs system. Total thickness of the electron gas is 50 nm.

CdTe-(InSb+~1%CdTe) where electron densities of 10^{19} cm^{-3} are within reach with an effective mass as low as $0.0145m_0$ for the InSb case, $0.005m_0$ for the InSb1%CdTe case and mobilities of 80 000 $cm^2/V.s$. The smaller band gap (0.17 eV or 7.3 μm) also makes it possible to design structures in which the same wavelength is used for the "source-to-drain" beam and the "gate" beam, opening perspectives for integrable all-optical transistors suited for digital applications.

Preliminary measurements on a device built in the GaAs system show indeed high modulation depths (additional illumination is needed to produce enough extra carriers).

Conclusion. The larger effect on TM polarized light of the matching of the plasma frequency of an electron gas to the frequency of the light allows to conceive light modulators and optical transistors based on modulable light confinement in waveguides limited by an integrated modulable mirror. The narrowness of the reflection peak in combination with the use of selectively doped heterojunctions in III-V compound semiconductors raises hopes for psec modulation and switching times.

References.

[1] R. Vounckx, patent pending, The Hague, 10 june 1988

[2] T. Mimura, S. Hiyamizu, T. Fujii, K. Nanbu, "A new field-effect transistor with selectively doped GaAs/n-$Al_{1-x}Ga_xAs$ heterojunctions", Japan. J. Appl. Phys., 1980, vol. 19, pp L225-L227.

[3] R. Dingle, H. L. Stormer, A.C. Gossard, W. Wiegmann, "Electron mobilities in modulation doped semiconductor heterojunction superlattices", Appl. Phys. Lett., 1978, vol. 33, pp. 665-667.

Reduced Waveguide Intersection Losses for Large Tree Structured Ti:$LiNbO_3$ Switch Arrays

T.O.Murphy, F.Hernandez-Gil, J.J. Veselka and S.K. Korotky

AT&T Bell Laboratories
Crawfords Corner Road
Holmdel, NJ 07733
(201) 949-4403

The prospects for realizing large integrated-optic switch arrays have been dramatically changed as a consequence of recent advances in both optical switch fabric architectures [1-3] and low crosstalk waveguide intersections [4]. The implementation of dilated versions [3] of standard and special optical switch architectures, for example, has had a significant impact in alleviating the accumulation of crosstalk from the constituent directional coupler crosspoints as the light signals traverse the switch. In fact, at present optical loss in the fabric is a limiting factor determining the overall switch size. The adapatation of switch architectures known in the field of electronic switching that grow only logarithmically in the number of switable coupler stages that are required, in principle permits switch line sizes as large as 1024×1024 for line rates as high as 1 Gb/s and an average loss per coupler of 1 dB [5,6]. These architectures make significant use of waveguide intersections, and consequently these intersections must be very efficient at angles for which crosstalk is negligible. In a previous Ti:$LiNbO_3$ 8×8 dilated-Benes switch reported by us, the excess loss for 10° waveguide intersections averaged 0.3dB/intersection [7]. This is consistent with independent measurements of losses for standard structures [4]. In this paper we report modifications of the waveguide intersection geometry which result in measured losses of 0.1 dB/intersection.

A typical waveguide intersection encountered in architectures such as the banyan, Benes, Clos, and shuffle architectures consists of two optical waveguides of transverse width W that intersect at an angle θ. For angles sufficiently large to ensure negligible crosstalk (> 5°) without the introduction of excessive fabrication tolerances, the coupled-mode formalism has proved inadequate to describe the evolution of the optical wave [8], and it is appropriate to consider the field evolution along the direction of propagation in terms of the distortion of the mode of the waveguide and the radiation caused by the presence of the second waveguide. From this point of view, low loss should be attained by minimizing the extent to which the field profile is steered away from the vertex of the intersection and also minimizing the asymmetry of the mode at that same point.

The peak index change for a Ti:$LiNbO_3$ waveguide has been described by

$$\Delta n_0 = \frac{2}{\sqrt{\pi}} erf\left(\frac{W}{2D}\right)\frac{b\tau}{D}$$

where D is the diffusion depth, W is the titanium stripe width, b is the constant of proportionality between the index change and titanium concentration, and τ is the thickness of the deposited titanium layer. Away from the intersection region $W/D \approx 2$. However, when the two waveguides meet $W/D \approx 4$ causing a large increase in the peak Δn_0. The authors have modified the geometry to minimize this peak Δn_0. The Beam Propagation Method (BPM) has been utilized to calculate losses for various intersection geometries. The variation in loss agreed quite well with fabricated intersections. We went on to simulate geometries that significantly reduce the intersection loss. Figure 1 illustrates a 10° intersection we have fabricated. This geometry starts with tapers on the inside edge of each waveguide down to a 2 um wide notch located 3 um after the inner vertex. From there another taper on the outside of the waveguides proceeds to a 4.5 um waveguide width at the center of the intersection region.

We fabricated the geometries using conventional Ti:$LiNbO_3$ waveguide technology. These guides exihibit low insertion loss, <2 dB, with a 2nd order cutoff frequency of 1.15um. With these optimized guides the best unmodified 10° degree intersection loss was 0.2 dB. Our mask contained normal and modified intersections for 7, 8.5 and 10 degree intersections. We measured a reduction in the loss of 30%, 28% and 50% for the 7, 8.5, and 10 degree intersections respectively.

Analysis of the intensity profiles of the intersections obtained from BPM calculations has been done in order to explain the mechanism for the loss reduction. We have seen a deformation of the intensity profile of the modified intersection before the center of the intersecting region is encountered. The profile for a regular intersection does not show this deformation. However, the intensity profile in the center of a regular intersection shows a greater displacement than that of a modified intersection. We feel the reduction in loss is due to better mode matching at the center of the intersecting region. Figures 2a and 2b show greater oscillation from the center of the waveguide for the intensity profile of the normal intersection than for that of the modified structure. We feel this is due to the radiation modes interacting with the fundamental mode.

In summary we have studied intersecting waveguides with the BPM arriving at modified geometries which, when fabricated in Ti:$LiNbO_3$, have reduced the loss as much as 50%. We acknowledge the valuable contributions of F. Heismann, R. Alferness, R. Bosworth, D. Herr, and J. Watson.

REFERENCES

[1] R. A. Spanke, J. Quantum Electron., QE-22, 964 (1986).

[2] L. Thylen, Tech. Dig. of Integrated ad Guided-Wave Optics, papers MAA1, 1989.

[3] K. Padmanabhan and A. N. Netravali, IEEE Trans. Comput., COM-35, 1357(1987).

[4] G. A. Bogert, Electron. Lett., 23, 72(1987).

[5] M. J. Wale et al., CLEO'87, Baltimore, paper WQ5.

[6] R. C. Alferness, IEEE J. Sel. Area Comm., 6, 1117(1988).

[7] J. J. Veselka et al., Conf. on Opt. Fiber Comm. 1989, Houston, 1989, paper ThB2.

[8] N. Agrawal, L. McCaughan, and S. R. Seshadri, J. Appl. Phys., 62, 2187(1987).

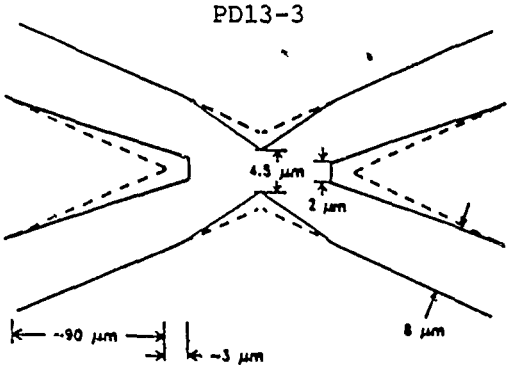

Figure 1.

Modified 10° Waveguide Intersection

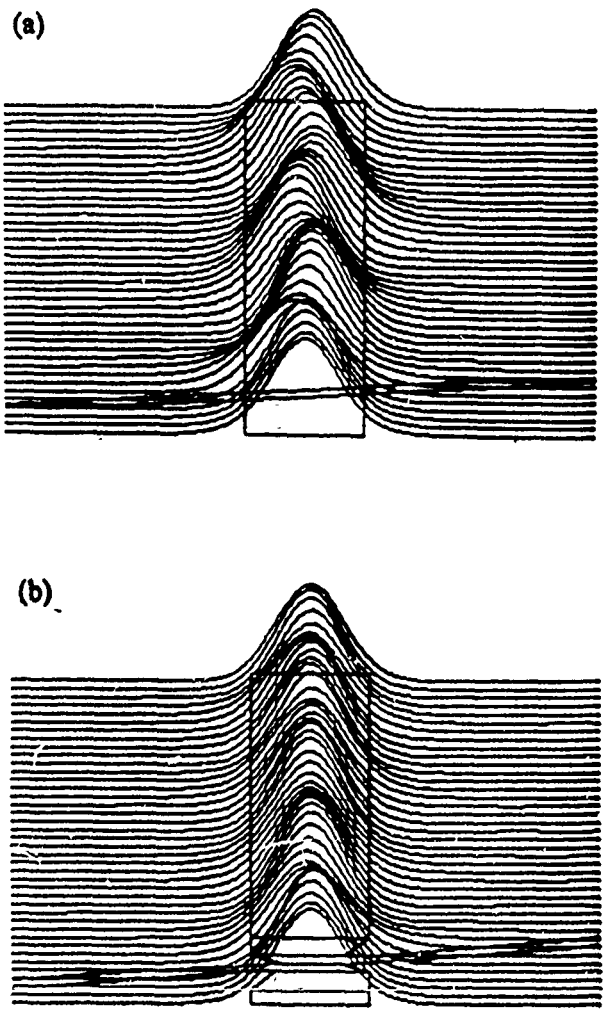

Figure 2. BPM calculation of the field intensity for (a) regular and (b) modified intersections.

PHOTONIC SWITCHING

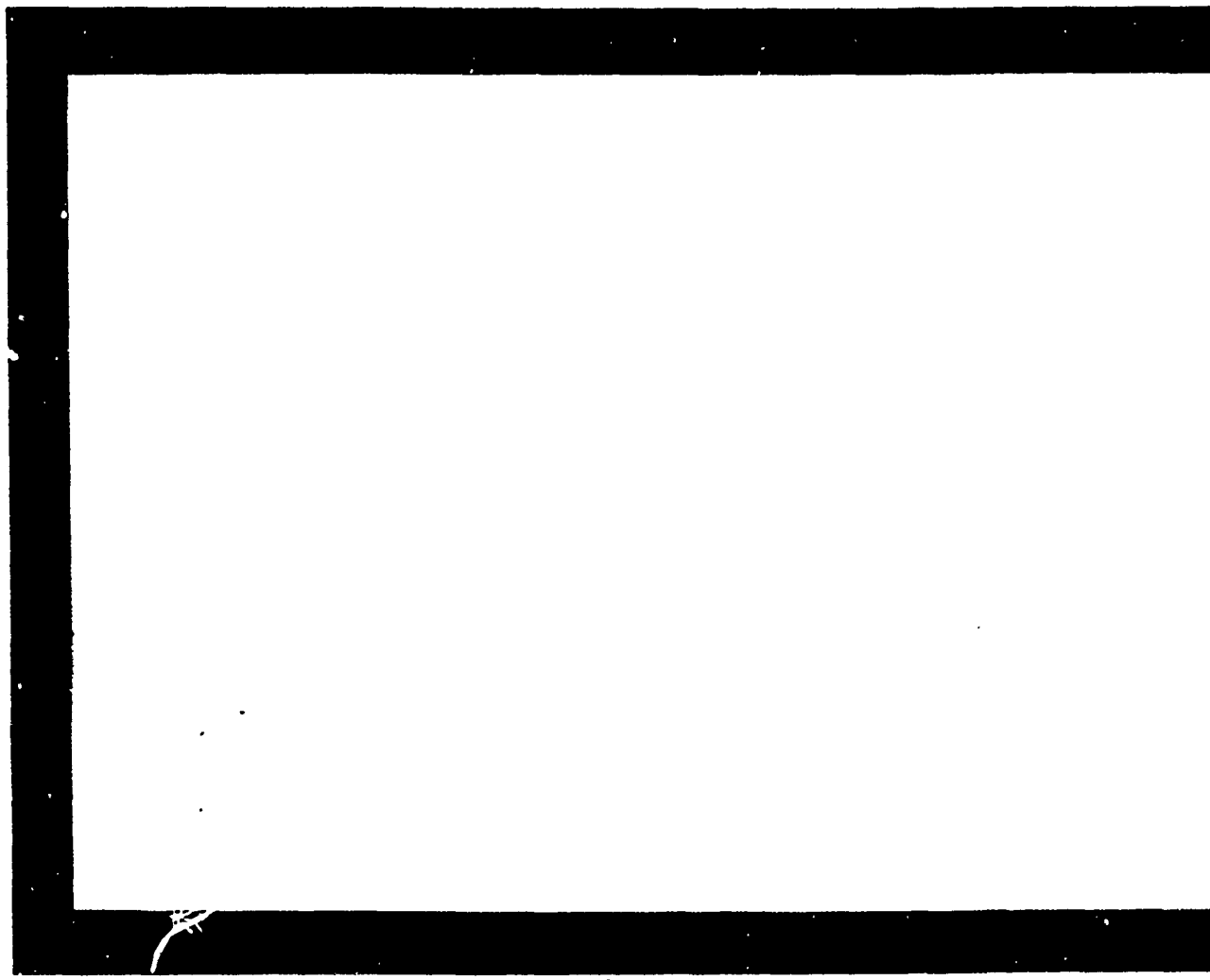

POSTDEADLINE PAPER ADDITION

MARCH 1-3, 1989
SALT LAKE CITY, UT

Soliton Switching in a Fiber Nonlinear Loop Mirror

M.N. Islam, E.R. Sunderman, R.H. Stolen, W. Pleibel and J.R. Simpson
AT&T Bell Laboratories
Holmdel, N.J. 07733

We observe complete switching of 310fsec soliton pulses at an energy of $\sim$55pJ with 90 percent transmission in a fiber nonlinear optical loop mirror (NOLM)[1]. Because of their low loss and fast nonlinearities, fibers are an attractive medium in which to implement ultrafast, all-optical switches. Switching in fibers generally occurs for only a part of the optical pulse since the nonlinear phase shift usually follows the intensity envelope[2]. However, solitons make possible the switching of the entire pulse because, in the anomalous group velocity regime, fundamental solitons show a uniform phase shift over the entire waveform[3]. To show complete soliton switching, Doran and Wood [1] first proposed the NOLM, which consists of a four-port directional coupler in which two ports on one side are connected by a loop of fiber. The device acts like a Mach-Zehnder interferometer whose two arms correspond to the two counter-propagating directions around the loop.

A multiple quantum well passively modelocked NaCl color center laser [4] provides τ=310fsec Gaussian pulses at λ= 1.692μm. As shown in Fig. 1, a variable attenuator is used to vary the input power, and an isolator prevents feedback into the laser. A 1cm thick uncoated quartz beam splitter picks off a fraction of the input and reflected light, and apertures are used to block multiple reflections. The NOLM is made of 25m of single-mode, polarization-maintaining, dispersion-shifted fiber with a zero dispersion wavelength of 1.584μm (at λ = 1.692μm the dispersion is 6.4 psec/nm/km). Germanium doping used to dispersion shift the fiber approximately doubles the solition self-frequency shift (SSFS) over fused silica. The coupler is made of quartz blocks in which the fiber is glued and polished. Thirty-two percent of the light is coupled over and the loss at the coupler is $\sim$8 percent. Although we varied the coupler between 20 and 70 percent coupling, the maximum transmission was achieved near values of $\sim$ 30 percent coupling. The loop is closed at a $\sim$90 percent transmitting splice. Throughout the set-up, the polarization extinction ratio is better than 15:1. For our fiber, the soliton period is $Z_0 \cong$ 5m, and the soliton fundamental power is $P_1 \cong$ 107W.

Figure 2 illustrates the nonlinear transmission (E_{out}) and reflection (E_{refl}) as a function of input power (E_{in}). The ratio of E_{out} to (E_{out} + E_{refl}) increases up to a peak and is then followed by a dip and an approximately flat region. After correcting for the various losses, the peak occurs at $E_{in}/E_1 \sim$ 1.66 and the transmission at the peak is $\sim$90 percent. This peak corresponds to a pulse switching energy of 1.66 $\times$ P_1 $\times$310fsec $\cong$ 55pJ. The peak and null are less pronounced than in the ideal case [1] because of SSFS effects. Since the coupler unequally divides the light in the two directions, the intensity dependent frequency shift is different in the two directions, and the interference is incomplete. To compare with theory, we numerically solved the modified nonlinear Schroedinger equation including only the first-order correction term from the SSFS. As the solid curve in Fig. 2a shows, the peak in $E_{out}/(E_{out} + E_{refl})$ occurs at 1.5 times the fundamental soliton energy and the peak transmission is 90 percent, in excellent agreement with the experiment. The $\sim$ 10 percent discrepancy in power may be from uncertainties in our assumed value for P_1.

At the peak of transmission, we see switching of the complete soliton waveform. We have studied the autocorrelations of the output pulses as a function of input power. At the peak of the transmission (point 2 in Fig. 2b), the output is slightly broader than the input pulse but otherwise identical in shape. If the pulses were not solitons, then only the center of the pulse would switch, and the autocorrelation would be narrower [2]. The solitons broaden slightly because, after dividing in the coupler, one arm has lower than fundamental soliton power. For this same reason, the transmitted pulses broaden with decreasing input power (point 1 in Fig. 2b).

As confirmation of the influence of SSFS, we see pulse break-up at higher powers. The pulse starts to change shape around the dip in transmission (point 3), where the output autocorrelation shows wings. At yet higher powers, the output splits into three pulses (corresponding to five peaks in the autocorrelation) that separate with increasing power.

In summary, we have studied the nonlinear transmission and reflection properties of a fiber NOLM operating in the soliton regime. The experimental results at the peak of transmission show switching of the complete pulse, thus proving the advantages of using solitons. An attractive feature of the NOLM as a switching device is that the pulse shaping is small up to the peak, so that the output can be cascaded to other fiber devices. Our observed 90 percent transmission at the peak is in excellent agreement with numerical simulations.

[1] N.J. Doran and D. Wood, Opt. Lett. **13** , 56 (1988). We thank N.J. Doran, K. Blow and B. Nelson for stimulating discussions.

[2] S.R. Friberg, A.M. Weiner, Y. Silberberg, B.G. Sfez and P.W. Smith, Opt. Lett. **13** , 904 (1988).

[3] N.J. Doran and D. Wood, J. Opt. Soc. Am. B **4** , 1843 (1987).

[4] M.N. Islam, E.R. Sunderman, I.Bar-Joseph, N. Sauer and T.Y. Chang, (March 27, 1989, Appl. Phys. Lett.).

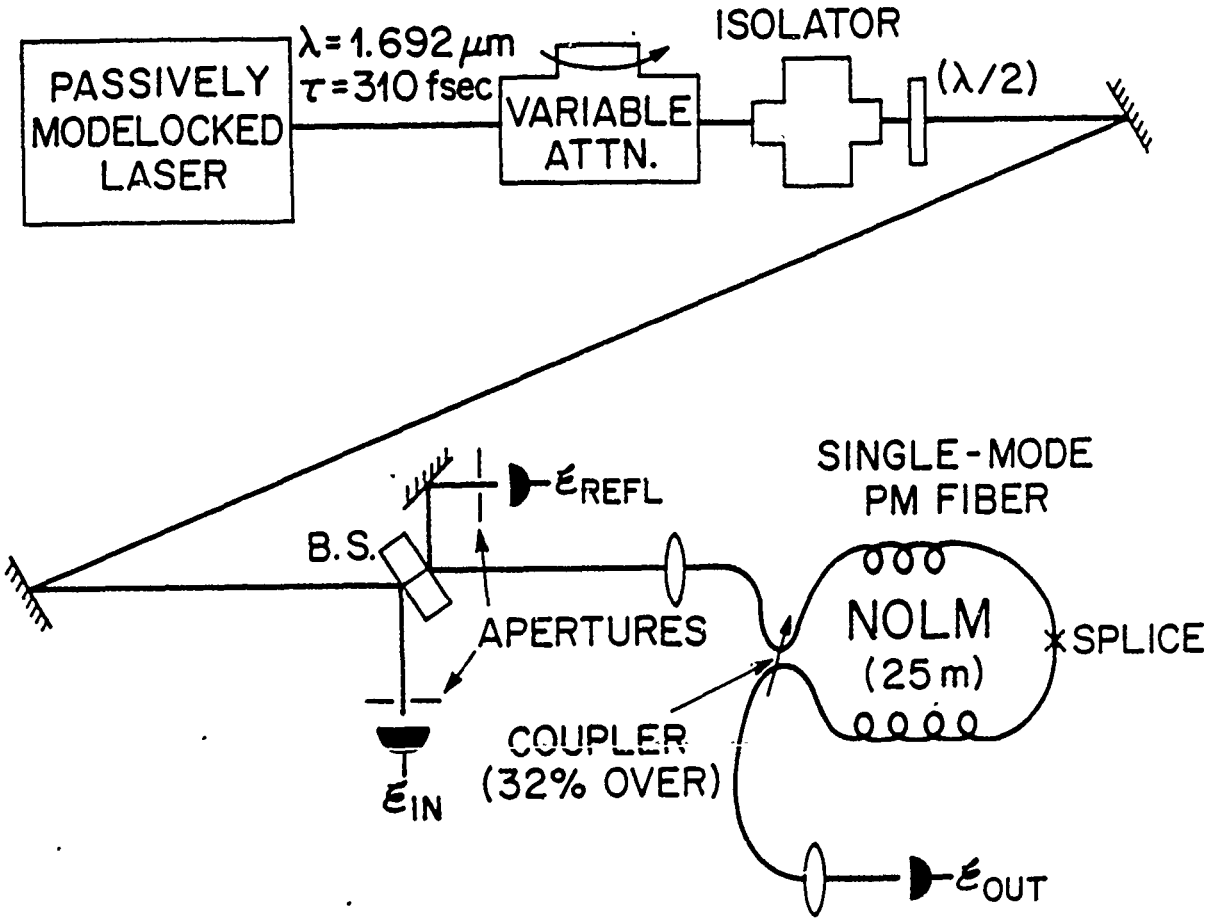

Fig. 1 Experimental configuration for the fiber nonlinear optical loop mirror.

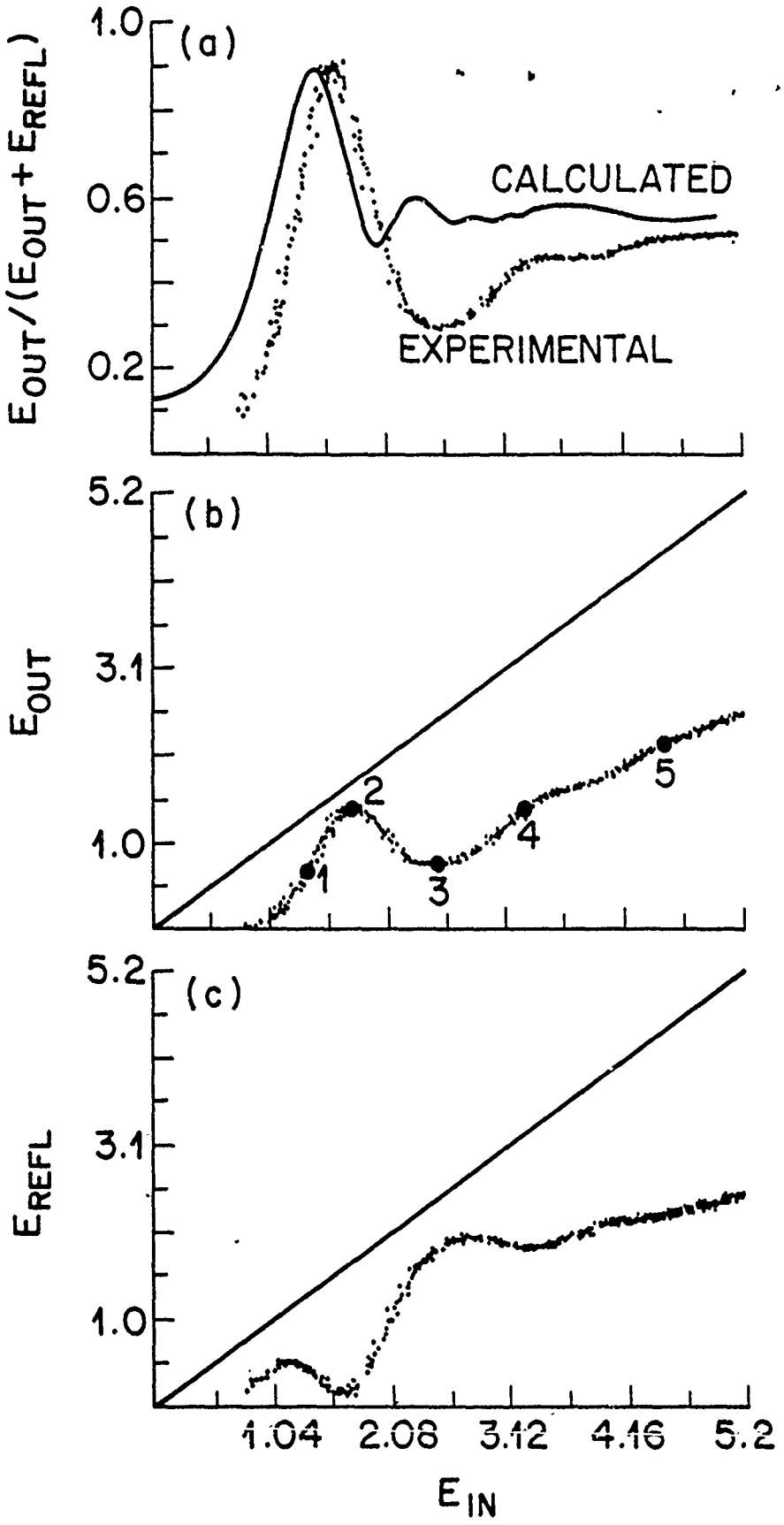

Fig. 2 Measured transfer characteristics of the nonlinear optical loop mirror. (a) $E_{out}/(E_{out} + E_{refl})$, (b) E_{out}, and (c)E_{refl} versus E_{in}. All energies are normalized to the fundamental soliton energy. The solid curve in (a) is computed by solving the modified nonlinear Schroedinger equation.